



# University of HUDDERSFIELD

## University of Huddersfield Repository

Butler, Simon

DNA Origami as a Foundry for Artificial Electromagnetic Materials

### Original Citation

Butler, Simon (2021) DNA Origami as a Foundry for Artificial Electromagnetic Materials. Doctoral thesis, University of Huddersfield.

This version is available at <https://eprints.hud.ac.uk/id/eprint/35663/>

The University Repository is a digital collection of the research output of the University, available on Open Access. Copyright and Moral Rights for the items on this site are retained by the individual author and/or other copyright owners. Users may access full items free of charge; copies of full text items generally can be reproduced, displayed or performed and given to third parties in any format or medium for personal research or study, educational or not-for-profit purposes without prior permission or charge, provided:

- The authors, title and full bibliographic details is credited in any copy;
- A hyperlink and/or URL is included for the original metadata page; and
- The content is not changed in any way.

For more information, including our policy and submission procedure, please contact the Repository Team at: [E.mailbox@hud.ac.uk](mailto:E.mailbox@hud.ac.uk).

<http://eprints.hud.ac.uk/>

DNA Origami as a Foundry for Artificial  
Electromagnetic Materials

Simon Butler

Thesis Submission – Doctor of Philosophy

The University of Huddersfield

284 pages

November 2021

This thesis describes work conducted to create a pathway for the fabrication of non-arbitrary nanomaterials using biological systems as foundries. Due to the difficulties of their fabrication by conventional nanofabrication systems we use an optical metamaterial sized split ring structure as an exemplar. We investigate all aspects of construction from design to fabrication. While we describe a specific design directly our method incorporates a modular system easily adjustable by other groups.

Unit cell size was determined using information available in the literature. A breadboard design was created employing the M13MP18 scaffold. Once a board size was confirmed split rings within the unit cell/feature size were simulated to ensure they displayed unusual optical effects. This design was then fabricated by decorating a scaffolded DNA origami breadboard with gold nanoparticles.

We demonstrate programmable metallisation of a DNA origami breadboard, in high throughput, via a near surface saturation layer of structures. We also address existing bottlenecks in the literature as well as other artefacts detrimental to fabrication. This is facilitated by creation of a novel functionalised gold nanoparticle purification device and adaptation of existing techniques to increase efficiency and fidelity.

*To Mum and Dad. Without you this wouldn't have been possible - I told you I'd finish it eventually.*

*To Emma for putting up with me spending weeks at a time working.*

*To Daphne, Winnie and Eva, who provided enforced breaks and spell checks by trying to sleep on the keyboard.*

*Thank you to all my lab partners and especially Simon Foulkes for your friendship and advice.*

# Contents

## Chapter 0 Summary

0.0 - Summary of contents - 10

## Chapter 1 Introduction

1.0 - Introduction -14

1.1 - Metamaterial Background - 15

1.2 – Nanofabrication – 20

1.3 -Technique comparison – 21

1.4 – Conclusion - 24

## Chapter 2 DNA and DNA origami

2.0 - Introduction – DNAs Elucidation and Use as a Building Block - 25

2.1 - DNAs Basic Structure as a polymer -25

2.2 - Watson and Crick Base Pairing and DNA as a Programmable Material – 28

2.3 - The Origins of Structural DNA Nanotechnology – 31

2.4 - DNA Origami – 32

2.5 - Conclusion – 52

## Chapter 3 Component fabrication and analytical techniques

3.0 - Component and Technique Examination – 54

3.1 - Scaffold synthesis - 54

3.2 - Staple Synthesis – 55

3.3 - DNA origami Fabrication and Physical properties – 57

3.4 - Characterisation – DNA and DNA origami – 60

3.5 - Agarose Gel Electrophoresis – 61

3.6 - Atomic Force Microscopy – 62

3.7 -Contact modes – 63

3.8 - Conclusion – 64

#### Chapter 4 Metallisation theory

4.0 - Metallisation theory – 66

4.1 - Gold nanoparticle synthesis -66

4.2 - Gold nanoparticle concentration - 67

4.3 - Nanoparticle functionalisation - 69

4.4 - Nanoparticle Characterisation via UV spectrography – 77

4.5 - Origami metallisation – 80

4.6 - Conclusion – 88

#### Chapter 5 Purification theory

5.0 - The requirement for purification – 90

5.1 - Existing component purification techniques - 90

5.2 - Centrifugation based techniques – 91

5.3 - Molecular Weight Cut of Columns - 92

5.4 - DNA precipitation - 92

5.5 - AGE based purification - 93

5.6 - The Freeze and Squeeze - 94

5.7 - Sucrose trapped elution method - 95

5.8 - Conclusion - 98

## Chapter 6 Simulation Methods

6.0 - Simulation Methods - 99

6.1 - Determining Material Parameters - 100

6.2 - Simulated structures - 101

6.3 - Test structures - 103

6.4 - Issues simulating curved structures – 106

6.5 Curvature and substrate - 107

## Chapter 7 Board design

7.0 - Modular board design considerations - 109

7.1 - Design itself - 109

7.2 - Board tail region - 112

7.3 - Lattice growth - 113

7.4 - Site specific attachment – tethering mechanism – 116

7.5 - Site specific attachment – binding sites - 117

7.6 - Recovery and modification of sequences - 119

7.7 - CANDO SIMULATION - 120

## Chapter 8 Fabrication methods

8.0 - Board fabrication, confirmation, and protocol refinement – 123

8.1 - Ionic conditions - 123

8.2 - Thermal cycle protocols - 124

8.3 - Staple concentration - 125

8.4 - Lattice protocols – 125

8.5 - Fixation protocols - 126

8.6 - AGE – 127

8.7 - AFM – 128

8.8 – Freeze and squeeze - 128

8.9 - DNA precipitation - 129

8.10 - AGE elution into sucrose - 129

## Chapter 9 Metallisation methods

9.0 - Au NP synthesis and preparation – 130

9.1 - Gold Nanoparticle preparation - 130

9.2 - Gold nanoparticle concentration - 131

9.3 - Nanoparticle functionalisation - 133

9.4 - Freeze and squeeze purification – 134

9.5 - Centrifugation – 134

9.6 - Metallisation enhancement – 134

## Chapter 10 EMA methods

10.0 - EMA – methods - 137

10.1 - EMA – Pathway overview - 137

10.2 - EMA – Device/component overview – 138

10.3 - EMA – Device fabrication – 139

10.4 - EMA – Device operation – 149

10.5 - DNA purification – 152

Chapter 11 Simulation results

11.00 Simulation results – 153

11.1 Conclusion – 160

Chapter 12 Fabrication results

12.0 - DNA fabrication results - 161

12.1 - Ionic conditions - 161

12.2 - Board tail region assembly interference – 163

12.3 - Thermal cycling protocols - 165

12.4 - Staple efficiency – 168

12.5 - One pot lattice growth - 169

12.6 - Post folding lattice fabrication - 172

12.7 - Imaging and fixation - 175

12.8 - DNA purification – Freeze and squeeze – 181

12.9 - DNA purification – PEG precipitation – 182

12.10 - DNA purification – sucrose lane elution – 183

12.11 - DNA purification – EMA based purification of DNA origami samples - 184

12.12 - Conclusion - 186

Chapter 13 Metallisation methods

13.0 - Gold Nanoparticle synthesis and concentration results - 188

13.1 - Au NP precipitation – 189

13.2 - Freeze and squeeze recovery - 191

13.3 - Centrifugation - 193

Chapter 14 EMA results

14.0 - EMA Results - 194

14.1 - Au NP recovered sample analysis – 195

14.2 - Functionalisation stepwise examination - 198

14.3 - Collecting specific Au NP sizes within an AGE band - 200

14.4 - BSPP resuspension and UV-vis observations - 201

14.5 - Au NP conclusion - 202

Chapter 15 Metallisation results

15.0 - Metallisation - 204

15.1 - Tether Length – 212

15.2 - Troubleshooting - 213

15.3 - Enhancement attempts - 213

15.4 - Conclusion - 216

Chapter 16 Final summary

16.0 - Conclusion – 219

References – 222

Appendices/Copyright statement – 231

# Chapter 0

## 0.0 Summary of contents

### Chapter 1 Introduction

Chapter 1 introduces the problem this work attempts to address: can DNA origami be used to create materials with programmable EM properties. The limits of naturally occurring materials, what artificial and metamaterials are, and the ability to program materials on a subwavelength level to create artificial effects (Significantly the manipulation of refractive index) is covered. The split ring resonator is described, in terms of overall design, and its functionality. Finally conventional nanofabrication techniques are critiqued and limits in their ability to create artificial materials in the optical regime discussed. DNA origami fabrication capabilities and suitability for task is assessed.

### Chapter 2 DNA and DNA Origami

A brief history of the elucidation of DNAs structure and function is provided, highlighting its highly programmable nature, and this leads to the theoretical origins of the field of structural DNA nanotechnology. DNA origami is introduced as a seminal DNA based nanofabrication system and significant paradigm changes within this field, such as the development of lattices from single monomer tiles, are highlighted. Emergent fabrication techniques, including bio-brick fabrication, and UV crosslinking, end the chapter.

### Chapter 3 Component Fabrication and Analytical Techniques

Chapter 3 discusses how scaffold and staples are synthesised and how the combination of biological and synthetic systems is a significant factor in the effectiveness of DNA origami as a fabrication tool. Fabrication considerations, notably thermal and ionic conditions, are explained. This chapter also covers the main methods of DNA origami characterisation: Agarose gel electrophoresis and atomic force microscopy.

### Chapter 4 Metallisation theory

Gold nanoparticles are a common unit for DNA origami decoration and are employed during this work. Specifically sub 10 nanometer synthesis is discussed, how these particles are manipulated and prepared for fabrication, and how they are characterised. Discussion of various origami metallisation attempts conducted by other groups are listed.

#### Chapter 5 Purification Theory

DNA based fabrication is a self-assembly system which relies on an excess of fabrication components. This can be problematic, due to interference in later fabrication steps, and purification is critical. Several common purification techniques are discussed.

#### Chapter 6 Simulation Methods

Discusses how a unit cell was chosen and created. Also details test structures to ensure simulations are somewhat representative of real world EM mechanics.

#### Chapter 7 Board Design

The design of the modular board we employ is discussed. Its general practical structure, addressable tethering sites, and lattice points for material expansion are listed along with relevant design motifs. A Cando simulation is provided to validate the overall stability of the design.

#### Chapter 8 Fabrication Methods

Experimental procedures for board fabrication and development of high efficiency protocols are explained. This chapter includes methods for single boards, lattices, and low excess staple fabrication attempts. A process for NaCl based fixation on mica is described. The main characterisation methods, AGE and AFM, have protocols listed.

#### Chapter 9 Metallisation Methods

Gold nanoparticle synthesis, functionalisation, and manipulation methods are listed.

#### Chapter 10 EMA Methods

A significant undertaking during this project was the creation of an easy to build purification column which can be used to purify functionalised sub 10 nanometer gold nanoparticles of excess thiolated DNA quickly and effectively with little to no loss of sample. The devices functionality, basic operation, and the process of fabricating it are all contained within this chapter.

#### Chapter 11 Simulation results

Two sets of split ring results are provided which could be created using the modular board we provide (With the limitations stipulated throughout the text and reiterated succinctly within Chapter 16/Conclusion).

#### Chapter 12 Fabrication results

DNA fabrication results are shown and discussed. Ideal pathways are put forward and justified. Lattice fabrication reduced staple excess samples, and the capabilities of NaCl based fixation are shown with beneficial combinations of the techniques undertaken and discussed. Attempts at purifying DNA origami samples using EMA are discussed and the significant edge charging issue when employed MgCl<sub>2</sub> containing gels highlighted.

#### Chapter 13 Au NP synthesis and concentration results

Refinement of the sub 10 nanometer manipulation process and attempts at gold nanoparticle sample purification using conventional methods are discussed.

#### Chapter 14 EMA results

EMA purification results are provided and UV-vis analysis of the entire synthesis to purification process undertaken. The importance of pre-characterisation BSPP resuspension is highlighted.

#### Chapter 15 Metallisation results

Metallisation is attempted under varying ionic conditions and different methods of producing samples, and specific fabrication products, displayed and discussed. High throughput metallisation is demonstrated with improvements suggested. Future work, including enhancement of existing metal

structures, the potential role of surfactant in this process, and the novel use of polyphosphothioate backbone DNA sequences to create metallic nanoparticles, and potentially nanowires, discussed.

#### Chapter 16 Conclusion

A rundown of individual chapter conclusions and discussion of significant findings.

# Chapter 1

## 1.0 Introduction

The elucidation of DNAs (DeoxyriboNucleic Acid) structure and the discovery of Watson-Crick base pairing [1] was the first point in a chain of scientific advances that would allow first sequencing, and later direct manipulation and synthesis of genetic material, creating the fields of molecular, and later synthetic, biology.

Structural DNA nanotechnology, essentially the field of using DNA as a building block to create devices and materials, would come when Seeman suggested that not only could DNA exist naturally in the mobile flux of states associated with living cells but also as “immobile junctions” [2].

This initial theoretical paradigm shift, suggesting that manipulation of sequence could be used to effectively create nanoscale structures, was further reinforced in 2006 when Rothemund described a method of ‘Bottom-up nanofabrication’ [3] matching the complexity of material fabrication achieved by more conventional ‘Top-down’ methods. He termed this method of fabrication scaffolded DNA origami and described a high throughput method of creating sub 6 nanometer feature size structures with high fidelity and efficiency.

This comparison of DNA origami to conventional nanofabrication techniques has also been extended further by suggesting that bottom up systems such as these will be required to bridge a physical limitation gap in Integrated circuit fabrication [4] as circuit feature size approaches the single figure nanometer level.

A contemporary example of an integrated circuit design which conventional top down methods cannot fabricate is a metamaterial active in, and around, the optical regime. An optical metamaterial [5] describes a material which presents a negative refractive index in the optical and near optical part of the EM (Electromagnetic) spectrum. Materials which present negative refractive indexes over broad frequency ranges do not exist naturally and must be engineered. A caveat of this type of fabrication is that the individual unit cell of the material must be on the order of magnitude of ten times smaller than

any specific wavelength of interest [6]. As the optical regime sits roughly between 400 and 800 nanometers in wavelength this would suggest a unit cell of between 40 and 80 nanometers with a feature size much smaller. Conventional nanofabrication techniques lack the fidelity coupled with throughput required but structural DNA nanotechnology [7] and more specifically scaffolded DNA origami based fabrication shows potential for success.

Due to DNAs relatively low conductivity [8] for many studies site specific or global metallisation must take place [9]. This can be conducted by exploiting the highly specific nature of Watson-Crick base pairing to attach a nanoparticle connected to a specific sequence to anywhere on the origami where that sequence is complemented [10].

Since the inception of the scaffolded method there have been numerous cases of highly detailed DNA origamis [11, 12], and later metallised [13, 14] origamis, being created. While the basic fabrication principles of these techniques is understood there is still a lack of a general fabrication tool [15] which could apply the science to the creation of both devices and materials in high fidelity on the nanoscale.

The aim of this thesis to present a pathway of ‘bottom-up’ DNA origami based fabrication that attempts to explore a pathway of metamaterial fabrication, for which current ‘top down’ conventional nanofabrication systems are unsuitable. We do this both by considering the creation of a designed material directly and then also as a broader pathway accessible for use by others. We also address bottlenecks observed in purification in the pathway and present potential solutions to these issues

## 1.1 - Metamaterial Background

The ability to create and construct EM based technologies is largely limited by the properties of the materials available. For decades researchers have used materials synthesised at the molecular level with peculiar properties, Polytetrafluorethylene (Teflon) and hafnium oxide are primary examples. Materials such as these can be used to modify the behaviour of an EM wave in a useful manner.

A materials interaction with EM wave is described by its permittivity (which couples the electric field to the material) and permeability (which couples the magnetic field to the material), while the

interaction between even single molecules and EM waves can be complex, and involve significant simulation, it is possible to recover bulk parameters which describe a material's response in averaged terms. Essentially molecules in a material in question respond to incident EM waves by forming dipoles, and it is these individual responses which are averaged over all molecules to yield the permittivity and permeability.

This response is fixed both by the fundamental properties (charge, mass) and the chemical bonds formed in the material, limiting the available parameter range materials can access. To get around these limitations researchers have created a range of artificial composite structures with periodic sub-wavelength functional inclusions [6]. Although these inclusions are much larger than the molecules in materials, they are still much smaller than the EM wavelength. To an EM wave these inclusions respond no differently than giant molecules with a very large polarizability. This enables the EM interactions between wave and collective structures to be described in terms of the abstracted bulk material parameters permittivity and permeability, again treating the structures collectively, but now as an artificial "effective" material.

Research into artificial EM materials began over a hundred years before the term "metamaterial" was introduced by Rayleigh, who proposed a system of small scatterers, with a period much smaller than the wavelength, as an equivalent continuous medium [16]. In this thesis, I refer to artificial EM materials as Metamaterials. The first application of metamaterials did not appear until the pioneering work of Kock [17] in the 1940s. Kock created Artificial Dielectrics from arrays of sub-wavelength metallic structures (spheres, rods and plates) to form Dielectric Lenses. All these materials had a positive permittivity, with a positive refractive index.

While many researchers have considered materials with a negative index of refraction [18] the first systematic study of the general properties of a hypothetical negative index medium is attributed to the seminal 1967 paper by Veselago [16]

In this seminal paper [16], 'left-handed materials', or negative index materials were described in terms of monochromatic waves interaction with an unusual isotropic material. Veselago begins by connecting

the wave vector ( $K$ ), the description of a waves propagation in terms of direction and magnitude, angular frequency ( $\omega$ ), a measure of the rate of rotation of the wave, and speed of light ( $c$ ), the absolute speed of EM waves in vacuum, to the refractive index ( $n$ ), a description of how light propagates through a medium.

$$K^2 = \left(\frac{\omega^2}{c^2}\right)n^2 \quad (1)$$

Equation 1 demonstrates the interaction between a monochromatic wave and an isotropic substance. While the angular frequency is defined by the frequency of a wave, and the speed of light remains constant, the refractive index comes directly from the material parameters of the medium the wave passes through.

$$n^2 = \epsilon\mu \quad (2)$$

Equation 2 demonstrates that the refractive index is a function of only the permittivity and permeability of a medium. These observations suggest that if these parameters can be engineered, and to what extent, defines our ability to manipulate or manufacture a specific refractive index.

While Veselago effectively describes a left handed material effectively, in terms of mathematical expression and displayed phenomena, he does not describe a structure, in terms of geometry or composition, which would present a simultaneously negative  $\epsilon$  and  $\mu$ . The first theoretical designs of a meta atom capable of displaying ‘left handedness’ are described by Pendry [19].

$$\alpha \ll \lambda = 2\pi c_0 \omega^{-1} \quad (3)$$

Pendry begins, before discussion of any device or material itself, to describe (Equation 3) the size of an individual unit cell ( $\alpha$ ), this describes the entire periodic unit that a single meta atom exists within (As opposed to the physical meta atom itself), and sets a limit that it is significantly less, in volume, than that of the wavelength of any specific EM wave of interest (The right hand of the equation describes

the size of a wavelength by its specific frequency). These conditions mean that any wave encountering a structure is refracted rather than partially or completely diffracted. These limitations also prevent chemical composition, rather than geometry, from dominating any response and providing a misleading result.

The design itself, the double Split Ring Resonator (SRR), further highlights the usefulness of materials with engineered properties over conventional materials by introducing the concept of artificial magnetism [19]. Where the magnetism of most materials begins to heavily diminish in the gigahertz range and most materials are effectively magnetically passive in the terahertz range, by harnessing sub wavelength split ring resonators it is possible to give materials composed of magnetically inert elements tailored permeability.

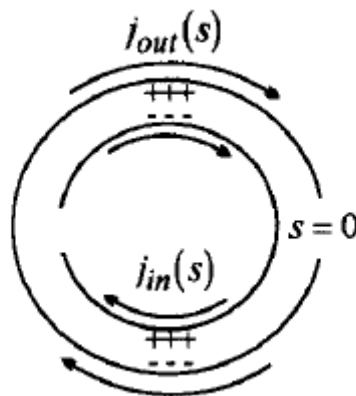


Figure 1 a Split Ring Resonator as described by Pendry [6].

Figure 1 describes a double split ring resonator. A magnetic field parallel to the rings induces a current around the ring. The flowing current combined with the split region leads to distinct regions of positive and negative charge. Due to the proximity and orientation of the 2 rings capacitance exists between the 2 sets of charged regions. The flux created in this system can be tailored to strongly enhance or oppose external fields.

It should be noted that while the double split ring is an effective tool for manipulating the effective permeability of a material a single ring also functions in a similar manner. The second loop reduces the resonance frequency and allows a greater degree of polarisation it is not a compulsory component.

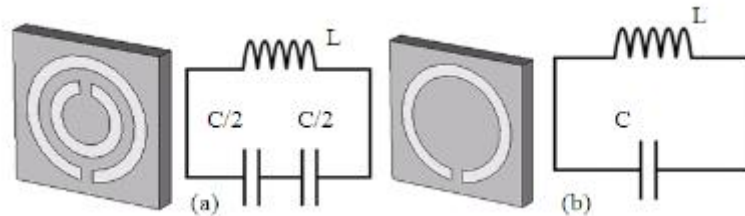


Figure 2 A diagram of double (a) and single (b) SRR designs and their respective comparative circuit diagrams [7].

Figure 2 shows how the SRR can be compared to a circuit diagram to show that the induced current in the system leads to highly polarised regions in both single and double SRR. However as seen from the comparative circuit diagram capacitance still exists in both cases– but only due to the proximal charged regions between the 2 ends of the single SRR rather than between the 2 sets of charged regions- At resonance it still gives a strong magnetic response [20].

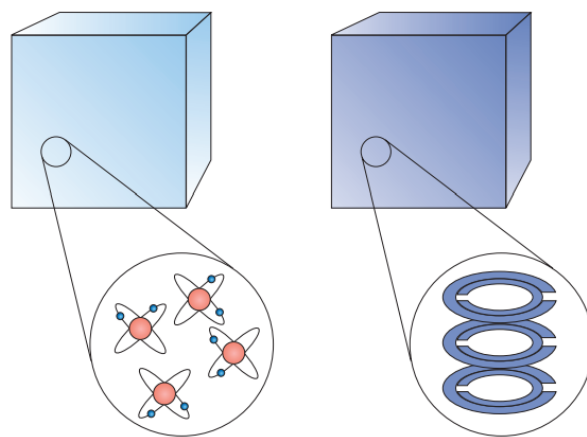


Figure 3 Atomic organisation of conventional material (left) and the higher order structures which comprise a metamaterial (right) [8].

Fig 3 demonstrates the difference between a conventional materials atomic based response and a meta materials more flexible response. Due to the less rigid, and much more tuneable nature of the artificial ‘meta atom’ topology and composition in comparison to conventional atoms and molecules, where rigid parameters of properties such as mass, charge and alignment strictly limit potential EM responses, a

wide array of polarisable states are possible [21]. As defined by Walser [20], while discussing the purpose of metamaterials over conventional composites and establishing a set of universal parameters to define these new materials by, a metamaterial is defined as a “macroscopic composite having a manmade, three dimensional, periodic cellular architecture designed to produce an optimised combination, not available in nature, of two or more responses to specific excitation”. This definition ends by highlighting the necessary property of simultaneously negative permittivity, and permeability, displayed by a specific device – as explained above. Before continuing we must examine the first requirement: the existence of these devices in rational, repeating, periodic lattices.

Walser makes the point that relative success in creating these materials could be defined as/be directly proportional to any volumetric analysis of specific properties matching the bulk parameters of the material as a whole. This ties the correct fabrication of meta-atoms and their correct inclusion into a larger periodic lattice to the displayed parameters of the metamaterial. We can now compare conventional materials and metamaterials directly. Both conventional material and metamaterial respond to incident EM waves, where any individual response due to discrepancy in composition or alignment, is averaged over all molecules, where any deviation describes any inefficiency of fabrication, to yield homogenised bulk parameters of permittivity and permeability.

## 1.2 - Nanofabrication

As stated an optical metamaterial must have a period cell significantly smaller than any specific wavelength of interest. As the optical regime lies, roughly, between 400 and 800 nanometres in wavelength, any metamaterial operating in this range would need to be between 40 and 160 nanometres in size (Assuming a unit cell between 5 and 10 times smaller than the wavelength). This caveat of optical metamaterial creation means that their construction sits firmly within the boundaries of nanofabrication (Where we define nanofabrication as the creation of an artefact with at least 1 feature size of less than 100 nanometres).

Nanofabrication can be examined broadly through 2 contradictory methodologies. The first approach, top-down fabrication, is a deterministic approach – where order is imposed on an existing system by

external forces to remodel it [23]. As stated by Moore, in the paper which pre-empted the creation of Moore's law, "No barrier exists comparable to the thermodynamic equilibrium considerations that often limit yields in chemical reactions" [24]. This would suggest that the limiting factor in the continued reduction of feature size are physical limitations in our ability to both provide a known system and to impose definite order on this system.

$$w = k_1 \left( \frac{\lambda}{NA} \right) \quad (4)$$

Equation 4 [25] is both an example, of a limiting step in creating a known system, and an example of a limiting step in our ability to rationally impose order on a system by external force. Where ( $w$ ) describes the smallest feature size,  $k_1$  defines the capability of a system to imprint onto a resist,  $NA$  is the Numerical Aperture of the lens which images any pattern.  $K_1$  essentially relies on our ability to create uniformly flat resists, where once a photo resist reaches a certain critical size it is no longer uniformly flat after spin coating (Or deviates in a significant enough manner to prevent its use in fabrication), and  $NA$  our ability to make a lens capable of accurately transferring information, where a wavelength too small will not accurately transfer a pattern onto the resist, using the defined wavelength. All top down systems essentially suffer from the same broad limitations, where throughput is limited by our ability to either create a completely defined system (Where nanofabrication approaches atomic definition), or wield external force in a manner capable of reproducibly modifying the system (Or accurately modifying enough systems within a time frame to make the approach viable).

In contrast bottom up fabrication, or self-assembly, is a product only of rational manipulation of thermodynamics and kinetics to create a desired structure in a specified yield [23]. These systems are beneficial over top down approaches because there is no longer a need to create a completely defined system – The fabrication system can be created, in large quantity, using our knowledge of chemistry and natural equilibriums. Typically, these fabrications rely on rationally engineering the interaction between individual components within a system then placing them in an environment where they will evolve into the predetermined final state [25].

### 1.3 -Technique comparison

## EUV Lithography

There are many conventional techniques associated with nanofabrication. In terms of creating detailed patterns and features, on a fixed substrate, lithographic techniques, which have been a huge focus of research and development due to the drive to continuously decrease the feature size of integrated circuits, are probably the most well-known category.

Extreme Ultraviolet Lithography is the current state of the art for the ‘routine’ production of sub 10 nanometer feature sizes [26] in industrial volumes [27]. EUV systems are highly costly, both in terms of setup and running costs [28], and are dedicated facilities with very large footprints [29]. It is very likely that if this type of production were employed for fabrication of any putative material or component it would be as part of large-scale production of a highly characterised design rather than for generic prototyping. Also, as typical wafers are relatively thick silicon [30], and typically a wafer is cut to size with the lithography product remaining on its surface, this makes them unsuitable for optical applications.

## Electron Beam Lithography

In contrast to EUV (A form of masked lithography) Electron Beam Lithography is conducted in a scanning fashion. While resolution using this technique is high, with sub 10 nanometer features possible [31], due to a combination of the scanning nature of the technique [32], and the increasing time requirements for complex designs [32], EBL is considered a low throughput technique [33]. As with EUV, EBL lithographic products are created upon a dedicated silicon substrate making removal/manipulation of the surface design a significant challenge.

EBL systems are significantly lower in purchasing and running cost than EUV systems [33], and combined with a lower footprint, are practical for academic/lab based applications [34]. It is also possible to retrofit existing electron microscopy systems with hardware that will allow them to act as lithographic tools although these systems are associated with a slightly lower resolution of around 20 nanometers [34].

## Scanning Probe Methods

Scanning Tunnelling Microscopy and Atomic Force Microscopy, unlike the lithographic techniques, employ a probe to directly interact and manipulate building blocks on a substrate. STM is a relatively low cost technique [35], capable of sub 10 nanometer (down to atomic) manipulation [36], which can be conducted on a variety of substrates [37]. Where STM employs quantum tunnelling effects (Meaning it is only effective in conjunction with conductors) AFM interacts with the sample directly via Van der Waals interactions [38], meaning that it can be used with a much wider variety of samples, and can also be used at ambient temperature (Without the need for a vacuum chamber). While occurring more recently AFM also demonstrates the atomic manipulation demonstrated by STM [39] while also showing potential for larger scale manipulation [40] (Although technically beyond the scope of nanofabrication). While potentially atomic in resolution scanning probe methods are characterised as low throughput [41] where atomic manipulation is described as exceedingly low throughput [41].

## DNA origami

DNA Origami offers a very high resolution, at a greatly reduced cost to the other techniques, and due to its organic, and self-assembling nature, could provide very high throughput without the cost and footprint associated with the EUV lithographic techniques. Furthermore due to the molecularly programmable nature of DNA, coupled with single nanometer length scale nanoparticle synthesis, the system presents a feature size potentially in the sub 10 nanometer regime.

DNA origami is not without its limitations: Functionalisation, where the other techniques directly manipulate or introduce materials DNA Origami provides a scaffold to which functional moieties are then attached, and aggregation, where the other techniques create meta-atoms in period directly DNA origami produces individual meta atoms which must then be navigated and fixed into lattice. However it is also certainly possible to interpret these limitations as advantages over the other techniques: Functionalisation, where the other techniques rely on the use of certain materials any functional moieties which can be modified to interact with the DNA construct can be used to fabricate devices,

and aggregation, where the other techniques are limited to 2D design (Or a crystalline structure), individual DNA constructs can be position and manipulated in solution, potentially, to create 3 dimensional lattices and super structures.

## 1.4 Conclusion

Our understanding of DNA has evolved significantly over time, not only in terms of DNAs role in genetic output, but also of its nature as a nanoscale programmable material and fundamentally a high throughput and precise building block. While conceptually DNA nanotechnology has existed since around the 1980s it was with Rothemunds [3] exploitation of a bacteriophage plasmid ‘scaffold’ loop and ~200 artificial ‘staples’ that provided the first demonstration of high throughput designs of around ~100nm<sup>2</sup> surface area, with sub 10 nanometer feature size.

Meta, and artificial, materials are theorised manmade structures created for the manipulation of EM waves using subwavelength periodic geometries. While these materials have been demonstrated to be effective at longer wavelengths creating bulk materials to interact at the optical range is challenging using conventional nanofabrication methodology. DNA origami could fulfil this role due to its ease of modification and experimentation, its high throughput coupled with sub 10 nanometer feature size, and its low cost and accessibility.

While creation of a true optical metamaterial would be significantly beyond the scope of this project we examine DNA origami as a foundry for such a system, create a high efficiency protocol which can be reproduced by others in a fairly facile manner while still allowing significant modification, address significant bottlenecks in the fabrication process, and provide the methods to create and use a device for the easy purification of sub 10 nanometer Au NPs (Which is challenging using existing purification methodology).

## Chapter 2

### 2.0 Introduction – DNAs Elucidation and Use as a Building Block

To understand the nature of DNA and its suitability as a building block for fabrication it is useful to briefly examine the unravelling of its structure and properties as a timeline of discovery. Traditionally DNA development is heavily tied to the advancement and understanding of genetics. However in this context it will be avoided in favour of focusing on the mechanical properties, mainly the strict combination of sequence and structure which must be present in union, and specific functional motifs such as the Holliday Junction, that make DNA such a versatile building material.

The concept of structural DNA nanotechnology, created by Seeman, preceded its eventual development by some decades. This quickly changed with the inception of the scaffolded DNA origami fabrication method, and later bio-brick based technique, with many examples of successful fabrication of intricate devices over the last 14 years.

However initially, for the purposes of DNA based fabrication, there are two significant properties of DNA which make it a desirable building material.

- It is a very stable polymer that can exist in very long chains.
- Base pairing and binding between these chains is highly predictable, reproducible, and stable.

This chapter will begin with a description of the elucidation of these motifs and then transition into the timeline of structural DNA based nanotechnology.

### 2.1 DNAs Basic Structure as a polymer

The initial discovery of the DNA subunits which form individual bases, nucleosides, and nucleotides was provided by Phoebus Levene in 1908 [41].

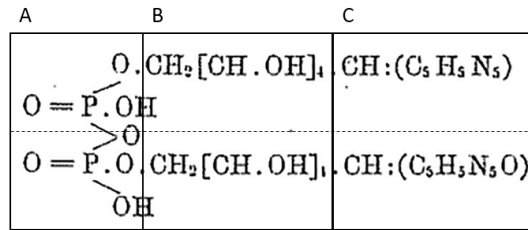


Figure 4 Levene observed a dinucleotide comprising adenine (C – top) and guanine (C – bottom), carbohydrate groups (B) and phosphodiester backbone (A) [41].

Levene postulated that these bases displayed in figure 4 (C) formed individual nucleosides when linked to carbohydrate groups (B). These individual nucleosides would then further link into nucleotides by the phosphodiester backbone (A). While the chemical structure displayed in figure 4 is slightly incorrect, as the phosphodiester linkage between the two nucleotides does not actually contain a hydrogen atom, it was the first demonstration of the individual subunits of a nucleotide and the mechanism of polymerisation that linked them. While the group also speculated that further integration between individual dinucleotides was likely, a specific mode or mechanism was not provided.

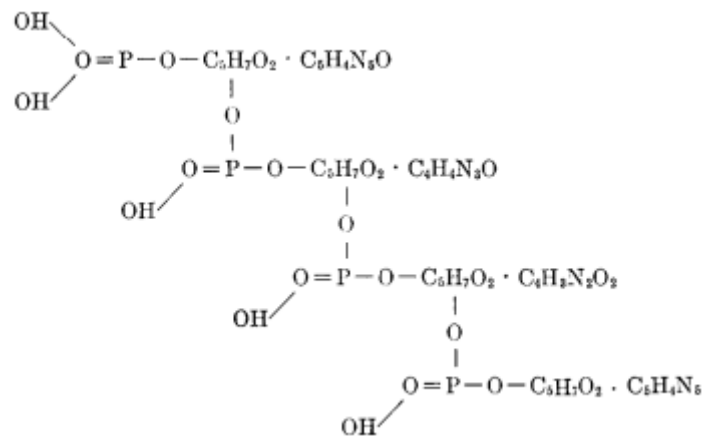


Figure 5 A tetranucleotide molecule as proposed by Leven [42].

While some aspects of the model show in figure 5 are incorrect, largely the assumption that all DNA molecules share the same sequence and are integer repetitions of the same four bases, it is the first demonstration of a polynucleotide system.

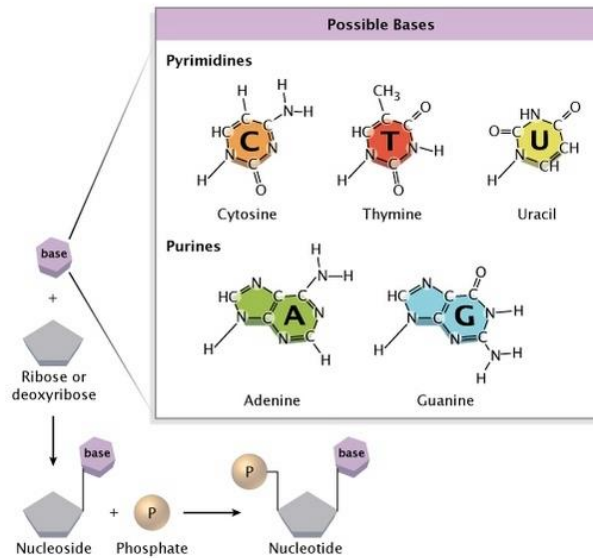


Figure 6 A map linking individual base to RNA or DNA species, then to nucleoside via base addition, and finally to nucleotide via phosphate backbone [43].

Leven was also responsible for the distinction between base, the sugar group separating DNA from RNA, and the mechanism by which individual nucleotides polymerise to become chains, as shown in figure 6.

The next evolution in the polynucleotide model came when Chargaff [44], who examined the content of each of the four individual bases in different animal species, noted that relative levels of individual nucleotides were not universal to all species. This challenged the previous assumption that polynucleotides were comprised of repetitions of the same four nucleotides.

The second observation made by Chargaff, which would become known as 'Chargaffs Rule' was that while the relative amount of individual sets of nucleotides within a specific sample differed there was typically near identical ratios of adenosine to thymidine and guanine to cytosine.

Essentially this observation combined with the pre-existing polynucleotide model presented the possibility of DNA sequences without fixed sequence with very strong correlations between individual molecules within any given sample. While there still existed holes in the theory – any links between the levels of A-T and G-C were purely speculation at this point – the theory had essentially encapsulated the structure of DNA and its existence as a continuous arbitrary sequence.

## 2.2 Watson and Crick Base Pairing and DNA as a Programmable Material

Watson and Crick's direct elucidation of the molecular structure of DNA [1] via X-ray crystallography showed interaction between both individual bases and the helical secondary structure created by chains, of multiple, interacting bases. Beyond the basic structure of the DNA polymer and interaction between individual mononucleotide bases it was also apparent that the hydrogen bonding which occurred between bases was very strict in compatibility.

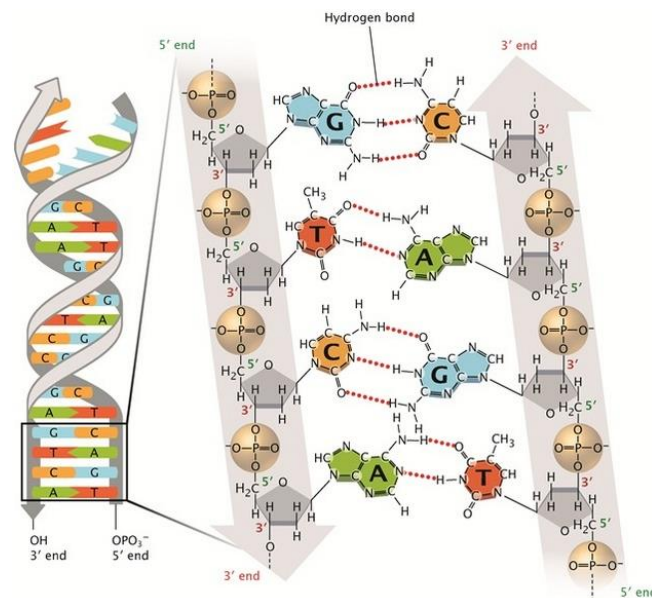


Figure 7 Left – a demonstration of Watson Crick base pairing and the anti-parallel nature of the DNA helix. Right – The chemical structure of DNA, already elucidated by Leven and Chargraff, where the external phosphodiester backbone and the internal nitrogen containing bases, and their complementary hydrogen bonding patterns, create a stable and predictable structure between two strands [43].

Watson and Crick extrapolated 4 features of the DNA polymer and its natural conformation to create a model of base pair bonding [43] that, while being expanded further by other studies, remains true today. The layout of the 4 rules is highlighted visually in figure 7.

1. DNA exists in a double stranded helix comprised of 2 distinct chains connected by hydrogen bonding. Specific hydrogen bonding exists between Adenine (A) to Thymine (T) and Cytosine

(C) to Guanine (G). This is reinforced by Chargraffs rule [43] which states that any cell of any organism should have a 1:1 ratio of the specific pyrimidine to purine bases.

2. DNA exists predominantly in a right handed confirmation.
3. The DNA helix is anti-parallel. Complimenting strands progress from the 5' to 3' carbon in opposite directions.
4. Internal hydrogen bonding exists between specific bases but there is also potential for hydrogen bonding interactions to exist at other points of bases. This facilitates interaction of the code within the helix to other mechanisms within the nucleus or external groups.

There is also some influence of specific sequence on the general physical properties of the DNA helix. As there are three hydrogen bonds between G-C in contrast to the two between A-T the former exist in a more stable state. This stability can be observed in higher melting points between G-C rich sequences [44,45].

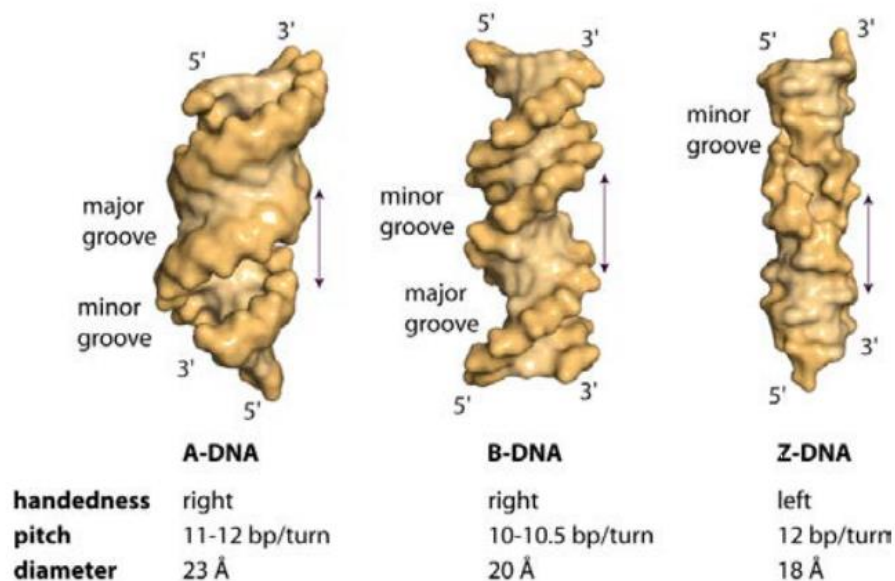


Figure 8 The 3 possible conformations of the DNA helix along with relative handedness, pitch and diameter [46].

While the initial A-T and G-C binding observations dictated the interaction between 2 strands in what is now known as the Beta helix there are actually several possible topologies of anti-parallel helix as seen in figure 8. These conformations affect helical pitch (The distance in base pairs it takes the helix

to travel a full 360° rotation), the handedness of the helix (The direction of base pair progression when viewed down the the helix) and the rise of the sequence (The distance between each individual base). For purely DNA to DNA interactions the most common topology is the Beta helix conformation.

Base interaction is a common way of defining how a helix, or DNA structure, maintains its stability. The planar arrangement of bases [46], with a constant progression of around 3.4 angstrom per base, maximises the Van der Waals interaction between bases, preventing other molecules, such as salt ions and water, from penetrating, and destabilising, the helix which greatly increase the integrity of these structures.

We have shown that the helix motif provides stable and highly predictable structures, however, to create structures using multiple strands requires a further mechanism. Described by Holliday as “Effective pairing over short regions of the genetic material occurs at the molecular level by separation of the strands at the DNA double helices” [47]. The concept of Holliday junctions allowed the understanding of strand exchange, and connection, between 2 proximal helices in a sequence dependent manner.

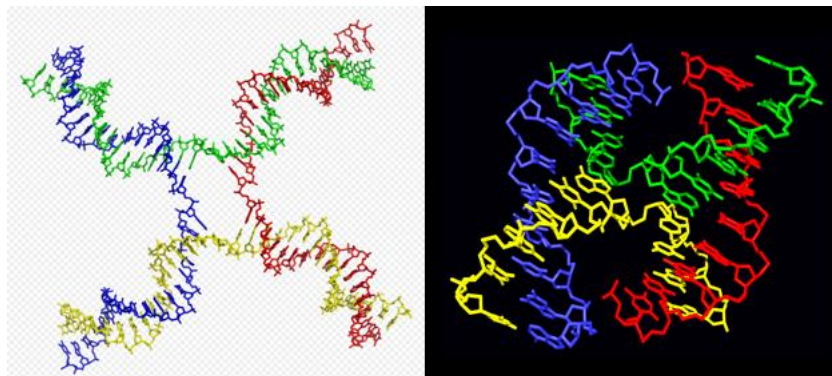


Figure 9 Left - an unstacked holiday junction. This junction accounts only for sequence migration and is not stacked correctly in terms of helical progression. Right – A stacked Holliday junction. Strand exchange has taken place and matches the specific helical pitch of each donating helix [48].

In Figure 9 two scenarios in which adjacent helices can exchange strands are depicted. Exchanges of these nature take advantage of sequence complementation on adjacent strands. While both strands rationally maintain base pairing rules to facilitate the exchange the left hand junction does not maintain helical stacking is more unstable. On the right helical pitch is matched between the helices and it is

observable that the red and blue strands continue base pair stacking as they progress past the site of the exchange leading to higher stability.

## 2.3 The Origins of Structural DNA Nanotechnology

As stated by Nadrian Seeman and Chad Mirkin, where Seeman originally theorised DNAs application as a nanofabrication tool, “Perhaps the most salient feature of DNA that can explain its versatility in biological settings is the specificity of canonical Watson-Crick base-pairing interaction (A-T and G-C), even those that are relatively short, results in an enormous library of orthogonal interactions that can direct hybridization to occur with high selectivity and specificity” [50]. It is this high specificity and selectivity, combined with our advancing ability to artificially synthesise arbitrary DNA strands cheaply and in high throughput, which allows us to consider DNA based construction as an effective nanofabrication tool. The key to self-assembly is understanding the specific thermodynamics of the systems in place and any possible final fixed energy states of the specific design. As Watson-Crick base pairing provides us with an extremely rigid and accurate prediction of how DNA sequences should behave [48], if observation doesn’t match expectation then it is usually another variable within the system which can be easily modified, such as buffer make up or stoichiometric ratios of DNA components, until prediction matches output.

The first theorised use of DNA as a programmable structural material, as oppose to a purely genetic mechanism, came in Nadrian Seemans seminal paper [52] where he speculated “It is possible to generate sequences of oligomeric nucleic acids which will preferentially associate to form migrationally immobile junctions, rather than linear duplexes, as they usually do”.

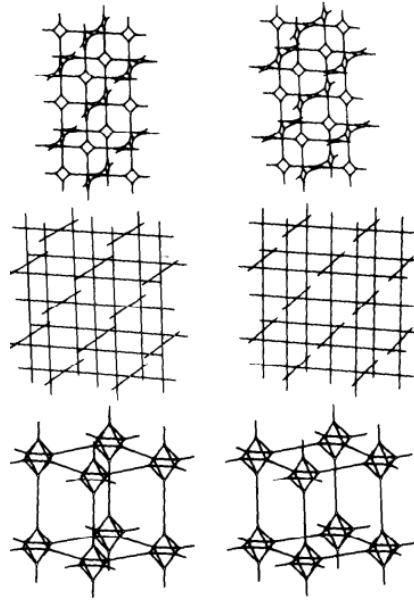


Figure 10 demonstrates, from top to bottom, 3, 4 and 5 branch connected networks [52].

The initial DNA fabrication system in figure 10 presented only the possibility to create linear repeating lattices and while it did include artificial groups they too were incorporated into the repeating lattice motif. It did however provide the key foundation of structural nanotechnology: That DNA can form rational immobile structures which can then be incorporated into higher order motifs [3].

## 2.4 DNA Origami

A significant leap in the possible size and complexity of structural DNA nanotechnology designs and devices came with Rothemunds seminal description of the Scaffolded DNA origami method. Until this point only artificially synthesised sequences had been considered as building blocks for DNA based designs. Rothemund [3] increased the limit significantly by incorporating the M13MP18 viral genome as a ‘scaffold’ strand. The viral genome provides a template of 7249 bases, of known sequence, whose secondary structures do not significantly affect origami fabrication, which can be complemented by shorter artificially synthesised sequences, identified as ‘staples’. The artificially synthesised staples are given sequences which complement 2 spatially distant regions of code on the scaffold strand. Binding between the scaffold and staple creates a small area of structure and changes the overall conformation of the scaffold. If many staples are added then the scaffold can be guided into rigid 2 and 3 dimensional shapes. These shapes have a feature size comparable to individual DNA bases (Making the feature size

of DNA origamis less than 5nm) and can be mass produced to the ‘bottom up’ or self-assembly fabrication methodology employed by the technique.

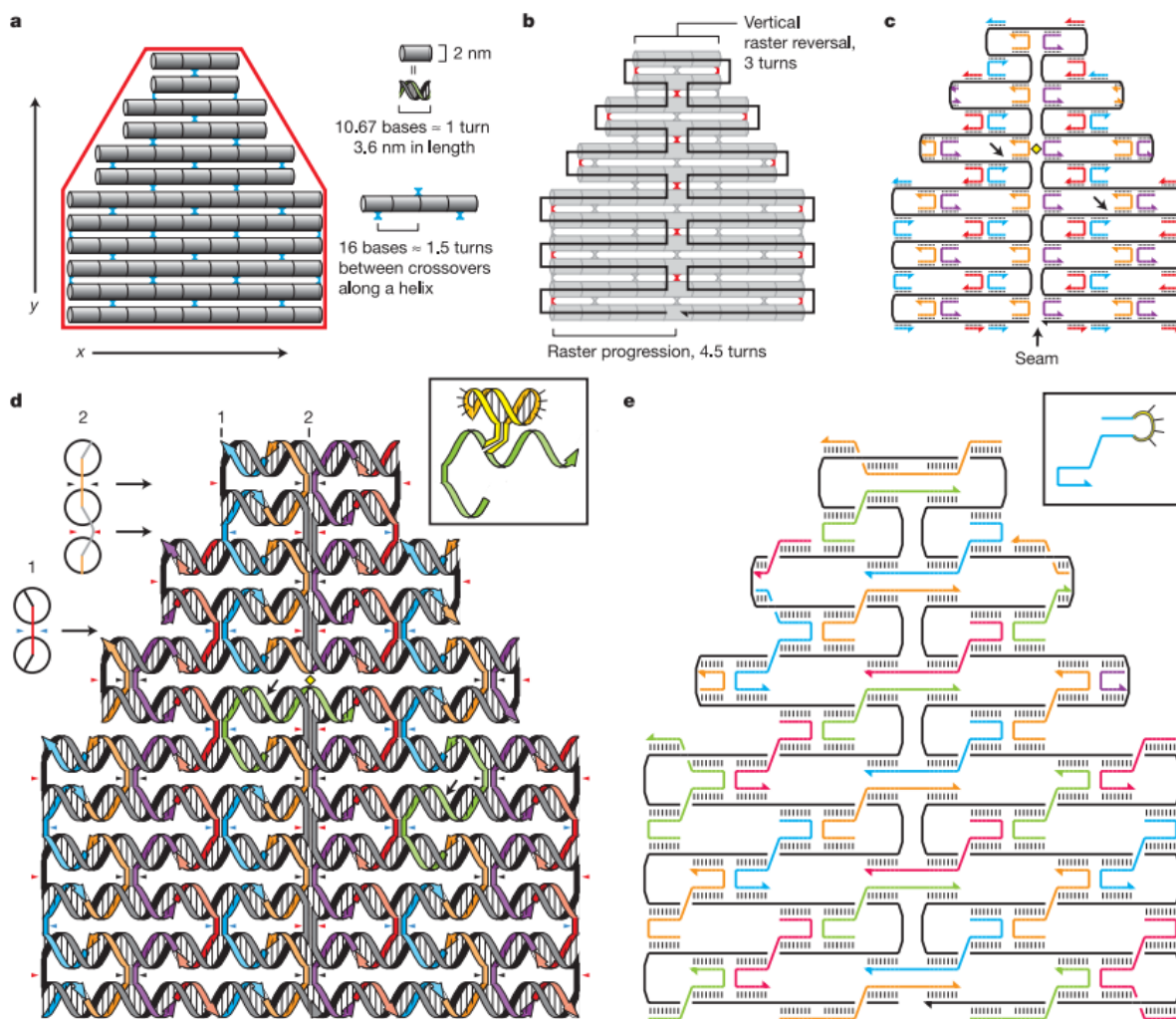


Figure 11 a – A template of the design is filled with 3.6 nanometer pixels representing a single complete turn of the DNA helix. Every 1.5 pixels there is a potential cross over. b – A scaffold sequence is overlaid travelling through each pixel and creating its own crossover points. c – 16 nucleotide long staples are added binding 2 domains of scaffold. d – staples are expanded and bridge the seam in the mid-section of the design. e – a finished with fine structure removed allowing easy addition of sequence to staples [3].

The initial design step shown in figure 11 is still a core fundamental aspect of origami design. The helical pitch of each interacting helix must be matched to allow for strand exchange in a manner which does not significantly disrupt base stacking rules. Once an initial schematic is created the scaffold can be overlaid, complementing staples added, and crossover junction points created which maintain base stacking rules (Figure 11. b). Once rational crossover points for both strands have been created and a continuous path for each helix created (Figure 11. c – d) all that remains is extending staples across the

mid-section seam. It is notable that in the original iteration of scaffolded origami the native secondary structure of the M13MP18 genome used in the fabrication attempt, a dumbbell hairpin and 4T oligonucleotide loop, were incorporated into the design to mitigate any adverse effect on fabrication. However further designs signified that these structures did not significantly interfere with fabrication. This is likely because the final energy state created by successful binding of all staples is lower than that of unsuccessful binding with secondary structures remaining intact.

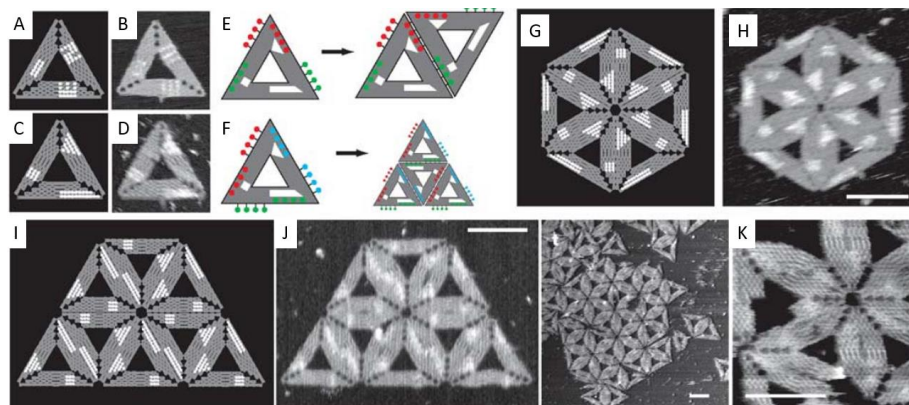


Figure 12 Expansion of the scaffolded DNA origami raster filling design methodology into lattice growth. A – D – DNA origami designs, and AFM images of the displayed designs, showing distinct markings on specific areas of the triangles surface providing clear distinction of a DNA origami's specific orientation. E and F – Specific lattice sequences allow controlled aggregation into both a superstructure hexagon, comprised of 6 individual triangles, or a continuous expanding lattice. G – the design of the hexagon superstructure. H – AFM visualisation confirming the presence of the hexagon superstructure. I – the design of the continuous expanding lattice structure. J – AFM visualisation confirming the presence of the expanding lattice superstructure. K – Breakage points within a triangle causing failure of the lattice at that point [3].

As well as providing the principles for design and fabrication of individual, and independent, DNA origami, Rothmund also explored the conjugation of individual units into larger lattices. Both finite superstructures, such as hexagons formed from 6 conjugated triangles, and periodic, continuous, lattices formed from complementary junctions between triangles. Lattice expansion, in both formats, was conducted by extending staples out from one design into another (As shown in figure 12 E and F) and all lattices were formed directly during the same fabrication protocol as singular designs. Yields were low using this method, putatively ascribed to poor overall stoichiometry between individual DNA origami and lattice staples, with hexagons having an overall estimated yield of <2% and lattice formation not being significant enough to be correctly measured.

In discussion of his new method Rothmund described a list of rules [3] which had been presumed by other groups to render a scaffolded approach, featuring hundreds of fabrication components used in tandem, impractical, but were inconsequential to fabrication success when tested.

1. Sequences must be optimised to avoid secondary structure or undesired binding interactions.

2. Strands must be highly purified.
3. Strand concentrations must be precisely equimolar.

Not only did Rothmund display that structures formed using the scaffolded approach whether or not secondary structure formations were taken into account. He also posited that as a naturally occurring sequence the M13MP18 genomes pre-existing secondary structures would be much lower in final energy state than any artificially applied to the sequence. Furthermore artificially synthesised staples contained at least 10% errors in sequence and truncation groups, with individual staple concentrations for certain designs varying by orders of magnitude, despite these factors all fabrication attempts were successful.

Further a list of factors the authors considered critical to successful fabrication were provided [3].

1. Strand invasion
2. Excess of staples during fabrication
3. Cooperative effects
4. A design which does not include staple to staple binding

Rothmund considered that an abundance of staple strands would overcome any secondary structure present in the scaffold during folding. This is due to small sections of staple-scaffold binding lowering the possible number unwanted secondary structures during folding. As folding progresses and more staples bind simultaneously the number of secondary structures possible is reduced to effectively zero with only the structure created by the correct binding of staples and scaffold remaining.

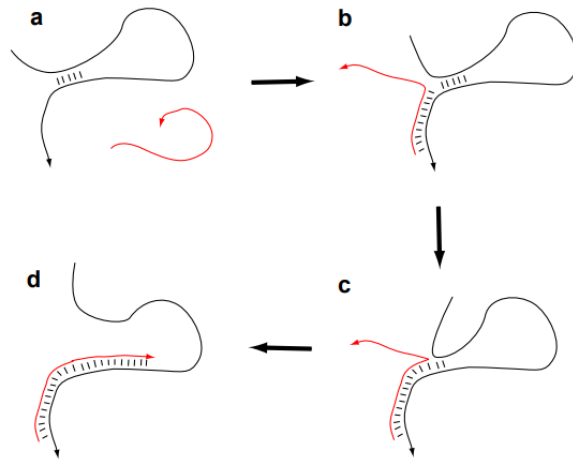


Figure 13 A scaffolds naturally occurring secondary structure is disrupted and replaced by scaffold-staple interaction. A – A 5 base secondary structure present in a scaffold DNA (Black) and a representative staple strand (Red) with sequence matching that area of scaffold. B – The staple binds to the region adjacent to the secondary structure. C – The secondary structure is in flux as base pair exchanges occur between the scaffold-scaffold structure and the scaffold-staple structure. D – The Scaffold secondary structure is overcome completely and the staple correctly binds [3].

Figure 13 demonstrates the interaction between scaffold and staple leading to the termination of a pre-existing secondary structure within the scaffold. This process also frees up the complementing region of the original secondary structure for complementation by other staple strands. During origami folding many interactions such as the one demonstrated in figure 13 would take place simultaneously. If fabrication is successful then all naturally occurring secondary structures within the scaffold would be replaced with the programmed origami design.

The next significant progression in the field of DNA origami occurred in 2009. Until this point shapes had been created in 2 dimensional motifs using a raster filling method. Douglas [51] demonstrated the possibility of fabricating 3 dimensional structures created using a layered honeycomb expansion by adapting the seminal raster technique. Essentially the honeycomb method takes into account potential crossovers as existing every  $120^\circ$ , rather than in a flat plane, with  $540^\circ$  helical pitch progression per crossover point.

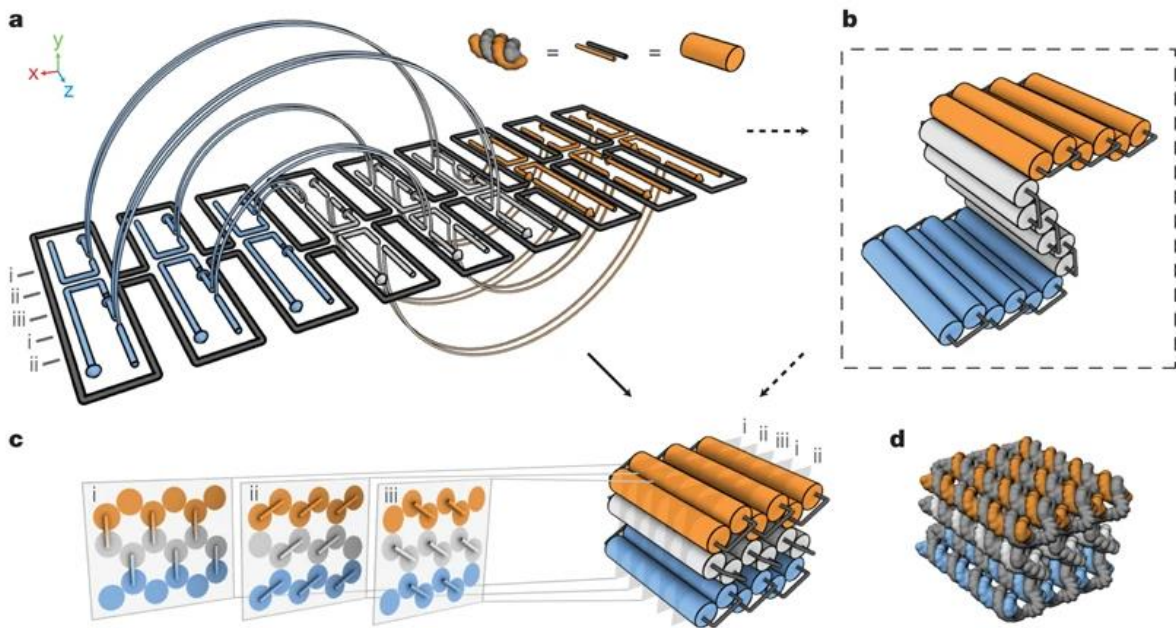


Figure 14 A visual description of the 3 dimensional honeycomb based approach to DNA origami fabrication. A – a 3D block design is demonstrated in 2D schematic. A continuous scaffold strand (Black) runs through the entire design. Staples representing independent domains in the Y axis are differentiated by colour (Blue, white, orange). The staples each crossover to other domains (Branching lines). b – the same design without the crossovers between domains in a semi conformed format. c – i, ii, iii a demonstration of potential crossovers between helices as each strand progresses. Crossovers occur every  $120^\circ$  of rotation. c middle – the design as it is predicted to fold. The scaffold runs continuously through the design over 3 levels with crossovers between the domains locking the structure into place. d – an illustration of the antiparallel helical conformation of continuous scaffold (Black) and staple domains (Blue, white, orange) [51].

Figure 14 demonstrates the shift in crossover domains which converts the existing continuous scaffolding method into a 3 dimensional structure. The key to the honeycomb method, as with all stable DNA origami structures, is the creation of crossover points between helices which maintain base stacking/helical pitch integrity.

Expansion into hierarchical fabrication using the method was also demonstrated by both the conjugation of 3 dimensional monomers into longer chains and 3 dimensional components into larger singular superstructures.

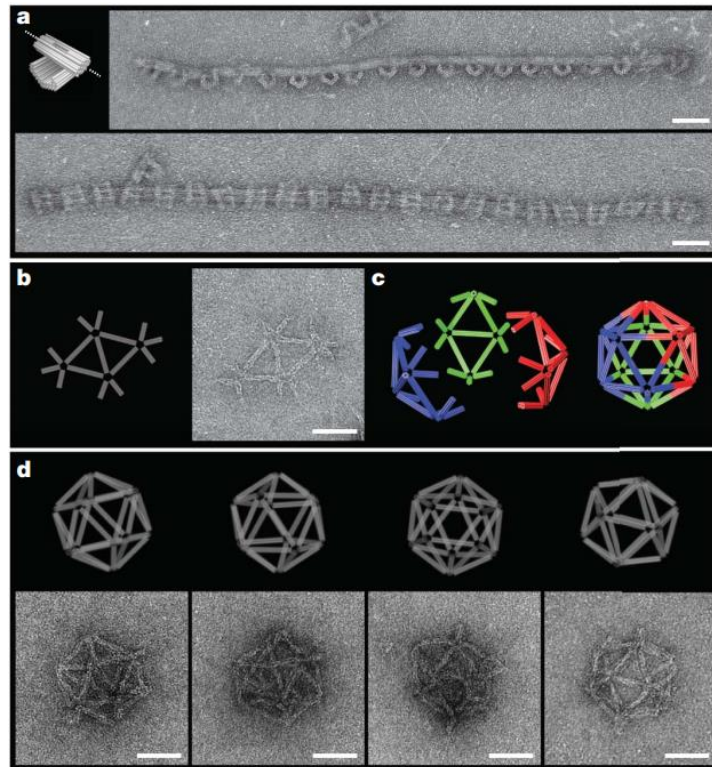


Figure 15 Expansion of DNA origami sub units into both chains and finite structures. A – A DNA origami design with its expansion pathway highlighted. B – honeycomb struts forming a single component of a larger structure. C – icosahedra design formed from 3 independent honeycomb strut components. D – Projections of the shapes conformation. E – TEM images of the correctly fabricated shapes matching the predicted design [51].

The fabrication method using to conjugate individual units into larger monomers was similar to the method originally described by Rothmund [3], figure 15, however this technique relies on the correct extension of scaffold loops from each structure provided anchoring points to neighbours similar scaffold loop. This contrasts the original technique where lattice staples were more embedded within conjugated units. Douglas also used an independent protocol [51], beyond the single step fabrication used to create individual DNA origami to create the icosahedra, where individual components were mixed in equimolar volumes and a 24 hour thermal cycling protocol took place. However even this expanded methodology led to the majority of visualised icosahedra being either damaged or malformed.

While the seminal raster filling and honeycomb based fabrication papers used their respective methodologies to demonstrate expansion of single structures into none continuous and periodic superstructures a lack of throughput and fidelity was described in all attempts [3, 51]. A more successful approach was later conducted by Seeman [53] who built on the work conducted in Douglas' attempt

where a single thermal incubation step had been combined with extended scaffold loops lattice junctions.

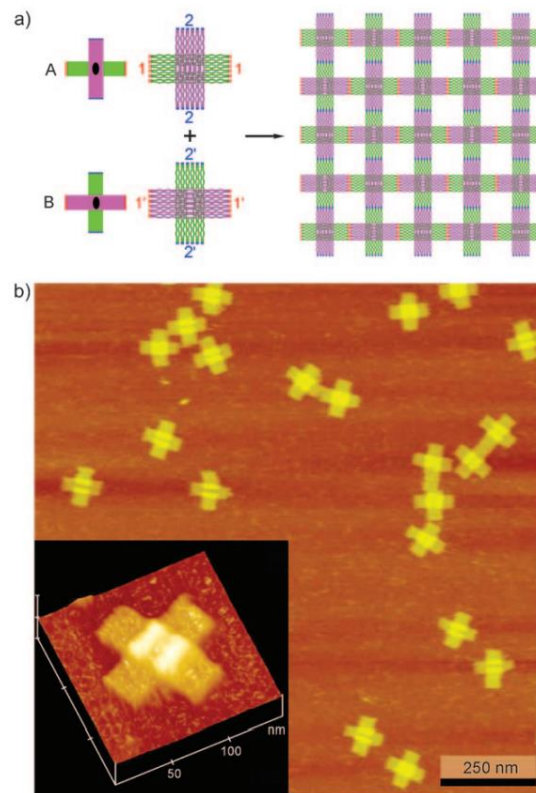


Figure 16 a double crossover lattice motif. A) 2 double cross over DNA origami designs featuring complementary lattice regions denoted by number. The individual designs create a periodic lattice. B) a single double cross over DNA origami structure confirmed by atomic force microscopy [53].

It was theorised by Seeman [53] that the previous attempts at tile based periodic lattice fabrication had been limited due to tile designs with a universal directionality of all helices within the structure. As shown in figure 16 a double crossover motif was employed allowing lattice expansion in both the X and Y direction parallel to the direction of helix progression.

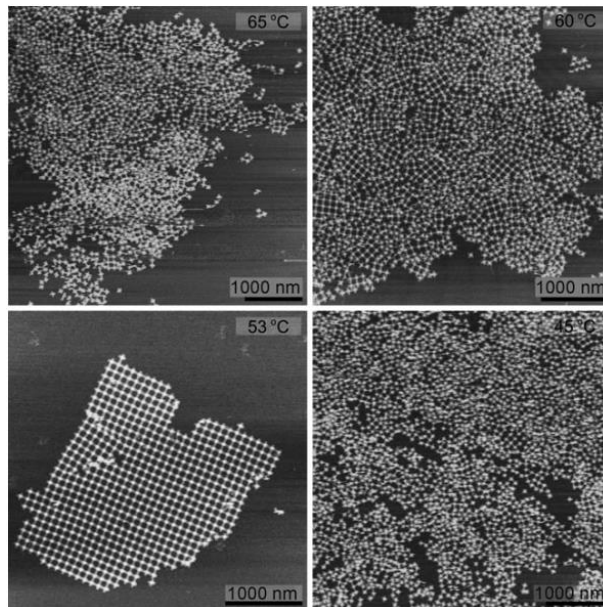


Figure 17 Solutions containing lattice structures are annealed at different temperature before imaging via AFM [53].

The group also ran serial examination of a post fabrication thermal cycle used to fold DNA origami into the lattice structure. The analysis showed that only specific thermal windows, for example only 53°C shows constructive lattice growth in figure 17, had the desired effect of creating long range order of structures.

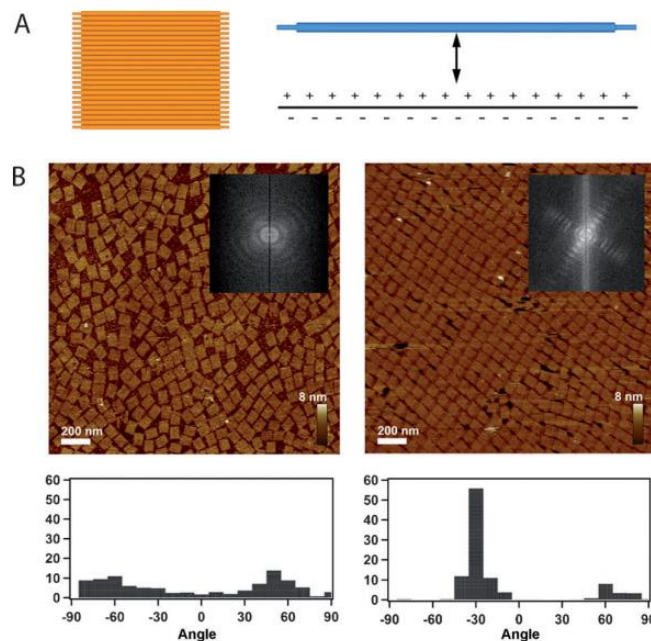


Figure 18 A combinatorial cation approach to lattice formation. A) A DNA tile and a visualisation of the process of tile attachment. The negative surface charge of mica is mitigated by positive ions allowing the origami to bond to the surface. B) A comparison of tiles attached to a mica surface

without 200mM sodium chloride (NaCl) present (Left) and in the presence of 200mM NaCl (Right). The angle of orientation of each shape within the image is also shown [54].

Typically a divalent ion is employed to fix DNA origami to a mica surface for visualisation as seen figure 18. The divalent acts as a salt bridge, mitigating the negative surface charge of both the mica sheet and negatively charged phosphodiester backbone of the DNA within the origami structure, allowing the 2 to form a strong bond. It has also been observed that if this process is combined with the addition of a monovalent ion to the solution being affixed [54], such as sodium chloride, that structures form larger lattices and align in orientation on the mica surface. It is theorised that this behaviour is due to the monovalent ion within the solution mitigating the surface charge of both the DNA within the origami and mica sheet without acting as a salt bridge and permanently binding the 2 together. This type of interference could also potentially interact with existing magnesium ions, displacing them, and allowing structures freedom of movement. Over time semi-permanent attachment of this type will begin to create equilibrium in the structures on the mica surface leading to large lattices of orientated shapes. This was demonstrated by the fact that even structures which did not contain complementary lattice binding points, but did have straight edges, formed large scale lattices over time. This effect could be further enhanced by creating blunt stacking edges which led to constructive interaction between the edge regions of tile based DNA origamis. Lattices stabilised by mono and divalent lattices are universally done so when imaged/suspended in buffer. This maintains the solution and prevents precipitation and crystallisation of the sample during evaporation. This is notable as a variant of this type of fixation was employed during chapters 12 and 13, which also makes use of a mono and divalent ion combination, but does so in air rather than in solution.

In contrast to both the original raster filling, and later the 3D honeycomb method, in which average DNA parameters are maintained to create a stable structure, Shih [55] used rational insertion and deletion of bases to alter the helical pitch of sequence to create curved structures.

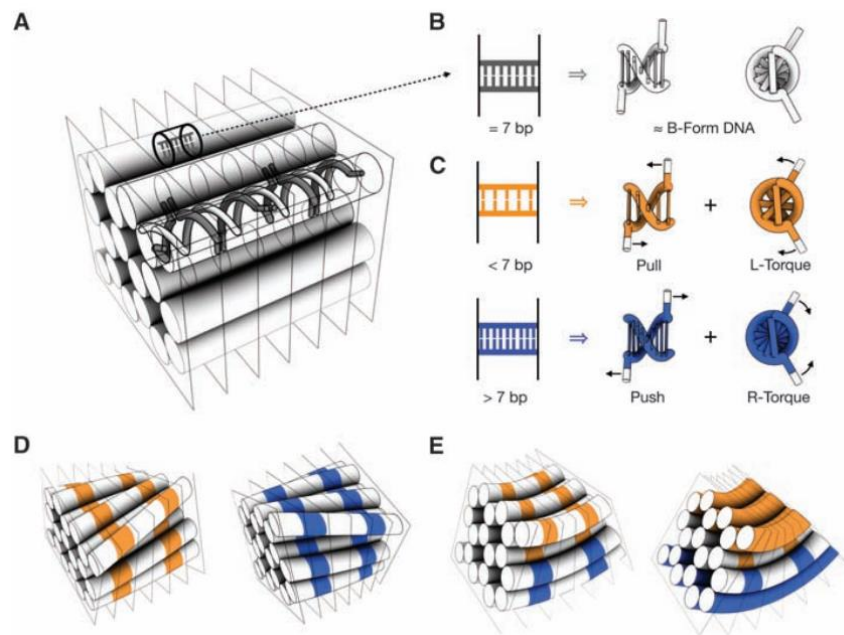


Figure 19 A representation of insertion and deletion events within a given staple strand leading to curvature of a DNA origami superstructure. A – A honeycomb lattice structure with no structural deformation. B – a 7 base pair sequence within the honeycomb lattice links 1 helix to 2 neighbours separated by  $120^\circ$  rotation. 7 bases separating a  $120^\circ$  crossover in this manner maintains a straight sequence as stable B form antiparallel spiral. C – In contrast to the 7 base pair gap between  $120^\circ$  crossover points between a helix with its neighbours we now have an example of both less than, and more than, 7 bases separating the same pair of Holiday junctions between 1 helix and its neighbours.

Due to the deletions in the orange sequence it exerts a pulling force on the Holiday junctions it facilitates. In contrast the blue sequence, which contains insertions, exerts a pushing force on the Holiday junctions it is attached to. D – Universal push and pull forces within a bundle of helices leads to torque forcing spiralling curvature of the entire honeycomb structure. E left – A combination of light push and pull forces leads to gentle curvature of a honeycomb structure. E right – A combination of light, and hard, push and pull forces leads to severe curvature of a honeycomb structure [55].

Figure 19 highlights the change in paradigm of both the method Shih [55] presents and the geometric nature of the structure it fabricates. By careful manipulation of sequence the helical pitch and base stacking of helices with a DNA origami structure can be altered in a stable manner to create curvature.

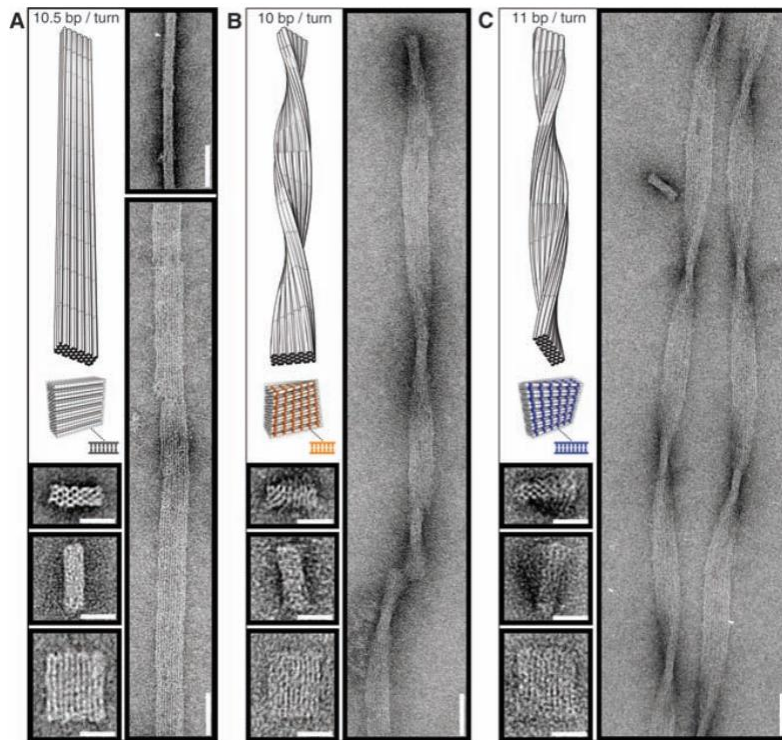


Figure 20 Direct TEM (Transmission Electron Microscope) images of structures where insertion and deletion events have been uniformly inserted into the design. A – Classical B form anti parallel helix is maintained and the structure remains straight. B – deletion events reduce the 10.5 base pairs per 360° rotation to 10 base pairs per 360° turn. C – insertion events have increased the average number of base pairs between each 360° rotation to 11 [55].

Figure 20 shows how universal manipulation of crossover events through insertion and deletion events leads to universal creation of twist and torque leading to uniform curvature of the design over its entire length. This can be seen by contrasting A – where the structure remains straight, with B, where the structure progresses from top to bottom there is significant spiralling the clockwise direction., and finally C, where significant spiralling is observed in the anticlockwise direction.

While the raster filling and honeycomb method offer a strong method of approximating shape on the nanoscale, through careful manipulation of sequence to create double crossover Holiday junction motifs, there are other alternatives. Wireframe architectures are appealing due to their lower reliance on positive ions to mitigate interhelical repulsion than more densely packed structures [56]. This is useful for applications which involve an environment prone to cation depletion or variation such as physiological conditions.

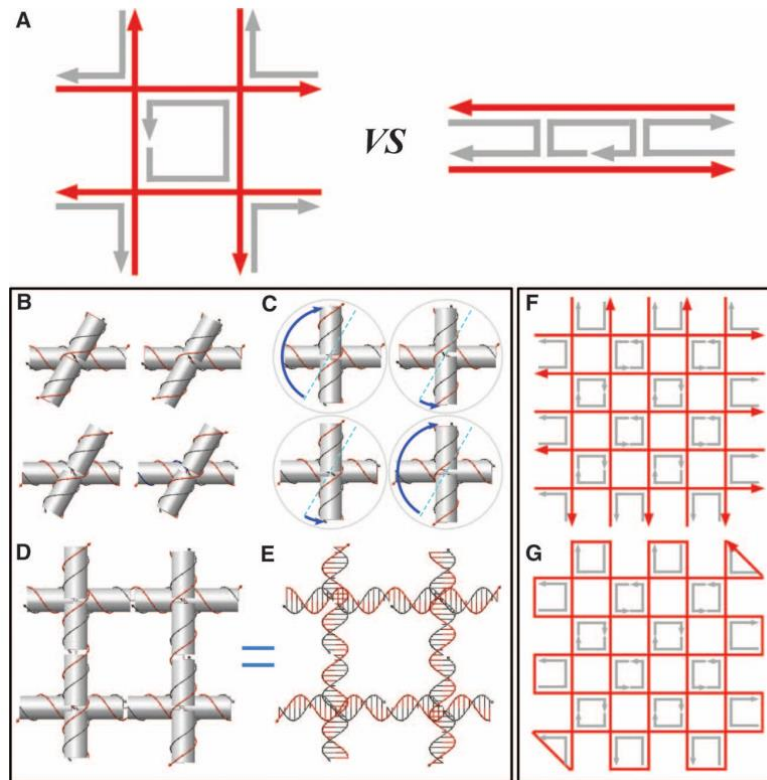


Figure 21 A visual description of the 4 crossover 'Grid iron' motif and its comparison to traditional Holiday junction based crossover. A All lines depict directional travel of the 5' to 3' strand of the anti parallel of helix. Left – The grid iron structure. Each staple is located within a unique pixel within the lattice structure. Right – The classical holiday junction structure. Each staple links at least 2 scaffold domains and the structure is much more densely packed. B – Models of individual grid iron structures where the orientation is no longer uniform and crossovers occur at an angle other than 90° perpendicular to the other helix. C – To form a correctly structured lattice the individual grid irons must deviate from their resting conformation and realign the lattice to match their deviation of structure. D – An example of a complete grid iron structure. E – A true B anti parallel helical representation of the same grid iron structure. F – An idealised grid iron design where each arrow represents the direction of travel of scaffold (Red) and staple (Grey). G – The same design where the continuous path of the scaffold through the entire structure is displayed [56].

Figure 21 shows that manipulation of crossover events can be used to exert force between connected helices and alter the structure of the DNA superstructure.

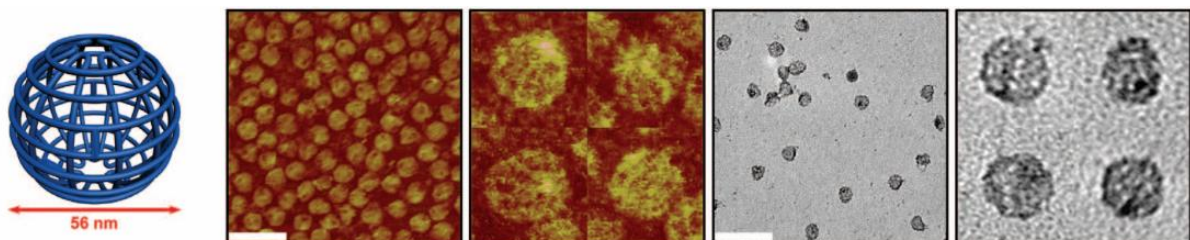


Figure 22 An example of a none continuous 3D structure, a sphere, created using the grid iron method. Middle – AFM images. Right – TEM images. White bar = 200 nanometers [56].

While the grid iron method does lend itself to 2 dimensional lattice or board based fabrication it also presents the possibility of none continuous structures as shown in figure 22.

Beyond manipulation of conventional scaffolded DNA origami technique there also exists the possibility of complete removal of the scaffold sequence from the method and utilise strictly staple, or ‘bio-brick’ [57], based fabrications. Initially conducted using 32 base pair sequences broken into 4 independent domains, each linked to potentially 4 other similar sequences, design was conducted in a similar manner to raster filling or the honeycomb approach. Shapes are approximated directly, where the feature size of the DNA is the limiting factor, and each pixel or voxel, is given the dimension of 2.5 x 2.5 x 2.7 nanometers.

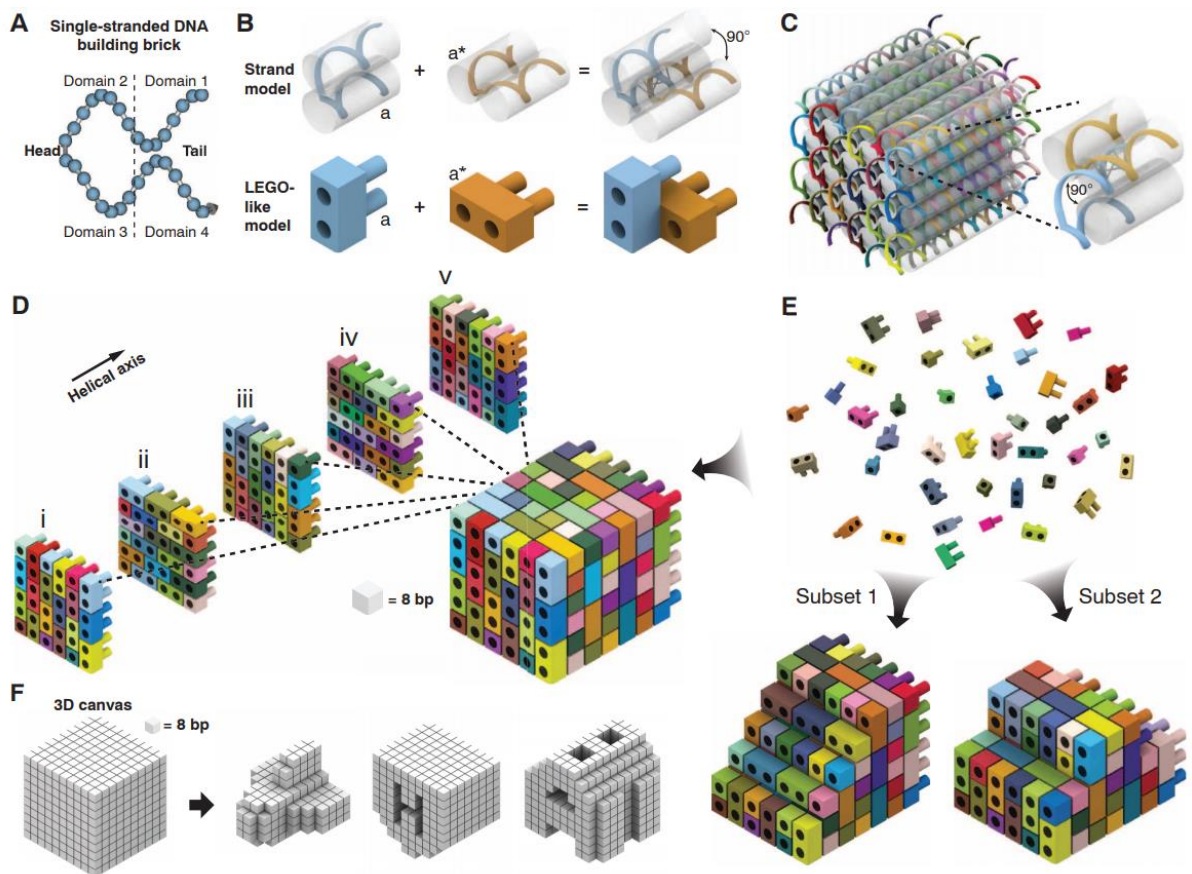


Figure 23 The ‘Bio-brick’ fabrication scheme from brick to final structures. A – A 32 base pair sequence is divided into 4 domains capable of interacting in a sequence dependent manner with other similar building blocks. B – Each block is considered to have 2 receiving and 2 donating domains. Blocks are not continuously stacked and 90° rotation occurs between each interacting block to create a square pixel based structure. C – a demonstration of the bio-brick method used to fabricate a cube structure where individual bio-brick are each distinguished as separate colours. D – Biobricks are assembled into 2D sheets which then further fabricate into a 3D structure. E – Using the larger 6 x 6 helix x 48 base cuboid as a canvas object other shapes can be created by removing specific bricks

from the complete set to sculpt defined shapes. F – An example of the canvas cuboid being used a tool whereby removal of individual bricks/pixels forms other unique shapes [57].

The biobrick method, explained in figure 23, is useful for creating many modular shaped designs within a specific volume of interest as once a large cuboid canvas has been synthesised any design within the specific pixel volume of the larger canvas shape can potentially be fabricated from the same bio-brick pool. This is not the case with conventional scaffolded fabrication where even minor structural changes require rerouting of the scaffold strand and significant alteration of the staple pool. It is notable that the authors of this paper reinforce the theory originally speculated by Rothmund that specific sequence of a construct is less pressing, in throughput terms, than the fabrication folding cycle.

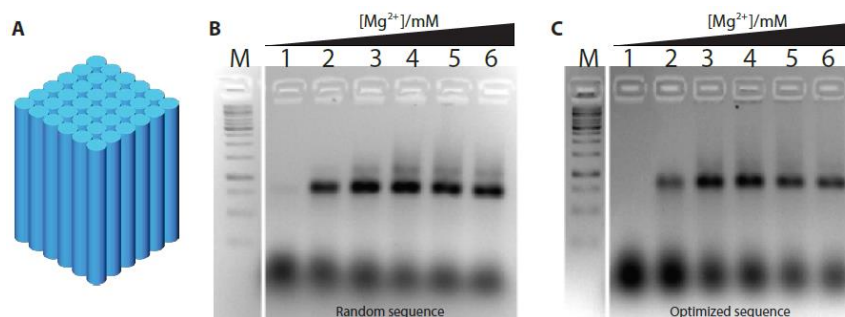


Figure 24 Random sequence assignment vs optimised sequence creation. A – An arbitrary 6 helix x 6 helix x 64 base pair bio-brick structure is used as a comparison fabrication objective to compare the 2 approaches. B – An agarose gel electrophoresis result comparing fabrications conducted, using a randomised sequence for the whole structure which was then used to sequence each individual bio-brick, at various  $Mg^{2+}$  concentrations. C – An agarose gel electrophoresis result comparing fabrications conducted, using an optimised sequence discussed below, at various  $Mg^{2+}$  concentrations [24].

Figure 24 contrasts a fabrication attempt where bio-brick pools have been created either by random sequence design and computationally optimised sequence where the following modifications (Used to create bio-bricks in the ‘X’ conformation where bio-bricks in the ‘Y’ conformation were creating by existing sequence complementation) have taken place:

1. GC content of the sequence has been modified to create as much uniformity as possible. This is done to reduce the binding energy between strands.
2. Minimisation of secondary structures within strands.
3. Reduction of sequence symmetry to avoid competition between possible folding domains.

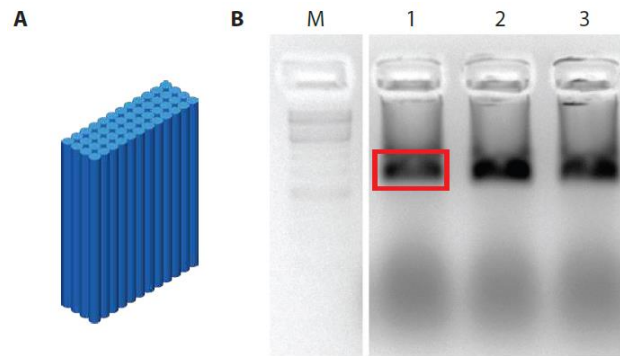


Figure 25 Further cross examination of random sequence assignment and fabrication efficiency. A – An arbitrary 4 helix x 12 helix x 120 base pair cuboid structure is used as a fabrication template. B – Lanes 1, 2 and 3 are each an independent random sequence assignment of fabrication components used to create the structure. Lane M is a DNA ladder used for comparison and the red box is the band from which structures were eluted and checked under TEM [57].

Figure 25 compares 3 random sequence assignments for fabrication efficiency. Little difference in throughput was visible between the final fabricated bands and each band, when checked directly via TEM, demonstrated correctly fabricated structures.

As shown in figure 24 and 25 there is very little difference in fabrication sequence between an optimised sequence and a randomly assigned one, this could suggest that co-operative folding domains are more important than the relative efficiency of any individual subset of fabrication components, even when the subset is >50% of all components.

A later paper [58] by the authors of the seminal bio-brick technique reinforced the capability of bio-bricks to address the lack of scalability present in the scaffolded origami approach. As DNA origami scaffolds are typically acquired by utilising pre-existing organic DNA structures, such as viral plasmids, they are of limited size in terms of specific base pair length. It was found that by increasing the binding domains of each individual brick from 8 bases to 13, meaning a total size change from 32 bases to 52, structures could be fabricated with molecular masses extending into the gigadalton range (Where an individual scaffolded DNA origami typically has a mass of around 5 megadaltons). In contrast to the original bio-brick work, where shapes were created using a canvas containing hundreds of individual bricks, the expanded method employed canvases with over ten thousand individual bricks.

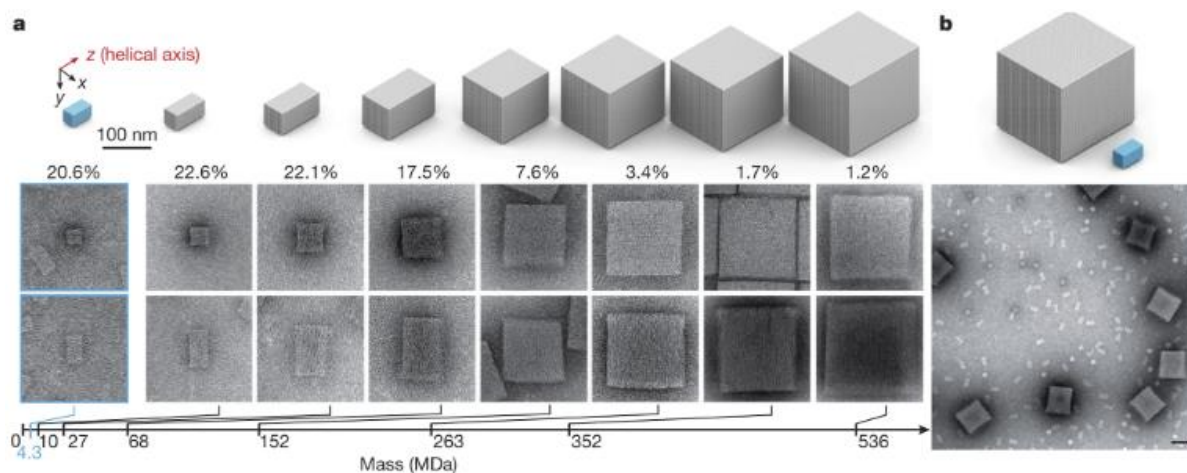


Figure 26 a comparison of fabrication size to relative throughput using the modified bio-brick method. A) A conventional scaffolded DNA cuboid (Blue) is compared to the size and throughput of progressively larger shapes fabricated using bio-bricks. B) the largest shape is compared directly to the scaffolded DNA based cuboid via TEM [58].

While comparable yield is observed in structures on a similar length scale to the scaffold origami cuboid as the mass of cuboid structures increases the relative throughput begins to drop off (Figure 26).

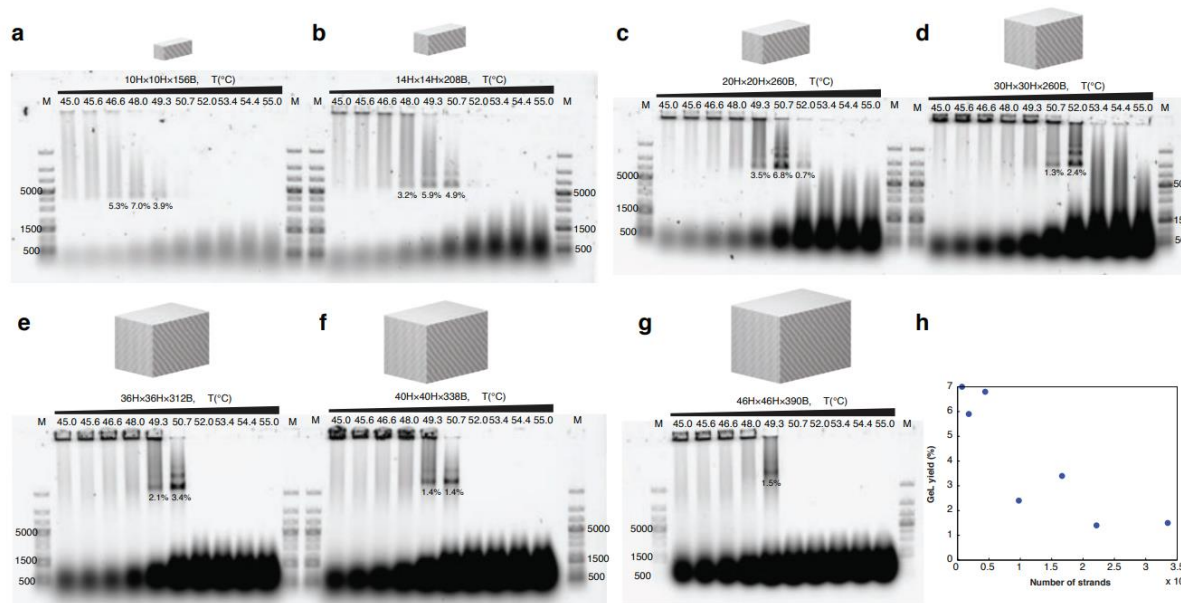


Figure 27 A five day isothermal thermal cycle is employed to examine specific structure formation. A – G) Various structures examined [58].

As the mass of the structures increases excess fabrication components (Lower bands) increase significantly (Figure 27). It is also of the note that significant aggregation can be seen in all loading wells, apart from the most successful lanes, and those where no structural growth occurred. H) The number of strands within a structure is proportional to its relative throughput in fabrication terms.

Figure 27 shows that bio-brick folding occurs in a very different manner to conventional scaffolded DNA origami. As demonstrated by Sobczak [59] typically significant levels of folding can occur over a

very narrow isothermal range, and with other fabrication considerations addressed, such as staple to scaffold ratio, successful fabrication can approach >90% using the scaffolded method. In contrast, while there is significant change in folding dynamics over a relatively small thermal window using bio-brick based fabrication, constructive folding remains quite low. Even for the smaller shapes which demonstrate a higher throughput less than 25% of all the total bio-bricks available are successfully incorporated into complete structures. However this is not to say the bio-brick method is not without benefit as it would take approximately 100 M13MP18 DNA scaffolds, the type used by Rothmund in the seminal origami attempt, folded correctly into a single tandem structure to approximate the 536 megadalton cube shown in figure 27. While 2 dimensional scaffolded origami lattice based fabrication is possible on the same length scale as the foot print of individual bio-brick structures of this scale there are no demonstrations of 3 dimensional fabrication on the same order of magnitude.

For these reasons it has been observed that the scaffolded DNA method, and bio-brick fabrication, should be considered as tools for different types of fabrication rather than direct competitors. The following observations are useful to determine the validity of either of the given approaches for a specific fabrication task [12].

1. DNA origami is typically produced in higher yields and with a higher fidelity. Staples are added in excess so missing components within a given design are rare. Because the bio-brick method is very dependent on equal stoichiometry between all components this throughput and fidelity is not observed in the same manner.
2. Scaffolded DNA origami are more resilient to changes in ionic conditions due to the continuous nature of the scaffold running through the entire structure. A bio-brick structure does not benefit from this stability.
3. DNA bricks are much more modular than DNA origami designs. A bio-brick canvas can be readily modified using the same set of sequences. The same is not true for the staple strands of a DNA origami where even small modifications lead to significant changes of sequence.
4. DNA bricks are artificial and their sequence can be easily modified. As all scaffold strands have a set sequence, and complement, this is not true for most staple strands.

As described the bio-brick method seeks to address the inflexibility and availability of suitably sized scaffolds by replacing them with shorter artificial strands completely. However there have also been attempts to identify or create novel custom scaffold sequences [50] for specific fabrication projects. This is typically done to facilitate fabrication of either larger, or smaller origami, but can also address other fabrication specific caveats, such as removing the use of a phage gene (For example the P7249 scaffold, and its variants, which are commonly used in DNA origami fabrication are derived from a bacteriophage plasmid) in *in vivo* projects.

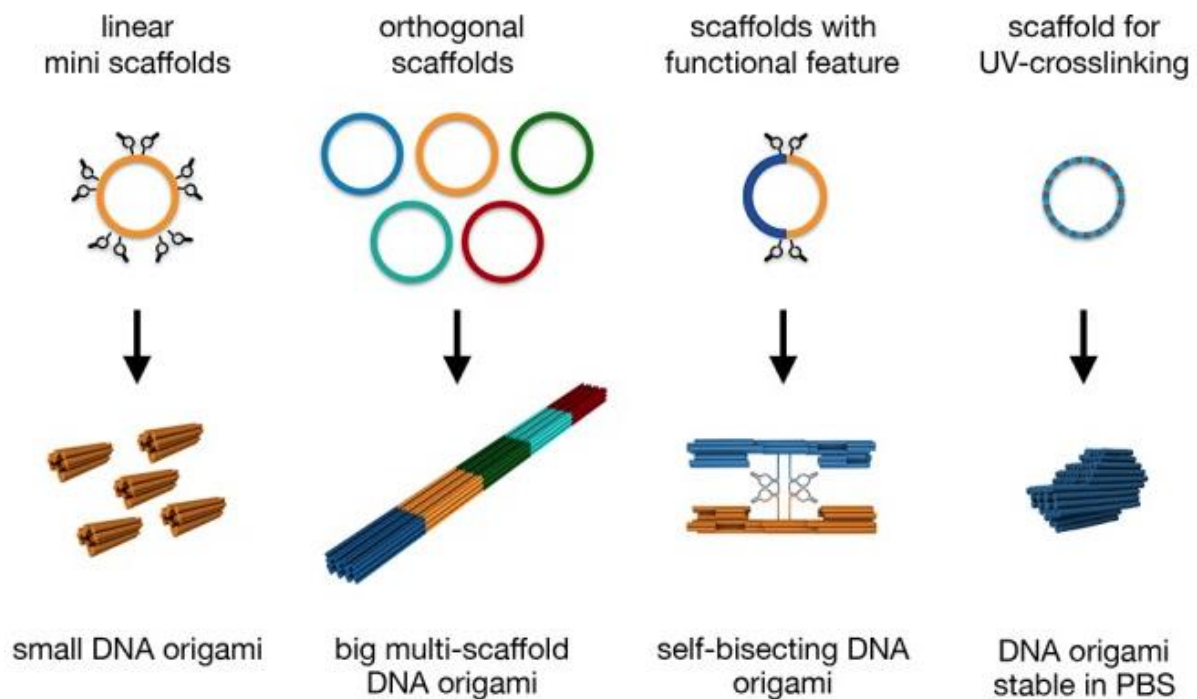
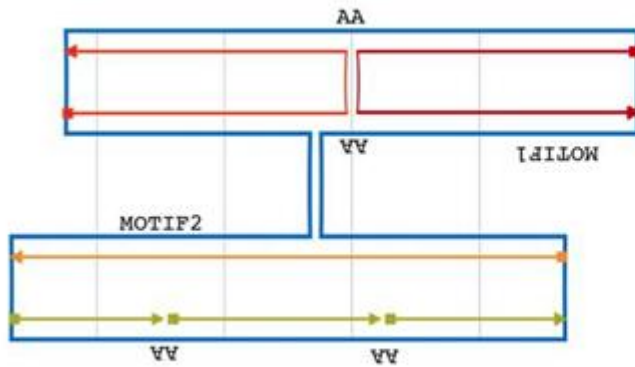


Figure 28 Various novel scaffolds presented by Dietz [46].

The scaffolds shown, figure 28, each have a specific function beyond pure DNA origami fabrication. Left to right – Linear mini scaffold fabrication - provides efficient throughput of ~1000 base pair scaffolds. Orthogonal scaffolds – distinct scaffolds can be used to fabricate multi scaffold superstructures. Scaffolds with functional feature – such as a structure with a self cleaving enzymatic domain triggered under specific conditions. Scaffold for UV-crosslinking – specific placement of thymidines within a structure can be used to create covalent dimer bonds on exposure to UV greatly increasing the structural stability of the origami structure.

Scaffold Smith [59] can be used to design specific custom scaffold sequences and integrates into the existing conventional scaffolded DNA origami methodology at the point a caDNAno strand diagram of the entire structure has been completed, but no scaffold sequence has been assigned.

### I. Design DNA origami



### II. Define constraints

MOTIF1	include at loc ...
MOTIF2	include at loc ...
<del>MOTIF3</del>	exclude globally
AA	include at crossovers
AA	include at nicks

### III. Define base pair step weights

	A	T	G	C
A	1	1	1	1
T	1	0	1	1
G	1	1	1	1
C	1	1	0	1

Figure 29 A walkthrough of the Scaffold Smith design process. I. A caDNAno design for modification by the Scaffold Smith software. II. Constraints created by the user under certain circumstances. In this example single stranded breaks, and holiday junction crossovers, are assigned AA as a sequence. III. Constraints to be taken into account by the program when creating a stochastic base distribution when the sequence is generated. In this example TT and CG motifs would not occur in any created sequence [60].

The pathway shown in figure 29 is finalised, with specific sequence creation, once all constraints and stochastic considerations have been selected.

It has already been mentioned that scaffolded DNA origami is comprised of a hydrogen bonded pair of DNA strands in an anti parallel helix knitted together by Holiday junctions between individual helices. While there is some flexibility in terms of various physical parameters, for example wireframe structures being more resistant to divalent ion depletion, and densely packed structures being more heat resistant, there are inherent limits on structural stability without further modification. Schemes for reinforcement of the origami structure can take place through direct modification of the DNA itself or complete encasement of sections of the origami superstructure.

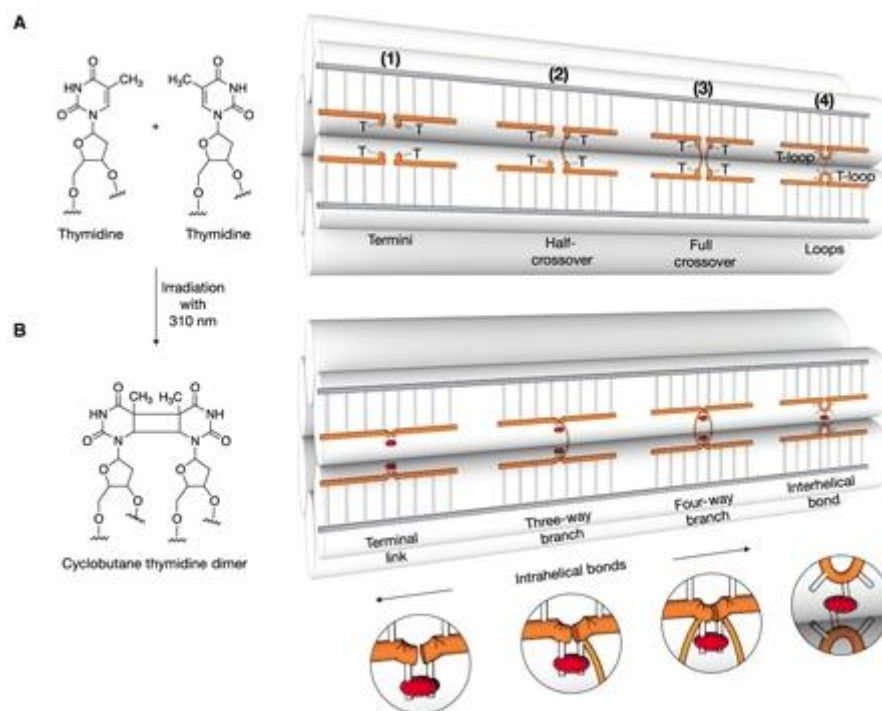


Figure 30 Conventional thymidine-thymidine motifs in proximal helices and the same thymidine motifs post UV exposure with covalent bonding present. A – adjacent thymidine bases (1) Adjacent bases in a broken strand with no crossover (2) adjacent bases with 1 Holiday crossover (3) 2 complete Holiday crossovers (4) 2 continuous strands with single stranded T loop motifs extending out of the helix. B – the same thymidine structures post UV exposure. Red ellipsoids show covalent cyclobutane dimer bonds between the existing bases [61].

Creation of the covalent bonds within DNA origami structures had significant effects on the structures resilience to both ionic conditions and heat as illustrated figure 30. While the test group of DNA origami designs, which had not undergone UV cross welding, displayed a heat resistance up to  $\sim 50^{\circ}\text{C}$  and showed significant degradation when transferred to a low monovalent ion solution, the UV (Ultraviolet) cross welded structures showed stability to at least  $90^{\circ}\text{C}$  and could be stored without degradation in distilled water without an ionic buffer.

## 2.5 Conclusion

DNA's structure, its programmable nature, and the interaction between localised chemical environment and its effect on the structure of the double helix were elucidated significantly before the theorisation of structural DNA based nanotechnology. Putatively this pre-existing knowledge and familiarity of DNA's structure and its manipulation could be one of the reasons that when artificial DNA synthesis,

and later harvesting of viral plasmids, became available there was significant activity, and many examples of fabricated devices, in what is still an emergent field.

Scaffolded DNA origami presented a significant step forward in DNA based fabrication as not only could larger structures be created but they could be done so in independent, none continuous motifs, with highly detailed surface features on a similar length scale to that of the physical size of individual helices and <10 DNA base pairs. However it also demonstrated potential expansion of individual subunits into repetitive lattices and superstructures.

While scaffolded DNA origami fabrication is a distinct field in the area of DNA based structural nanotechnology it demonstrates a high degree of interaction with other similar and none similar approaches. An example of a similar approach would be the divergence of the method into bio-brick based fabrication. There is also potential for these fields to recombine with bio-brick based features used to decorate the surface of a larger DNA origami. In contrast a none familiar field would be the use of high intensity UV waves to chemically alter the DNA used to compose DNA origami to significantly improve the samples stability in terms of both physical robustness and resistance to ionic degradation.

## Chapter 3

### 3.0 Component and Technique Examination

Discussion of specific lab technique, and its development over time, is useful when examining the field of structural DNA nanotechnology and the mechanics of DNA Origami fabrication. Many of the techniques used are adapted from other disciplines, significantly molecular biology, or evolved to address requirements which modern synthesis and manufacturing techniques no longer present, such as the rate limiting thiol reduction and purification steps (which as mentioned in chapter 9 has no effect on functionalisation if not conducted). This chapter can be used to provide an understanding of the general theory behind common lab-based technique used to fabricate structures.

#### 3.1 Scaffold synthesis

When creating the seminal scaffolded DNA origami method Rothemund used a pre-existing viral genome as a template. The M13MP18 scaffold, commonly used in DNA origami synthesis, is typically synthesised in vitro using an E Coli bacterial host as a biofoundry. In a series of bacterial transformations using a viral phage plasmid, which also serves as the scaffold post amplification, the product is recovered from solution and can be conducted in a continuous manner without destruction of the host culture [62]. Initially yields using this method were limited to ~10 milligrams per litre of culture [63]. This yield has improved over time and more recent biofoundries have demonstrated yields in the region of ~0.4 grams per litre of culture [63].

While it is possible to synthesise DNA scaffolds in a lab based setting it is also convenient to purchase them commercially at a relatively low price. Regardless of specific acquisition pathway DNA origami scaffolds are typically resuspended to somewhere within the 100s of nanomolar range (All fabrication attempts in this thesis were conducted using a 100 nanomolar P7249 scaffold as detailed chapter 8) and stored in Tris (trisaminomethane) base buffer to maintain pH. While scaffold DNA can be frozen it is prudent to allow the solution to completely dethaw, to avoid shearing effects, before removing aliquots

for fabrication [64]. For this reason aliquots of scaffold can be removed from a mother solution which can then be placed in a freezer for long term storage.

## 3.2 Staple Synthesis

For work conducted in this thesis all short staple strands were purchased from Integrated DNA Technologies (IDT). All oligonucleotides produced by IDT are synthesised via solid-phase support [65].

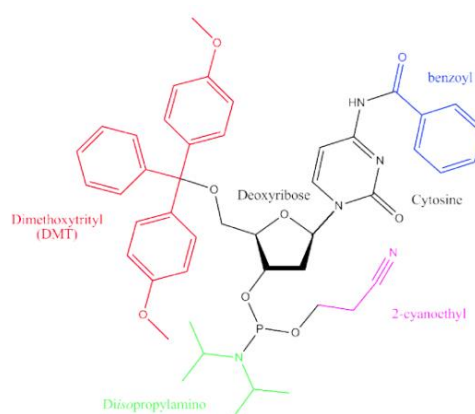


Figure 31 A cytosine molecule protected by various groups on its amine, hydroxyl and phosphate groups [65].

Figure 31 demonstrates the general scheme of solid-phase oligonucleotide synthesis. Capping molecules are used to protect the various reactive groups of the individual mononucleotide and it is the exchange of these molecules with others that leads to the controlled growth of a specific DNA sequence. While several parts of the oligonucleotide can be modified [65], for example the phosphodiester backbone, or the 5' or 3' terminus, only modification of the 5' terminus, using dimethoxytrityl [65] is consistent throughout oligonucleotide synthesis as it is by this mechanism that a synthesised strand is sequentially extended.

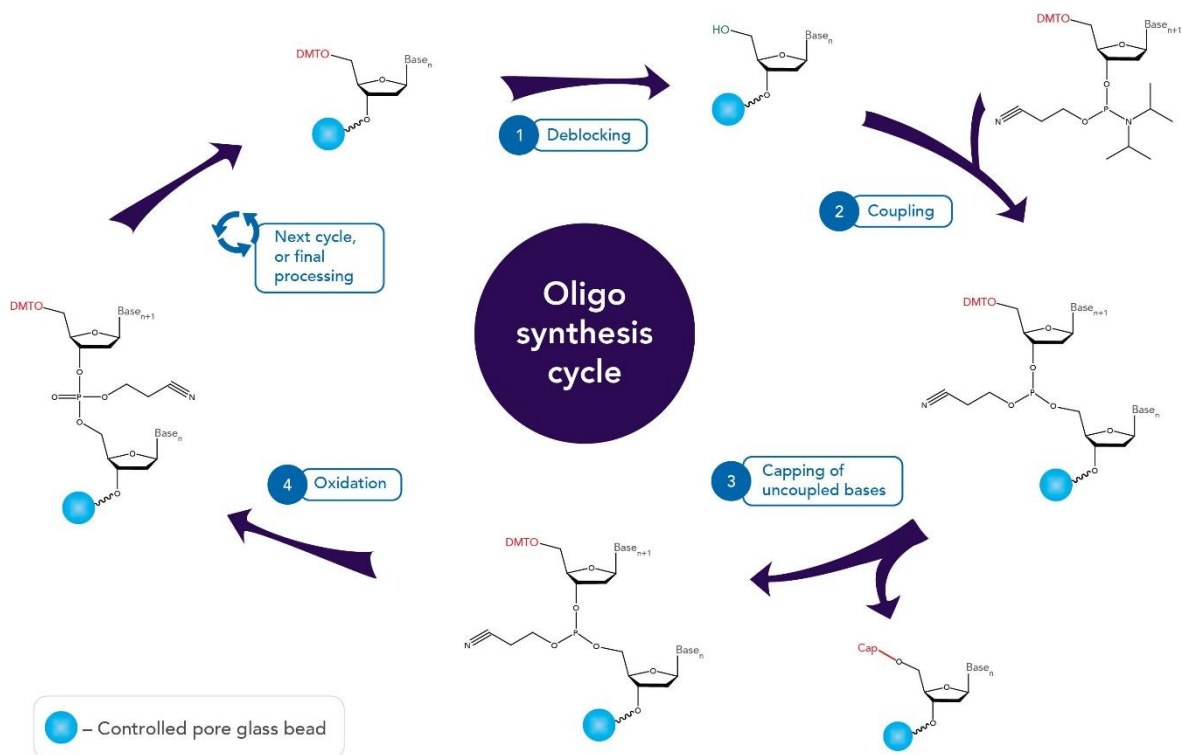


Figure 32 These 4 steps of sequence extension are conducted until the sequence is complete. Step 1 – the DMT group is removed from the 5' carbon of the nucleotide at the end of the growing oligonucleotide chain presenting a binding site for the next nucleotide in the sequence. Step 2 – new nucleotides react with a weak acid leading to covalent bonding with the unprotected 5' region on the exposed nucleotide. Step 3 – Efficiency of this method can never be 100% as some sequences which have not correctly received the next oligonucleotide in the chain, and therefore exhibiting deletions in sequence when compared to successfully extended chains, are incorporated into the final synthesis product. Step 4 – once the nucleotide is incorporated into the chain and capped its 3' phosphite linkage is oxidised leading to the phosphotriester joining unit displayed in naturally occurring DNA [65].

This cycle growth process is conducted, figure 32, until the sequence is of the correct length. All protection molecules are then removed, and the chain is ejected from its glass support. Once all sequences from the synthesis have been collected the solution is desalted and is ready for use in lab-based fabrication.

When using the P7249 scaffold, and staples of around 32 base pairs in length, it is likely that a typical origami will use over 200 individual staple sequences in fabrication. During the course of the work conducted in this thesis staples would be ordered in 384 well plate format. Other sequences, such as thiolated, or phosphothioate, modifications of the existing design would be ordered separately in a 1 millilitre tube format.

It is notable that DNA sequences terminated with either a 5' or 3' thiol group, which are purchased commercially from sources such as IDT, are capped with small alkanethiol molecules [66,67]. Many papers describing the functionalisation of gold nanoparticles, in a manner identical to that demonstrated in the work conducted in this project describe the process of reducing [68,69], and then in some cases purifying, the thiolated DNA from excess reduction agents before functionalisation takes place. The reduction agents used in this manner if left unpurified from the final solution could be considered contaminants [67] in the system as they do not feature in the fabrication protocol in any other steps.

### 3.3 DNA origami Fabrication and Physical properties

Once a DNA origami design has been confirmed staple sequences are recovered computationally and then synthesised. For lab-based fabrication synthesis is typically done commercially and is received either in a multi-well 'plate', containing many wells with each well containing a single staple sequence, and then a single tube containing the relevant scaffold sequence. If received dehydrated sequences must be re-suspended into a concentration conducive for fabrication. If the staples or scaffold are received pre-suspended it is crucial they are in a concentration which allows dilution to effective fabrication solutions. For applications requiring significant amounts of either raw origami or fabrication components both scaffold and staples can be synthesised in a lab environment using PCR [70] or chip based amplification [71].

Once obtained staples and scaffold are mixed in solution, typically at a ratio of 10: 1 - Staple: Scaffold [72, 73]. There is evidence to show that staple to scaffold ratio of 5:1 can lead to <50% of scaffolds incorporated into monomeric DNA origami post fabrication [51]. Other groups suggest that for arbitrary DNA origami design a ratio of 20:1 staples to scaffold is required to ensure high fidelity fabrication [74]. This would suggest that while there is some dependence on design and other fabrication consideration a key factor of DNA origami fabrication is a significant excess of fabrication components to scaffold.

The chemical composition of the solution the sequences are contained within must be changed for fabrication conditions to become favourable. Adjusting of the sample is typically done with a

concentrated ‘Fabrication buffer’ which is added to solution containing scaffold and staples before fabrication takes place.

Tris is commonly used to maintain the pH in buffer solutions containing DNA. While Tris, or other pH maintaining compounds, are used almost universally with DNA containing solutions (from storage of oligonucleotides to fully constructed DNA origami) they do so in a passive manner. No modification of Tris content was attempted during fabrication.

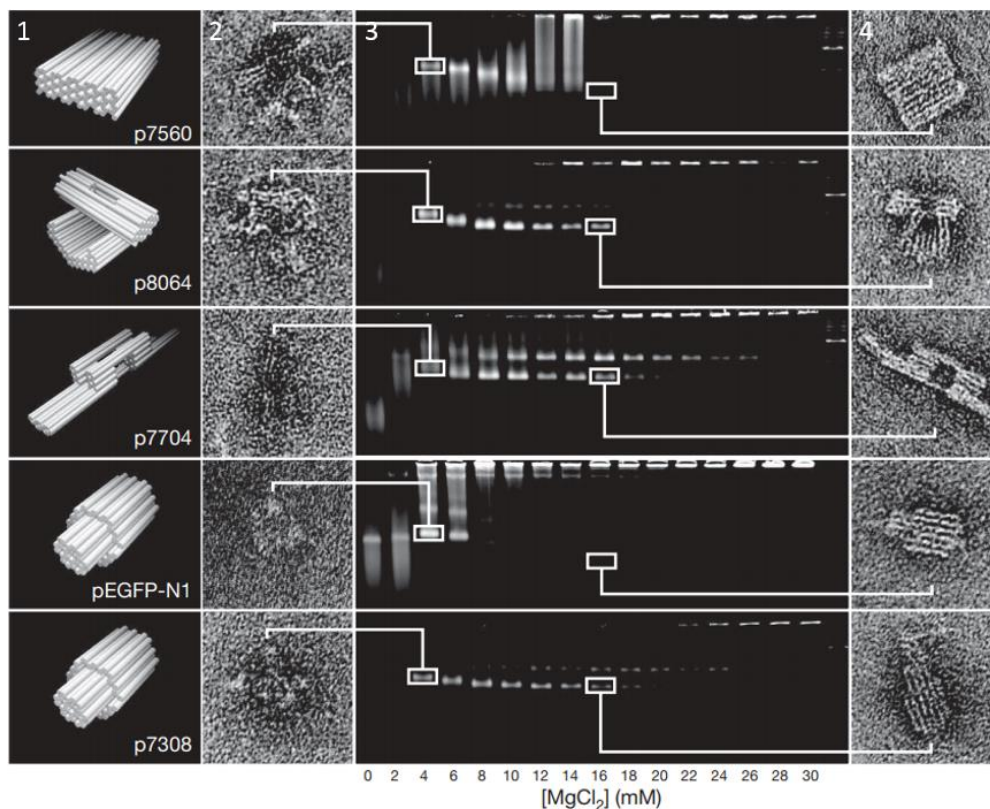


Figure 33 Columns - 1 - A selection of simulated origami designs. 2 – TEM images of samples of the predicted designs folded under conditions where 4mM magnesium chloride ( $MgCl_2$ ) is present. 3 – Gel electrophoresis of samples at various concentrations of  $MgCl_2$  where 16mM  $MgCl_2$  is highlighted. 4 – Successful fabrication observed via TEM [52].

As DNAs phosphodiester backbone is highly negative this charge must be mitigated in order for stable DNA helices, with Watson Crick base pairing maintained, to be formed. Typically divalent magnesium ions [3,61] are used for this purpose however other monovalent ions [75] have also been employed. As DNA origami are created from many helices in close proximity this mitigation is critical to not only fabrication but also stable storage, in solution, of completed origami. The specific ionic levels required for DNA origami fabrication have been shown to be structure specific as can be seen in the variation of

ions required for successful fabrication in figure 33. Designs in which there is limited interhelical proximity, such as skeletal or frame designs, are shown to fabricate in buffers containing less positive ions than more densely packed 3 dimensional honeycomb structures [12].

Once the fabrication sample has been finalised it is thermally cycled. This process involves the rational breaking of hydrogen bonding within a sample which is then restored, over time, in a manner which maintains Watson-Crick base pairing and enables origami formation. The initial step, where a fabrication solution is heated to the point that all hydrogen bonding breaks down completely and all DNA within the solution becomes single stranded, is universal to all successful fabrication attempts.

While some studies begin with a temperature ramp as high as 85°C there is strong evidence to suggest that bringing a sample to 65°C for 15 minutes is sufficient to neutralise any anomalous secondary structure formation within the sample [72]. Once this step has taken place the temperature is lowered over a specified temperature range and correlating time domain. Originally thermal cycling protocols were highly varied and would last from several hours to several days and occurred arbitrarily over a wide temperature range [3,51,55]. This also leaves a somewhat trial and error method of protocol identification as designs can only be confirmed once analysed through either direct imaging of a finalised solution or indirect results via agarose gel electrophoresis (AGE).

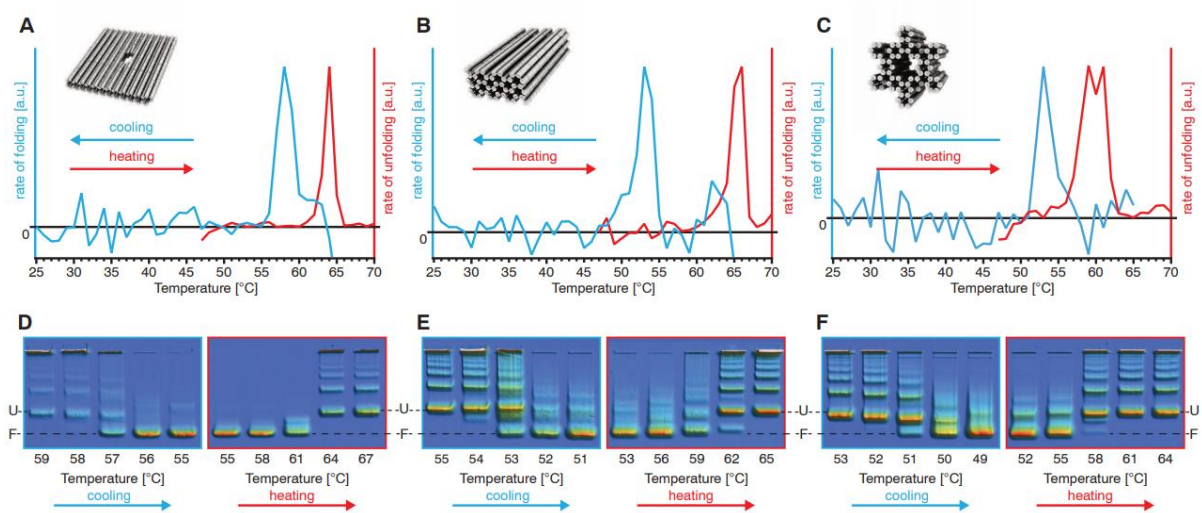


Figure 34 A, B, C – The levels of folding occurring during cooling transitions (Blue) and unfolding occurring during heating transitions (Red) during a heating cycle between 25 and 70 degrees Celsius. D, E, F – Gel electrophoresis analysis of samples cooled to, from an initial heating temp of 65 degrees Celsius (Blue), and heated to (Red) specific temperatures [72].

Figure 34 shows the levels of relative folding which occur at certain temperatures in a folding cycle (After an initial temperature spike at 65 degrees Celsius for 5 minutes) by quenching the thermal cycle reaction instantaneously by inserting the reaction vessel into liquid nitrogen. It is clear that there are significant levels of folding and unfolding at certain design specific temperatures during relatively short periods of time. It is also clear that there is an almost universal temperature window in which all constructive folding occurs. An iteration of this method of tracking and refining origami fabrication was employed during our fabrication attempts and is discussed more in chapter 11.

Typically the more successful a fabrication protocol is the more conformed a sample will be in comparison to un-complemented scaffold and misfolded origamis. This allows separation of individual species within a sample by their relative conformation using methods such as agarose gel electrophoresis. It is clear from this work that significant levels of folding, certainly for at least some origami designs, do not occur over wide, and universal, temperature dependent domains but quickly over very structure specific thermal transitions.

### 3.4 Characterisation – DNA and DNA origami

As DNA in single or double strands sits well below the double figures nanometer level (0.34 nanometers base width and 1.1 nanometers per base height) imaging is well beneath the diffraction limit of any visible light microscope and this remains the case for even large scale DNA origami which incorporate many thousands of individual base pairs into fabrication.

Typically visualisation is divided into 2 distinct methodologies: indirect visualisation, in which DNA and DNA origami structures are examined indirectly and only general properties can be ascertained, such as conformation or concentration within a solution, or directly in which very specific structural information can be obtained, but this process usually involves fixing of a sample onto substrate and the loss of information pertaining to the original bulk sample.

It is usual for studies involving DNA origami to make use of both methods in a feedback cycle usually beginning with indirect imaging followed by direct visualisation and mapping. This feedback process is described in more detail along with the progression of our own structural work and evolution of

protocol in chapter 5. In contrast this chapter contains a general description of the mechanics behind most common imaging techniques used during DNA origami fabrication.

### 3.5 Agarose Gel Electrophoresis

The first use of electrophoresis as a method of separating different conformations of DNA and RNA came in 1962 by Matsubara and Takagi [76]. This method of electrophoresis is used to effectively separate DNA fragments between 100 and 25000 Bases in length. When an agarose gel is created its polymers form non-covalent networks of bundles where the gels effective pore size is directly proportional to the concentration of agarose present [77]. Once a gel is set it is placed into an electrophoresis tank, filled with electrophoresis buffer, and a current passed between an anode and cathode at separate ends of the tank. Due to DNAs highly negative phosphodiester backbone it will migrate towards the positive end of the tank.

There are 7 characteristics which affect the migration of DNA through a gel [77]

1. The size of the DNA molecule
2. The concentration of agarose in the gel/its relative pore size
3. The conformation of the DNA
4. The voltage applied
5. Other contaminants within the solution/DNA stains
6. The specific type of agarose used to create the running gel
7. The buffer used

Electrophoresis running buffer contains chemicals which maintain the current across the tank and buffer the pH of the solution to protect the sample held within from degradation. There are 2 main electrophoresis buffers used TAE and TBE. Each buffer contains Tris, which regulates the pH of the running buffer, acetic or boric acid which maintain the electric current across the tank, and ethylenediaminetetraacetic acid (EDTA) which is traditionally used to protect DNA within the sample from nuclease activity. While both buffers can be used to separate DNA sequences from several hundred

to several thousand bases TBE is associated with analysis of sequences smaller than this and TAE with sequences larger [64]. A further requirement for analysis of DNA origami structures via gel electrophoresis is the addition of MgCl<sub>2</sub> to the running buffer. If MgCl<sub>2</sub> is not present then the structures will degrade very quickly as they travel through the gel.

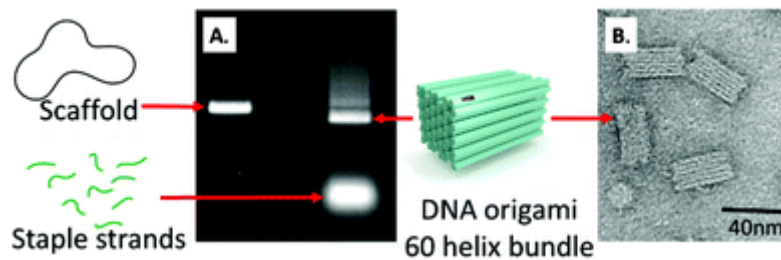


Figure 35 A – 2 samples being analysed by agarose gel electrophoresis. The sample on the left contains only scaffold. The sample on the right contains a successful fabrication of scaffold, staples, and origami. B – The sample in the highlighted band visualised via TEM [79].

Figure 35 offers a good examples of a typical agarose electrophoresis visualisation of a successful fabrication run. It is notable that there is a smear above the band containing the correctly fabricated DNA origami. This is likely misfolded origami and aggregates of scaffold DNA. There is also a distinct band visible parallel to the scaffold lane on the left likely containing un-complemented scaffold. As the staples used for fabrication are much shorter than both scaffold and origami they travel relatively quicker through the agarose gel. The staple band also appears as a less defined band as the scaffold and agarose because it likely contains DNA sequences with varying lengths.

### 3.6 Atomic Force Microscopy

AFM is distinct from many other forms of microscopy in that it does not rely on direct examination via EM waves, or electrons, but rather uses a probe to interact with a sample directly. AFM is useful for examining naked DNA based materials as they are smaller than the visible light range, meaning they cannot be effectively illuminated by wavelengths within the optical regime [66], and typically require staining/coating when examined by wavelengths of sufficient size to interact correctly with the structure, such as electrons [80].

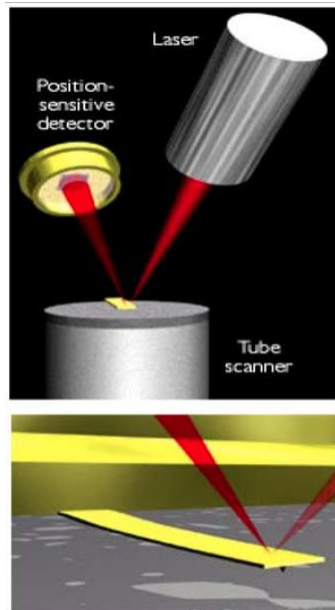


Figure 36 A illustration of the major interactions used by an atomic force microscope to analyse a surface [81].

AFM operates by examining, in a raster fashion, the interaction between tip and surface over a given area (Figure 36). A laser beam is bounced from probe mount to detector and the difference in reflection intensities, as the probe interacts with the contours of the surface as it scans, is interpreted by software connected to the AFM and converted into mechanical properties or surface maps.

### 3.7 Contact modes

There are 3 main methods of AFM which reflect the tips relative position, and interaction with, a sample during mapping.

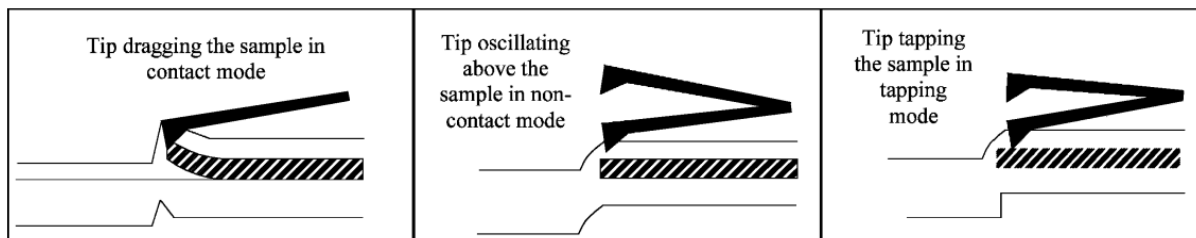


Figure 37 The three main modes of AFM operation: Contact, none-contact and tapping mode [82].

Contact mode is employed when a probe contacts a sample during measurement and is then dragged across the substrate. This mode provides a great deal of information about a sample, as information can be gathered directly without the significant extrapolation steps involved in the modes discussed below,

however contact mode can be damaging to soft samples and debris can become stuck to the probe [80,82].

Non-contact mode describes measurements taken when the probe does not directly interact with the sample being analysed [80,81]. The probe is oscillated closely to the surface of the sample, within range of Van der Waals interactions, changes in oscillation measured, and the forces acting on the probe calculated which can be used to define the surface layer. This method is challenging due to the range of Van der Waals interactions being very low, and measurements taken in ambient conditions being susceptible to airflow and fine layers of moisture, sometimes meaning the true surface cannot be found correctly or accurately [81].

Tapping mode is a development which utilises aspects of both contact, and non-contact, measurement. The probe is oscillated above the surface of the sample (at, or near, the probes resonant frequency) and lowered towards the sample. The probe now gently interacts with the sample and is then lifted away. The changes in the probes oscillation due to the interactions with the surface, as well as information about adhesion etc, can then be calculated and the surface mapped.

Of the three main modes associated with AFM, seen figure 37, typically imaging of DNA origami will occur in none contact or tapping mode. This is due to damaging effects which can occur on DNA based structure when scratched with sharp AFM tip [80,82] which could also lower the resolution of the recovered surface.

For the images presented as evidence for fabrication of both naked, and metalised, DNA origami structures in this work, Quantitive Mechanical Mapping mode [83] which is a tapping mode technique, was used on a Bruker Dimension Icon AFM with the protocols provided in chapter 8.

### 3.8 Conclusion

DNA origami is dependent upon a combination of biological (Scaffold strand) and synthetic (Staple strand) processes which exploits the benefits each system provides. Employing biological foundries mean large, 1000's of bases long, scaffold strands can be created in significant throughput but are reliant

on pre-existing sequences (For example the common M13MP18/P7249 scaffold is a bacteriophage plasmid) and therefore highly inflexible in sequence (A different scaffold can be chosen – but a small section of its code cannot be modified independently). In contrast artificially synthesised sequences are very short, where most of the strands used in this project were 32 bases in length, but are highly programmable. Also, artificial sequences allow for the addition of chemical groups, such as thiols, which allow for interaction with metals and other external groups. Combining the throughput and size of biological scaffolds with the flexibility and functionality of artificial staples allows for large scale nanostructures with programmable metallisation.

Specific protocols for DNA origami preparation and fabrication vary significantly between groups. In terms of preparation the rate limiting thiol purification step is a strong example of a protocol which has become redundant over time (Or is certainly redundant in the DNA based solutions employed during DNA origami fabrication). While thermal cycles are broadly understood, in that it is recognised that there is an initial hydrogen bond breaking step, at a high temp, which is then lowered over time to allow a structure to form, it is common for this to be an unrefined process which is not examined further once a fabrication is at least somewhat successful. While this may not be an issue for lab-based fabrication for material applications it is crucial to ensure throughput and fidelity.

Once fabricated the two main methods for analysing samples are AGE and AFM. AGE is an indirect method, which only charts the flow of a species within a sample through an agarose matrix, and only speed of migration is displayed with all other information being inferred from pre-existing knowledge of the sample being monitored. In contrast AFM provides very detailed information on the fine structure of a DNA origami but only represents a small fraction of the volume of the sample being analysed.

## Chapter 4

### 4.0 Metallisation theory

For studies focusing on DNA origami as a foundry for optical or electronic devices and materials metallisation must take place. There are several methods of metallising the DNA structure, and more specifically DNA origami, and also approaches which take advantage of Watson-Crick base pairing, or other means, to attach metals to specific sites on a DNA origami. In broad terms these metallisation approaches can be divided into 2 categories: Site specific or global. Site specific metallisation requires a seeding site to which a particle can be attached, or from which further metallisation can take place, in contrast global metallisation methods target the DNA structure as a whole and metallisation occurs universally. A common method of site-specific metallisation of DNA origami is via conjugation of thiolated DNA tethered gold nanoparticles which are bound to a region of the DNA origami which displays an available DNA sequence complementing that of the thiolated DNA. Use of such nanoparticles requires an understanding of the synthesis processes used to fabricate them and the physical properties associated with specific size ranges post fabrication. Furthermore, synthesised nanoparticles must be stabilised and then reduced in volume/significantly increased in concentration to provide a solution appropriate for fabrication.

### 4.1 Gold nanoparticle synthesis

The first synthesis protocol for Au nanoparticles in the sub 100 nanometer domain was created by Turkevich [84] who used sodium citrate as a reduction agent to nucleate gold chloride ions in a controlled manner. This ‘Turkevich’ method is still used today, in a modified format, and is associated with the fabrication of monodisperse nanoparticle solutions down to 10 nanometers in size. Furthermore, the citrate layer stabilising the nanoparticle is easily replaced by other chemical groups allowing quick functionalisation of the nanoparticle surface without further purification steps [85]. However, for synthesis of sub 10 nanometer Au nanoparticles, which offer an increased feature resolution for origami decoration, many methods require the use of stronger reducing agents which can

block the surface of the nanoparticle preventing further functionalisation [86]. The dual use of sodium citrate and tannic acid was first conducted by Muhpfordt [87] but more recently refined [85] to allow the synthesis of fairly monodisperse 3.5 nanometer gold nanoparticles. This method provides both the smaller scale of nanoparticle associated with stronger reduction agents while also allowing post functionalisation of the nanoparticle.

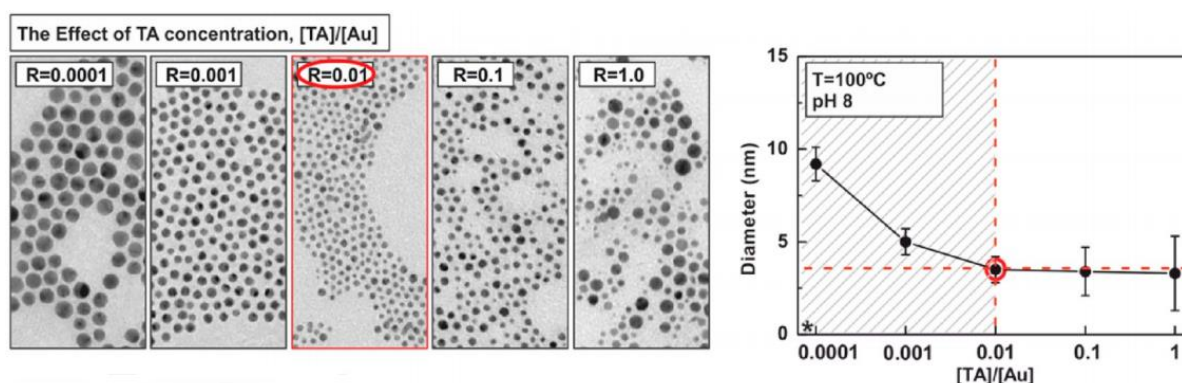


Figure 38 Left - nanoparticles observed directly by TEM and the respective tannic acid to gold chloride ratio used (The concentration of sodium citrate remained constant). Right – The diameter of particles measured at the various concentration ratios. Red highlights the 3.5 nanometer solution [85].

This method also provides a pathway for the synthesis of particles of 9 and 5 nanometers directly (figure 38) and also the indirect synthesis of a range of particles between these sizes by careful extrapolation of the ratios used in fabrication. The synthesis is conducted by boiling ultra-purified water followed by stepwise addition of reagents making the process quick and facile to reproduce.

The process used in this iteration of the tannic acid gold nanoparticle synthesis was utilised significantly during the course of this work. Full synthesis protocols are given chapter 9.

## 4.2 Gold nanoparticle concentration

Before nanoparticles can be used as decoration for a DNA origami sample they must be concentrated to a level high enough for a significant percent of binding regions on each origami to be quickly and effectively occupied. While estimates vary a typical reaction uses around 10 nanoparticles per binding site [14]. Typically gold nanoparticles synthesised by the classical Turkevich or reverse Turkevich method or the modified tannic acid route have an as synthesised concentration of between  $\sim 1$ , for larger

10 nanometer particles, and 35, for the smallest 3.5 nanometer particles [85], nanomolars. To functionalise a 10 nanomolar DNA origami solution, with only 4 binding sites per DNA origami, a functionalised nanoparticle solution of at least 400 nanomolars relative concentration would be required. A very common method of increasing the relative concentration of a gold nanoparticle solution, as well as increasing its resilience to ionic degradation, is an initial replacement of surface bound citrate ligands with more strongly bound phosphine ligands using dipotassium bis(p-sulfonatophenyl) phenylphosphane dehydrate (BSPP) [14,67]. The ligand exchange process means that the nanoparticles can now undergo reversible aggregation when NaCl is added to the nanoparticle solution.



Figure 39 A gold nanoparticle solution is aggregated, pelleted and resuspended into a lower volume solution with a higher concentration. Left to right – 1. The as synthesised solution which has undergone surface ligand exchange via BSPP. 2. Solid NaCl is added to the solution until distinct color change (From the very distinctive wine red associated with small gold nanoparticles to purple/blue/grey). 3. Once aggregation has occurred the sample can be centrifuged and the colloid stably pelleted. 4. The pellet is resuspended with a lower volume creating a higher concentration solution than the original.

Figure 39 outlines the process whereby a low concentration nanoparticle can be used to create a higher concentration solution of smaller volume. This process is typically 2 set: Firstly the as described NaCl aggregation step is performed but this is then followed by a second methanol based precipitation, once the NaCl containing supernatant has been discarded. This increases the effect of any residual NaCl, aggregating the solution again but with significantly less NaCl present and the surpennatant again discarded. As methanol readily evaporates at room temperature this process uses the initial high NaCl

step to aggregate the solution completely and then the second methanol step to remove any residual NaCl remaining from the first step leaving a relatively uncontaminated pellet, which can be readily resuspended in ultra-purified water once the process has been completed.

### 4.3 Nanoparticle functionalisation

Until this point we have discussed DNA in terms of only its physical properties and interaction with other strands/helices. DNA modified either on its 5' or 3' terminator, or with many other similar modifications, still maintains its ability to bind to its complementing sequence. The first use of DNA to bind an artificial group took place when Mirkin used a thiol group [88] attached to the 3' terminator of a single stranded oligonucleotide to bind it to the surface of a colloidal gold nanoparticle.

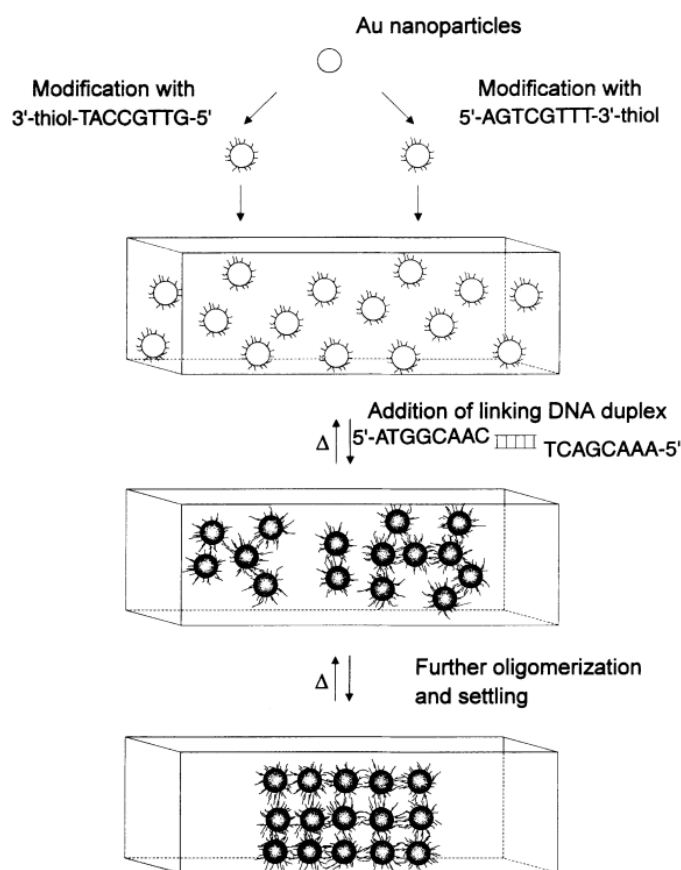


Figure 40 Au nanoparticles are functionalised with uncomplementing sequences both terminated on their 3' with a thiol group. A sequence complementing both thiolated sequences is added. The nanoparticles begin to aggregate. Over time aggregation becomes universal and little to no individual nanoparticles remain in solution [88].

Mirkins group used the method illustrated in figure 40 to show that DNA could be used to reversible bind gold nanoparticles in a controllable manner. When the aggregated solution is heated until the point that hydrogen bonding between the linker strand and the 2 thiolated strands breaks down the nanoparticles are released and go back into solution. As the temperature is lowered the linker strand again binds the thiolated sequence attached to the nanoparticles and the aggregate begins to reform.

This initial study highlights the ability to use Watson Crick base pairing as a guide to attach nanoparticles at a site-specific point on another sequence. It also highlights that this attachment can be manipulated by effecting the physical environment of the DNA sequences in question in a reproducible manner.

Another significant development highlighted by Mirkins work was the use of the thiol as a binding agent between DNA and nanoparticle. As thiols contain a sulphur atom, which forms a very strong naturally occurring bond with gold, they provide an ideal pathway for the secure attachment of a DNA strand to the surface of a particle while still allowing it to extend outwards into the space proximal to the particle making them available for complementation.

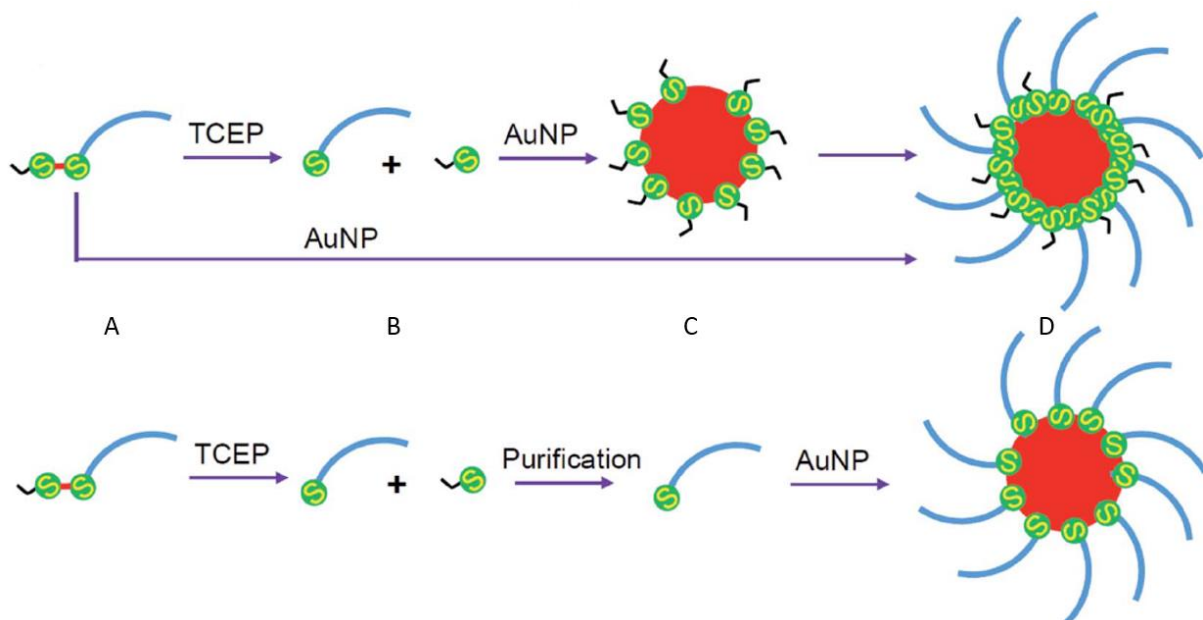


Figure 41 The effects of dithiol cleavage and purification on gold nanoparticle DNA functionalisation density. A. A di-thiol molecule with an attached DNA sequence is cleaved via TCEP. B. Cleavage leaves a thiol with attached DNA sequence and an unassigned thiol. C. If unpurified from the solution

the unassigned thiols quickly bind to gold nanoparticles. D. Due to the small size of the unassigned thiol the loading density of DNA on the gold nanoparticles surface essentially remains the same [88].

As mentioned above, a thiol group is not synthesised independently, two thiol groups, which present as a disulphide bridge, are created with one attached to the DNA sequence of interest. It is possible to cleave the two thiol groups, using a reduction agent such as TCEP as shown in figure 41, and then purify the solution of unassigned thiols and excess reduction agent leaving only thiolated DNA present. If this step is not conducted the smaller thiol sequences bind to the nanoparticles surface. It is possible that this, potentially unwanted, binding could lead to a lower number of DNA sequences attached to the nanoparticles surface. However, none DNA presenting thiol groups are shown to be much smaller in footprint compared to a thiol group with a DNA sequence attached and, it has been shown that a 13nm gold nanoparticle can absorb ~1200 unassigned thiols and only ~100 thiolated DNA sequences [22].

Given that when using commercially obtained dithiols [23] the ratio of unassigned and sequence attached thiols is 1:1 this would suggest that only 1/12<sup>th</sup> of all sequence attached thiols would be displaced. If a 13nm gold nanoparticle was functionalised with unpurified dithiol sequences 92 sequence assigned thiols would be present out of a possible 100 with the remaining regions taken by 100 unassigned thiols. Given the rate limiting process of reduction and purification of dithiol linkers, any small loss of loading density would be outweighed by the significant reduction in thiol DNA availability due to a solutions reduced concentration post purification.

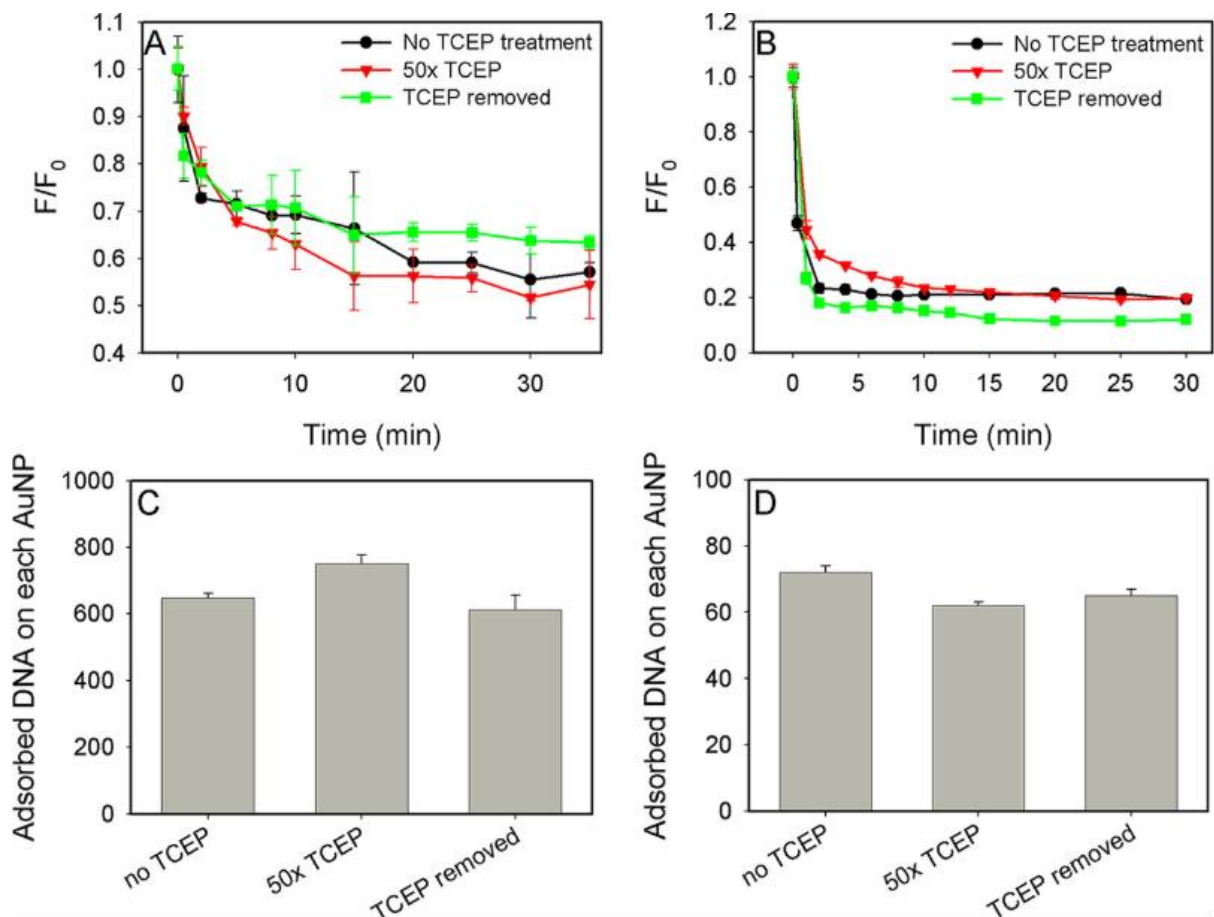


Figure 42 The effect of TCEP reduction of thiolated DNA conjugated to 13 (A) and 50 (B) nanometer gold nanoparticles. Specific loading capacity is shown for 13 (C) and 50 (D) nanometer gold nanoparticles [67].

When observed directly there is little difference in loading capacity between thiolated DNA which has been treated with TCEP, thiolated DNA that has been treated with TCEP and then purified, and then thiolated DNA which has not been reduced (Figure 42). Certainly, in the case of 13 nanometer gold nanoparticles, closer in size fit to those used in the fabrication work conducted in this project, loading density is higher when TCEP based reduction does not take place.

Studies have shown that when creating self-assembled monolayers disulphides can be cleaved by interaction with the gold surface without external interference [70]. This would suggest that the same is also true for gold nanoparticle surfaces. It is possible that as this reduction method was first cited in the seminal gold nanoparticle functionalisation paper conducted by Mirkin [88], conducted in 1996, that the post TCEP purification step was conducted due to residual contaminants from DNA synthesis techniques at this period potentially interfering with functionalisation or causing aggregation of the gold

nanoparticles. Over time DNA synthesis techniques have improved and the purification step has become redundant.

Since this inception point there have been a significant number of studies conducted for the creation DNA functionalised nanoparticles. As both gold nanoparticles and DNA are negatively charged molecules effectively mediating attachment requires specific protocols. This concept can be extended more broadly to encompass the conjugation of any functional group to a DNA sequence. Essentially the DNA sequence, or nanoparticle, must display a group capable of binding them securely together and any repulsion between the 2 groups must be mitigated allowing the binding to take place.

When working with colloidal nanoparticles the capping agent used during synthesis must always be considered as there will need to be an exchange, or interaction, between the ligand which has stabilised the colloid during synthesis and the functional group used to attach the DNA sequence of interest to the nanoparticles surface. This exchange must also take place in a manner which maintains the colloid. For example if both nanoparticle and DNA sequence have a negative charge, which must be overcome for the two to come into proximity, it is not enough to add positive ions until all negative surface charge on the nanoparticle sample is mitigated as doing so in an uncontrolled manner would lead to failure of the colloid/complete aggregation.

For our purposes synthesis is always conducted via a modified Turkevich method where trisodium citrate and tannic acid become the ligands on the nanoparticle surface. While many of the methods we will discuss were conducted before tannic acid was used as an additional reduction agent, during our work we have observed no anomalous effects arising from the presence of tannic acid on the nanoparticles surface. This is likely due to the significantly stronger affinity of the thiol group to the nanoparticles surface, than tannic acid, and the natural and efficient exchange of the two groups.

An unrefined approach, employed by the Mirkin group in the seminal gold nanoparticle functionalisation paper, is to add the particles required for functionalisation and thiolated sequences in solution and then leave the solution to incubate at room temperature. Over time thiols will attach to the surface of the gold nanoparticle. To expedite this process the ‘Salt aging method’, was developed by

Mirkin [88], this method employs the serial addition of positive ions, such as NaCl, over time, to mitigate the negative charge of nanoparticle and DNA in such a manner that facilitates gradual attachment but does not lead to irreversible aggregation of the colloid before functionalisation can correctly take place [90]. While the original salt aging method can be successful it is also associated with long reactions times (Up to 40 hours) and can lead to irreversible aggregation of the solution [91]. Further enhancements of the method involve using surfactants to stabilise the solution during functionalisation, preventing aggregation of the colloid even when exposed to high levels of NaCl [92]. Using surfactants as a stabilising agent significantly increases the size of nanoparticle it is possible to functionalise using the salt aging method [93]. Sonication has also been shown to be effective in increasing loading density and attachment speed during functionalisation [93]. This effect is likely due to sonication dislodging any sequences not correctly attached to a nanoparticles surface creating space for new sequences to properly attach.

An alternative approach [94] uses a low pH solution to mitigate surface charges in a reversible manner. As the colloid in solution is not threatened with aggregation a relatively high concentration of positive ions can be used.

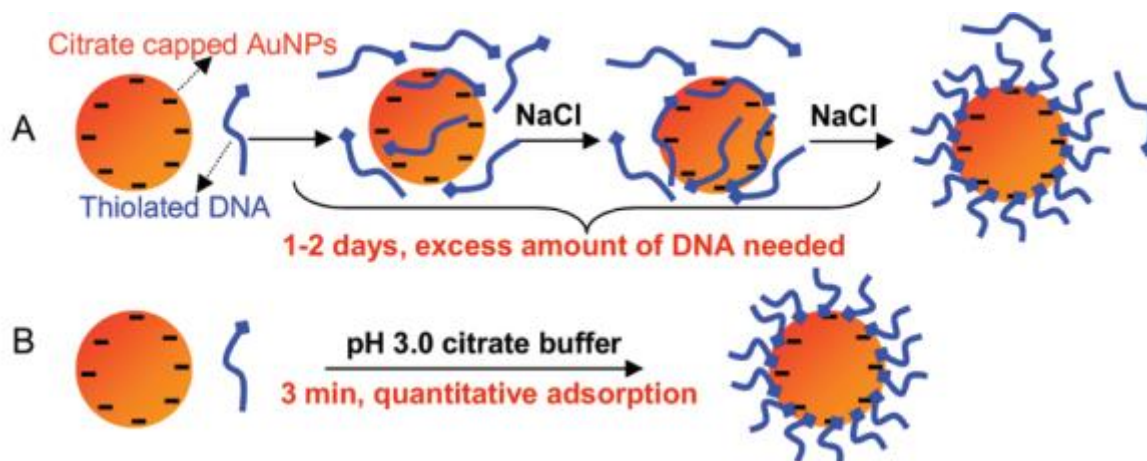


Figure 43 a comparison of the methodology of salt aging nanoparticles (A) and the low pH approach (B) [94].

In the low pH route the addition of NaCl over time is replaced with the addition of a single solution of pH3 sodium citrate buffer. As figure 43 highlights this method presents the potential of very quick reaction times, and unlike the salt aging method, with no risk of degradation of the sample.

The use of a thiol group to attach the terminal base of a DNA oligonucleotide to a gold nanoparticle was the first demonstrated of using a DNA sequence to create a programmable effect in a metallic nanoparticle system. Since this inception point there have been many protocols suggested for the functionalisation of gold nanoparticles, with DNA oligonucleotides, using a thiol group as the primary ligand. However more recently there have been other demonstrations of DNA sequences adhering to gold nanoparticles using an artificial group at the terminator of the sequence, but also using artificial sequences embedded in the phosphodiester backbone of the sequence, or by taking advantage of the naturally occurring properties of the backbone itself [95].

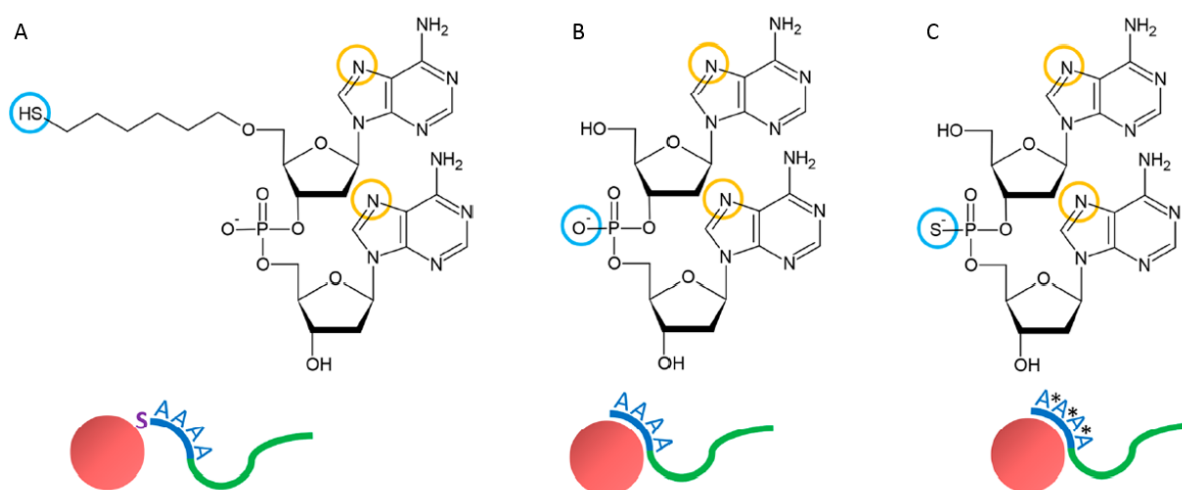


Figure 44 The primary group of attachment of DNA sequence to gold nanoparticle by various strategies. A. A thiol group present at 5' terminator of DNA oligonucleotide. B. The negatively charged oxygen atom present in the naturally occurring phosphodiester backbone of a DNA oligonucleotide. C. A sulfur atom replaces the negatively charged oxygen atom present in the phosphodiester backbone of a DNA oligonucleotide [95].

Figure 44 A. Presents the seminal thiol based route of attachment between gold nanoparticle and DNA oligonucleotide we have already discussed. In contrast figure 44 B. and figure 44. C. present back bone attachment points potentially present in continuous DNA oligonucleotide sequences rather than just the terminal 5' or 3' group. Terminal attachment and backbone attachment are characterised in different ways as highlighted at the bottom of figure 44. In thiol, or terminal attachment, the DNA sequence is attached to the surface of the nanoparticle at a single point, this leaves the rest of the oligonucleotide free to extend into the space away from the nanoparticle. In contrast when the tethering group of interest occurs in the backbone of the attached DNA oligonucleotide creating a different geometry whereby the

attachment point of the strand is adhered to the nanoparticle in a parallel fashion and the sequence is not available for complementation.

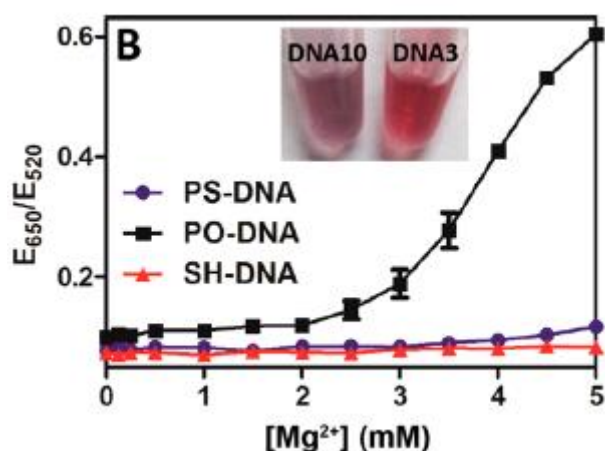


Figure 45 The stability of nanoparticles functionalised via different strategies and their stability in various levels of magnesium chloride. PS-DNA – A poly adenosine DNA sequence containing sulfur modifications along its phosphodiester backbone. PO-DNA – A poly adenosine DNA sequence without artificial modification. SH-DNA – A DNA sequence terminated with a thiol group [95].

Figure 45 demonstrates successful functionalisation by treatment of functionalised samples with ionic solutions that would irreversibly aggregate naked colloidal gold nanoparticles. The surface coverage of the nanoparticle by the DNA oligonucleotide, and the binding affinity between the nanoparticle surface and attachment group on the DNA oligonucleotide, define the ionic resistance of a sample. While poly adenosine DNA shows successful functionalisation and protects the nanoparticles at the lower end of the magnesium chloride concentration scale it becomes displaced at above 2mM and the sample aggregates. The sulphur containing attachment points present in the PS and SH containing DNA displays a much higher resistance to ionic interference of the colloid. It is notable that while the functionalisation protocols remain similar for backbone and terminal groups, in that ionic changes of the solution are employed to defeat point charges between nanoparticle and attachment site in a controlled manner, the low pH method does not occur instantaneously in backbone-based attachment. This attachment is instead conducted via a low pH initiation followed by an overnight salt aging step [95].

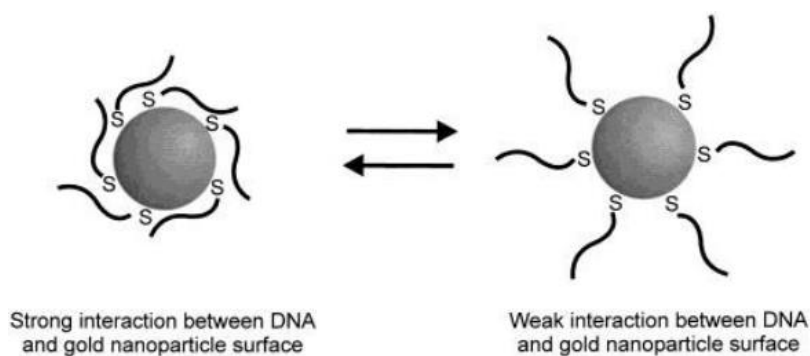


Figure 46 Demonstration of sequence affinity to nanoparticle surface on the availability of attached sequences for complementation [96].

Understanding the interaction between specific DNA base and gold nanoparticle is key not just for the attachment of sequences but also making the sequence of successfully bound DNA oligonucleotides available for complementation in further fabrication steps. It has been demonstrated [96] that thymidine has a significantly lower interaction with a gold nanoparticle surface than any other nucleotide. Thiol terminated poly thymidine sequences are ideal conjugates, allowing a much greater loading density on a gold nanoparticles surface than the other nucleobases [96], while the lack of affinity between nanoparticle and sequence leaves the oligonucleotide free to complement other sequences without interference. Conversely adenosine has been showed to have a very high natural affinity to the surface of sodium citrate stabilised gold nanoparticles [96]. This could potentially make thiol terminated adenosine sequences a poor choice of conjugate due to the adenosines propensity to wrap around the nanoparticles surface [97] and being unavailable for complementation in further steps (Figure 46).

#### 4.4 Nanoparticle Characterisation via UV spectrography

Once nanoparticles have been synthesised, they need to be somehow characterised to ensure relatively low polydispersity of size within the correct range predicted. While this can be done to an extent, via SEM and TEM, these systems only provide a snapshot of part of the solution, and do not provide any way of gauging a solutions specific concentration. Beyond this initial raw synthesis characterisation step it is also useful to be able to analyse a solution which has undergone the BSPP, NaCl, methanol stabilisation reduction method to ensure it has remained stable and there has been no significant loss of concentration.

A highly useful resource for the quick characterisation of nanoparticles within the 5-100 nanometer range is available using only UV-vis spectrography [98]. The tabular information provided as supplementary information [98], allows both the size and concentration of arbitrary nanoparticle solutions to be calculated quickly using only absorbance at 2 specific wavelengths (Although the method does assume that any nanoparticle sample being examined is relatively low in polydispersity in terms of nanoparticle size and shape) [98].

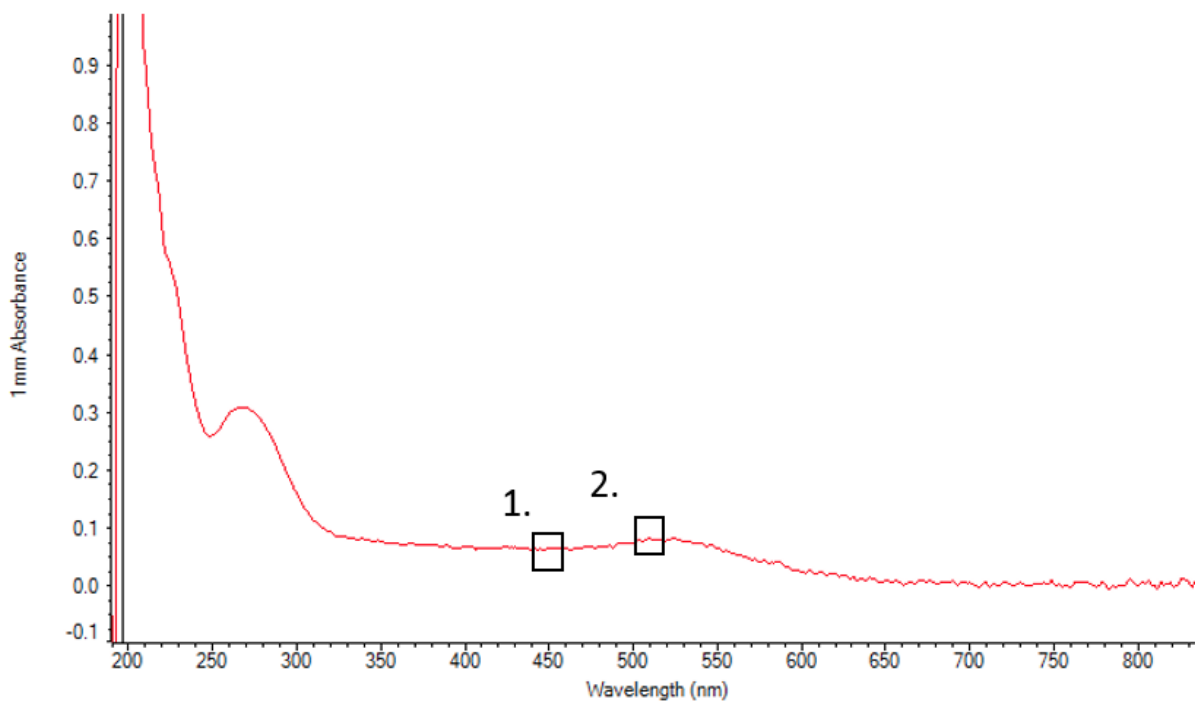


Figure 47 A nanodrop microspectrometer analysis of a 5 nanometer gold nanoparticle sample in, and around, the visible light range. There are 2 key results for determination of both nanoparticle size and relative concentration within the solution. 1. The result at 450 nanometers wavelength. 2. The peak absorbance above the 450 nanometer wavelength mark in the spectrum.

Value 2. in figure 47 is the surface plasmon resonance peak ( $\lambda_{spr}$ ). This value can be used to confirm the size of nanoparticles above 32 nanometers in size relatively easily by direct observation.

$\lambda_{\text{spr}} / \text{nm}$	$d / \text{nm}$
525.0	32
525.6	34
526.2	36
526.8	38
527.5	40
528.2	42

Figure 48 The specific surface plasmon resonance wavelengths of spherical nanoparticles between 32 and 42 nanometers in diameter.

As each spherical Au NP has a unique SPR it can be identified using tabular information alone. However because SPR effects become lower below this size range the ratio of absorbance between 2 individual wavelengths can be used to determine the size of nanoparticles down to the 3 nanometer diameter range (Figure 48).

$A_{\text{spr}}/A_{450}$	$d / \text{nm}$
1.10	3
1.19	4
1.27	5
1.33	6
1.38	7

Figure 49 The ratio of the absorbance at SPR and at 450 nanometers wavelength is correlated with nanoparticles between 3 and 7 nanometers in diameter.

The initial step of size identification is conducted using tabular information [98] as shown in Figure 49.

$d/$ nm	$\epsilon_{450} /$ $M^{-1}cm^{-1}$
2	4.25E+05
3	1.49E+06
4	3.62E+06
5	7.20E+06
6	1.26E+07
7	2.03E+07
8	3.07E+07
9	4.43E+07
10	6.15E+07
11	8.27E+07
12	1.09E+08
13	1.39E+08
14	1.76E+08

Figure 50 Nanoparticle diameter and associated extinction coefficient.

Once a diameter has been established this can be used to identify a specific extinction coefficient (Figure 50). Once this step is completed the molarity of the solution, in terms of gold nanoparticle concentration can be found by dividing the solutions absorbance at 450 nanometers wavelength by the extinction coefficient.

This initial step to determine size and concentration does not need to follow the more exhaustive method, used to determine size and concentration of nanoparticle solutions post functionalisation/purification, detailed in Chapter 13. As some losses are inevitable during the concentration steps it is advisable to confirm the nanoparticle solution is within the size range of interest and recover a broad concentration. As nanoparticle synthesis using the tannic acid approach is very sensitive to interference/contaminants if the solution appears as ruby red the synthesis has likely been successful. However, any recovered size and concentration values, even if rounded, can be used to determine the number of tethers required for functionalisation and the volume of raw synthesis to concentrate (There should be at least a 50% margin of error considered during this step – if the solution is too concentrated it can be easily diluted). More specific identification of concentration can be undertaken post functionalisation.

## 4.5 Origami metalisation

As mentioned for its use the field of nanoelectronics or optics DNA origami must be metallised. While there were previous examples of DNA being functionalised to create devices such as transistors [99] and globally metallised to create nanowires [100] the DNA was employed as an unstructured scaffold, whose chemical and physical properties could be exploited, rather than a spatially programmable material. The first example of metallisation of a DNA origami was conducted by Woolley [101] who described metallised DNA origami as making possible “the increased complexity and flexibility needed for both the design and assembly of useful circuit templates”.

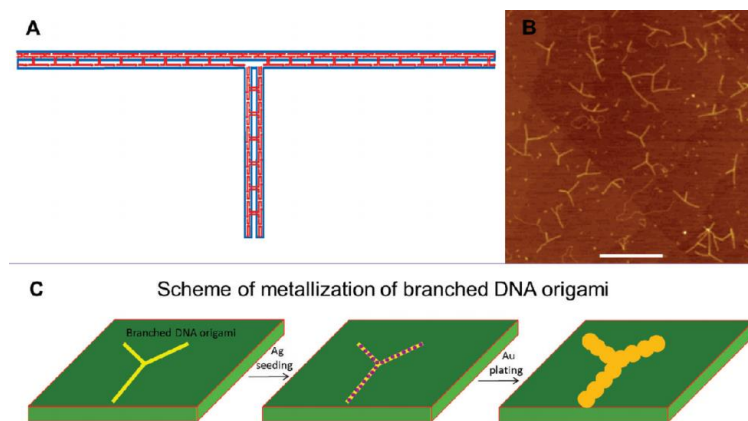


Figure 51 A DNA Origami pathway leading to metallisation as described by Wooley. A. The origami design. B. Images of confirmed origami displaying the broad design trend shown in A. C The metallisation process itself. Left – Naked origami on mica. Middle - Origami is seeded with silver ions. Right – The origami is further enhanced with a layer of gold bringing the diameter of the wire to >30 nanometers diameter [101].

While the metallisation pathway, shown figure 51, was successful it only provides a method for metallisation once an origami has been anchored to the origami surface. Furthermore, while deposition rates can be tuned to control the specific layer thickness of applied substrates, it is done in a global manner. For more precision and utilisation of DNA origamis low feature size metallisation would have to occur in a controllable or site specific manner.

Building on the practical description of the global metallisation method itself several challenges associated with the ongoing field of DNA origami metallisation, as opposed to challenges associated only with metallisation of the DNA molecular or double helix, were also discussed.

1. The stability of origami during the fabrication process
2. Increased selectivity to require metallisation of small origami designs

3. Securely attaching an origami to a substrate during the metallisation process
4. Interference from excess fabrication components (Staples) during functionalisation

While caveats 2. and 3. are only applicable to a strategy based on global metallisation conducted on a solid support 1. and 4. are more universal in scope. The stability of origami is dependent upon the ionic make-up of the buffer they are contained within and the reduction it provides to interhelical repulsion. Any modifications to origami which interact with these parameters must be carefully monitored to maintain structural stability. Interference from excess fabrication components is a still very much a key issue in origami-based construction and is discussed significantly in chapter 5.

An option for metallisation of DNA origami in a site-specific manner is the conjugation of nanoparticles tagged with complementary DNA sequences to sites on a DNA origami structure. The first demonstration of this method was described by Pilo-Pais [102] and provided a method by which these seed particles could be enhanced by the electroless deposition of silver.

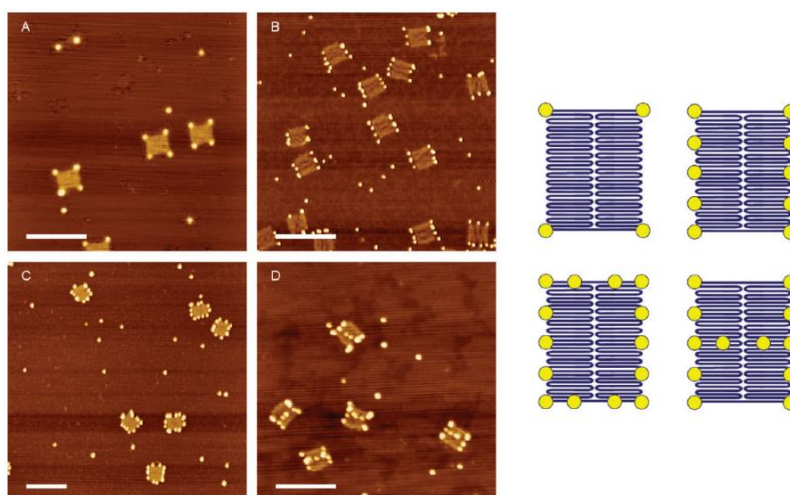


Figure 52 A-D – AFM images of various Origami templates metallised with gold nanoparticles in a site-specific manner. Right – The design templates showing the rational placement of nanoparticles at specific points on the origami design [102].

Figure 52 compares AFM images of site specifically metallised origamis to their respective design templates. Due to the careful monitoring of helical pitch during origami design it is relatively simple to extend a staple, already woven into the design, ‘out’ into the space surrounding an origami. This is discussed more significantly in design terms in chapter 7. This is done by selecting a sequence for the

extension which does not complement any existing sequence used in the origami design code. This extended, uncomplemented, sequence now presents a binding site for nanoparticle conjugation. The complementing sequence can be attached to a nanoparticle, such as through thiol groups attached to its 3' or 5' terminator and will naturally complement the sequence. This seminal work also mentions the key fabrication need of purifying excess fabrication components before successful fabrication can take place (However this time in the context of excess thiolated DNA used to functionalise gold nanoparticles rather than origami fabrication staples).

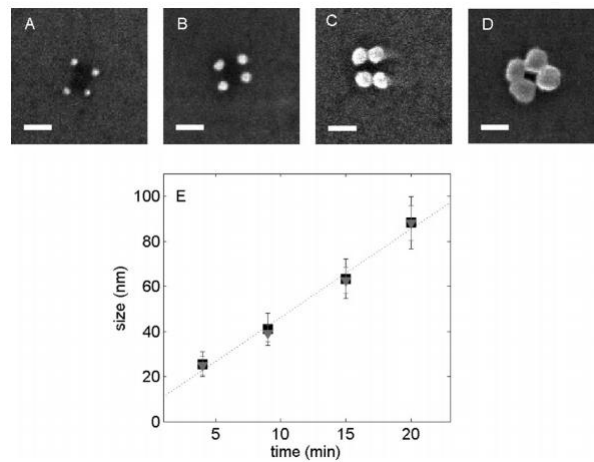


Figure 53 A-D - Reduction of silver used to enhance nanoparticles conjugated to a DNA origami. Bottom – the time scale associated with growth to certain sizes [102].

For the creation of continuously metallised circuits from individual seeding sites enhancement must take place in controllable manner. Pilo-Pais [102] also provided a method for this process, figure 53 demonstrates the time dependent reduction of silver onto metallic nanoparticles attached to an origami leading to continuous metallisation. This method is ideally conducted once a sample has already been attached to a substrate as the reaction can quickly be quenched by the washing of the substrate with ultra-purified water. The final width of any created continuous metallisation is largely dependent on the size of the nanoparticle and its proximity to other seeds. This length is controlled by both length of the sequence used to complement the nanoparticle to the origami, due to this value presenting the distance which must be overcome to fuse two particles, and the size of the nanoparticle itself, which dictates the starting width before enhancement of the exist nanoparticle takes place.

While the initial work conducted by Pilo-Pais was a step forward for site specific metallisation it still represents a fundamental limit in that both conjugation, and further enhancement, of the DNA origami structures must take place on a solid support. Furthermore, as shown in figure 91 even relatively short incubation periods create significant enhancement of the nanoparticles attached to the origami. This means that while continuous metallisation is possible using this method its feature size is still very high in relation to the potential, sub 10 nanometer, feature size presented by naked DNA origami fabrication itself.

Later work conducted by Wooley [103] refined the seeding approach by using sequential palladium seeding steps.

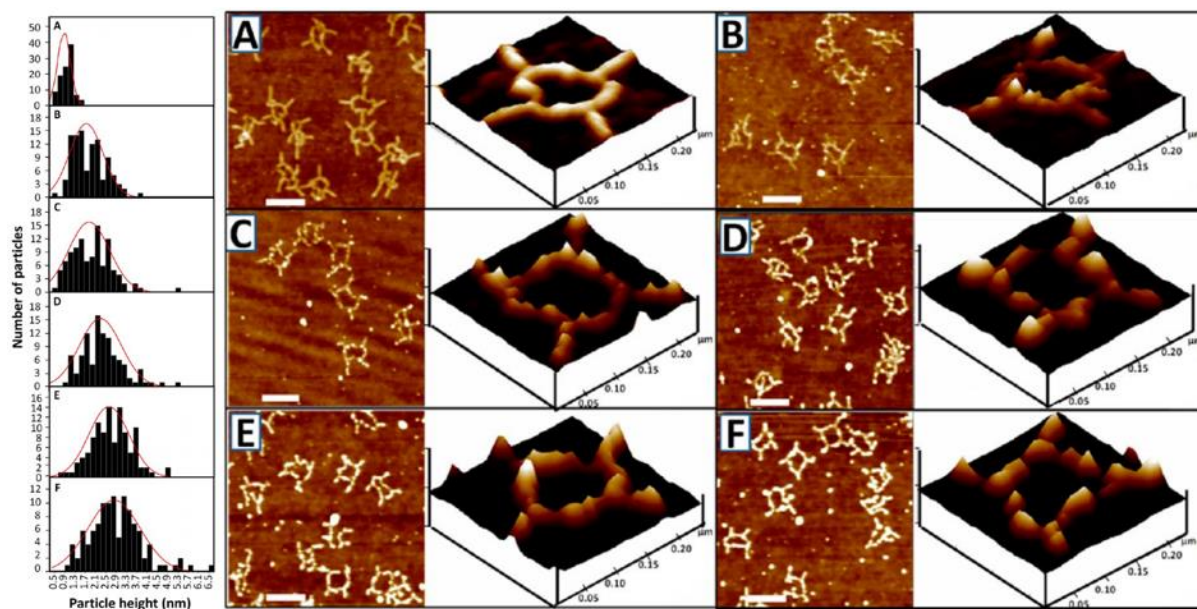


Figure 54 Sequential palladium seeding steps of DNA origami on mica. A. Unseeded origami. B. 1 seed. C. 2 seeds. D. 3 seeds. E. 4 seeds. F. 5 seeds [103].

The approach of multiple initial palladium seeding steps took significantly longer than the initial approach (25 minutes per seed vs 20 for the longest seeding step) but demonstrated a higher feature size resolution as shown in figure 54.

In contrast to methods where seeding of existing metallisation is conducted, in an unrestricted steady rate manner, where quenching of the reaction is conducted by washing away the reactants once a

predicted dimension has been achieved, there is also a strategy of using DNA origami as a restrictive mould [104].

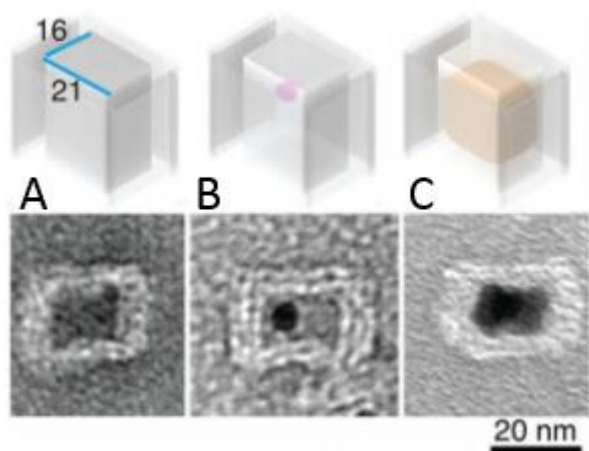


Figure 55 A pathway showing a DNA origami cast. A. The origami cast showing dimension size in nanometers. B. A conjugated gold nanoparticle which will act as the seeding particle. C. The cast once the nanoparticle has successfully been enhanced [104].

Figure 55 demonstrates the validity of using a DNA origami as a mould, or interactive component, rather than a passive scaffold. The method also details a 2-step enhancement process which is conducted in solution as opposed to on a solid support as was demonstrated by previous studies. While this study, which employs ascorbic acid as the reduction agent, makes no distinction between differing cast shapes or recovered concentrations it is likely that by doing so tuning of specific enhancement levels could be conducted in a similar manner to previous work [104,105].

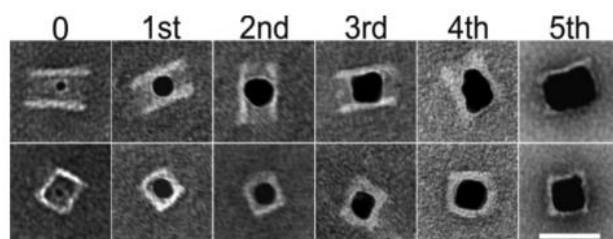


Figure 56 [105] A DNA origami casting approach utilising multiple seeding steps. Left to right – A DNA origami mould with single nanoparticle which will act as the seed. The seed increases in volume due to successive exposure to further enhancement steps until its growth is prohibited by the wall of the DNA origami cast

Similar work conducted by Seidel [105] demonstrated a similar DNA origami casting method but utilising a differing enhancement process. Concentration of origami casts present in solution is considered and hydroxyl amine is used as the reduction agent. The enhancement is conducted by

additions of either a single high concentration, or multiple low concentrations, for size tuning purposes as shown in figure 56, injections of gold chloride. Particle growth is suggested to resolve in less than 60 seconds using this method.

While the DNA origami mould casting technique does demonstrate success its enhancement level is dictated by the size of the origami structure cavity rather than the enhancement process itself. This makes the resolution of the feature size relatively low and, and while simple variations of shape, such as discs, and 'Y's have been shown, feature sizes below 10 nanometers have not been demonstrated.

While these techniques lack the required feature size resolution for nanofabrication on the sub 10 nanometer scale they do present many pathways and methods of interest. Enhancement of nanoparticle size, and continuous metallisation, through the tuning of reducing agent and metallic ion is demonstrably possible. Furthermore, the work conducted using DNA origami moulds suggests that DNA layers can be used to effectively end this enhancement, this would pave the way for distinct metallisations on either side of a structure.

A more recent metallisation method describes a high-resolution enhancement of naked single stranded DNA with copper or silver [106]. Condensation of DNA is seen in a wide variety of life forms and is facilitated by positively charged ions causing negatively charged DNA molecules to create tightly compact structures.

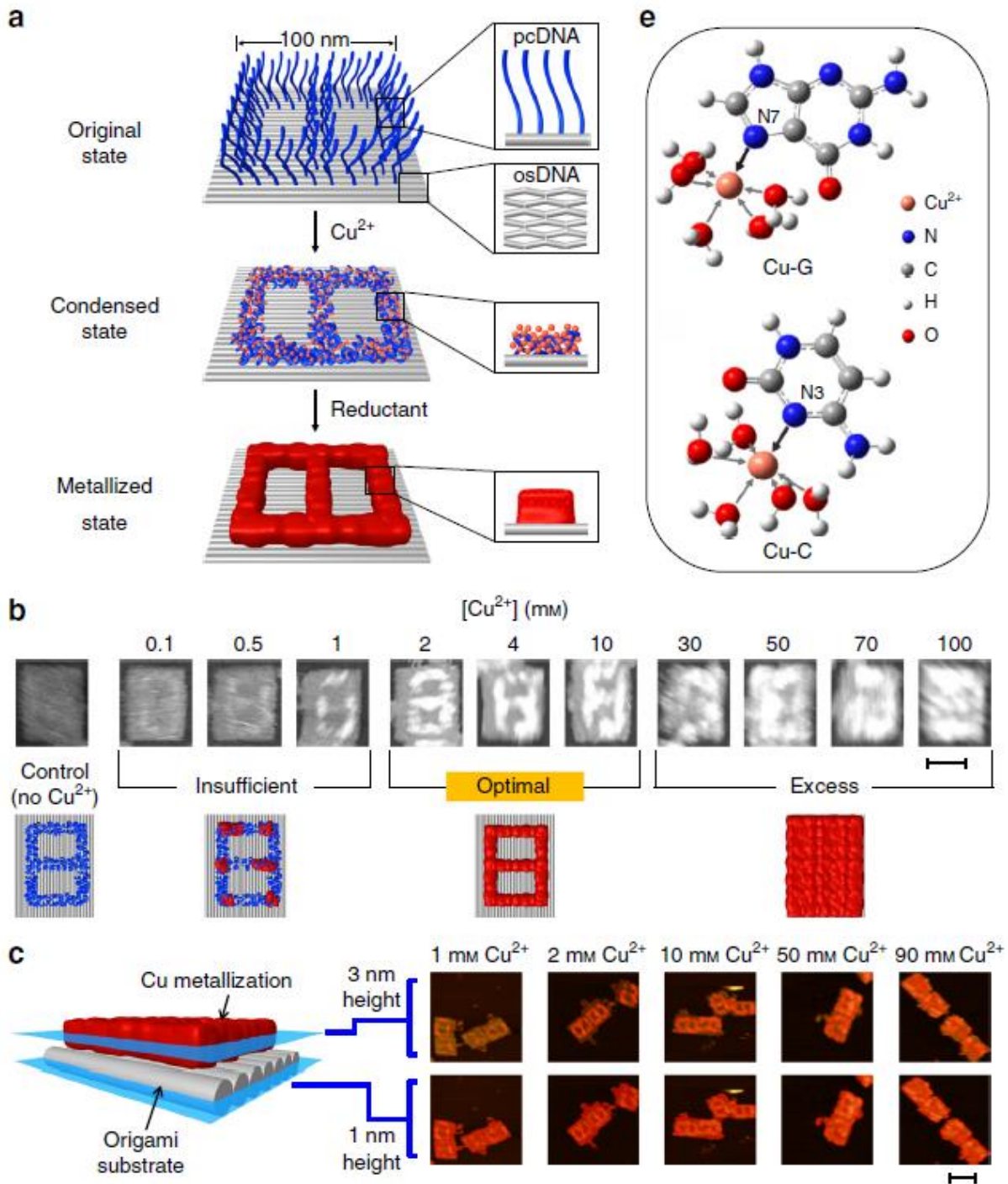


Figure 57. A condensation-based pathway of site specific metallisation. A. An origami with single strands extending out in an ‘8’ motif. Copper ions are condensed into the ssDNA. Further metallisation is conducted using the initial site as a seed. B. Concentration of the initial seeding step is key to overall metallisation. C. A 3 nanometer copper height is observed D [102].

Unlike previous methods the condensation approach, shown figure 57, allows selective placement of metals on a structure without the use of complementing strands. It does this by taking advantage of the uncondensed state of single stranded DNA protruding from the board at desired sites for metallisation.

When exposed to copper and silver ions the single stranded DNA collapse into a more condensed state while incorporating the new metals into its structure. It is notable that this pathway does not lead to any metallisation of the double stranded DNA making up the rest of the DNA origami board, likely due to its more condensed hydrophobic state, allowing feature size selective metallisation on a similar scale to DNA itself.

While the condensation method has a very high resolution it is not without drawbacks. Firstly, the concentration of ions used to condense DNA is crucial to the level of metallisation of the structures. If this level is too low metallisation will not be continuous. In contrast if this level is too high metallisation will overcome the design motif and become global across the board. The method demonstrates around a 3nm feature size and does not significantly rise away from the board even once metallisation has become global. As the board is secured to a mica sheet for metallisation there is no possible further manipulation of the board once this step has taken place.

While metallisation of DNA origami either directly through deposition of metal ions onto the structures surface, or site specifically via completing strands attached to gold nanoparticles, has been demonstrate in a variety of formats there are still significant challenges to be overcome. Protocols which rely on the adherence of structures to mica before functionalisation limit post treatment fabrication steps. This method also limits the throughput of the technique as only a small fraction of origami within a given fabrication solution will bind to the mica. There is also a fundamental limit of the number of structures bound in a single layer preventing further expansion. Further enhancement of site specific metallisation protocols is required to create truly continuous metallisation in a controllable manner between individual origami units. Currently enhancement of single nanoparticles leads to a granular effect and a vastly reduced feature size resolution. While metallisation of DNA universally through exploitation of its inherent physical properties allows more control, in regard to specific metallisation intensity, it does not allow site specific metallisation. Condensation, a promising technique that blends the 2 approaches, only allows very fine metallisation, leading to the risk of noncontinuous tracks.

## 4.6 Conclusion

Gold nanoparticle synthesis can be conducted efficiently, in a modest lab setting, creating nanoparticles down to the sub-10 nanometer level. The tannic acid/sodium citrate route is capable of producing 3.5, 5, and 9 nanometer nanoparticles with very slight modification of the method with high fidelity.

Gold nanoparticles are also beneficial due to characterisation of a samples size and concentration being achievable by simple measurements of absorbance in and around the visible light range of the electromagnetic spectrum.

In contrast direct metallisation of DNA itself, using classical methods, create significant global metallisation, that is well above the feature size presented by DNA itself and likely beyond the scope of the fabrication work required within this project. Newer metallisation attempts [106] provide a significant increase in feature size and allow selective metallisation of DNA within an origami design but in this case demonstrate a rough higher limit of 3 nanometers thickness before the design motif is lost. This low higher limit is also unsuitable for the work required within the project.

It is likely that enhancement of existing decorative nanoparticles [102,103] would be the most appropriate method of creating continuous metallisation to the levels and feature sizes required for the design specifications optical metamaterial fabrication dictates.

## Chapter 5

### 5.0 The requirement for purification

A common theme in structural DNA nanotechnology is the need for isolation of a finalised sample from its fabrication components after every fabrication step. Typically, fabrication of origami, or functionalisation of nanoparticle, features one larger fabrication unit being modified by many smaller units. To ensure fabrication, or functionalisation, is successful a higher ratio of smaller fabrication units is used.

Typically, origami fabrication is conducted at ratio of 10:1 Staples to scaffold. For nanoparticles this ratio is even greater, with 13 nanometer particles, a fairly common size for fabrication projects, employing a ratio of at least 100:1 thiolated DNA: nanoparticle [97] during functionalisation.

This ratio difference is increased by the need for the presence of multiple nanoparticles being available per binding site during fabrication. If each nanoparticle requires 100 DNA sequences to correctly functionalise, and each nanoparticle binding site requires at least a tenfold excess of nanoparticle to be correctly attached, then there are potentially one thousand complementary DNA sequences available for complementation per single binding site with the majority being unattached and highly mobile.

It is likely that if these smaller, unattached, fabrication components are present during the next step of fabrication they will be more mobile than those correctly attached to larger groups. Interference in fabrication will occur as these smaller unattached sequences bind their complementing sites on larger structures [103] before slower moving sequences which are correctly attached to either origami or nanoparticle.

### 5.1 Existing component purification techniques

During the fabrication work conducted throughout the project many different purification techniques were examined and/or tested on a variety of samples. Each technique can be associated with certain benefits and limitations; however, many techniques represent a combinatory approach (For example the

‘freeze and squeeze’ approach combines centrifuge, membrane separation, and AGE to recover a sample). We will begin by discussing separation by centrifuge and then progress into combinatory approaches. The novel approach developed as part of our work is discussed later in chapters 10 and 14.

## 5.2 Centrifugation based techniques

An option for the purification of gold nanoparticles, from another species of significantly lower molecular weight, such as thiolated DNA, is a series of spin cycles at gravities sufficient to bring the colloid out of solution (while not effecting the contaminant) in a reversible manner. Once the sample of interest is brought out of solution, or ‘pelleted’ at the bottom of the container it has been centrifuged in, the supernatant can be removed, and fresh solute added. After several cycles the sample of interest will be effectively purified of any contaminant.

SGNP Size (nm)	Speed (rpm)	Notes
1.8-5	150000	Ultracentrifuge
7	20000	
10	15000	
15	12000	
20	10000	
30	6000	
40	5000	
50	4000	
60	3500	
70	3000	
80	2500	
90	2000	
100	1500	

Table 1 [107] The associated centrifugal forces to ‘pellet’ gold nanoparticles from solution (It is assumed that revolutions per minute is equivalent to relative centrifugal force)

While the centrifuge method is viable for nanoparticles above 10 nanometers in diameter, in a lab-based setting, upwards of 15000 RCF requires the use of industrial centrifuge. These centrifuges are typically larger units as they must be able to control the strong forces being manipulated within. Also, in ultracentrifuge volumes centrifuged are at the millilitre and above level making manipulation of the microliter volumes associated with origami decoration highly challenging or not possible.

For these reasons it is uncommon to see centrifuge without modification used as a purification method for functionalised gold nanoparticles any smaller than 10 nanometers in diameter. Beyond this point

even small reductions in size require significant jumps in the centrifugal force required to sediment the colloid from the solution.

Raw centrifuge is not appropriate for purification of excess staple DNA from fabricated structures, for the same reasons it is not practical to pellet near ultra-small gold nanoparticle samples due to their low molecular weight, therefore DNA origami cannot be practically centrifuged using conventional centrifuge.

### 5.3 Molecular Weight Cut of Columns

A modification of the classical centrifuge method, a MWCO membrane is fixed in the centrifuged device, when centrifuge is engaged a fraction of the solution travels through the membrane. Anything smaller than the membranes pore size is taken with it and anything larger is retained in the sample. This approach requires multiple cycles, as only a fraction of the solution is purified in one cycle, as opposed to the almost complete purification demonstrated in a full sedimentation run. It has been noted that for removal of >99% of staple strands from a solution using the MWCO method requires at least 5 cycles with a recovery of <50% of the original DNA origami sample after the same 5 cycles [108]. Furthermore, high concentration, fragile samples, or samples containing a species of interest close to the MWCO point, which includes functionalised gold nanoparticles, destruction of sample and/or clogging of the MWCO membrane is observed making this approach sometimes unviable [102].

### 5.4 DNA precipitation

DNA origami precipitation is a method for DNA origami purification, and concentration, which integrates centrifuge with PEG based precipitation. The technique builds upon existing methods of native DNA purification via the use of PEG polymers as crowding agents [109]. The method is straight forward, employing a single calibrated buffer to bring the fabrication solution containing the DNA origami to a specific chemical composition, followed by a centrifuge step and an incubation period [108].

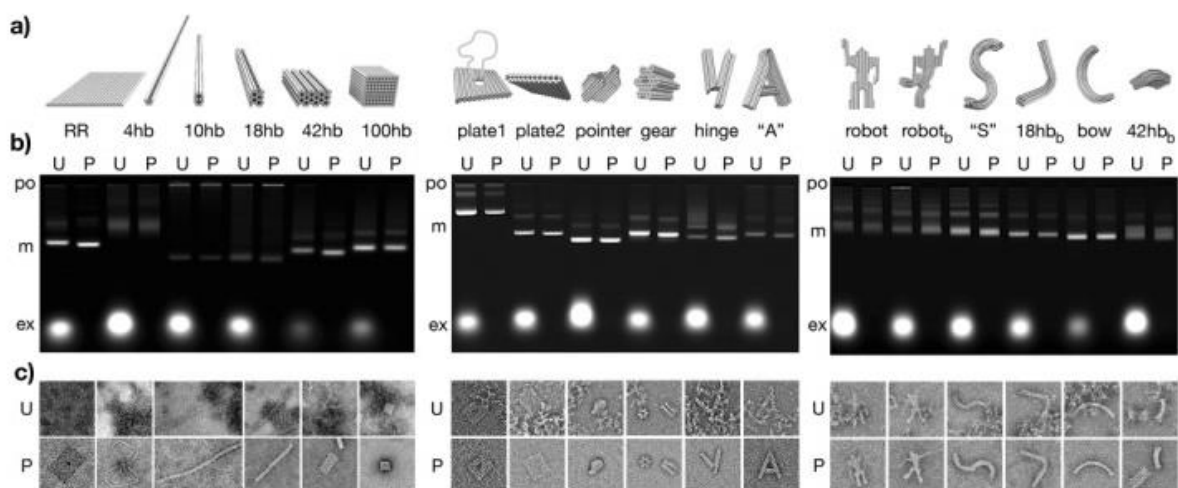


Figure 58 AGE and TEM analysis of structures shown in a). b) AGE of samples where po in the loading pocket, m is the origami band, and ex is the excess staple band. Below each structure is a ‘u’ unpurified sample and ‘p’ purified sample. C) ‘u’ unpurified and ‘p’ purified samples are examined via TEM.

It is notable that of the examples provided by the paper two specific DNA origami geometries have similarities to the one we employ [99]. Structure ‘RR’ figure 58 is a flat sheet, as is our breadboard, and the purified sample displays slightly higher mobility than the unpurified sample. Furthermore, sample ‘plate 1’ contains a single strand loop which ejects out from the structure in a similar manner to the tethers our design employs to conjugate nanoparticles to the boards surface. It is noticeable that ‘plate 1’ displays a lower intensity purified, than unpurified, DNA origami band when examined via AGE. While our work using this technique was somewhat successful, some losses were detected, and purification of excess staple strands not complete. It is likely our structure, which contains many single stranded domains, was not an ideal candidate for PEG based precipitation. Furthermore, the chemical used to stain DNA within AGE gels during this work, ethidium bromide, is not an ideal marker for single stranded DNA [110] and characterisation of remaining strands post purification was not total.

## 5.5 AGE based purification

As discussed in more detail in chapter 12, and demonstrated in images from most papers featuring DNA origami fabrication [3,51,57,58,59], AGE is a very common technique for the separation and analysis of DNA origami and their fabrication components. Beyond use as a purely analytical tool agarose gel

electrophoresis has also been demonstrated as a means of purification/recovery of DNA origami and its fabrication components from AGE.

## 5.6 The Freeze and Squeeze

The Freeze and Squeeze recovery method [110] is a commonly used technique to recover DNA origami post AGE but is associated with a low yield of recovery [111] which was observed when the technique was applied to fabrication work conducted in the creation of this thesis.

A significant advantage of the freeze and squeeze method is that it can be used to purify any species from a pre run AGE that can survive the process.

Originally described as a method of freezing a block of agarose, post electrophoresis, it presents a quick and easy method of recovering a specific DNA, or DNA conjugated, species from an agarose gel electrophoresis run by hand.

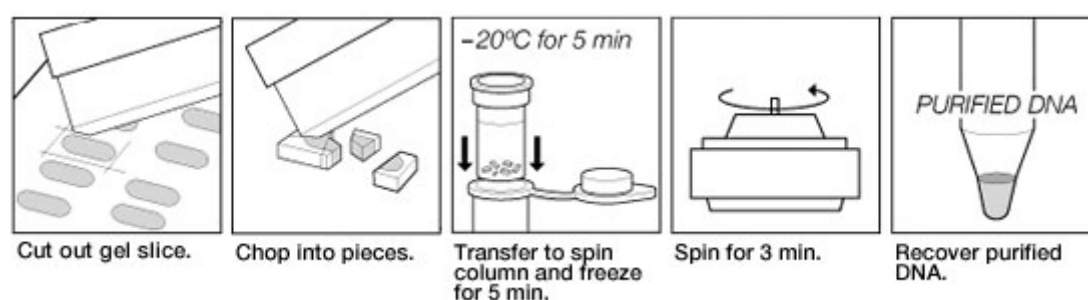


Figure 59 Left to right - the process of Freeze and Squeeze based purification with a commercially available kit [110]

Contemporary Freeze and squeeze kits use centrifugal force to 'squeeze' a sample and a size exclusion membrane is used to retain any agarose as the sample is expelled as shown in figure 59. While the kits are effective for quick recovery of a sample they are associated with low recovery of origami, this is likely due to the  $MgCl_2$  contained within the buffer lowering throughput [3], and the relatively large size of the origami preventing their elution from the agarose matrix as it is dehydrated.

As the relative concentration of any sample is dictated by the volume of buffer within the gel slice excised to recover it, rather than the initial volume inserted for electrophoresis, purification of indistinct

species becomes challenging. The more distinct a band appears the lower the amount of agarose required to be eluted for its recovery. An indistinct, or smeared band, leads to lower concentrations recovered due to the larger volume of gel being eluted. In practical terms this means that nanoparticles <10 nanometers provide limited throughput using this method as they present as a smear during AGE separation even at relatively high agarose concentration.

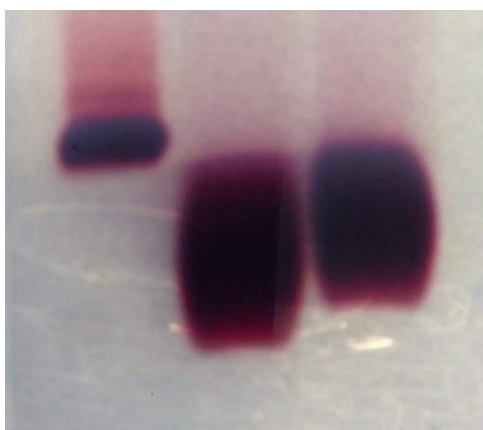


Figure 60 Various size nanoparticles separated via AGE– left to right – 9, 3.5 and 5 nanometer functionalised gold nanoparticles.

Figure 60 shows that as the size of the nanoparticle decreases the size of the band increases and the smearing effect becomes prominent. Overall yield can be increased by lowering the concentration of agarose used in the separating gel, but this will also increase the smearing effect of any band recovered, meaning that a larger quantity of agarose needs to be excised to recover all the sample, this in turn means a lower relative concentration. Conversely if the concentration of agarose is increased the band will appear less smeared but due to the increased density of the agarose matrix less sample will be eluted during the freeze and squeeze spin step.

## 5.7 Sucrose trapped elution method

A method which builds upon the Freeze and Squeeze method, and other techniques which recover a DNA origami sample directly from AGE, is the creation of a recovery well in the path of a migrating sample during electrophoresis [111].

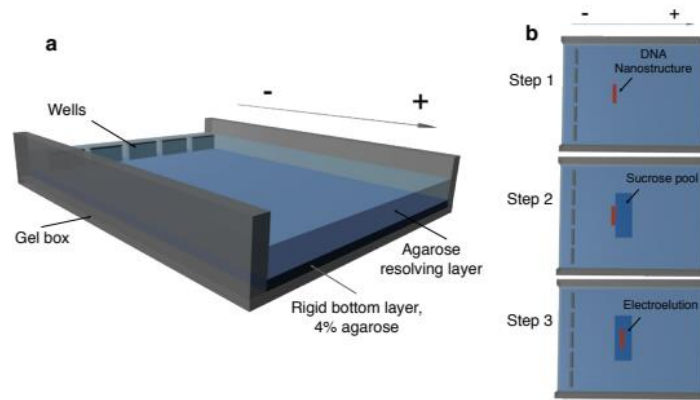


Figure 61 A modification of the standard AGE setup used for separation and analysis of DNA bands to allow recovery of a specific sample directly. A – a typical AGE casting system. In contrast to standard runs, in which a uniform gel is cast, a high concentration gel is used as a base and a lower concentration gel is applied once the foundation gel has set. B.1. – DNA nanostructures are electrophoresed into the gel. 2 – A section of the lower concentration gel in front of the DNA nanostructures being electrophoresed is excised and replaced with a recovery solution containing sucrose. 3 – Electrophoresis is continued leading to the sample eluting from the agarose into the recovery well where it can be collected directly [111].

Figure 61 shows that with simple modifications a traditional AGE setup can be used to recover nanostructures directly during electrophoresis. Instead of a single uniform gel being cast in a single step a thin, high concentration gel, is used as a base onto which a lower concentration, which will be the running gel, is set upon. Using this technique allows wells to be cut in the path of oncoming bands (As seen figure 61) without cutting through the thick gel at the bottom of the setup which would allow the sample to escape. However, the efficiency of this process is largely dependent upon nanostructure geometry.

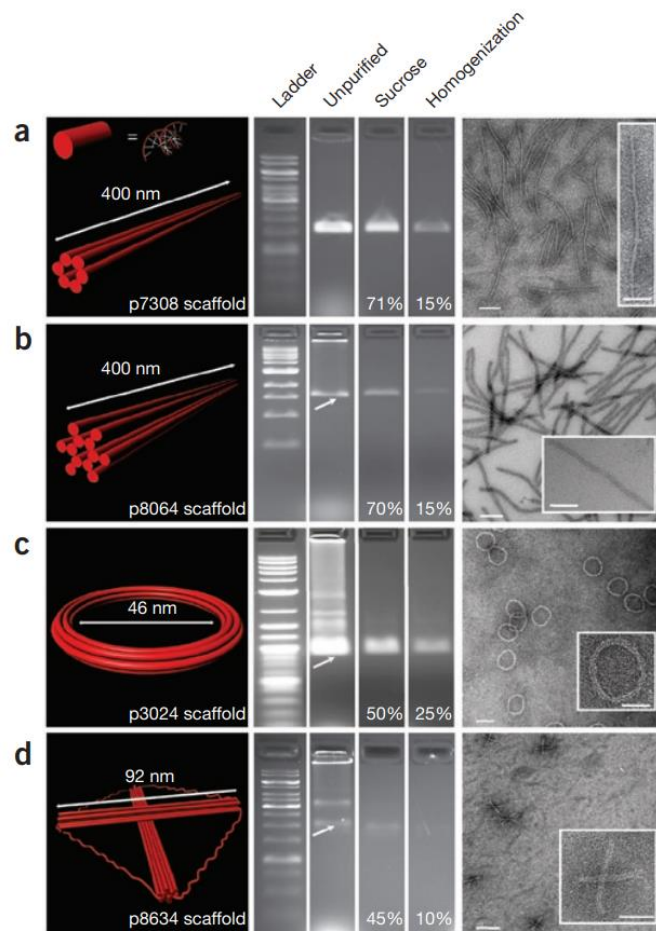


Figure 62 A contrast of recovery yields of various structures using AGE where final structure integrity is confirmed via TEM. Ladder – a standardised ladder used to measure band migration in contrast to arbitrary sequence progression. Unpurified – the raw fabrication sample. Sucrose – the method detailed above is used to elute DNA origami nanostructures into a sucrose solution. This solution is then analysed via AGE in contrast to a raw fabrication sample. Homogenization – the freeze and squeeze method is also used to recover DNA origami nanostructures from AGE [111].

Figure 62 compares the recovery yields between different structures and the 2 techniques. While the yield using the homogenisation technique varies by 15% from highest to lowest yield when using the sucrose-based recovery method the yield is universally higher but the variation between the highest and lowest yield increases to 25%. The sucrose is cited as an agent to effectively mitigate DNA origami structures dispersion into the AGE media and allow its efficient recovery [8]. While addressing the speed of sample migration through the recovery solution and back into AGE is likely a factor in recovery yield it is also notable that the shapes with the smallest cross sections, and the highest relative mobility through electrophoresis as indicated by their passage when compared to the progression of the DNA ladder, show the highest recovery yield. This would suggest that both a samples ability to migrate from

the AGE matrix into the sucrose collection well and a samples tendency to remain in the recovery well once this has occurred are both defining factors of final recovery yield.

## 5.8 Conclusion

As a self-assembly technique DNA origami, and components created for its decoration such as functionalised Au NPs, is reliant upon excesses of fabrication components to ensure high levels of fidelity. Purification is key, due to DNAs programmable nature, as excess fabrication components likely share complementing regions with the components used in further fabrication steps leading to interference and inefficiency.

Purification methods are broadly split into two methodologies, those that employ centrifugal force to separate different groups within a sample, and those that use an AGE run to do the same. Centrifuge based techniques range from raw centrifuge, where a sample is spun at sufficient speed to ‘pellet’ a group of high enough molecular weight from solution to novel variants of this technique such as PEG based DNA precipitation, where the molecular weight of DNA is much too low for traditional lab based centrifuge to be viable and polymer crowding is used to ‘push’ larger double stranded DNA structures from solution. Molecular Weight Cut Off columns also employ centrifuge and essentially use a fine mesh to sieve a solution of smaller components while retaining those larger than the MWCO in question. AGE based purification begins with a standard AGE run to separate a sample out into species of interest. Once separated they can be removed from the gel as distinct bands and purified. Freeze and squeeze-based purification is quick to perform, and while yields are low, can provide purified DNA origami and Au NP samples with relative ease. Sucrose lane based recovery is a more and emergent, and novel technique, but is challenging to perform and results are varied as discussed later in section 11.10.

## Chapter 6

### 6.0 Simulation Methods

One of the aims of this thesis is to present a potential fabrication system for the creation of artificial materials and devices, which are challenging to create using current nanofabrication methodologies. As discussed in chapter 1 one such application of the technique could be the creation of a materials with tuneable refractive indices which would potentially allow materials with novel optical effects.

To understand the interaction of an EM wave with our unit cell, we undertook a series of numerical simulations using the commercial EM solver HFSS [112]. HFSS is a finite element solver [112], which allows the user to create arbitrary 3D structures/geometries and simulate a predicted EM field under frequency sweeps of interest. This is achieved by discretising the domain into an irregular triangular mesh where Maxwell's equations are solved in their integral form on each triangle. HFSS simulations were undertaken to determine the scattering parameters  $S_{11}$  and  $S_{21}$  of the S-matrix which relates incoming and outgoing EM waves to the system. Essentially the parameters  $S_{11}$  and  $S_{21}$  relate to the reflection ( $S_{11}$ ) and transmission ( $S_{21}$ ) of the wave over the structure. Our simulations subjected the system to a spectral sweep, between 1 – 1000 terahertz (in 0.1 THz steps) encompassing the entirety of the visible light spectrum.

A single split ring structure was simulated, where a ring with no split was used as a comparator, and the gap size varied to examine its effect on EM response. The split ring size was created using the design methodology discussed in chapter 7. In brief, a unit cell of 45 x 55 nanometers was employed, as this is both within our manufacturing capabilities of interest and theoretically an ideal unit cell to interact with EM waves within the visible range (Where wavelength is between 5 and 10 fold the unit cell length). The board was metallised with sub 10 nanometer Au NPs which would act as seeding templates for enhancement into continuous metallisation in further work.

#### 6.1 Determining Material Parameters

There are several techniques that can be used to determine the material properties of metamaterials using the parameters of the scattering matrix (S-matrix). The approach presented here uses the Nicolson-Ross-Weir (NRW) technique [113,114] adapted [115] to account for possible negative responses in the real component of the refractive index. The NRW uses a closed-form expression allowing the complex form of the permittivity and permeability to be determined directly from S-parameter measurements. The approach starts from the assumptions that the media is in the form of an infinite free-standing slab in the x-y plane (thickness d) surrounded by a vacuum, with normal incident plane wave propagating in z.

Using the approach of [112] and the  $S_{11}$  and  $S_{21}$  values recovered from the simulation of the impedance ( $Z$ ) is given by;

$$Z = \pm \left[ \frac{(1+S_{11})^2 - S_{21}^2}{(1-S_{11})^2 - S_{21}^2} \right]^{\frac{1}{2}} \quad (1)$$

The root of equation (1) for a passive material is chosen such that the imaginary component of  $Z$  is positive. The refractive index, a complex parameter of the form  $\mathbf{n} = \mathbf{n}' + i\mathbf{n}''$ , is given by;

$$\mathbf{n}' = \pm \frac{1}{kd} \Re \left[ \cos^{-1} \left( \frac{1-S_{11}^2+S_{21}^2}{2S_{11}^2} \right) \right] + \frac{2\pi m}{kd} \quad (2)$$

$$\mathbf{n}'' = \pm \frac{1}{kd} \Im \left[ \cos^{-1} \left( \frac{1-S_{11}^2+S_{21}^2}{2S_{11}^2} \right) \right] \quad (3)$$

$\mathbf{k} = 2\pi / \lambda$  is the free space wave vector, and  $m$  is an integer. For a passive media the refractive index is chosen such that the  $\mathbf{n}''$  component is positive [115]. The second condition on  $\mathbf{n}'$  is to select the correct solution branch of equation 2 by choosing the correct  $\mathbf{m}$ , to ensure that  $\mathbf{n}'$  is continuous across the frequency range [115]. Once  $Z$  and  $\mathbf{n}$  have been determined the permittivity and permeability can be determined directly from;

$$\epsilon = \mathbf{n}/Z \quad (4)$$

$$\mu = \mathbf{n}Z \quad (5)$$

These equations, and variables, were translated into a MATLAB script importing the  $S_{11}$  and  $S_{21}$  values from the HFSS simulations to determine the effective material parameters; refractive index ( $\mathbf{n}'$ ), permittivity ( $\epsilon$ ) and permeability ( $\mu$ ), and the extinction coefficient ( $\mathbf{n}''$ ) that relates to loss.

## 6.2 Simulated structures

Split square structures were simulated within putative fabrication capabilities, where the Au NPs we employ were between 3.5 and 9 nanometers in diameter, and some electroless deposition techniques have been shown to be effective in enlarging Au NPs from between and 1 and 5 nanometers [103]. Five and 10 nanometer major radius structures, with 35 and 45 (32.5 and 42.5 nanometers in the case of the 10nm diameter design) minor radius, representing an area within the boundary of a single unit cell/DNA breadboard. This also gives 5/2.5 nanometers freedom of movement to allow for deviations in metallisation.

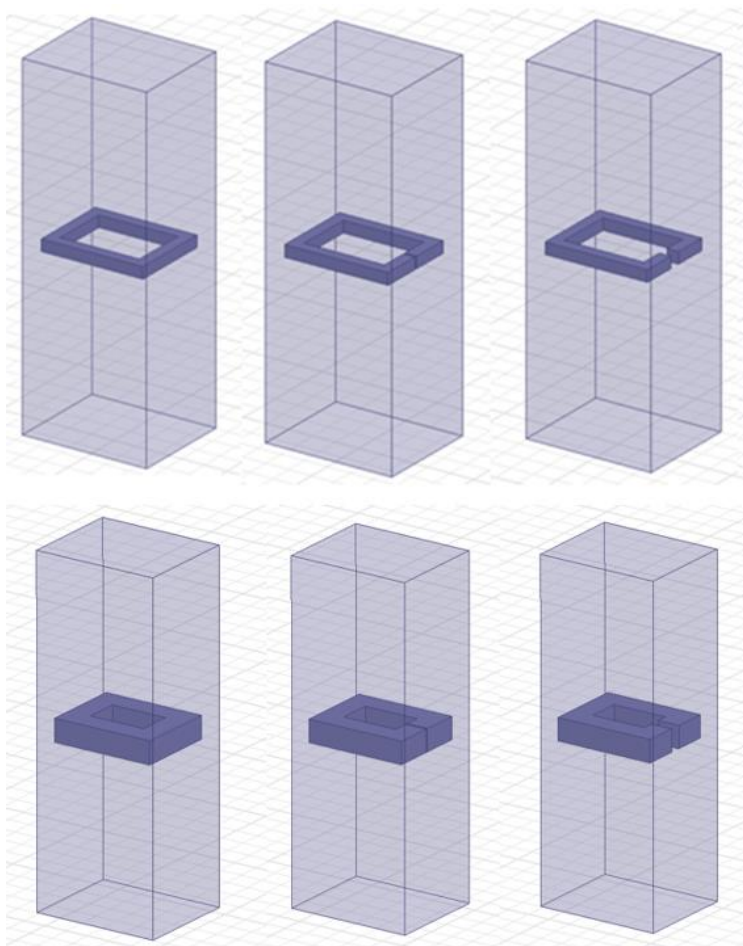


Figure 63 Square gold square ring structures (Described above) with increasing gap size starting 0nm, 1nm, 5m and 10nm from left to right. Top = 5 nanometers major radius. Bottom = 10 nanometers major radius.

The only change between individual simulations, with the same diameter, was the increasing of the split gap in the ring. No further changes to design or unit cell took place.

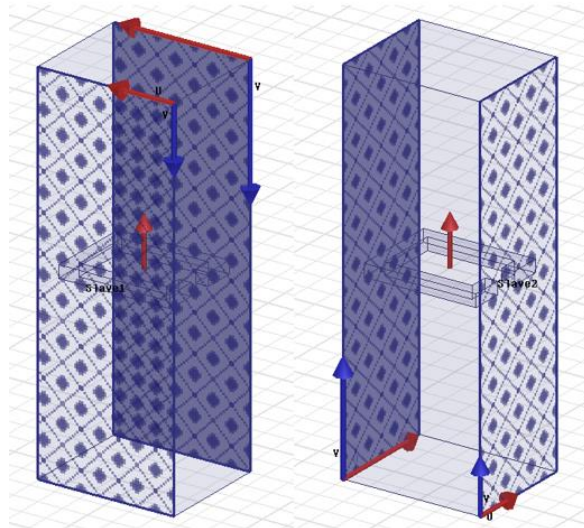


Figure 64 Master and slave boundaries were employed to simulate a single layer thick, infinite sheet, which extends in both X and Y – The central red arrow denotes the direction of wave propagation during simulation

While only one unit cell was created it is used to simulate a sheet of structures. This means that any fabricated structures must be created in fixed lattices to present the spectral properties produced during simulation.

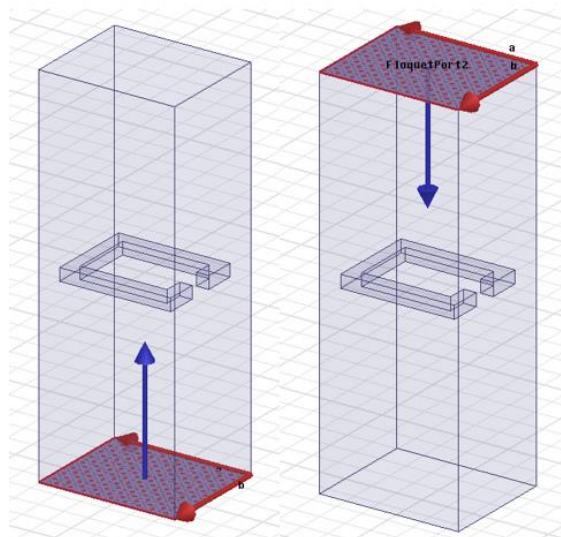


Figure 65 floque ports are employed to dictate where the wave enters and leaves the unit cell. Blue arrows show where spectral information is collected (S11 and S21 are measured 50 nanometers away from the region where waves enter/leave the unit cell to avoid interference)

We employ a 45 x 55nm unit cell. While the unit cell in HFSS extends above and below this ‘true’ unit cell, which the structure is contained within, this is to allow for effective measurement of transmission

and reflection at the ports highlighted above. Structures were simulated under frequency sweeps between 1 and 1000 terahertz at 0.1 terahertz intervals.

### 6.3 Test structures

To ensure the structures representing our fabrication designs would be simulated in a test environment at least somewhat representative of real-world conditions simple test structures were simulated and analysed.

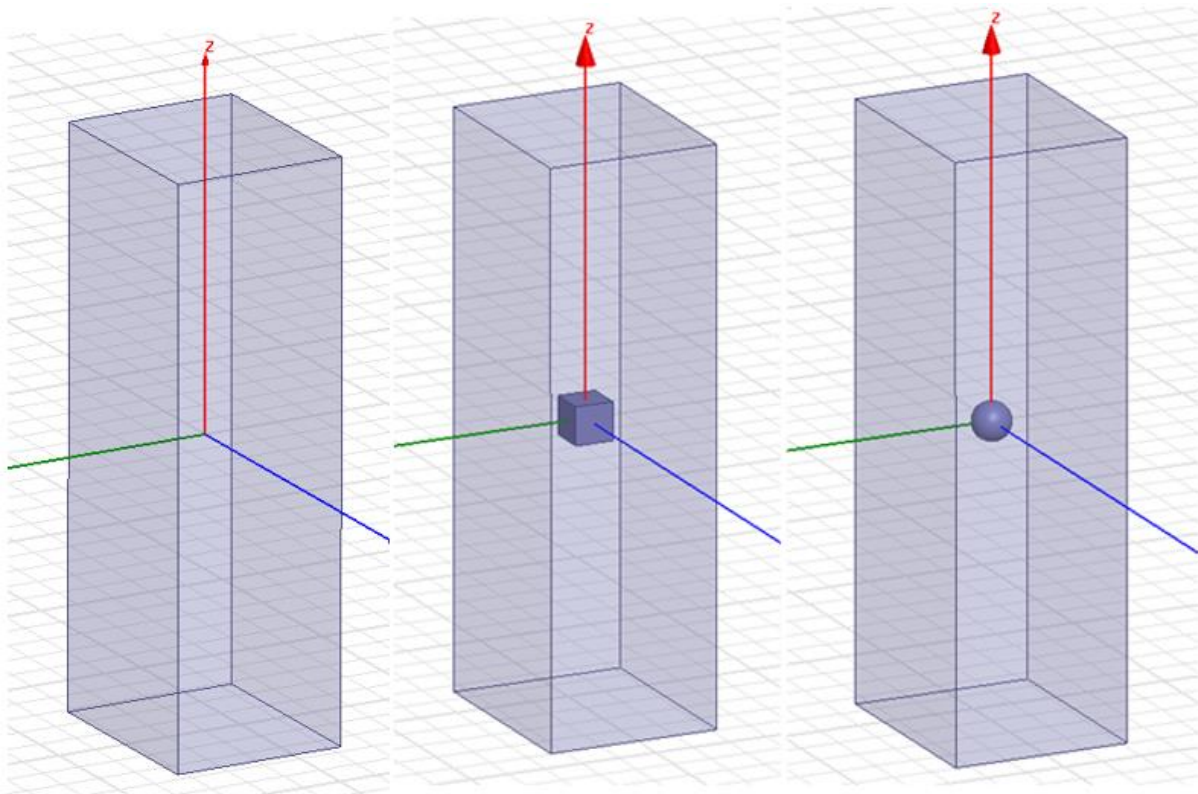


Figure 66 an empty unit cell (Left) a 10 nanometer cube (middle) and a 10 nanometer sphere (Right) were used to validate the simulation environment.

The empty unit cell is used to demonstrate there is no interaction between the frequency sweep and the empty cell. Small nanoparticle structures were also simulated to ensure a small shift in parameters occurred (As we only simulate a single infinite sheet of ~10 nanometer Au NPs it is probable that there would be very minimal interaction with light within the frequency sweep – a more significant interaction would require many multiple layers – or structures tailored to interact in an artificial capacity).

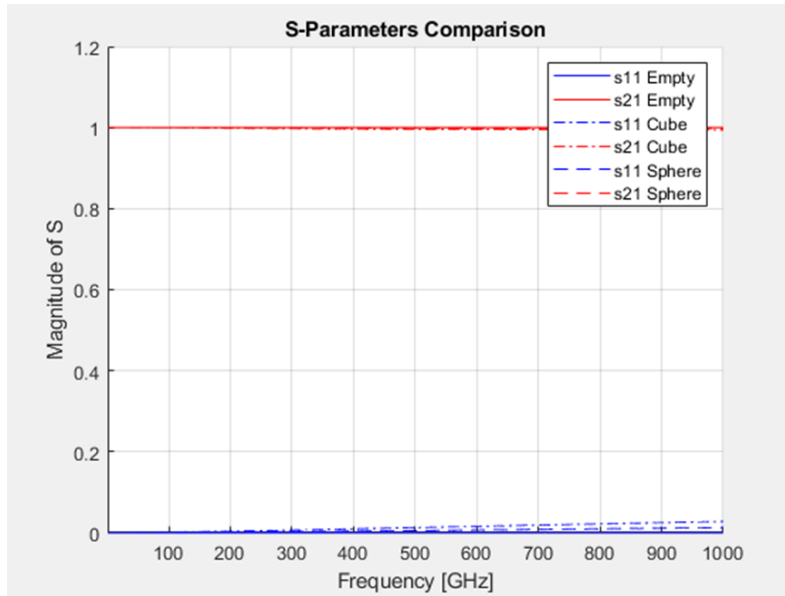


Figure 67 S11 (Reflection) and S21 (Transmission) results from the test structures

Figure 67 shows that there is almost complete transmission in each of the simulations. The nanostructure simulations demonstrate that, while there is little interaction with the single layer of nanoparticles, reflection can be seen to rise over the frequency sweep. There is also some minor change in transmission.

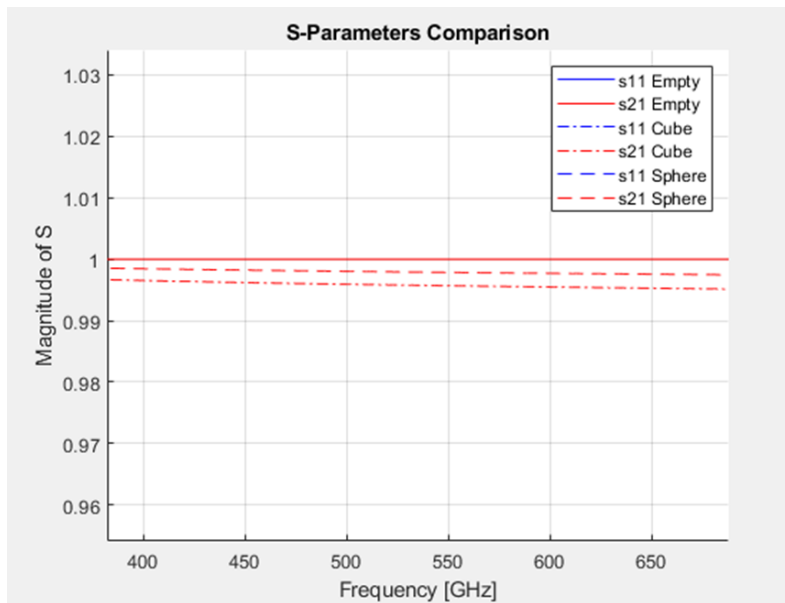


Figure 68 A zoomed in region of the transmission S parameters over the ~-visible range

Figure 68 shows a zoomed in region of the transmission shown via each system. While the empty unit cell remains essentially featureless over the frequency sweep, nanoparticles within the system cause a

lowering in this value, with the cube causing the greatest drop likely due to its slightly larger volume (While still very small in overall magnitude).

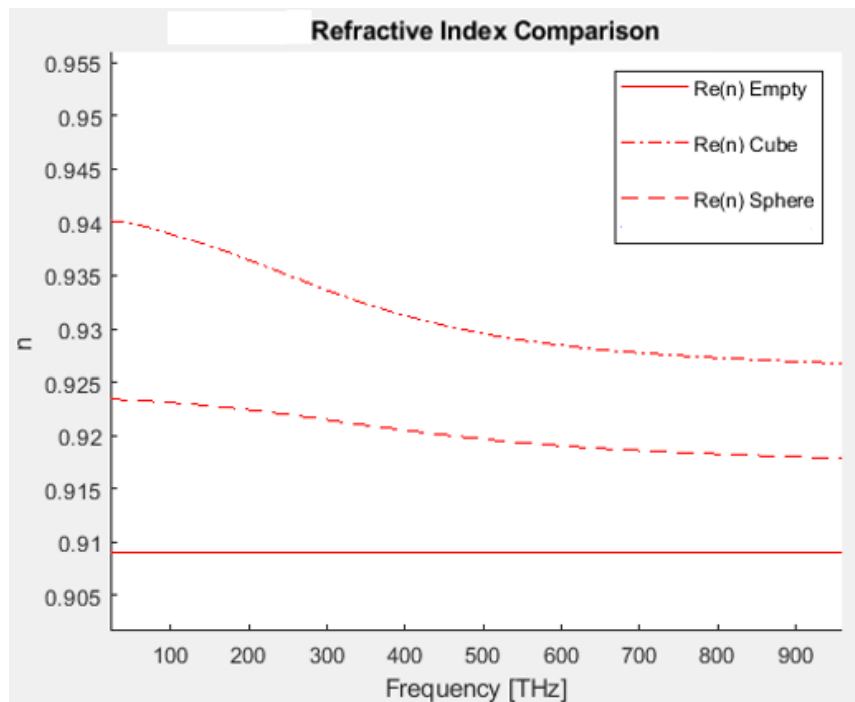


Figure 69 The differing simulation environments cause differing effects on the refractive index (Or no effect whatsoever in the case of vacuum)

Figure 69 shows that while the relative refractive index of the empty cell (Which should be exactly 1) is slightly out, when analysed in our artificial empty unit cell environment, it does correctly display that there is no change throughout the frequency sweep (As there is nothing to interact with). In the case of our cube and sphere structures there is minimal, but dynamic, interaction over the frequency range, suggesting that the change is down to the structure of the shapes interacting with different wavelengths in differing manners, rather than a singular constant effect.

The results described above show that while our results may not be exactly true to reality they do abide by normal physical conventions and expectations. This means that while any exact values cannot be guaranteed by the simulation any changes in dynamics offered by the more complex simulations conducted in Chapter 11 are likely to be based upon, true, observable effects.

## 6.4 Issues simulating curved structures

Initially the 10nm Au sphere was simulated and the intention was to then move on simulated curved ring structures (In an attempt to simulate structures similar to those we would fabricate). However this attempt highlighted the difficulty of simulating curved nanoscale structures using HFSS with the computational resources available. While simulations of the sphere could be completed using a high performance PC it was not possible to extend to same method to large curved structures. To demonstrate the problem a 10nm Au diameter cube, and sphere, were simulated using insufficient computational resources to correctly resolve the sphere (16GB RAM and a quad core intel I5 processor at ~3.4Ghz).

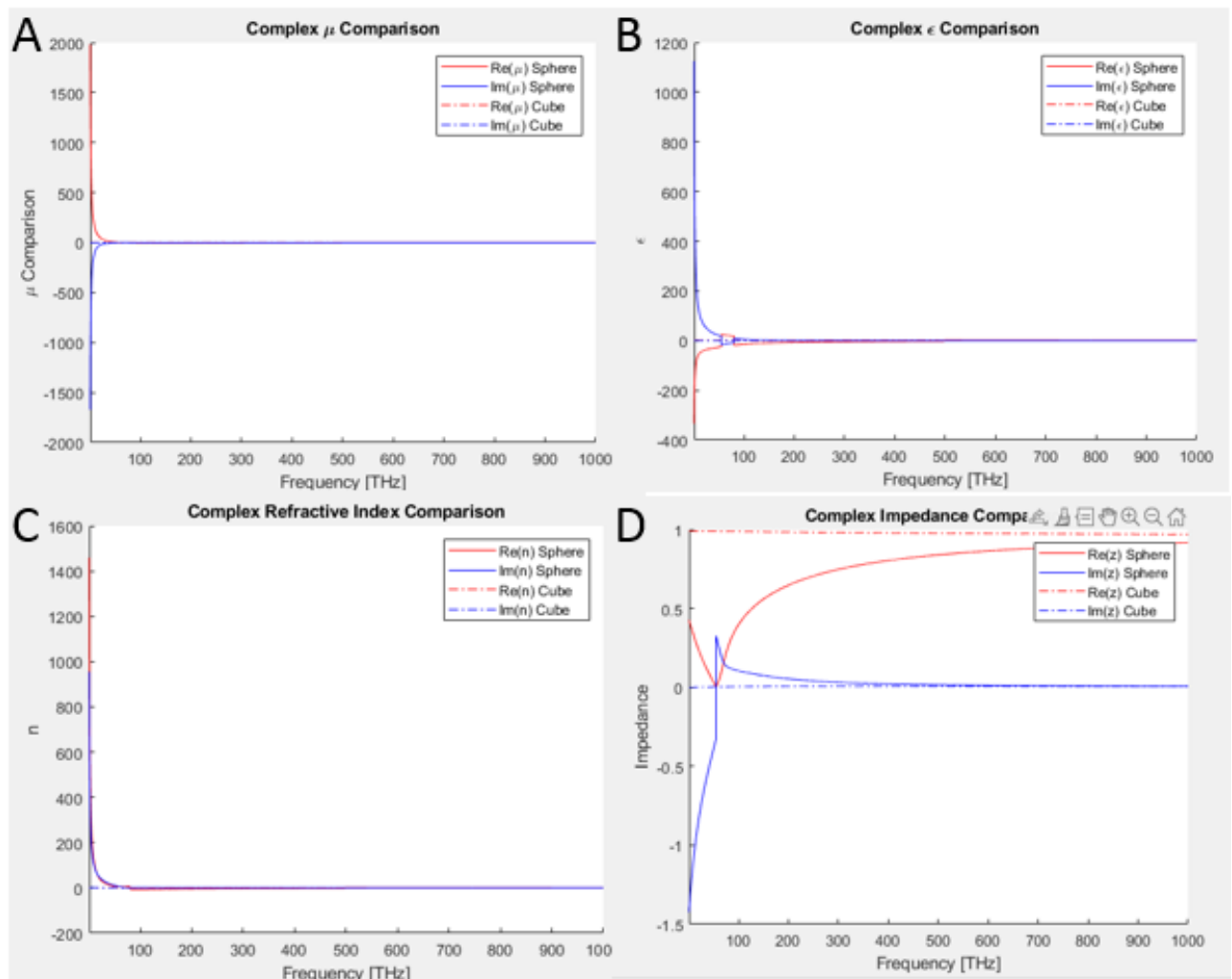


Figure 70 Initial simulations comparing the sphere and the cube. A – Complex Mu. B – Complex epsilon. C – Complex refractive index. D – Complex impedance

Figure 70 shows that the results for the 10nm sphere, solid blue and red lines, jump very significantly at the beginning of the frequency range and also show disjointed results around 100 terahertz. These errors are associated with incorrect branch selection via the Nicholson Ross Weir extraction process. This form of inconsistency is due to many potential results being possible from experimental data and this ambiguity means it is necessary to select the correct ‘branch’ (Where the correct branch is continuous over the entire frequency range). ‘Noisy’ or poorly collected results are cited as a cause for this problem [117] and given the issues we encountered when simulating the sphere lack of computational resources are likely the case.

## 6.5 Curvature and substrate

Due to the issues described above it was decided to pursue square based simulations rather than truer to life (But beyond our means to simulate) curved setups. While we acknowledge there will be differences between simulated results, and anything created using the method, the emphasis of our work is the creation of a pathway through which material properties can be altered rather than any specific application. Meta, and artificial, materials have been demonstrated in many straight [119], and curved [120], geometries, and while the effect may be slightly changed, the use of the system remains valid.

It was also chosen not to simulate a substrate layer/s. Firstly, due to practical computational resources it would be challenging (As DNA has a very complex structure – and the boards themselves are also very complex in design), further the DNA aspect of the substrate would likely have mitigable interaction with EM waves in the spectrum of interest [121], and while mica was employed as an effective substrate during the project this was through a necessary process (As mica is commonly used as an AFM slide for DNA structures). So, while it is likely mica could be used as an exemplar substrate it would require a cleaving/preparation method which left a defined surface layer, and again while this is an interesting and highly practical prospect, and would then potentially allow simulation, it was beyond the scope of work conducted within this project. Additionally, even though the addition of a substrate would modulate the effect of the resonators (By creating another set of scattering parameters), assuming any

substrate was a homogenous material, it would still allow programmable effects defined by the tailored structures annealed to its surface.

## Chapter 7

### 7.0 Modular board design considerations

Initial critical requirements of the modular board design were that it was capable of being produced in high throughput using conventional fabrication methodology and that once fabricated it was stable and robust enough for purpose. These considerations were addressed by the mechanics of the individual staple domains and where these domains terminate at the edges of the design.

Once a suitable base design has been identified, to fulfil the project requirement of site specific metallisation, it needs to be easily modifiable across the entire surface of the design. Beyond the addressability of a single board, the project also aims to create materials built from many individual unit cells, so methods to link individual boards together in clear, and stable, geometries also need to be considered.

### 7.1 Design itself

A square design was chosen as it facilitates easy comparison of a single tile to a unit cell and presents the most balanced surface area for designs to extend into both the X and Y dimensions. The board is interwoven between two layers, rather than being only one helix thick with a larger surface area, to promote stiffness and prevent the design folding around nanoparticles or other functional groups, when multiple tethers are attached to different areas on its surface or ‘creasing’ into a none-flat configuration when applied to substrate.

A common scaffold, P7249 (So called because it has 7249 base pairs in its sequence), was chosen due to its success in many other studies. To create a roughly flat square design the board was chosen to be 128 bases x 2 helices x 24 helices. Assuming each helix is 2.2 nanometers in diameter and each base pair is 0.34 nanometers across we present a design roughly 43.5 x 4.4 x 52.8 nanometers. This slight deviation from a true square geometry is due to the importance of maintaining base stacking rules,

which dictate the location of interhelical crossover points which give the DNA origami structure, limiting the number of possible structural motifs.

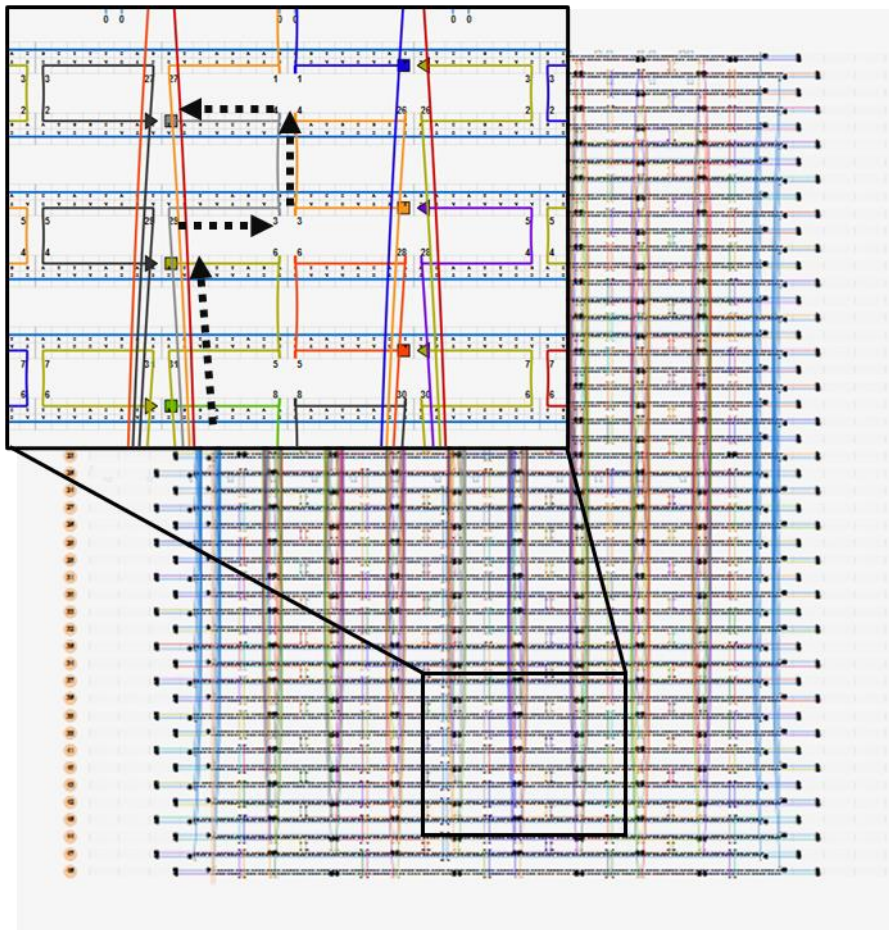


Figure 71 The full caDNANO design of the modular DNA origami board and a zoomed in look at staples (Coloured lines) interacting with the continuous scaffold (Blue line) to form the structure of the board. Staple 'direction' is denoted by a dotted black arrow in the direction of 5' to 3' along the DNA strand (Where the strand enters the helix from the domain above shown by the slanted line)

Figure 71 shows staples travelling through regions of the scaffold on one face of the board and then crossing over to domains on the other. Figure 43 also demonstrates that most individual staples travel through 4 separate scaffold domains (With 2 domains being crossed on each side of the board). Using the 8-base pair per domain rule also means that each staple is terminated when its helical pitch is close to the nearest external edge of the board allowing easy extension of sequences to connect external groups (Such as the Au NPs employed to create EM circuits).

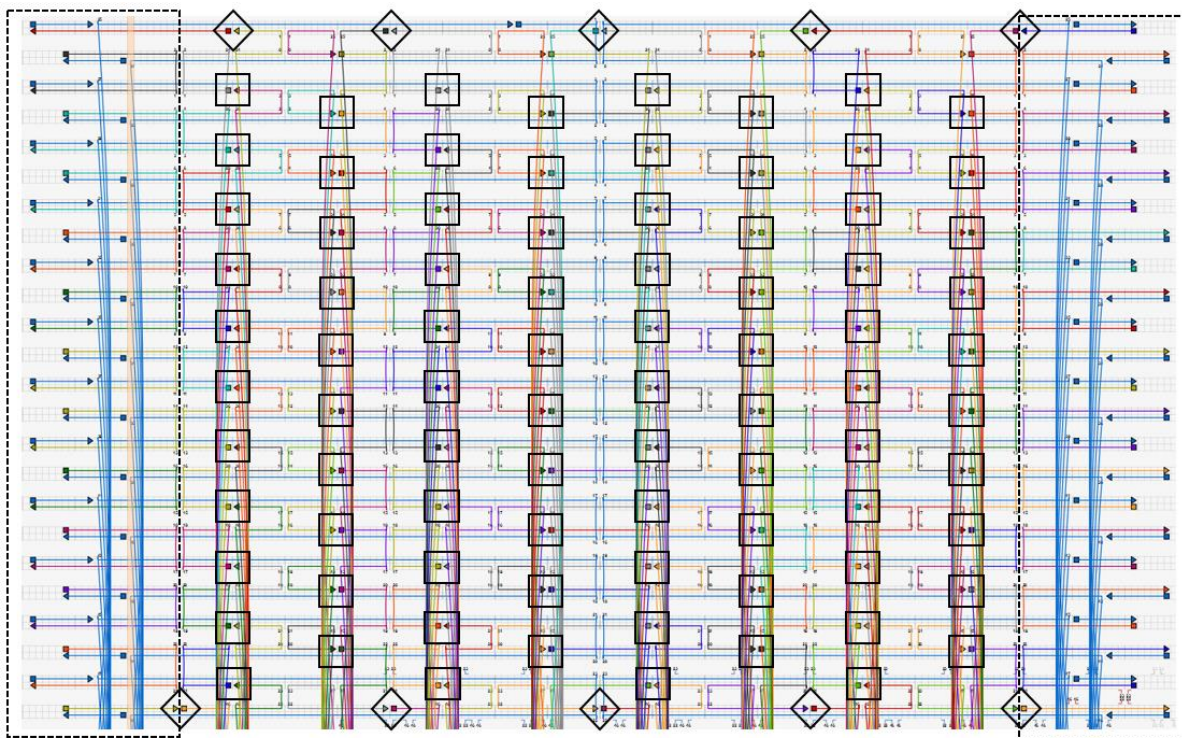


Figure 72 One face of the modular board. Distinct board regions are highlighted. Dashed boxes – Board tails/lattice points. Diamonds – Lattice points. Squares – Nanoparticle/Component tethering sites.

The putative board schematic can now be divided into 3 distinct regions (Figure 72). The tail regions (Dashed boxes) must be examined to ensure successful fabrication [122]. As these tail regions are also terminal regions they are potential candidates for lattice expansion. Dedicated lattice points (Diamonds) terminate in staples facing outwards parallel to the surface of the board potentially allowing extension/binding to other boards when resting on a substrate, or, binding of external groups when in solution. The surface of the board is populated by 84 binding sites (Squares) which terminate on the outer edge of their respective helix proximal to the surface of the board. These sites will be used to bind external groups decorating the surface of the board leading to metallised structures.

- The key requirements for a successful modular board design would begin with a board that can be fabricated in high throughput and fidelity and lies flat on the surface of a substrate. Once this objective is complete examination of the board's suitability in metallisation attempts, for example if the board folds around individual nanoparticles in solution rather than acting as an

robust sheet for multiple individual attachments, and then if the board can be folded into continuous geometric lattices without loss of unit cell symmetry, can be examined.

## 7.2 Board tail region

There is a need to prevent non-constructive base stacking effects between helices during fabrication, or when fabricated structures are attached to a substrate for imaging or spectral testing, and to prevent nonconstructive aggregation leading to failure of the design. Initially a poly thymidine tail spacer was employed to protect this region, which has been shown to be highly successful in other studies [122], to create a base protocol. However once general fabrication was confirmed these tail regions were re-examined as poly thymidine sequences are also highly efficient at binding Au NPs, another key aspect of the project (Where using poly T sequences for both tasks would create very high levels of interference), so experimentation of other tail region strategies was conducted as detailed below.

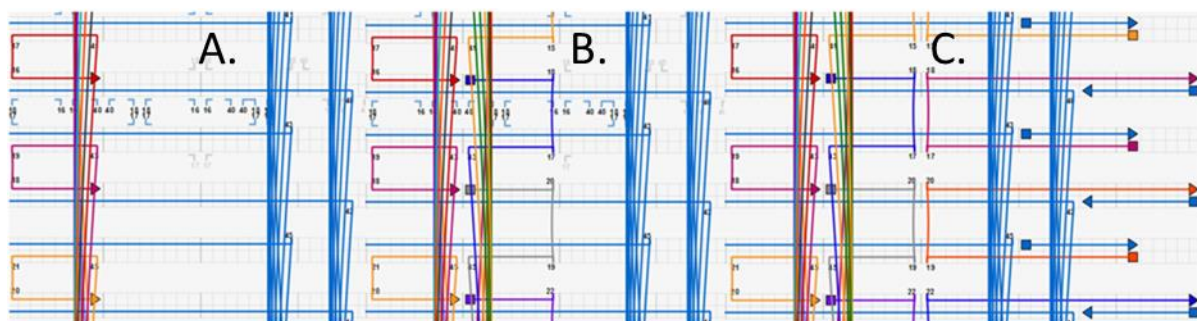


Figure 73 A section of the tail region of the breadboard design representing differing capping strategies. A – highly uncomplemented tail region. B – Uncomplemented tail region. C– Poly mononucleotide capping of the tail region.

As shown figure 73 tail regions are protected either by removal, or addition, of sequences at the terminal edges of the board. This effectively presents a trade-off between losing surface area, where sequences are removed as in fig. 73 A and B, or losing potential lattice sites, where poly mononucleotide sequences are added as protective spacers, as shown fig. 73 C. It should be noted that while the general methodology of fig. 73 A and B is the same (Removal of ‘edge’ staples to promote stability) it highlights that the number of staples removed could potentially be increased to promote stability if required.

Once the modifications shown figure 45 were incorporated into a fabrication attempt samples were fabricated under the full sweep, ionic conditions, and molar ratios of scaffold to staple identified and discussed more fully in chapter 11. All fabricated samples were analysed and compared via AFM and AGE.

- Three capping motifs were experimentally examined each representing one of the methodologies shown figure 45. The only changes in design/sequence between each fabrication attempt were those located at the ‘tail’ region of the board (Shown figure 44 dashed boxes).

### 7.3 Lattice growth

The potential of lattice fabrication was examined by the addition of staples joining the edges of 2 independent boards potentially creating 1 or 2 dimensional chains or sheets of monomer boards. These staples were anchored within the tail region of the board (Where the remainder of the tail region was unpopulated) so this method of lattice fabrication requires some variation of the uncomplemented capping strategy discussed figure 73.

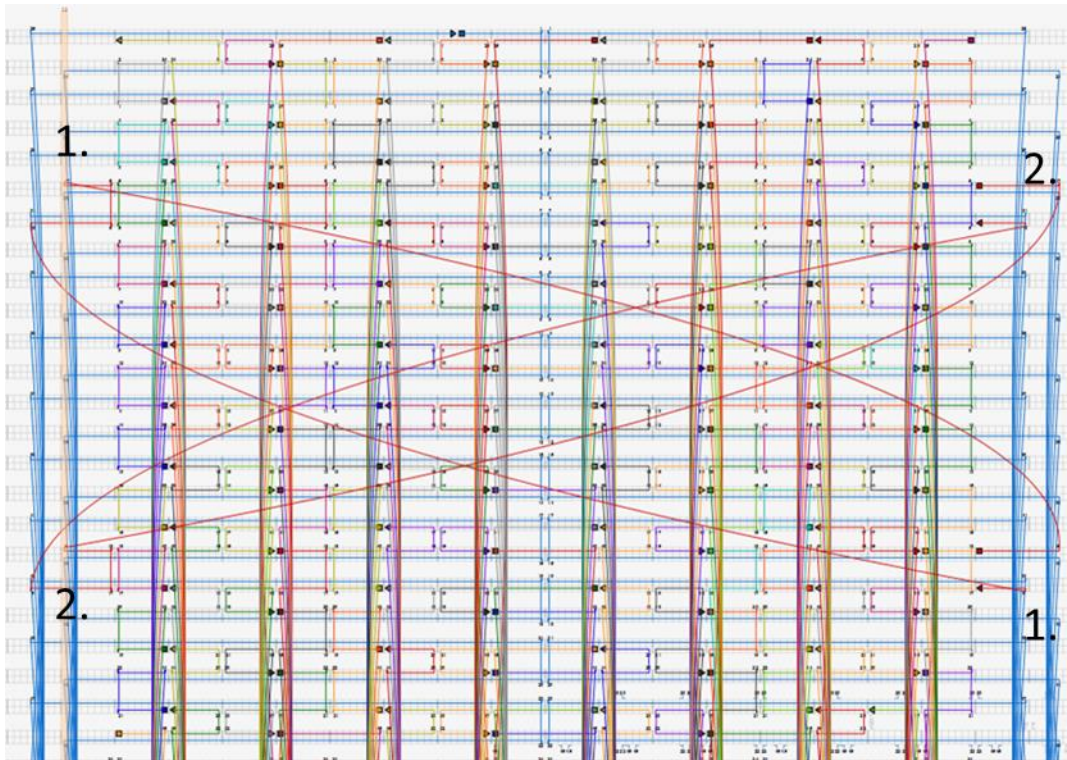


Figure 74 An example of lattice staples which would lead to lattice growth in 2 directions. 1. The top left quadrant anchors to a complementing sequence on the bottom right quadrant. 2. The top right strand anchors to a complementing sequence on the bottom left.

When staples are extended to connect to domains at an angle, as seen in figure 74, lattice expansion will occur in both X and Y facilitating the creation of a sheet of monomer boards. For the work conducted in this thesis a significant aim was the creation of a continuous sheet of material, where a substrate would ideally be covered by regimented boards without gaps, or small geometric clusters of correctly formed units which would simulate the same effect when packed onto a substrate, so the chosen lattice points were equidistant (If a continuous string of boards is considered). However it would also be a simple task to modify the position of the lattice point, breaking the equidistant symmetry in lattice sites, in an attempt to make a less tightly packed lattice if required.

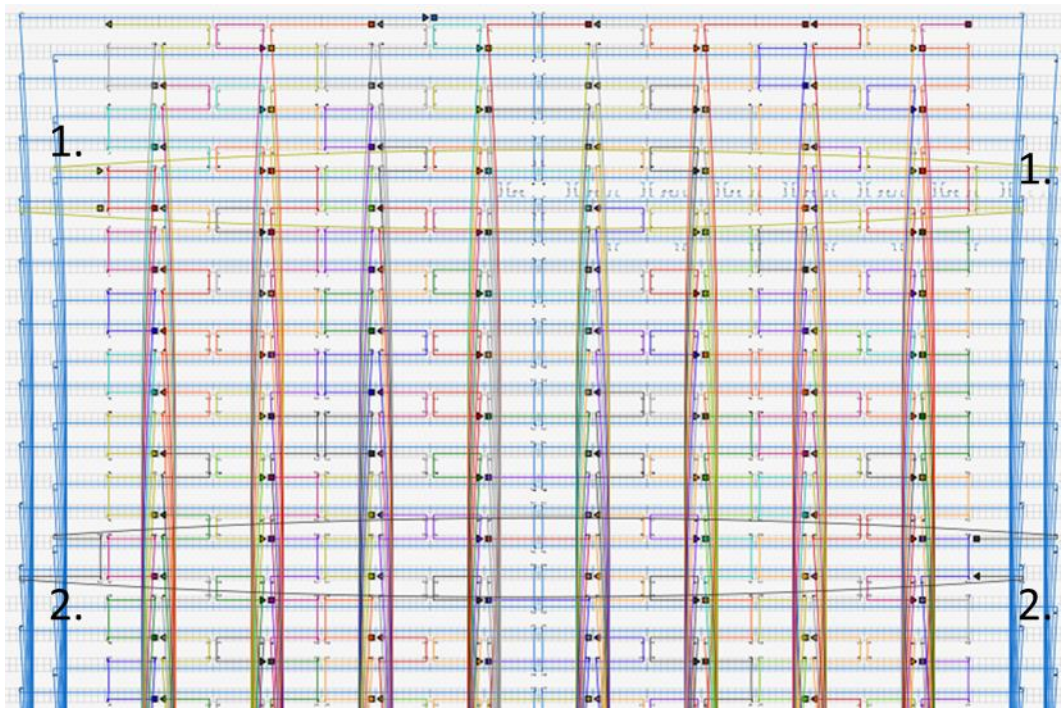


Figure 75 An example of lattice staples which lead to lattice growth in 1 direction. The anchoring points are parallel in relation to their placement on the board and no crossover occurs. Lattice strands remain within parallel domains – 1. binds to 1. and 2. binds to 2.

In contrast to lattice expansion in X and Y by creating lattice points which anchor parallel binding sites on sister boards, as show figure 75, it would be possible to create long chains of boards. Obviously this approach would (potentially) present a lower surface area per individual chain than X Y lattice conjugation, however, it may be possible to group chains within regimented rows to create high surface coverage.

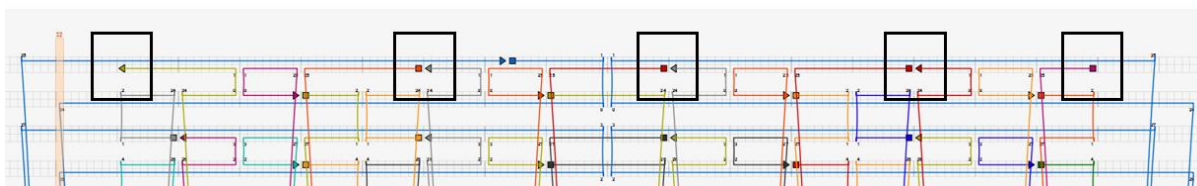


Figure 76 Black squares - All possible binding sites located at the ‘top’ of the board design  
There are additional potential lattice binding sites located at the top and bottom of the board (Figure 76 black squares). Unlike the tail regions, where lattice growth is conducted by extension of existing helices, these potential lattice points are created by extension of single staple strands out from the design

when their helical pitch is aligned with the edge of the board facing out into the empty space surrounding the design.

- Lattice expansion was attempted using the embedded design (Figure 45. B) modified with lattice sequences in the same motif as those shown figure 46 and 47.
- Molar concentration was also a variable considered with ratios of 3:1, 2:1, 1:1, 1:2 and 1:3 (In the format of Scaffolds:lattice components within a fabrication solution).

## 7.4 Site specific attachment – tethering mechanism

Attachment of nanoparticles, or other functional units, to the boards surface is dependent on staples extending out from the board surface, complementing sequences attached to the external group, leading to anchorage between the two. The specific variables associated with this process include the length of the tethering sequence and the number of individual tethers needed to bind a specific nanoparticle.

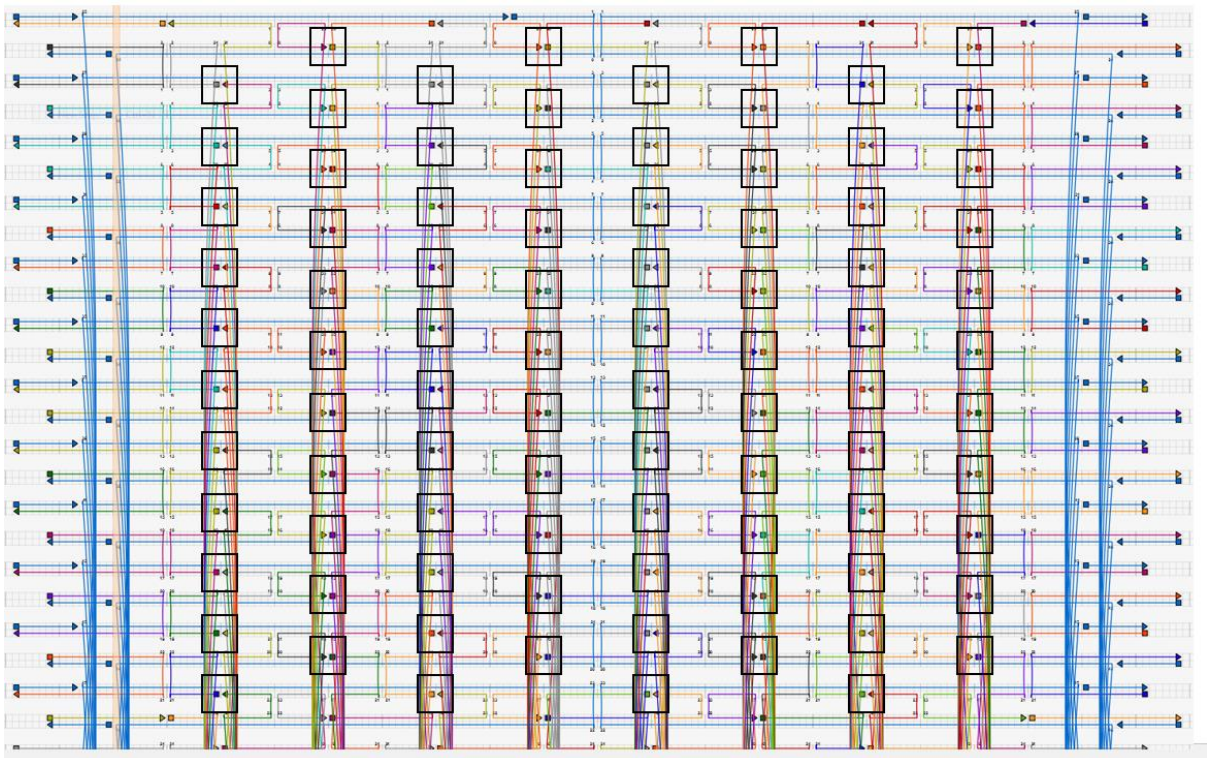


Figure 77 All possible attachment points on one face of the board.

Sequences which extend out from the board must do so at locations where the helical pitch of the donating DNA strand is parallel to the surface of the board with suitable binding sites of the board used in this work shown in figure 77.

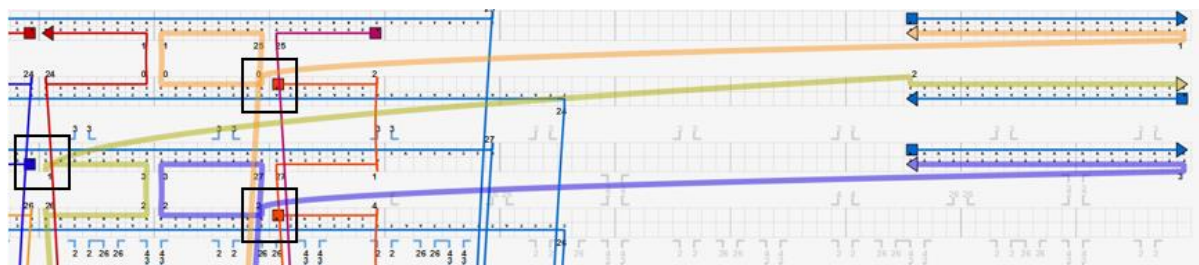


Figure 78 Staples extending out from the board, left, domains to complement none scaffold sequences on the right.

Once attachment sites have been chosen staples are extended and paired to sequences external to the board (As seen figure 78). These external sequences represent the sequences which will be attached to functional groups such as gold nanoparticles. Typically more than 1 strand is used to attach each particle with each particle tethered between multiple points as discussed in chapter 9. While there is no distinction of sequence between individual tethers (All tethers share the same sequence and any functionalised nanoparticle can bind at any point) assuming the board does not fold around individual particles each attached particle will have a limited binding domain footprint on the board leading to similar metallised circuits to those envisioned even if there are small discrepancies between individual designs. Poly T tethers were chosen due to their high efficiency of binding as discussed in section 9.3.

- Initially 20 base pair tethers were employed to test the design as these lengths have been shown to be highly effective in other studies [127].
- To examine tether lengths effect on binding 5, 10, 15 and 20 base pair tethers were examined both in solution-based fabrication and through metallisation of a sheet of boards already fixed to a mica substrate.

## 7.5 Site specific attachment – binding sites

2 distinct designs (Figures 77-78) were employed in attempts to create metallised circuits representing the structures, and structures similar to, those simulated in chapter 11.

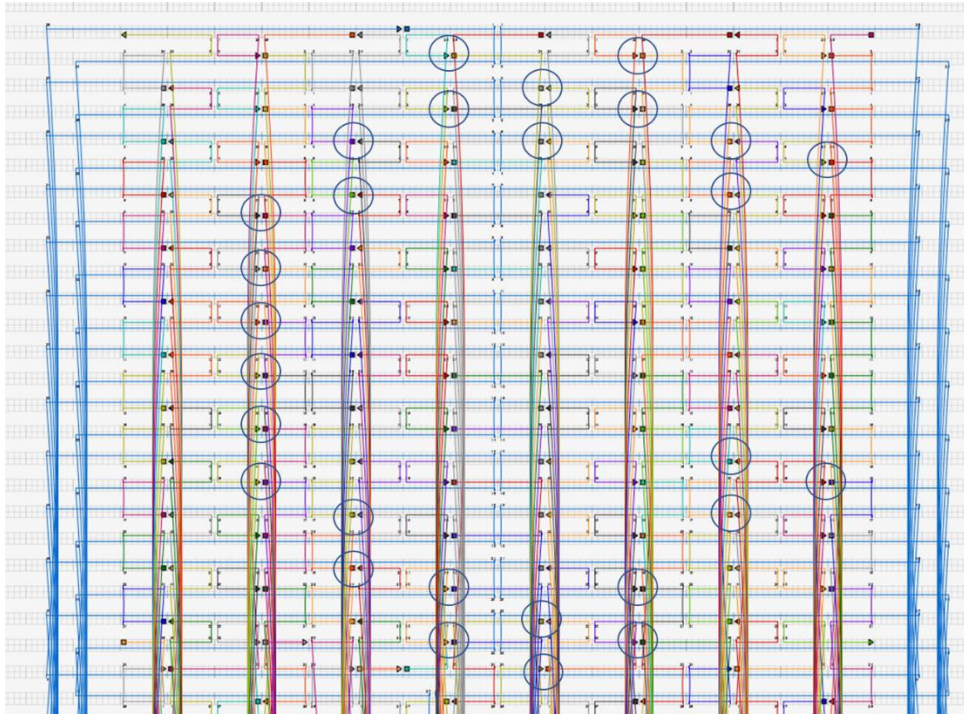


Figure 79 Tethers employed to bind nanoparticles in a 'C' resembling the simulated structure.

Figure 79 is an example of identifying binding sites on the modular board which would lead to the creation of a metal 'C' on the board if they were successfully functionalised.

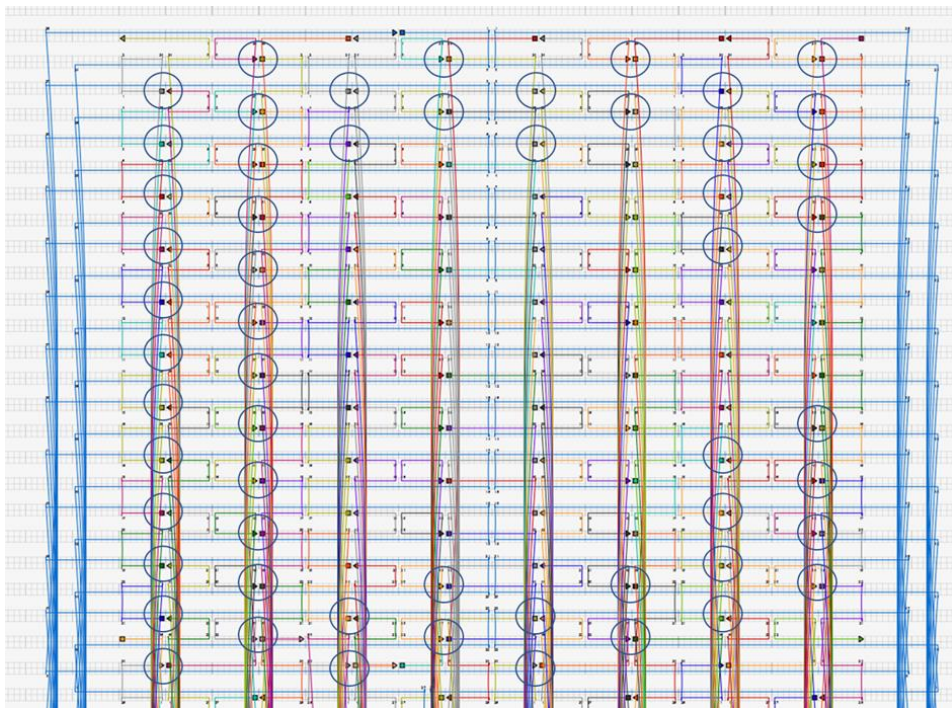


Figure 80 High density square 'C'

Figure 80 employs a higher density of binding sites which extend out to the terminal edges of the DNA board in a square resonator motif.

- The 3 designs shown figures 79 and 80 were fabricated and metallisation was attempted in both solution and on structures fixed to a substrate.

It should be noted that the tethering systems shown in figures 79 and 80, are not a precise replica of the simulated structure, due to the pixelated nature of the regimented binding sites created using the suggested crossover points provided by the caDNAno design/sequence recovery software. This could be partially addressed (Where feature size could be increased but would still rely on the underlying helical pitch of DNA) by breaking the 8 base pair domains used in the design of our modular board.

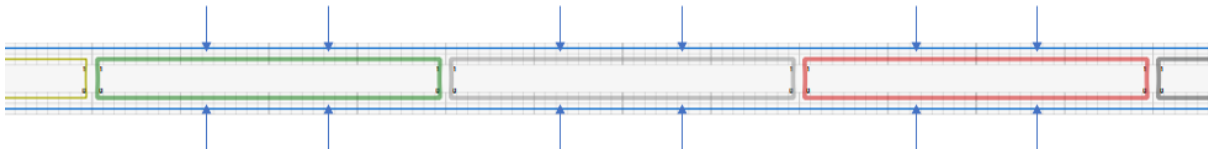


Figure 81 - 3 potential staple sequence sites crossing over 2 domains using the crossover points suggested by caDNAno (Green, grey, red lines) and potential crossover points which occur roughly every 360° rotation of the staple sequence (Blue arrows)

The distance between two proximal crossover sites in caDNAno, on the same helix, is 32 bases, and the helical pitch of beta helix DNA is 10.5 bases per 360° rotation. This suggests that between each of the binding sites described in figure 81 is two putative sites (Blue arrows) which could be created by removing two staples and replacing the location of the binding site. This method would reduce the feature size of plugin sites (On the same helix) on the breadboard from ~10 to ~3 nanometers. Combining this approach with multiple custom sites would potentially allow a significant increase in feature size without adding excess stress to the superstructure of the board.

## 7.6 Recovery and modification of sequences

Once the design is complete, and all lattice points and component strands have been added, the specific sequence for all staples can be recovered. Staple sequences are not created independently: a scaffold

sequence is applied to the design with all staples being recovered from the scaffolds complimenting sequence.

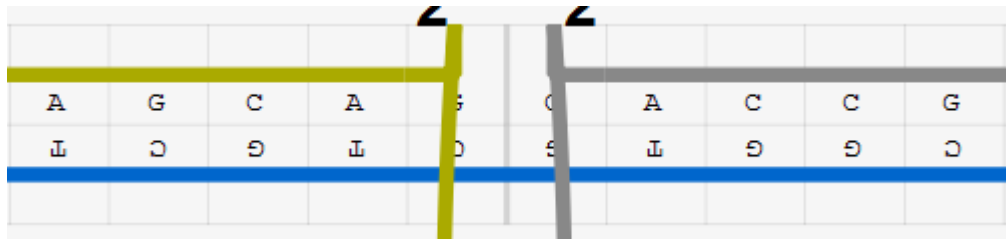


Figure 82 Scaffold sequence (Blue) is paired to staple sequences (Gold and grey)

Figure 82 demonstrates how an imported scaffold sequence can be used to assign complementing sequences to staples. Where there is a change in the sequence, such as when scaffold reaches the end of a design and loops back on itself, or staples jump across Holliday junctions to neighbouring helices, the scaffold sequence at the new landing site will be now be used.

	A	B	C	D
1	Start	End	Sequence	Length
2	26[95]	5[95]	CAAAGCATCCGGAATGGTGCCAAGCACGACGT	32
3	25[80]	1[95]	CCCGCCGCGCTTAATGTATCATTAAACGTCAA	32
4	21[64]	46[64]	GGAAGTTTATTTCTTATGAGGCTTTCAACAG	32
5	4[79]	27[79]	CCTGCAGGGCTGCATTAAGCCTGGCCCCAGCA	32
6	47[112]	20[112]	CAGGCGGAGACTCCTCTACAGGAGAGCGTCAT	32
7	10[111]	34[96]	GTAGGGCTAAGCCTTTAAATTTAAGCCTGTTT	32
8	2[143]	25[143]	ATAGAACCACGCAAACCTTGCTGGCGTATAAC	32
9	3[128]	28[128]	TAGTCTTTCACCTAACAAATATCAAAAAGAAAC	32
10	38[95]	17[95]	GCCGAGGGTGCCACTTCATTCAACATCAGTTG	32
11	6[47]	29[47]	TATCGGCCGATGTGCTTATTACGCTTCCTGTG	32
12	43[112]	16[112]	ATTTGGGAGAAATTATAAAGAAACCATACATA	32
13	25[48]	1[63]	GTGTAGCGGTACGCTAACGTGGCACAAGAGT	32
14	37[48]	10[48]	TCATTTGGGCAAAGAATAAAGCTATTTTAAAT	32
15	12[111]	36[96]	GTTTTATTCCATATAAATAGATAAGCTACAA	32

Figure 83 Staple sequences exported from caDNAno

Once exported sequences will be available in tabular data, as seen figure 83, this is useful for checking bulk details, such as the length of all sequences within the design to ensure there are no ‘clipped’ sequences too short to be synthesised or other similar practical considerations.

## 7.7 CAND0 simulation

While not strictly necessary, or part of our experimental protocols/results, it is very pragmatic to check a caDNAno design before sequences are finalised. Cando is a powerful tool for this purpose and provides a direct simulation of a DNA origami structure by analysing a caDNAno design schematic. The process has many advantages over the native visual interpretation of structure provided by the caDNAno program, which does not simulate curvature or check structure in any way, relying on the simulated geometry of helices within the defined honeycomb interface it provides.

Cando does this by treating double stranded DNA as a homogenous elastic rod whose physical characteristics, such as twisting and bending stiffness, have been determined and measured experimentally [124]. Beyond this initial approximation of double stranded DNA more complex motifs, such as Holliday junction crossovers, are incorporated to allow simulation of full-scale origami structures in a huge variety of conformations.

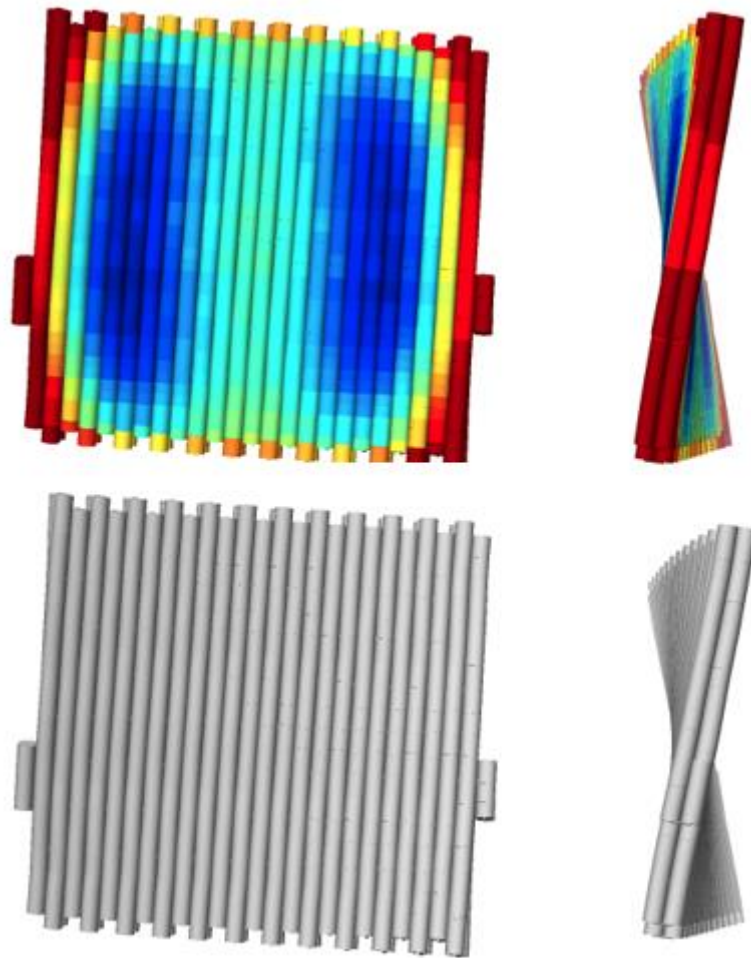


Figure 84 Cando outputs of the modular DNA origami breadboard (Bearing no surface modifications). Top – flexibility maps describe which areas of the structure are more prone to movement. Bottom – the native structure of the design once it has been fabricated (Both simulation outputs assume the structure is at room temperature)

Figure 84 shows that the sections within the greater body of the board show lower mobility than those at the board edges. This is likely due to higher interconnection with other strands, while the absolute edge strands, are only connected to other helices on one side (With no further helices at the terminal edge of the board). It is noticeable that in simulation there is some global twisting effect which runs through the design. This effect is due to the generalised 10.5 bases per helical rotation which caDNAno uses to rationalise crossover points in designs not meshing completely with the actual, or at least somewhat more precise, figure of 10.67 bases (Dependent on specific sequence) per helical rotation [3]. However, it has also been stated that this low level of twist would be difficult to visualise and confirm in solution and would be dampened by the structure being adhered to a flat substrate for imaging [54].

## Chapter 8

### 8.0 Board fabrication, confirmation, and protocol refinement

Once a DNA origami has been designed specific staple sequences can be synthesised and then complemented to a scaffold sequence in a fabrication attempt. However, while a functional design is partially key to creating stable origami in high throughput, any putative design is equally reliant upon the fabrication cycle which is employed to fabricate it correctly.

Essentially fabrication of DNA origami structures has two significant variables. Firstly, the ionic conditions of the solution must be raised to allow origami formation and stability. Secondly a thermal cycle must be employed to break hydrogen bonding within the scaffold, and potentially staple strands, and allow rational Watson and Crick base pairing to take place in a controlled manner with all sequences correctly available for complement.

Initially it is useful to conduct protocols over wide sweeps, in terms of both ionic conditions and specific thermal cycles, then once structures have been confirmed, the protocol can be modified to increase fidelity or efficiency.

#### 8.1 Ionic conditions

Regarding the ionic concentration and chemical makeup of the solution, discussed in chapter 3, Tris and  $MgCl_2$  are both employed to ensure stability of DNA origami in solution. Several companies [125,126] who provide DNA synthesis services suggest DNA is stored in a solution containing 10mM Tris and as such our fabrication buffer also contains this concentration to promote DNA stability when in solution.  $MgCl_2$  was employed as the divalent ion used to mitigate interhelical repulsion and facilitate fabrication. It is notable that during fabrication our buffer did not contain ethylene-diamine-tetraacetic acid (EDTA). While EDTA is commonly used in molecular biology as a metallic ion chelation agent, to prevent activation of metal dependent enzymes which would damage DNA and

RNA samples, it has been shown to leech divalent ions from DNA origami structures [75] and did not show any effect when removed from all protocols.

- All DNA samples were raised to 10mM Tris.
- To examine the effect of changing  $MgCl_2$  levels on fabrication 4 solutions were raised to differing  $MgCl_2$  concentrations, 7.5, 12.5, 17.5 and 22.5mM respectively, and a thermal cycle conducted.
- Like for like samples, with or without EDTA present, were fabricated to examine EDTAs effect on fabrication.

## 8.2 Thermal cycle protocols

An adaptive tuning of thermal cycle windows was employed to focus on areas where constructive folding occurred and to reduce interference in fabrication caused by unnecessary or unwanted folding, to create rapid and effective creation of both the base DNA origami structure and further modified structures and geometric lattices.

Initially thermal cycling was conducted over pre-existing windows like those employed in many DNA origami fabrication attempts (Which also confirmed the validity of the design blueprint). Once confirmed the cycle was divided into smaller segments and the fabrication product re-examined. This process was then repeated to increase granularity of the folding information provided.

Beyond increasing the efficiency of fabrication of the standard DNA breadboard the effect of specific thermal cycles on board metallisation and lattice growth was also examined. This examination would be conducted on a confirmed fabrication attempt which would then have further fabrication components added and a secondary thermal cycle employed to facilitate attachment/modification.

- The initial denaturation step was conducted at 65°C for 15 minutes. This remained constant throughout the course of work.
- For the full sweep protocol used to verify design stability - the second restorative step was initially conducted from 60-40°C over 20 hours.

- Further thermal cycles were tested over smaller temperature windows. Firstly over 5 degree windows: 60-56°C, 55-51°C, 50-46°C, 45-41°C and then over smaller single °C steps.
- All thermal cycles conducted during fabrication analysis were conducted at ~1 hour per change in 1°C where any slight variation in time at a specific temperature was due to the thermal cyclers taking extra time to recalibrate sufficiently to continue the cycle.

### 8.3 Staple concentration

As staples are sequence dependent upon the complementary sequence of the scaffold only the scaffold used to create a design can be used during fabrication. As discussed in section 1.3 staples of interest are mixed with their complementing scaffold in excess. Classically [3] at least a 10:1 molar ratio of staples to scaffold is used to ensure successful fabrication in high throughput. Reduction of staples would be beneficial not only in terms of raw efficiency, and reduced cost, but also to reduce, or possibly mitigate entirely, the amount of purification a sample requires before it is used in further steps (Purification is a significant issue in DNA based nanotechnology and is discussed in more detail in chapter 5).

- Staples solutions were mixed from wells containing each, unique, addressable, sequence within the board to create specific master mixes at 500 micromolars. All sequences required for a specific design (Typically ~200 staples) were then mixed to create a master mix solutions of 2.5 micromolars.
- Scaffold sequence at 100 nanomolars was used for all fabrication attempts.
- Initial fabrication analysis experiments were conducted using a molar ratio of 10:1/Staples:scaffold.
- Examination of the effect of reduced staple concentration on fabrication was conducted by diluting the staple concentration to 3, 2, and 1:1 of scaffold concentration.

### 8.4 Lattice protocols

A further challenge in DNA origami fabrication is the creation of long-range order structures created from individual monomers. A simple method of lattice fabrication was examined, by the addition of a single staple joining the edges of 2 independent boards, creating potential chains of monomers into the

X and Y direction. The lattice design motif is discussed more thoroughly in chapter 7. Comparison of the folding dynamics of the new structural motif, created by addition of the lattice components to the existing fabrication solution, were conducted in a similar manner to the original monomer tiles however as the mono tile structure had been stably identified it was used as a comparator during migration.

## 8.5 Fixation protocols

DNA origami imaged via AFM was affixed to a mica substrate. The effect of incubation length and the addition of monovalent ions to the fabrication solution being analysed (Where there is evidence that divalent ions favour double stranded fixation while monovalent ions mitigate single stranded fixation) as well the length of time a sample was incubated upon a substrate, and the washing solutions used before a substrate was dried, were also examined.

- 1 microlitre samples were applied to freshly cleaved mica in all imaging attempts.
- For standard fixation attempts the fabrication solution was applied directly, for attempts using a combination of divalent and monovalent ions NaCl was added to raise the solution to the required level before the sample was administered.
- Samples were then left to incubate for 30, 60 or 90 seconds before washing, or until completely dehydrated.
- Samples were washed with ultra-purified water – 100 microlitres was ejected over the sample using a micropipette, where the sample was wicked using a paper towel on its corner, without the tip of the pipette touching the mica surface. This process was repeated twice.
- Samples were then dried with a constant gentle (Where the pressure of the stream would cause minor disturbance of a latex glove worn over the hand and would be barely audible) for 60 seconds at which point they would be completely dry.
- Where a second fixation step was conducted (Whereby an attempt to attach nanoparticles to a pre-existing layer of DNA breadboards was conducted) the origami sample was fixed using the steps above and then a second microlitre solution applied containing the Au NPs required for fabrication.

- This second fixation step was also conducted using various  $\text{MgCl}_2$  and  $\text{NaCl}$  concentrations as noted in their corresponding results in chapter 10.
- Samples were then dried with a constant gentle (Where the pressure of the stream would cause minor disturbance of a latex glove worn over the hand and would be barely audible) for 60 seconds at which point they would be completely dry.

## 8.6 AGE

AGE is an effective tool for examination of DNA length and conformation and is discussed more in section 3.5. AGE was used to examine all DNA origami structures and other groups such as Au NPs.

For examination of DNA origami (Including metallised origami)

- Agarose gels were run universally at 1% agarose with 0.5X tris boric acid running buffer. For standard visualisation gels were run at 100 volts for 60 minutes. This would typically provide strong visualisation of dominant bands. For closer examination of sub species within dominant bands the gel was run for a further 60 minutes at 100 volts. However after 120 minutes had passed all bands had lost their definition and only contrast between individual species, as oppose to clear examination of specific species, was possible.
- Agarose gels containing DNA origami structures running buffer MUST be raised to 10 millimolar  $\text{MgCl}_2$ . This use of divalent ions is critical to maintain DNA origami super structures. Use of divalent ions within electrophoresis causes a residual build-up of heat within the tank. To mitigate heat build-up the tank was placed in a water basin containing ice. For longer runs ice should be replenished.
- Using  $\text{MgCl}_2$  containing gels in AGE leads to precipitate on the cathode (An effect not observed where no  $\text{MgCl}_2$  is present). This is likely some form of  $\text{MgCl}_2$  and agarose gel interaction which is then leeching from the gel and becoming fixed to the cathode. For this reason if a run lasts longer than 3 hours the buffer should be exchanged.

For examination/purification of gold nanoparticles:

- For effective separation of gold nanoparticles higher concentration AGE gels should be employed than those used to separate DNA and DNA origami: 3.5 nanometer functionalised Au NPs were separated using a 3% gel however this was only possible using finer high grade agarose powder, where lower grade agarose powder did not form a usable gel at 3% concentration, so it may be necessary to modify protocol slightly depending on supplier.
- $MgCl_2$  should not be present in gels used for Au NP separation. For reasons discussed more fully in the results section (Chapter 11) this method will not allow effective purification.

## 8.7 AFM

Once a sample had been fixed, washed, and dried upon freshly cleaved mica it was examined using a Bruker Dimension Icon AFM, in quantitative nanoscale mapping mode, with a Bruker SNL-10 C probe. All recovered images were then created, and examined, for structure specific measurements, using Nanoscope software where the only manipulation was the use of the ‘flatten’ function to create a flat exportable image.

## 8.8 Freeze and squeeze

Freeze and squeeze based purification (Discussed chapter 10) was employed to purify DNA origami structures of excess staple DNA post fabrication. This process begins with an AGE separation step, followed by an excision of the origami band, following by a freeze spin cycle.

- An unpurified DNA origami sample was electrophoresed for 45 mins in a 1% agarose gel using 0.5X TBE buffer with 10mM  $MgCl_2$ .
- The band of interest was carefully excised, trimmed, and crushed.
- Freeze N Squeeze DNA gel extraction columns were used.
- The crushed sample was frozen, inside the column, for 3 minutes.
- The column was centrifuged for 5 minutes at 8000RCF and used immediately post recovery.

## 8.9 DNA precipitation

PEG precipitation was conducted on DNA origami breadboards, to both concentrate and purify a sample, post fabrication and is discussed in more detail in chapter 14. This is a PEG crowding technique which precipitates larger DNA structures, such as DNA origami, from a solution while smaller strands, such as staples, remain in solution and can be discarded.

- The buffer of the solution was raised to 7.5% PEG, 10mM Tris, 2mM EDTA and 250mM NaCl.
- Samples were then centrifuged at 16000G for 30 minutes.
- The supernatant was discarded and samples were resuspended to ~100nm DNA origami concentration in 10mM Tris 12.5mM MgCl<sub>2</sub> buffer and left to incubate at room temperature for 20 hours.

## 8.10 AGE elution into sucrose

One potential method of purification of DNA structures involves eluting the sample directly from AGE into a sucrose containing well cut into the agarose block in the path of band migration.

- A thin layer of 3% agarose was set on the bottom of an AGE loading tray.
- A thicker layer (The running layer) was set using 1% agarose 0.5X tbe and 10mM MgCl<sub>2</sub>.
- Electrophoresis was conducted until the origami band had completely separated from the staple band.
- A small trough was cut in front of the DNA origami band and filled with 10% w/v sucrose containing 0.5X tbe and 10mM MgCl<sub>2</sub>.
- Electrophoresis was then re-engaged until the band had eluted completely.
- The sucrose containing solution is then eluted directly via pipette.

## Chapter 9

### 9.0 Au NP synthesis and preparation

Gold nanoparticles were employed for all work conducted in the metallisation aspect of this project. A further focus was on specifically sub 10 nanometer Au NP particles as these represent a potential feature size where most conventional nanofabrication techniques become unviable (As discussed chapter 1). >10nm Au NPs have been used extensively in the literature and the methods for their manipulation and functionalisation provided a solid base for the work we conducted into use of sub 10 nanometer Au NPs.

While using Au NPs to recreate simulated designs in a pixelated manner was conducted the goal of the project was to provide a template for continuous metallisation. This was not completed but potential novel pathways, both for the enhancement of existing metal particles into continuous structures, and the direct metallisation of sulphur containing artificial DNA sequences, was undertaken and provide some progress towards this future goal.

### 9.1 Gold Nanoparticle preparation

Sub 10 nanometer Au NPs were chosen as the initial metallisation seeds which would be applied to DNA modular breadboard designs in similar motifs to those simulated in chapters 6/11. Au NPs were prepared using a modified Turkevich method (With tannic acid used as a secondary reduction agent).

#### Gold nanoparticle synthesis

Protocols were taken directly from the synthesis techniques described by Piella [85] but some indirect modifications, such as the volume to concentration ratio of solutions, did take place.

TA 2.5 mM (mL)	Temperature	K <sub>2</sub> CO <sub>3</sub> 150 mM (mL)	pH before gold injection	pH after gold injection	Reaction time (min.)	Size ± SD (nm)
0.001	100 °C	1	10.2	8.3	6	9.1±1.0
0.01	100 °C	1	10.4	8.3	<1	5.0±0.7
<u>0.1</u>	<u>100 °C</u>	<u>1</u>	<u>10.3</u>	<u>8.2</u>	<u>&lt;1</u>	<u>3.5±0.7*</u>

Figure 85 Effects of variables in Au NP synthesis as observed by Piella [85]. Our experimental work was conducted using 3.5, 5, and 9 nanometer Au NPs whose synthesis methods are described above. TA refers to Tannic acid and K<sub>2</sub>CO<sub>3</sub> refers to potassium carbonate

Our synthesis was conducted using the overall concentrations/volumes of reagents above, however sodium citrate, which is not mentioned, was added as 1 millilitre of 330mM solution. 10 micrograms of BSPP were added to each 150ml reaction which was then left to incubate at room temperature, overnight, before any further experimental steps were conducted.

#### Au NP nanoparticles synthesis methods

- Glassware and stirrer must be thoroughly washed with aqua regia and copiously rinsed with ultrapure water before synthesis is conducted.
- 150ml of ultrapure water is brought the boil and constant vigorous (~1000rpm) stirring is engaged.
- 1ml of 330mM sodium citrate solution, 500ul of 300mM potassium carbonate solution, and 0.1 (3.5nm), 0.01 (5nm) or 0.001 (9nm), microlitres of 2.5mM tannic acid solution are then added to the synthesis solution.
- The synthesis solution is left to equilibrate for at least 60 seconds.
- 1ml of 25mM AuCl solution is added to the synthesis solution (at this point the solution should begin to undergo colour change).
- Once colour change is complete, and the solution is ruby red, the heat is removed and the solution left to stir.
- The solution is then placed on a heat mat, 10mg of BSPP added, covered, and left to incubate overnight.

## 9.2 Gold nanoparticle concentration

Before nanoparticles can be used as decoration for a DNA origami sample they must be concentrated to a level high enough for a significant percent of binding regions on each origami to be occupied.



Figure 86 A gold nanoparticle solution is aggregated, pelleted and resuspended into a lower volume solution with a higher concentration. Left to right – 1. Post BSPP addition Au NP solution. 2. Solid NaCl is added to the solution until distinct color change occurs. 3. The sample is pelleted ready for resuspension

Figure 86 outlines the process whereby a low concentration nanoparticle solution can be aggregated to create a higher concentration solution within a smaller volume. Once this process is complete a similar secondary resuspension cycle is conducted in which the pellet is resuspended using ultra purified water and then aggregated again by addition of a volume of pure methanol. The addition of methanol increases the effect of any residual NaCl, aggregating the solution again but with significantly less NaCl present and the supernatant again discarded. As methanol readily evaporates at room temperature this process uses the initial high NaCl step to aggregate the solution completely and then the second methanol step to remove any residual NaCl remaining from the first step leaving a relatively uncontaminated pellet, which can be readily resuspended in ultra-purified water once the process has been completed.

It was observed that complete aggregation of sample was not observed in the initial NaCl based aggregation step when the technique was applied to 5 and 3.5 nanometer Au NPs (As discussed section 4). For this reason, to improve efficiency, the potential role of methanol in the initial aggregation step was also examined.

#### Au NP aggregation methods

- 20% W/V NaCl crystals were added to the BSPP ligand exchanged Au NP samples.
- Experimental - at this step the addition of 10% W/V methanol to 5 and 3.5 nanometer Au NP samples to improve aggregation levels was also examined – however this process was conducted to increase efficiency and is not typically conducted in the literature.
- Once aggregation was complete samples were centrifuged at 13.7RCF for 15 minutes.
- The supernatant was removed carefully, leaving the pellet intact, and the pellet was resuspended in 500ul ultrapure water.
- 500ul methanol is added to the resuspended pellet solution causing re-aggregation.
- The sample is centrifuged at 13.7RCF for 15 minutes.
- The supernatant was removed carefully, leaving the pellet intact, and the tube was left to air dry for 120 seconds.
- The pellet is resuspended to the required concentration.

### 9.3 Nanoparticle functionalisation

As discussed in Chapter 4 Au NPs are attached to DNA origami template via thiolated DNA, where the thiol group is bound to the surface of the Au NP, and the DNA tether extends away from the Au NP making it available to bind to complementary sequences. Only once Au NPs have successfully undergone BSPP ligand exchange and resuspension into a solution of volume/concentration of interest can functionalisation take place as functionalised samples will be highly resilient to the NaCl aggregation method described above.

It should be noted when using thiolated DNA reduction followed by purification via a Freeze and Squeeze or DNA KIT extraction led to all attempts at functionalisation of gold nanoparticles to fail when tested with destructive divalent ions. This is likely due to significant lowering of thiolated DNA concentration within the solution being purified. Given these observations during both our project and others for functionalisation of gold nanoparticles below 10 nanometers in size, the reduction, and purification, of thiolated DNA should be avoided as it is a rate limiting step.

### Functionalisation method

- Thiolated DNA is mixed with Au NPs at a molar ratio of 50:1 (3.5nm), 75:1 (5nm) and 100:1 (9nm), thiolated DNA: Au NP, and the solution mixed via pipetting.
- 10% V/V 500mM pH3 sodium citrate solution is added, and the solution mixed by pipetting.
- Once the process is complete a sample can be tested by taking 1ul, placing it on a waterproof surface (Such a weigh boat) and then add 1ul of 20mM MgCl<sub>2</sub> solution, if functionalisation was successful the sample will remain ruby red (If functionalisation was not successful it will undergo color change to purple/grey – if this is the case it is likely a higher concentration of DNA is required in the functionalisation step).

## 9.4 Freeze and squeeze purification

Freeze and squeeze based purification (Discussed chapter 5) was employed to purify Au NPs of excess thiolated DNA post functionalisation. This process begins with an AGE separation step, followed by an excision of the Au NP band, following by a freeze spin cycle.

- An unpurified Au NP samples was electrophoresed for 90 mins in a 3% agarose gel using 0.5X TBE buffer.
- The band of interest was carefully excised, trimmed, and crushed.
- Freeze N Squeeze DNA gel extraction columns were used.
- The crushed sample was frozen, inside the column, for 3 minutes.
- The column was centrifuged for 5 minutes at 8000RCF and used immediately post recovery.

## 9.5 Centrifugation

Centrifuge based purification, in pellet/resuspension cycles, is a common method for purification of >10nm Au NPs using desktop centrifuges with RCFs up to 17K. We attempted to extend this method to sub 10nm Au NPs by employing an ultracentrifuge, capable of up to 250K RCF, with limited result discussed chapter 12.

## 9.6 Metallisation enhancement

The work conducted within this thesis provides a template for the creation of DNA origami/Au NP scaffold which could be further enhanced into continuous circuitry to create materials with properties similar to those simulated in chapter 11. One method of enhancement, a process which increases the volume of existing Au NPs via electroless deposition, is conducted using a reduction agent and metallic ion.

- A solution containing an attempt at DNA origami metallisation (i.e. a sample which contained purified Au NPs and DNA origami with tether sites to bind such nanoparticles) was required for enhancement attempts. Attempts were conducted on raw metallised samples, freeze and squeeze purified Au NP samples and metallised structures attached to a mica surface.
- The solution was raised to between 2.5 and 25mM AuCl and gently mixed via pipetting (In the case of surface bound structures solution at varying levels between 2.5 and 25mM AuCl was applied directly to the substrate).
- The solution was then raised to between 2.5 and 25mM ascorbic acid (In the case of surface bound structures solution at varying levels between 2.5 and 25mM ascorbic acid was applied directly to the substrate).

A novel method of continuous metallisation was also attempt using polyphosphothioate DNA strands. These sequences contain sulphur atoms in the backbone region of the DNA strand, rather than the terminal 5' or 3' region displayed by thiolated DNA sequences, meaning that they display many potential Au binding sites per sequence. It was thought that if these sequences could be metallised directly in an electroless deposition method, similar the step above, it would allow selective metallisation of DNA within a solution.

- 10% W/V PEG was employed as a surfactant which was added to the solution BEFORE metallisation took place
- 20 base pair poly T polyphosphothioate sequences, at 100 nanomolars, were employed in all attempts.
- The solution was raised to between 2.5 and 25mM ascorbic acid and mixed via pipetting.

- The solution was then raising to between 2.5 and 25mM AuCl, mixed via pipetting, and kept in a dark drawer for 1 hour.

## Chapter 10 Electrophoresis Matrix Alternator purification Methods

### 10.0 EMA - methods

As discussed in chapter 5, and demonstrated in results chapter 12, existing protocols for the purification of excess thiol DNA from a thiolated gold nanoparticle solution are each associated with specific limitations and bottlenecks with purification of sub 10 nanometer Au NPs in high throughput being unavailable. As the work conducted in this thesis is an attempt to provide a putative pathway towards high throughput material fabrication methods to mitigate the purification limitation were significantly examined. In terms of increased purified Au np output, when compared to existing methods, a novel electrophoresis trap system was created and tested.

### 10.1 EMA – Pathway overview

The EMA purification system uses a direct recovery from pre run AGE approach, similarly to the techniques described Chapter 5, but uses a trapping system to prevent any loss of sample, or if required, to concentrate single or multiple individual samples into a known volume.

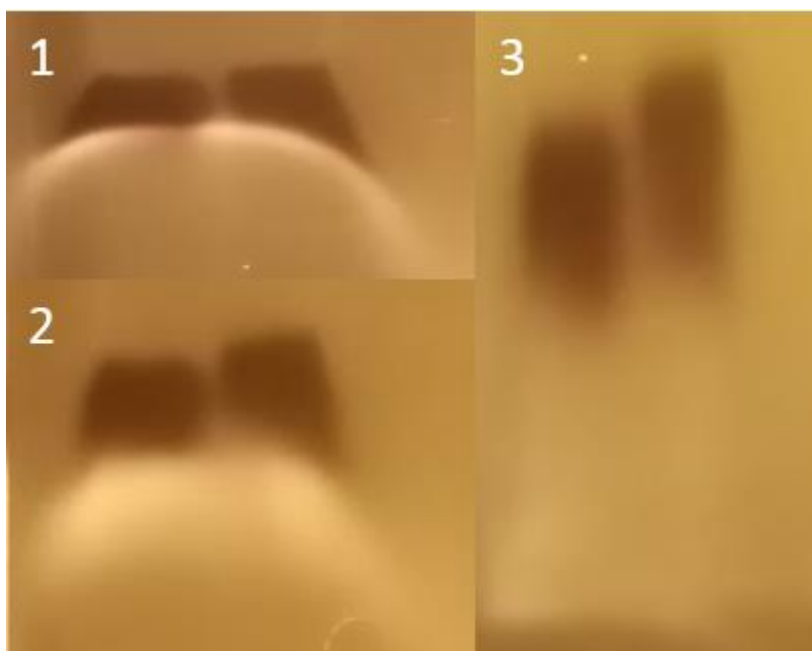


Figure 87 using the EMA technique the first step of purification is the complete separation of nanoparticle from excess thiolated DNA via native AGE. 1. The sample needs to be run for a time

before separation of nanoparticles and excess DNA takes place. 2. Over time both bands will regain conformation and stably travel through the gel as the excess thiolated DNA can be seen dispersing away from the nanoparticle band. 3. Once all traces of excess DNA have been removed recovery can be conducted and the nanoparticle band excised.

The initial step of purification is conducted in native AGE with a concise description shown in figure 87. Complete separation of the nanoparticle DNA conjugates and excess thiolated DNA must occur before the sample is recovered – if this does not occur completely then excess DNA will be trapped in the recovered sample – rendering the process ineffective.

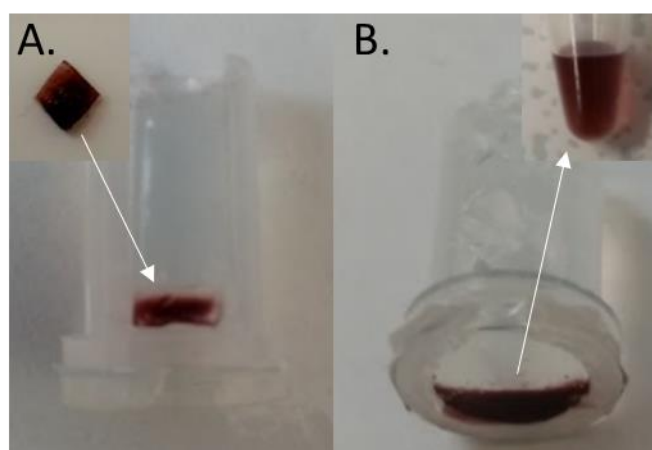


Figure 88 A sample contained within agarose is eluted into solution. A. An Au NP sample recovered from an AGE step (This sample was collected from the gel run in figure 102) is inserted into the body of the recovery device. B. The device is electrophoresed, and the sample is eluted from agarose into solution where it can be recovered directly.

Figure 88 shows the basic pathway of recovery of Au NPs from agarose back into solution in a single electrophoresis step using a lab made device. Once the electrophoretic separation, seen figure 86, is complete the sample containing agarose is excised, and then re-set into an agarose cap filling the device, and a secondary electrophoresis step is conducted on the device itself to elute the Au NP sample into solution.

## 10.2 EMA – Device/component overview

The device itself is fabricated using cheap and widely available materials typically found in most DNA, or similar molecular biology, focused wet labs. The device has 2 main sections, the agarose containing cap in which the sample is eluted from, and the recovery reservoir which the sample is eluted into.

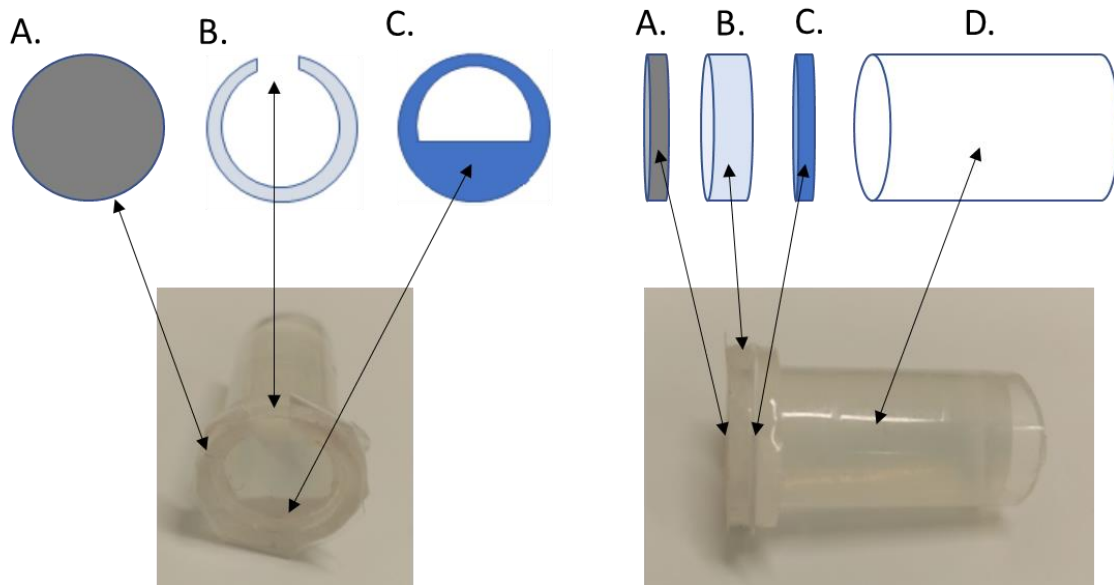


Figure 89 shows the features displayed by the device used to facilitate recovery of Au NPs from agarose back into solution. A. A dialysis membrane which caps the cathode facing end of the device. B. A small section of pipeway containing an opening to insert/remove buffer. C. A washer matching the shape of B. but also containing a small, protected region where sample will collect. D. the agarose containing body of the device into which the sample is initially inserted.

The device operated effectively during electrophoresis due to being ‘open’ to the electrophoretic field, which is created between the anode and cathode in a conventional electrophoresis tank, but ‘closed’ to Au NP elution due to the semi permeable dialysis membrane which caps the device. This can be seen in figure 89 in which every part of the device contains a hollow window or channel (Bar the semi permeable dialysis membrane).

### 10.3 EMA – Device fabrication

Each device requires 2 x 1.5 millimetre Eppendorf test tubes, a small piece of dialysis membrane and a standard weigh boat. Beyond these materials all that is required to fabricate the device is a scalpel for cutting, tweezers for manipulation, and cyanoacrylate to seal the components/sections together. It

should be noted that several adhesives were tested for use in device fabrication. Cyanoacrylate was chosen because it is cheap, highly watertight with no visible sample leakage, and very quick setting.



Figure 90 a 1.5 millilitre Eppendorf.

The test tube should be cleaned with isopropanol before it is used, and sterile gloves and equipment should be worn as once it is sealed as it is not possible to effectively clean inside the compartments created during fabrication.

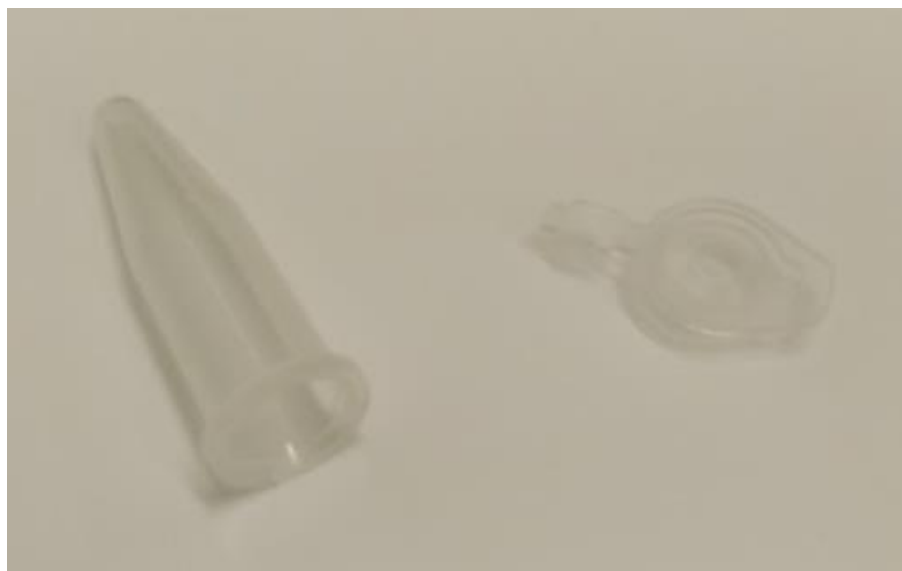


Figure 91 the lid is removed.

The lid should be cut quite close to the rim without damaging the lip of the test tube which it is attached to as it will later form a seal with another test tube.



Figure 92 the lip is removed from the test tube.

This should be conducted carefully. Cracking the lip will render it useless and the process will need to be restarted. Rather than cutting into the test tube it is effective to create an incision and then roll the tube back into the blade of the scalpel – this method leads to a smoother cut.

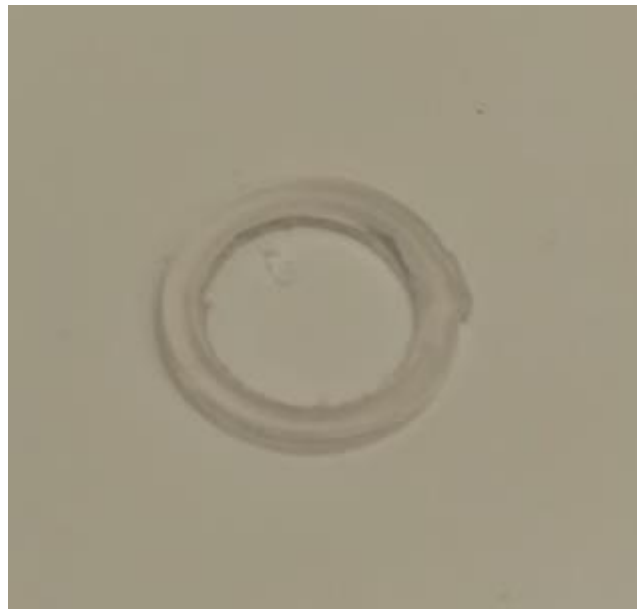


Figure 93 the removed test tube rim.

The rim should be trimmed along the edge which has just been separated from the greater body of the test tube. This edge forms a seal so should not present any gaps, which would allow sample to escape, or sharp edges, which would damage the components it is sealed too.



Figure 94 A standard weigh boat.

As with the test tube used to fabricate the device, if not sterile, the weigh boat should be cleaned before fabrication.

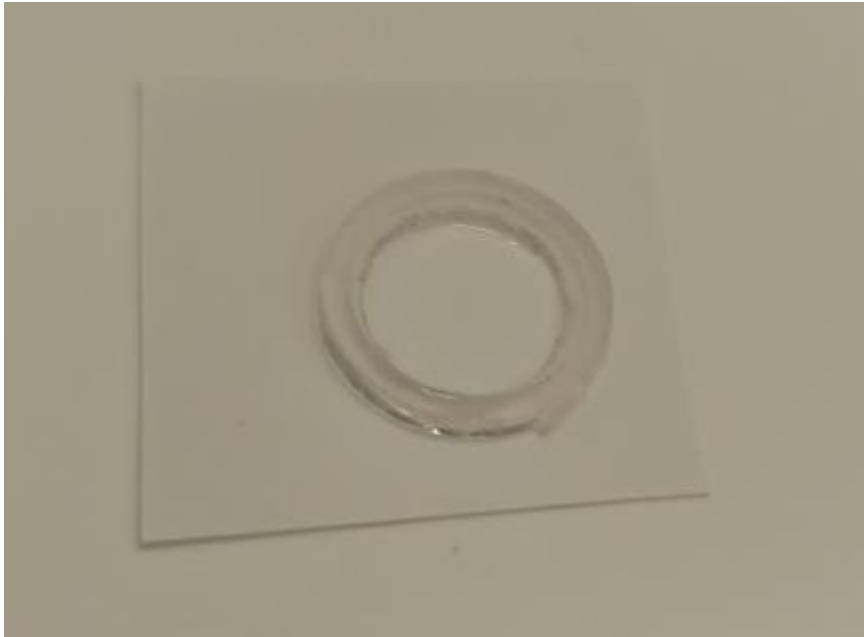


Figure 95 the rim of the test tube is attached to the excised centre of the weigh boat. Due to the thinness of the rim it is much more viable to use tweezers, or the end of a scalpel, to move the rim into, and around, a small pool of adhesive than to use gloved hands. Once the adhesive has been applied the rim should be carefully placed on the weigh boat surface and gently pushed down so any air pockets between the 2 surfaces are expelled. Gentle pressure should continue for roughly 20 seconds until a semi-permanent bond has formed.



Figure 96 excess weigh boat is trimmed. Once the adhesive has completely set the outer edges of the weigh boat can be removed completely. The inner surface should be trimmed completely aside from a flat edge 5mm above the centre of what will be the lowest point of the device when it sits in the electrophoresis tank. Images of the device post

electrophoresis, shown figure 134 and 135, demonstrate that this will be roughly the level at which the nanoparticle sample will sit once it has been eluted from the agarose. Aside from this catchment area the rest of the surface should be completely removed to allow effective travel of the electric field through the device during electrophoresis.



Figure 97 A channel is cut through both connected sections of weigh boat and test tube lip. This channel is where the sample will be withdrawn from. For this reason, it must be wider than the widest part of the pipette tip which will be used to evacuate the device once the sample has been successfully eluted.

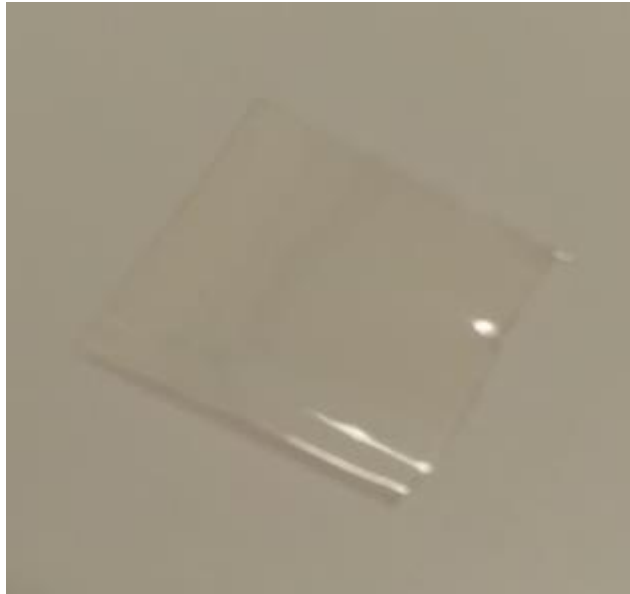


Figure 98 a piece of dialysis membrane large enough for the test tube to lay face down on. There should be sufficient room for the device to be placed on dialysis membrane without having to alter or adjust its position once it has been placed. As this membrane will function as the ‘window’ capping the device while allowing the electric field to propagate if the rim is moved across it before the adhesive is set, causing adhesive to permeate the matrix, it will lower the efficiency of the device considerably and/or stop its proper functioning.



Figure 99 the rim of the test tube is applied with adhesive and placed onto the dialysis membrane. As mentioned above the rim should be carefully applied once it has been rolled through a small pool of adhesive. While drift of the components once they have been placed is problematic so is use of excess adhesive which will be pushed out from between the surfaces, and onto the centre of the membrane, when gentle pressure is applied to push air pockets out from between the surfaces. Gentle pressure

should be maintained until a semi-permanent bond is formed between the 2 surfaces at which point it can be left to set.



Figure 100 Another test tube is now required which will form the body of the device. A second 1.5 millilitre test tube should now have its lid removed, in the same manner as the first, and then the tail region of the structure. The tail region should be removed from the point that any tapering of the test tube from cylinder into point is absent. If the structure is tapered i.e., one opening has a larger surface area than the other it will inhibit the effective propagation of the electric field through the device during electrophoresis and efficiency will drop and/or the device will not function correctly.



Figure 101 The body of the device is secured and capped with agarose.

If a sample is being eluted from agarose it can be inserted directly at this point. It should be gently pushed to the bottom of the device before the agarose sets. This step is not essential but the further the sample is from the bottom of the agarose cap the longer it will take to electrophorese out into the capture reservoir. To achieve a flat seal we placed the rim of the test tube onto a strip of cello tape, molten agarose could be then added directly, and the device could be left to set until solidified.



Figure 102 The 2 sections of the device are prepared for attachment.

The easiest way to join the 2 sections is to carefully apply adhesive to the lip on the agarose containing body and then place it directly onto the weigh boat surface, parallel to the sister lip beneath it, and gently press down until a permanent bond is formed. As mentioned above, it is imperative that adhesive does not contaminate the windows in the device in which the electric field propagates (The surface of the agarose being such a window). For this reason it is useful to create a small pool of adhesive and then gently roll the edge of the lip of the body of the device through it. Surface retention will effectively ‘pull’ adhesive onto the entire surface area of the lip without contaminating the surface of the agarose.



Figure 103 a tight seal is formed between the 2 surfaces and the device is complete.



Figure 104 running buffer can be injected directly into the collection reservoir.

As cyanoacrylate rapidly polymerises when it comes into contact with moisture the injection and elution cycle, of buffer into the reservoir, can be quickly conducted (Where the initial buffer is discarded and replaced in a cleaning step) to remove any excess adhesive present within the device or fix any areas in which have not set completely.

## 10.4 EMA – Device operation

Samples can be inserted into the device either directly as the molten agarose cap is setting or once the device is constructed by cutting a channel into the agarose cap, by removing a section of the insulated structure, and filling the enclosure it is within with running buffer allowing efficient transit of sample from agarose shard, to buffer, to the columns agarose cap, to collection reservoir. It should be noted that if the latter method is conducted the insertion cut into the agarose body must be conducted above the water line of the buffer filling the greater volume of the tank to prevent sample dissipating when it leaves the insertion agarose and is eluted into the running buffer before it enters the agarose making up the main body of the recovery device.



Figure 105 A sample is placed into the device

If a sample has not been set directly into the body of the device when it was cast with agarose then a small section of agarose can be excised and a sample inserted directly into the body of the device. The area surrounding the implanted agarose shard should be filled with running buffer to facilitate transference of sample from the inserted agarose, into the body of agarose in the device itself, before it is eluted into the capture reservoir.



Figure 106 the sample is eluted through the device into the collection reservoir over time. Typically the capture reservoir is filled with buffer before the greater volume of the tank. However once filled, and secured to the bottom of the tank, it can be completely submerged within the buffer reservoir of the electrophoresis tank (ONLY if the sample was inserted directly into the molten agarose cap). If

conducted as described, with a sample proximal to the collection reservoir, complete elution should be completed within 15 minutes, when the tank is operating at 100 volts.



Figure 107 Excess running buffer is extracted from the recovery reservoir.

Over time the sample will sediment in the bottom of the collection reservoir below the line cut into the weigh boat/insulated back plate. If increase in overall concentration is required the supernatant/excess buffer can be discarded. However, care should be taken when extracting excess running buffer as the nanoparticle solution typically exists as a concentrated solution, rather than solidified pellet, as is the case during purification by centrifugation, and some colloid can be carried into the solution being discarded if care is not taken. Finally, the nanoparticle sample can be extracted via the recovery window via pipette.

Any functionalised nanoparticle sample should be used immediately prior to recovery as over time oxidation of thiol attachments will lead to excess, unattached, DNA tethers accumulating in the solution.

#### Device based purification method

- Functionalised Au NPs are first separated via AGE using 3% agarose gels and 0.5X TBE running buffer.
- The body of the device (Figure 103 D) is filled with 1% molten agarose (Figure 129) the Au NP sample can be inserted into the body while the agarose is still molten or it can be inserted as described above (Figure 133).

- The body is attached to the recovery reservoir (figure 131) and left to set.
- The device is fixed in an electrophoresis tank, parallel to the direction of the electric field, with the recovery reservoir facing the cathode.
- The tank is filled until only the recovery window at the top of the device is above the buffer line.
- Electrophoresis is engaged at 100 volts until complete elution of the sample into the recovery well is observed (Typically around 15 minutes).

## 10.5 DNA purification

Attempts were also made to use the EMA system to purify DNA origami fabrication solutions of excess staple components. The only difference in protocols was the exchange of the membrane employed during electrophoresis and how the sample was inserted into the device (Directly into the recovery reservoir in solution rather than into the main agarose cap as an excised sample post AGE). During purification attempts of DNA origami based samples fabrication solution was inserted directly into the recovery reservoir briefly due to the charging effects discussed more fully in section 10.5.

The step described in figure 130 must be altered to employ a PES based membrane rather than the cellulose based dialysis membrane employed during nanoparticle purification. Briefly, this is again due to unwanted surface charging effects displayed during  $MgCl_2$  containing buffer during electrophoresis, but this is discussed more fully in results chapter 14. Another modification is the use of cyanoacrylate, which was employed for cellulose based membrane attachment, being unsuitable for PES based membranes as it destroys them, so epoxy type adhesives were employed but with limited success as described Chapter 14.

# Chapter 11

## 11.0 Simulation results

Results were collected from the simulations described in Chapter 6. We begin by comparing results between structures sharing the same diameter, but with differing split sizes, and then by structures with the same split size but differing diameters.

### 5nm diameter structures

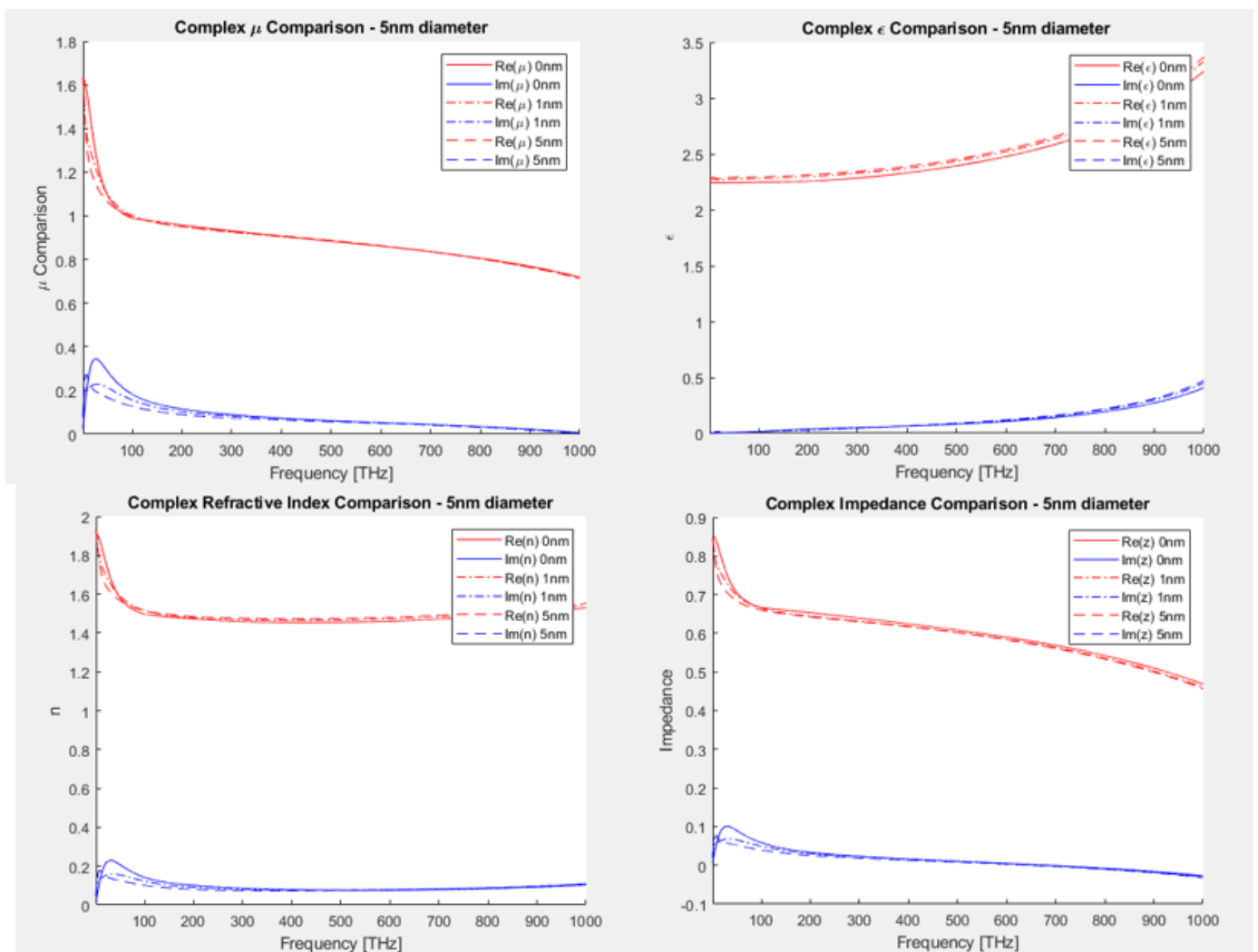


Figure 108 – 5nm diameter structure results. Top left – Complex permeability. Top right – complex permittivity. Bottom left – complex refractive index. Bottom right – complex impedance. Legend – Split sizes

The 5nm structures showed minor deviation due to split size in both permittivity and refractive index. There are also some changes in imaginary component behaviour at the beginning of the frequency sweep.

There seems to be some form of resonance occurring just before the frequency sweep begins in terms of the real components of all parameters bar permittivity. The imaginary components show a peak at around 40 terahertz (Also barring permittivity) and interestingly the addition of a split gap lowers this effect with the largest split gap having the greatest effect.

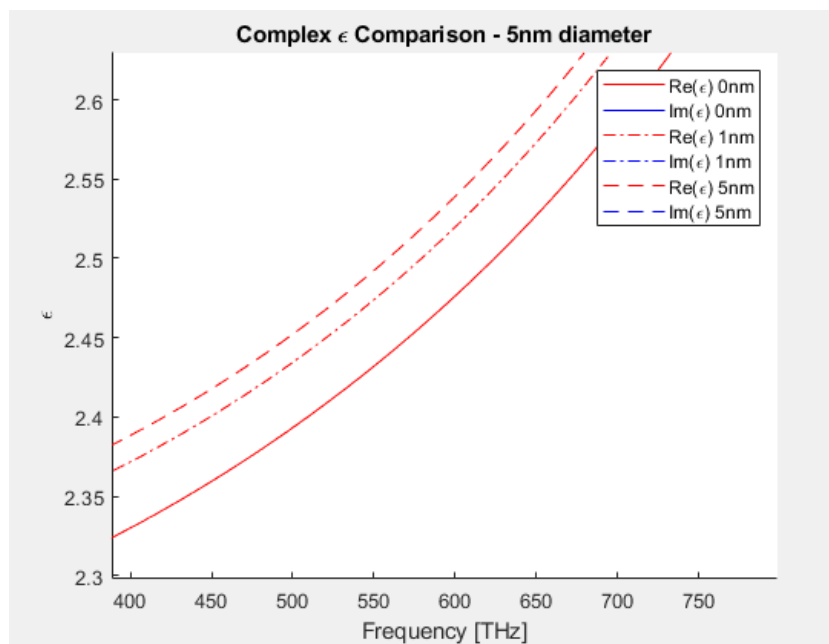


Figure 109 Real permittivity (Complex results magnifying area of interest) over the visible range.  
Legend – Split sizes

Figure 109 shows that the inclusion of a split in the ring structure increases electrical permittivity over the visible range with the largest split size displaying the largest increase. While not a huge increase it does validate the system as a tool for interaction (Although likely with further modification) with visible light.

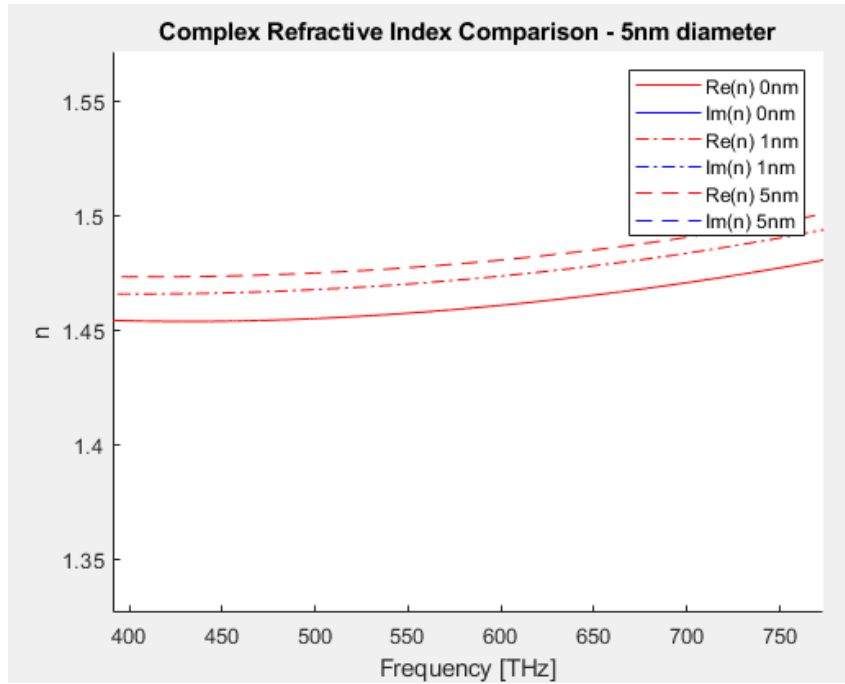


Figure 110 Real refractive index comparison (Complex results magnifying area of interest) over the visible range. Legend – Split sizes

Figure 110 displays that there is an increase in the real component of the refractive index over the visible range. The level of increase is again matched to the change in gap size of the structures being simulated.

### 10nm diameter structures

While the 10nm diameter structures do not show significant deviation over the visible range there are points of interest at the beginning of the frequency sweep.

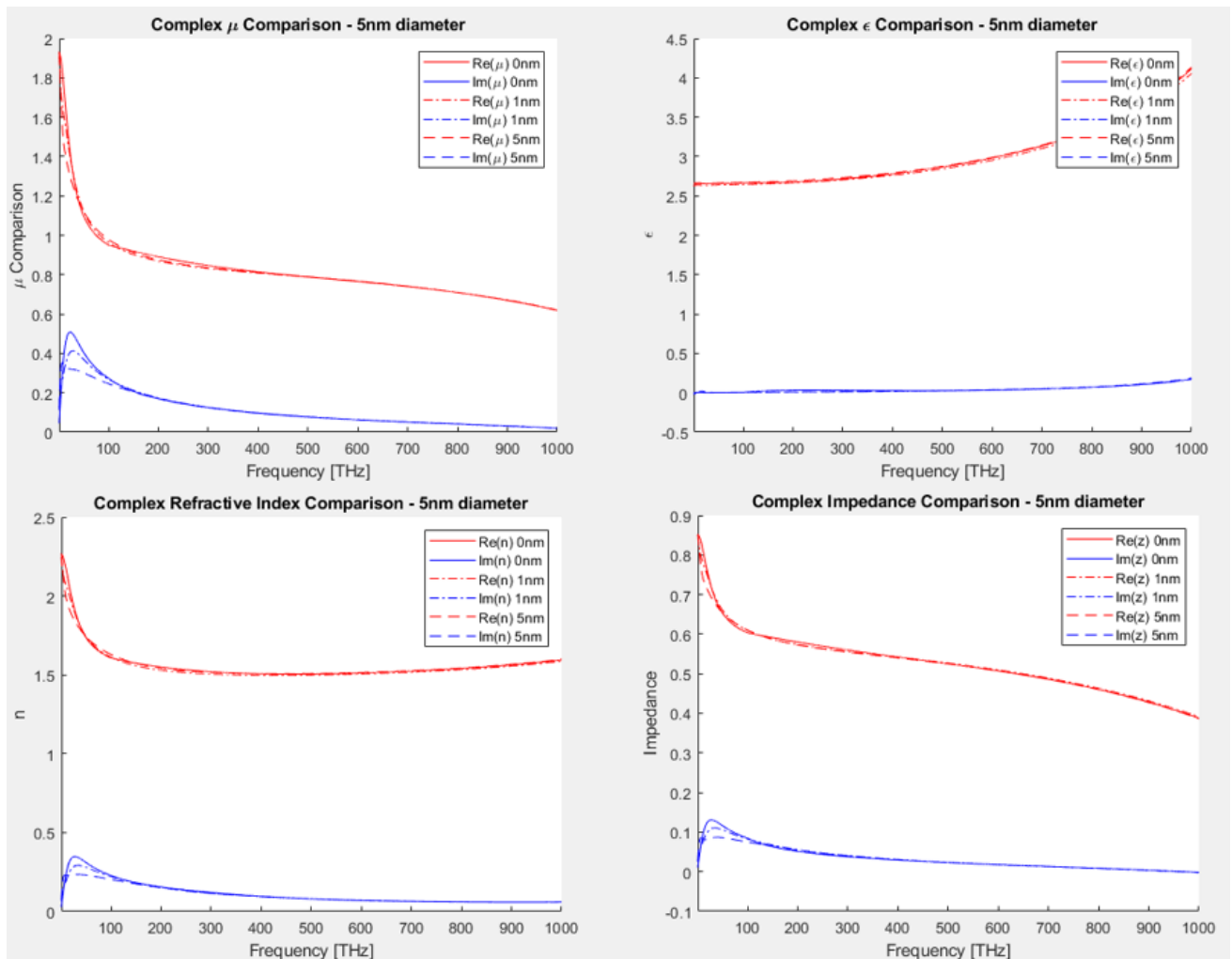


Figure 111 5nm diameter structure results. Top left – Complex permeability. Top right – complex permittivity. Bottom left – complex refractive index. Bottom right – complex impedance. Legend – Split sizes

The resonance observed at the beginning of the frequency sweep is more significant in the 10nm diameter structures. Also of interest is the significant reduction of the imaginary component of the permittivity and refractive index at beginning of the frequency sweep (Where the reduction in peak is ~40% magnitude). This would suggest that employing a split gap could be used to reduce loss in these frequency ranges.

## No gap

5 and 10nm diameter square ring structures (With no split) were compared.

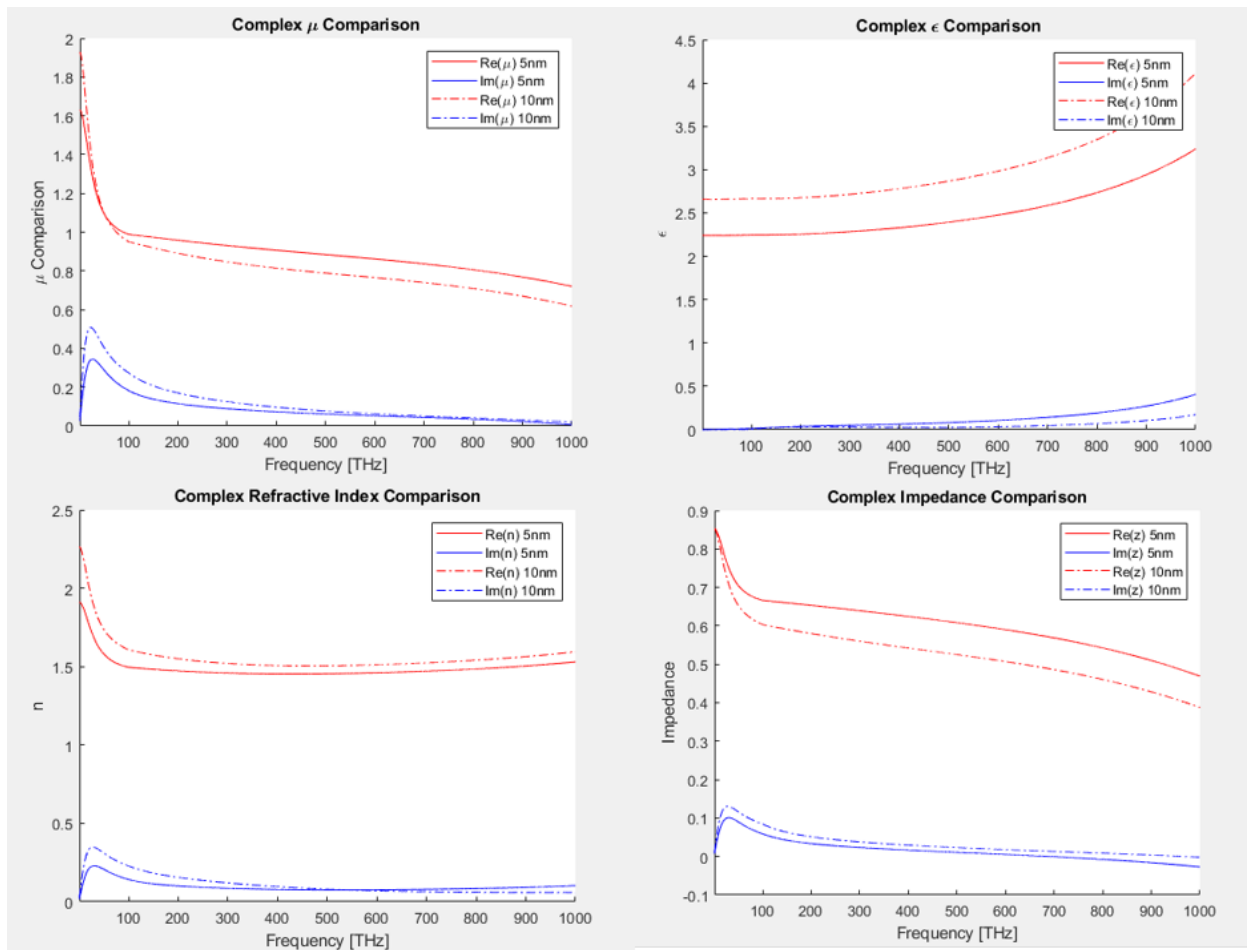


Figure 112 5 and 10nm diameter, no split, structure results. Top left – Complex permeability. Top right – complex permittivity. Bottom left – complex refractive index. Bottom right – complex impedance. Legend – diameter sizes

Figure 112 shows that the diameter of the ring shows significant effect on the structure's interaction with the frequency range even when no split is present. The real permeability of the 5nm diameter structure is around 20% higher over the visible range where the imaginary component is reduced by 50% in the larger 10nm structure at the beginning of the frequency sweep. In contrast the larger 10nm diameter structure shows a similar increase over the 5nm structure, in permittivity, over the entire frequency range. The larger structure shows a higher refractive index coupled with a higher loss until the end of the frequency range, where the real component remains higher than the 5nm structure, but the loss becomes lower. Real impedance of the 5nm structure is ~10% higher across the frequency sweep and it also displays a slightly lower imaginary component also.

## 1nm gap

The results of the 1nm gap are very close to those recovered from the no gap group but there are subtle changes which imply that in some cases the system is behaving quite differently.

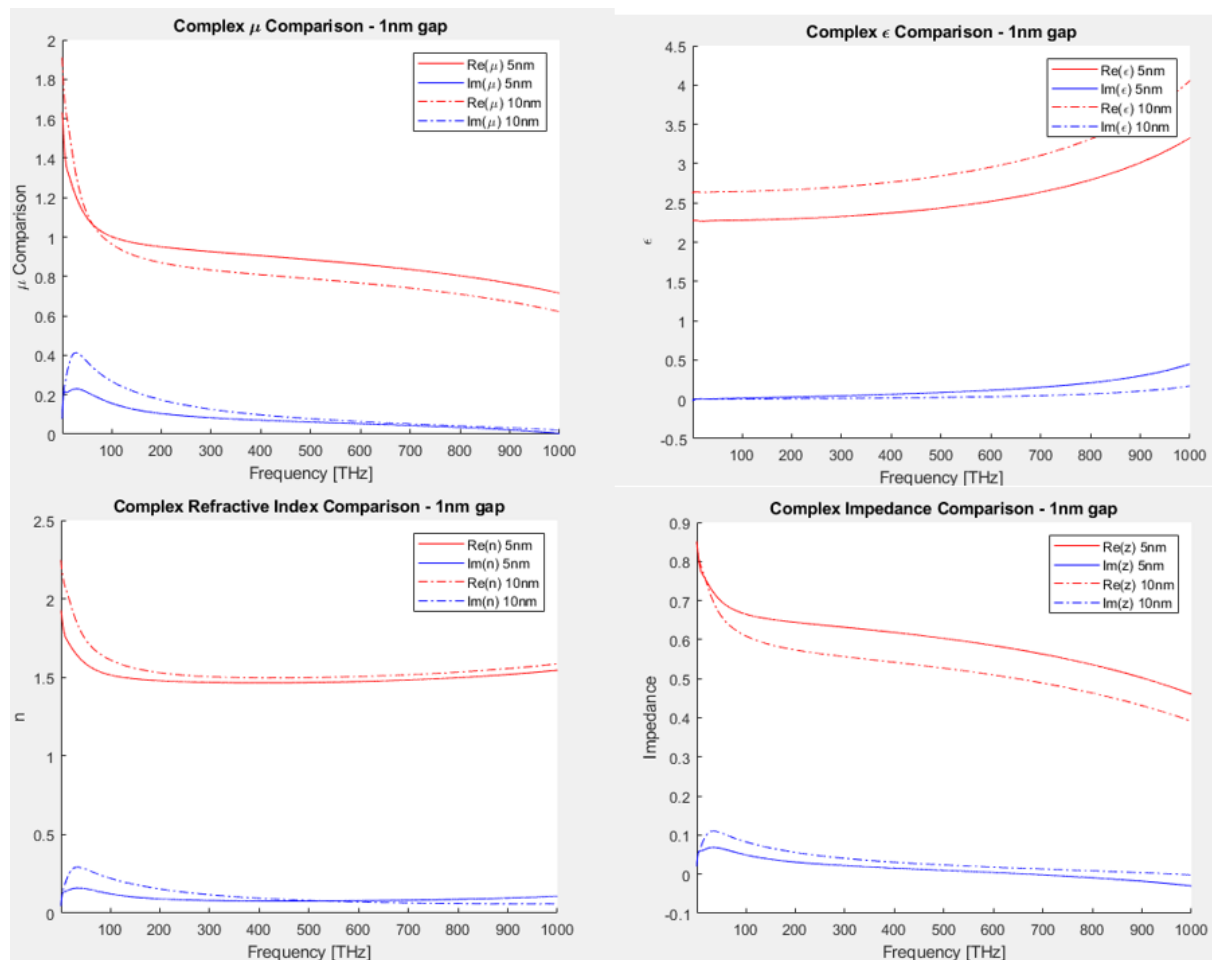


Figure 113 and 10nm diameter, 1nm split, structure results. Top left – Complex permeability. Top right – complex permittivity. Bottom left – complex refractive index. Bottom right – complex impedance. Legend – diameter sizes

While overall results are similar the addition of the 1nm gap in the 5nm structure nearly halves the imaginary component of the permeability at the start of the frequency range when compared to the 10nm result. There is further evidence that there is a resonance peak before our frequency range begins as the imaginary component of the impedance becomes negative during the beginning of the sweep, and in the case of the 5nm structure, again from ~650 terahertz. As this imaginary component relates to loss in the system when negative it implies that energy is being created/stored (Likely in the form of capacitance and in a passive system this is only possible at resonance [116]). A similar effect is also observed in the permittivity, although in this case much smaller, again signalling that energy is

remaining within the system. In terms of refractive index the imaginary component becomes smaller, in both cases, at the beginning of the frequency sweep.

## 5nm gap

The 5nm system has lost the negative value of permittivity at the beginning of the frequency sweep and the dynamics effecting the imaginary components at the start of the sweep have also changed further.

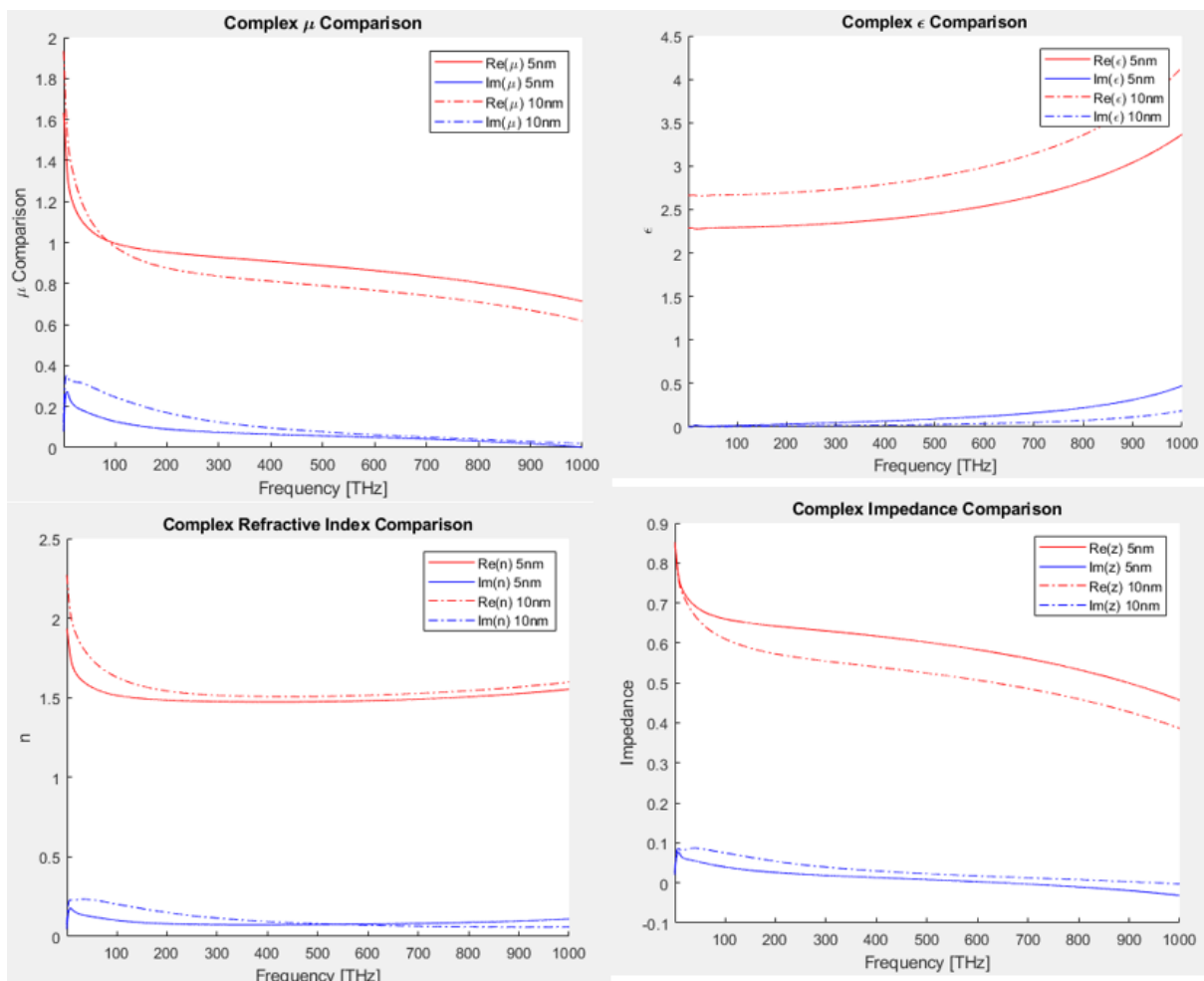


Figure 114 5 and 10nm diameter, 5nm split, structure results. Top left – Complex permeability. Top right – complex permittivity. Bottom left – complex refractive index. Bottom right – complex impedance. Legend – diameter sizes

In the 5nm gap structures the peak in imaginary permittivity at the start of the sweep has been lowered in intensity, reducing the peak to a gentle curve in the case of the 10nm structure, and creating a relatively sharp peak which quickly dissipates in the case of the 5nm example. The negative effect of the imaginary component, of both structures, is further increased with the 10nm structure passing from

a positive to negative value for the last 25 terahertz of the run. The imaginary component of the refractive index is further lowered at the beginning of the sweep, in the same manner as the permeability, with a faint peak in the 5nm structure followed by a gentle curve, and only a gentle curve (With no peak) from the 10nm.

## 11.1 Conclusion

On the surface simulations were challenging and there was no significant change in the real component of the refractive index by modification of the structures. However, upon further examination, there are significant changes in dynamics created by only very small modifications to the structure. In terms of refractive index the reduction of imaginary component, at the beginning of the sweep, by addition of split in the structure demonstrates that this structure will display a lower loss when frequencies in this range are transmitted through it.

Another significant effect is the demonstration of capacitance, when the imaginary components of the permittivity, and impedance, become negative in the split ring structures. This shows that the structure is acting as intended and a current is being formed due to the effect of the external EM field. While rather mild in intensity, and for real world applications this effect would likely need to be increased, it serves as a strong proof of concept. Finally the change in diameter of the structure itself, with or without split in the structure, is shown to have a significant effect on the dynamics of interaction with the frequency sweep. Given the different levels of metallisation displayed in various studies shown in chapter 4 it is likely many levels of metallisation could be employed for varying effect.

Our results strongly suggest the structure is resonant at some point before 1 terahertz (Where our sweep begins). While unfortunate that it was not more central in our results this does reinforce that it is possible to create resonances with these types of structures around the wavelengths of interest. With further tuning, and simulation, it is likely that resonance could occur within the optical range (Rather than just outside it) and further interesting (and/or useful) effects created.

## Chapter 12

### 12.0 DNA fabrication results

Experimentation was conducted on each step of the fabrication process. This begins with the choice of ionic conditions in which fabrication takes place, identifying specific design motifs to address weaknesses in the tail region of the board design, and an effective thermal cycle which folds boards in high throughput without degrading the sample. We also examined expansion of single boards into 1 and 2-dimensional lattice strings and methods for recovering such structures.

Beyond basic fabrication considerations we also explored the efficiency of fabrication which could be achieved when a fabrication solution is ‘starved’ of staple strand components and if the fixation step, used to prepare DNA origami for visualisation via AFM, could be modified to effectively differentiate between certain sample types and become an effective part of the fabrication process for surface based materials.

Due to the excess of fabrication components employed during self assembly it is likely that any DNA origami fabrication which employs a secondary fabrication step (Such as metallisation) needs to highly purified of excess DNA to avoid sequence interference. We examine various common methods of purification including novel substrate based fixation and attempts at purification using the EMA method.

### 12.1 Ionic conditions

Initially tests were conducted on the effect of varying  $MgCl_2$  concentrations within the fabrication solution during the full sweep thermal cycling step, as while a thermal sweep can be adjusted for efficiency, DNA origami formation will not occur without the correct concentration of divalent ion [59].

Identical samples, in terms of scaffold and staple sequence, as well as the specific ratio of scaffold to staple, were altered with differing ionic conditions and were subject to a full sweep thermal cycle. These

samples were created using a poly T spacer tail region. Once thermal cycling was complete samples were analysed via AGE as described in section 8.6.

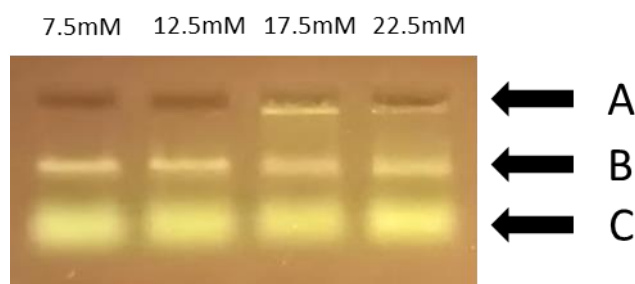


Figure 115 Scaffold and staple samples annealed over the full sweep thermal cycle with varying  $MgCl_2$  levels present are analysed via AGE. From left to right the levels of  $MgCl_2$  are increased in increments of 5mM beginning 7.5mM, 12.5mM, 17.5mM and 22.5mM. A – Insertion pocket. B – folded scaffold DNA band. C – Excess staple band.

Figure 115 shows that, in terms of the relative  $MgCl_2$  levels required to fabricate correctly folded boards, there is a broad window in which successful fabrication, which exists in the B band, can occur. However when the  $MgCl_2$  increases beyond 12.5mM slow moving aggregates become visible in proximity to A. The intensity and sharpness of band B in both the 17.5mM and 22.5mM lanes are comparatively lower those in the 7.5mM and 12.5mM samples, and there is significant trailing effect behind the correctly formed B structures in the higher  $MgCl_2$  lanes. There is also a slight change of relative mobility within the bands as  $MgCl_2$  concentration increases with band B at 22.5mM progressing slightly further through the gel than band B in the 7.5mM and 12.5mM lanes. These effects would suggest that the fabrication process loses efficiency beyond the 12.5mM level and there exist many different species of incorrectly folded structures, and completely unfolded aggregates, when the  $MgCl_2$  level in the solution increases beyond this threshold.

- 12.5mM  $MgCl_2$  was chosen as the level used in fabrication. While there is little difference between samples at 7.5mM and 12.5mM, due to potential strain put on individual tiles in future work, such as linking boards, and Au NP attachment, it was decided that the increased divalent ion levels would be of benefit due to the higher concentration of negatively charged DNA present in these runs.

- Poly T spacers were initially employed at tail regions. As these sequences did not significantly vary the overall number of DNA bases within the design it was theorised effective ionic conditions would not be affected.

## 12.2 Board tail region assembly interference

There is a need to prevent base stacking effects between helices during fabrication, or when fabricated structures are attached to a substrate for imaging or spectral testing, and to prevent nonconstructive aggregation leading to failure of the design. This set of fabrication attempts was conducted using the idealised ionic conditions described above.

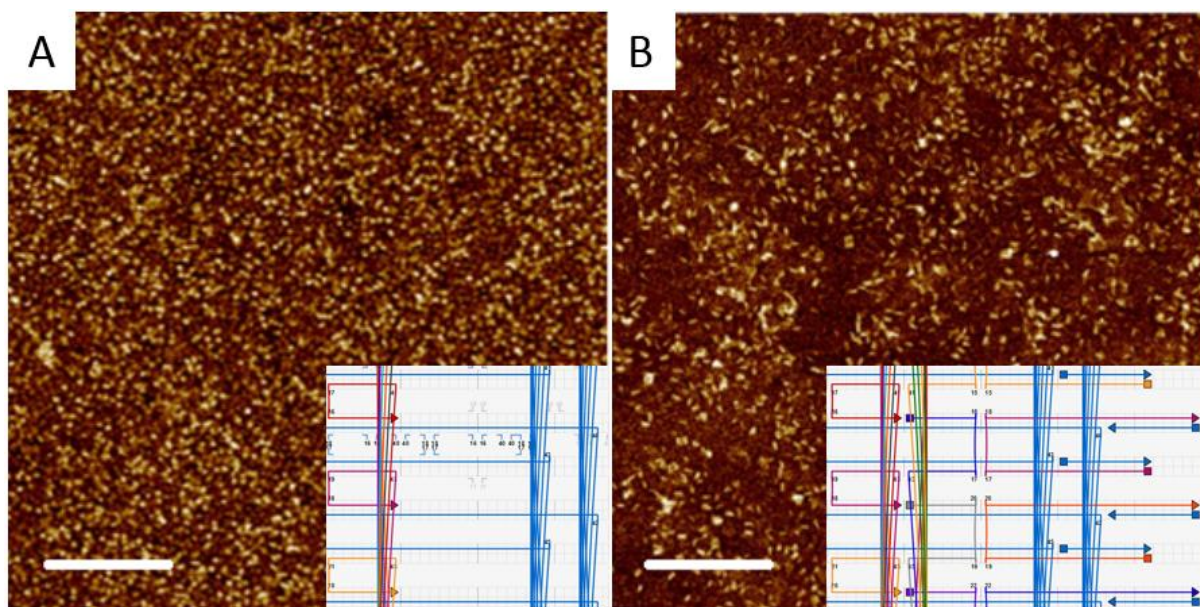


Figure 116 AFM images of fabrication solutions thermally cycled over the full sweep of temperature ranges with varying tail regions. A. The sample featuring the highly embedded tail motif. Bottom right - caDNAno schematics of the edge of the design. Between 16 and 22 bases are left uncomplemented. B. The sample displaying Poly C tails extended out from the main body of the structure. Bottom right - caDNAno schematics displaying the poly C tails extending out past the boundary of the scaffold by 10 bases. White bar – 1 micrometre.

As shown in figure 116. Both the highly embedded and poly C tail designs failed during fabrication and or imaging. While there is evidence of some distinct formations within the samples, it is nonconstructive, and when examined further there was no evidence of constructive fabrication of any kind and both samples also contained extensive aggregate (In contrast to the board structures highlighted below/figure 108).

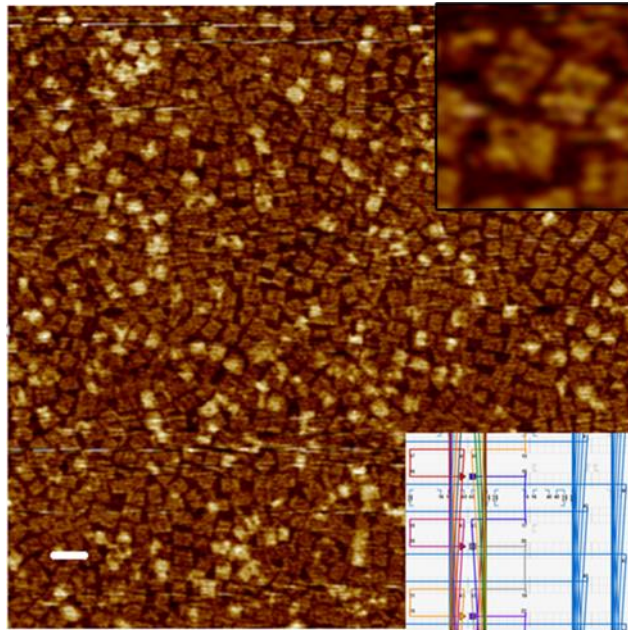


Figure 117 AFM image of a fabrication solution thermally cycled over full sweep of temperature ranges. Bottom right -The caDNAno design showing uncomplemented scaffold at the edges of the design. Between 9 and 14 bases are left uncomplemented. White line – 100 nanometres.

However, in the case of the moderately embedded design, figure 117, the initial fabrication attempt was successful. Boards are present in high throughput and appear to be fully formed. While ‘junk’ is visible in this sample, both on and around DNA origami board structures, this can be removed in later purification/fixation steps, discussed more significantly in chapter 5, and is due to the large excess of fabrication components within the fabrication solution. It is notable that the boards are rectangular (Rather than the square  $\sim 50 \times 50 \text{ nm}$  predicted) this is likely due to the single stranded, uncomplemented, tail regions at the ‘sides’ of the board being flexible and not providing as strong a signal when probed by the AFM.

- The moderately embedded design (With 9 to 14 base pair uncomplemented scaffold in the designs tail region) was shown to be successful and employed as the fabrication template for further experimentation (Such as lattice formation and Au NP attachment).
- Protocols used to create the poly T confirmation design were also highly effective when used with the moderately embedded design.
- Boards are present in high number, without noticeable defect, and seem to lie flat on the mica surface without folding or bending.

- Boards measure 45 x 55nm with ~2nm thickness

## 12.3 Thermal cycling protocols

Fabrication experimentation was conducted to determine a thermal cycling protocol for the efficient and stable fabrication of the modular board. This was done by examining narrower thermal windows within the full thermal sweep and imaging fabrication solutions exposed to these cycles directly via AFM. Efficiency protocols were conducted using the design in which the modular board is in its base configuration, with no sequences extending out of the structure to bind external groups, and lacking components able to bring individual boards together into a rational lattice.

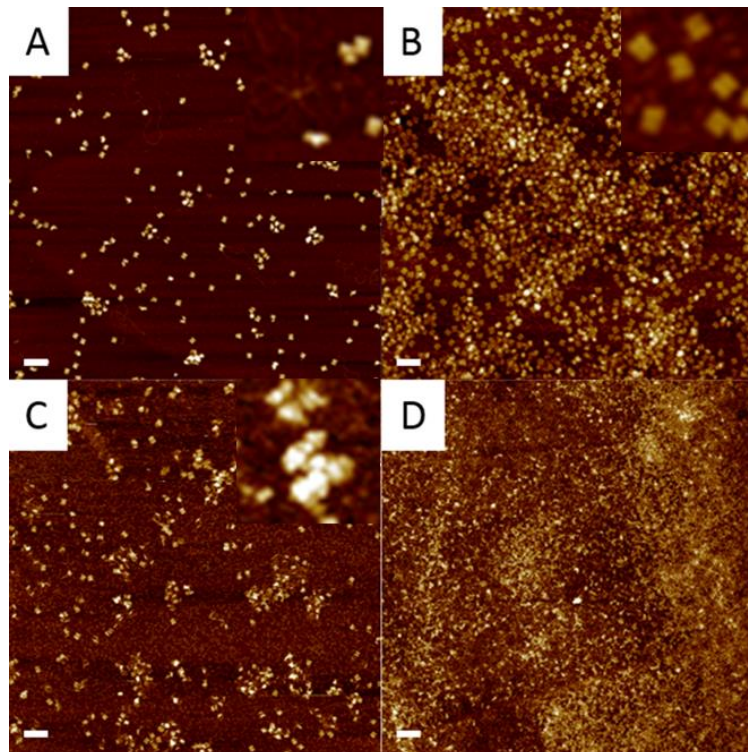


Figure 118 Fabrication solutions thermally cycled from high temp to low temp, over 5 hours, at various temperature windows. A. 45-41°C B. 50-46°C C. 55-51°C D. 60-56°C. White line – 200 nanometres.

Figure 118 illustrates that there are very significant, and distinct, levels of constructive folding which occur over relatively small temperature domains. Figure 57 would suggest folding which leads to the correct assembly of the DNA origami boards we envisage likely occurs within a relatively small

temperature range between 50 and 46°C. It is also worth noting that while temperature domain A shows some correctly folded structures it is at a significantly lower throughput.

Further analysis of folding patterns was conducted by examining the folding windows which showed the highest relative levels of folding over a relatively short period of time. To examine the effects of folding at certain temperatures, in terms of relative activity rather than of absolute fabrication within the folding range of interest, we significantly reduced the thermal cycle to 30 minutes at 65°C, to break hydrogen bonding in the scaffold strand, and then 15 minutes over a single °C temperature change. It was hoped that by reducing the folding time complete folding would be significantly hindered, or at least retarded, and folding dynamics could be examined in more detail than that which is presented by a single correctly folded band.

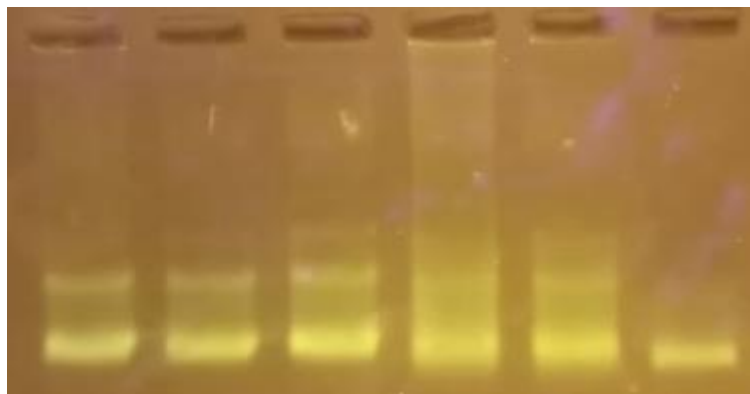


Figure 119 Folding over single °C temperature steps in 15 minutes contrasted with a sample folded over the full temperature sweep. Folding domains – Lane 1 – 50-49, lane 2 – 48-47, lane 3 – 47-46, lane 4 – 46-45, lane 5 – 45-44, lane 6 – sample folded over the full sweep thermal cycle (60°C to 40°C over 20 hours).

Figure 119 shows folding dynamics occur and change over a relatively short thermal window. Lanes 4 and 5 seem to show the fastest migration of the semi-fabricated bands but still do not migrate as quickly as the product of the full sweep thermal cycle. It is notable that the fastest migrating products also show the highest levels of aggregation displayed as immobile bands proximal to the loading pocket at the top of the gel. This effect is further reinforced in lane 4 as a smearing band showing many different species of misfolded products from complete aggregate to the highly mobile species at the bottom of the gel. Lanes 1 to 5 also show a clear lower mobility band, trailing the most mobile species of each

lane, with faint aggregate between them. While there is no significant band visible in lane 6 there is a very faint smearing band trailing the correctly fabricated band in the same manner.

Analysing lanes to their nearest neighbour is also useful as it can show over which domains significant activity is occurring and where significant changes in folding dynamics take place. Lanes 1 and 2 share very similar patterning bar the light aggregation observed in the loading well in lane 1. Lanes 2 and 3 are also similar but lane 2 contains much less visible aggregate. There is a very distinct shift in folding between lanes 3 and 4 with lane 4 showing the greatest levels of overall folding and a high mobility band. In lane 5 the overall folding is reduced, with a significant reduction in aggregate, and the high mobility band is retained.

This examination suggested that while significant folding occurs at the lower end of the 50 - 46°C range it also extends into the high end of the 45 - 41°C domain. Taking these observations into account we ran a sample over the observed high folding temperatures.

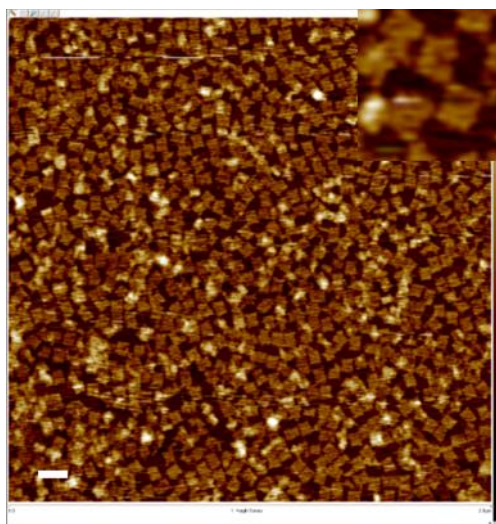


Figure 120 A fabrication solution incubated between 46 to 44 degrees C over 2 hours. White line – 100 nanometers

Figure 120 shows that when the window was extended to cover the region between two of the original five degree thermal windows, as showing in Figure 58. A and B, large scale constructive folding was observed.

- High efficiency folding of the DNA origami breadboard could be achieved in a single ~2 hour step between 46°C and 44°C.
- It should be noted that when tested with all surface modified designs (Such as those used to anchor Au NPs to the boards surface) the high efficiency protocol remained equally effective suggesting that double stranded folding dominates the thermal requirements while staple length (Or certainly the sub 50bp lengths used in this fabrication) has a limited effect on required thermal cycle.

## 12.4 Staple efficiency

It has been stated that an excess of fabrication components, in this case staples, is crucial for fabrication success. Having identified what seemed to be a highly efficient folding pathway we re-examined the effect of staple reduction on a fabrication conducted over the high efficiency thermal domain.

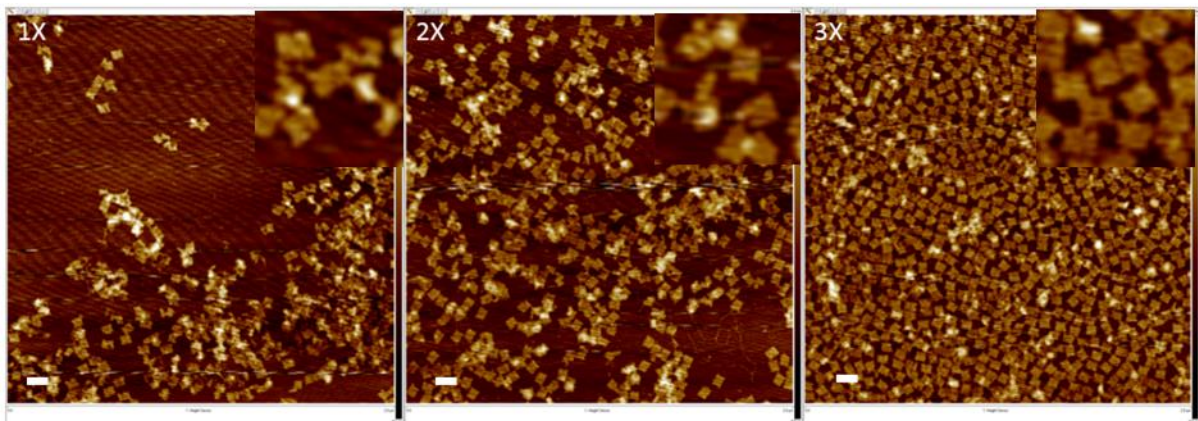


Figure 121 DNA origami boards folded between 46 and 44 degrees C with an hour cycle per complete transition over the thermal range. White lines – 100 nanometers

The images in figure 121 suggest that in the case of the modular DNA origami breadboard, efficient, high fidelity, fabrication can occur at a significantly lower staple to scaffold ratio than that which has been suggested in the literature. This is likely due to the boards relatively thin nature, which would allow access to every point of the board during fabrication, rather than a thick structure whose outer domains could possibly seal inner sites from fabrication if complemented first during a thermal cycle.

- Some board formation was observed at the lowest staple ratio with high throughput formation observed at 30% staple concentration when compared to a standard 10X staple excess reaction.

## 12.5 One pot lattice growth

Initial lattice fabrication was conducted in a single reaction where all correctly identified fabrication components and methods were employed with the addition of lattice sequences in the 2-dimensional motif discussed in chapter 7.

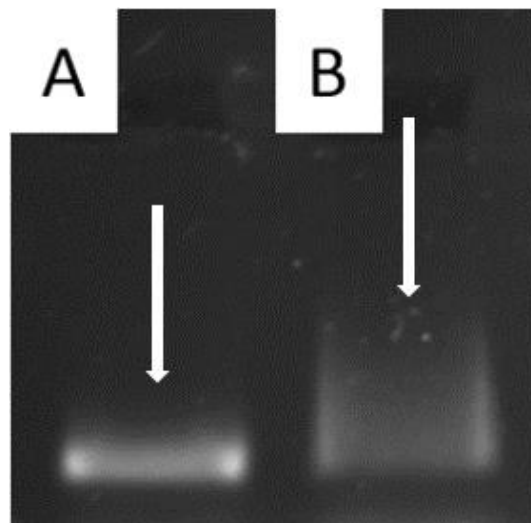


Figure 122 AGE results of monomer and lattice fabrication samples cycled over the full temperature sweep. A monomer DNA origami board sample B. A fabrication solution containing all fabrication components present in sample A and also lattice components extending in the X and Y dimensions. White arrows highlight the difference in mobility between the 2 species with lane A exhibiting a significantly more defined and uniform band than lane B.

Figure 122 shows that the addition of lattice components changes the species which make up the fabrication samples significantly. The species within lane B are different in conformation and over time they are separated due to their varied mobility by the uniform lattice of the agarose gel in a similar manner to the unfolded samples seen figure 59. The formation of the band would also suggest that while there are very likely certain species within sample B that are different to sample there are also a small fraction that are either the same or very similar as the most mobile species, travelling further down the gel during electrophoresis within both bands, terminate at the same point. The smearing effect is also unbroken suggesting that while the species within sample B are diverse they are not regimented into the envisaged monomer tiles or extended geometric lattices (Which would present as many individual

bands rather than a smear). This implies that while there are possibly correctly folded boards, and regimented geometries containing multiple boards, there are also significant incorrectly fabricated artefacts preventing formation of clear and regimented bands within the sample.

Further analysis of the sample was conducted by excision of a piece of agarose at the base of the fabrication band in lane B. The sample was recovered via Freeze and Squeeze column which is discussed in more depth in the purification chapter 5. This sample was compared to the raw fabrication sample it had been recovered from under AFM.

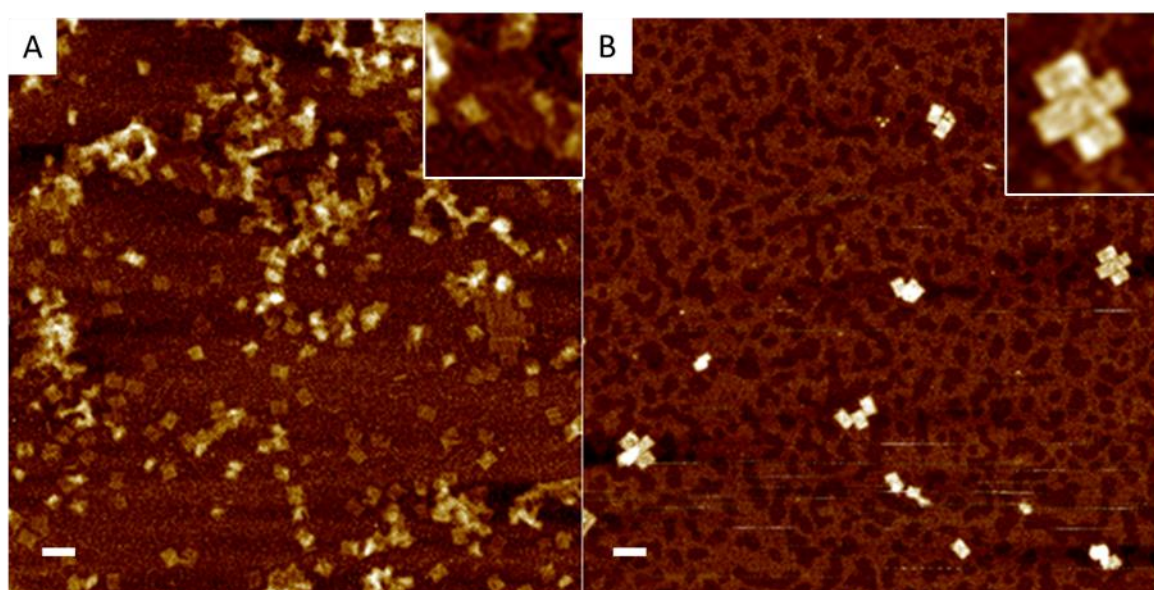


Figure 123 A. The initial raw lattice fabrication sample B. The sample recovered from the most mobile section of a band (Shown in Fig. 4.) purified using AGE. White line – 100 nanometres.

While sample A contains unfolded boards there is also significant evidence of controlled lattice growth (Figure 123). Sample B represents the lower mass/tighter conformation, and more mobile during AGE, species of the raw lattice fabrication solution and contains the smallest geometric representations of lattice expansion in both X and Y and also demonstrates that correctly folded structures are present in the sample. There is evidence of geometric units of 2, 3 and 4 boards within both samples as well as partially folded boards.

Once lattice growth had been observed within a sample, confirming the design methodology, the fabrication protocols were re-examined. By comparing lattice structure fabrication solutions thermally cycled using the full thermal sweep and others over the high efficiency fabrication window it was

theorised that many different lattice conformations were occurring over the wide temperature range of the full sweep thermal cycle.

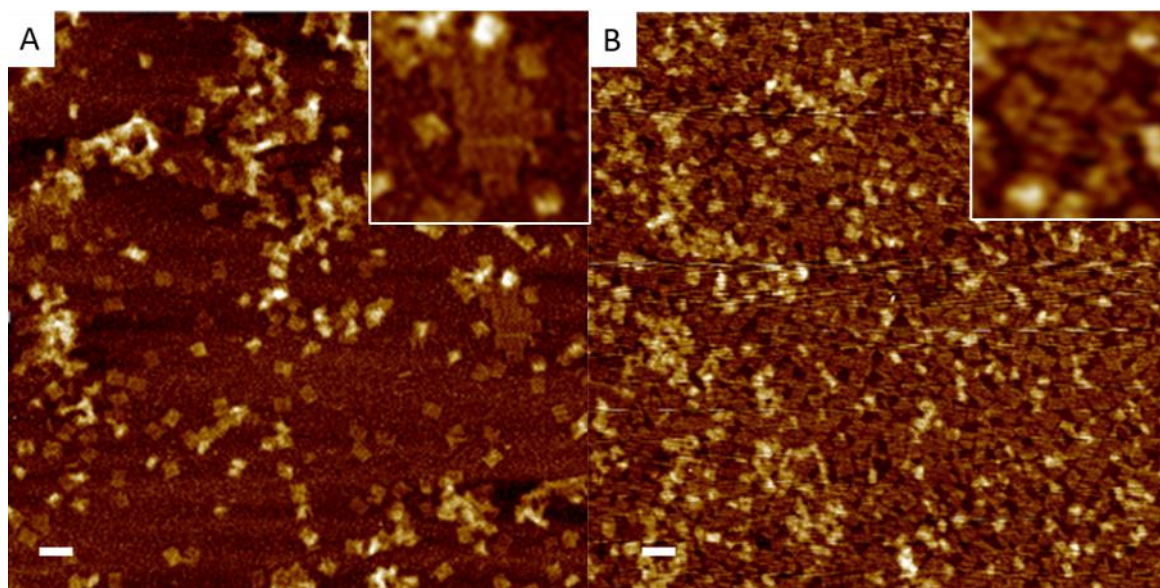


Figure 124 Fabrication solutions containing lattice components thermally cycled at different temperature windows. A. 'Full sweep' thermal cycle. B. High efficiency cycle between 46 and 44°C. White line – 100 nanometres.

Figure 124 Unlike the monomer fabrication attempts, in which both full sweep and high efficiency were highly successful in fabrication, there is little correlation between a large temperature sweep covering many likely folding domains and a smaller more targeted sweep created using analysis of the monomer unit. Though the fabrication solution employed in figure 64. B. contains lattice components there is very little evidence that significant constructive, or unstructured, lattice growth has occurred. The concentration of DNA adhered to the mica slide in figure 64. B. is significantly greater than that in figure 64. A. This is likely due to larger geometric lattices, and unstructured aggregates, having a much larger surface area than the structures visible in figure 64. B. making them much more exposed to the washing process which is used to clean slides of crystallisation effects before AFM imaging takes place.

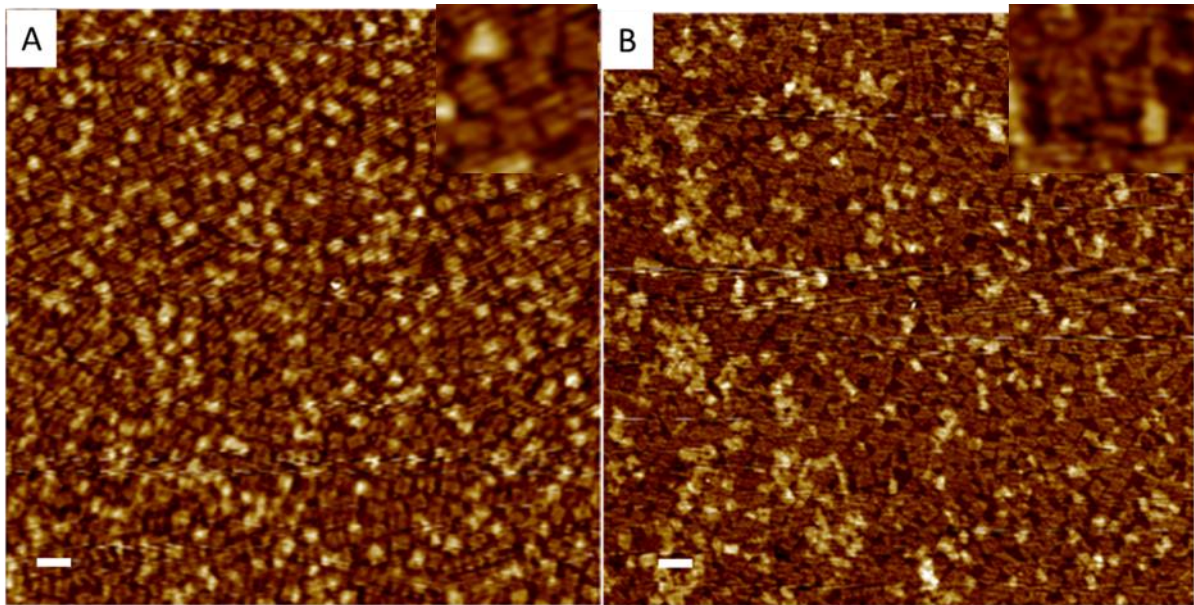


Figure 125 A. A monomer fabrication solution is compared to B. A solution containing lattice components under AFM. Both solutions have been fabricated and applied to mica under the same conditions. White line – 100 nanometres.

Direct comparison between 2 samples created using the short sweep thermal cycle protocol, figure 125, demonstrates there is no significant distinguishable difference between boards fabricated in this manner when lattice components are present. This suggests that successful geometric lattice formation, and unstructured aggregate folding, occurs at other points within the larger thermal sweep originally conducted.

While lattice formation of this manner was partially successful, and the possibility of one pot lattice fabrication remains open, experimentation moved to the use of pre-fabricated tiles.

- One pot lattice formation is possible and with a post fabrication purification step specific species of geometries can be recovered.
- It is likely that lattice folding occurs outside the high efficiency thermal cycling protocol developed earlier in this chapter. This would suggest that it would be possible to trigger differing fabrication stages at different temperatures.

## 12.6 Post folding lattice fabrication

There are many advantages to the concept of one pot creation of large-scale origami lattices. However as demonstrated above this method presents significant difficulties and, in many cases, even when constructive lattice formation is observed there is also significant defective tile formation and aggregation.

Another approach is to take tiles which have already been folded and then use a further reaction to bind them into lattices. One of the significant advantages of this technique is that the initial fabrication step ensures a very high number of correctly folded tiles exist within the sample. As it has been theorised previously [3] that creation of continuous origami lattices via self-assembly would require precise stoichiometric control of any lattice components to their complementing sites on origami structures there is also benefit to having higher confidence in initial DNA origami molarity within a lattice fabrication solution.

Also, as it is possible that lattice strands present in board fabrication potentially break the fabrication pathway of some boards, and act as negative interference, an observation reinforced by the evidence shown in our previous lattice attempts, it is likely that lattice growth conducted in 1 pot lowers the number of initial tiles present. There is also benefit in being able to select an optimal folding window for both tiles and lattice independently which could lead to constructive lattice growth without reducing sample stability or damaging existing tiles.

A further advantage of this technique is using the uncomplemented tail regions on our DNA breadboard design: because the lattice sequences in our design bind to areas of the scaffold which are not bound by staples, as discussed in section 4.2 they are free to be complemented post fabrication, they benefit from potentially higher selectivity (The only domains remaining on the folded origami boards are the correct lattice domains) and lower interference (All excess sequences still present have not bound to the lattice domains). The lack of interference between components also means that there is no requirement for purification post fabrication which is associated with lowering throughput (As discussed in chapter 5)

A relatively broad temperature cycle, 50-40 over 3 hours, was conducted on pre-fabricated boards with specific integer molar ratios of lattice components added to the fabrication solution.



Figure 126 left to right – 3:1, 2:1, 1:1, 1:2 and 1:3 lattice staples to origami boards

Figure 126 highlights that as the molar ratio decreases greater levels of aggregation are observed. When the ratio of staples to boards is at its highest little to no aggregation is observed, as this ratio approaches even, between boards and lattice staples, aggregation occurs and as board number overtakes lattice staple number the effect becomes more prominent.

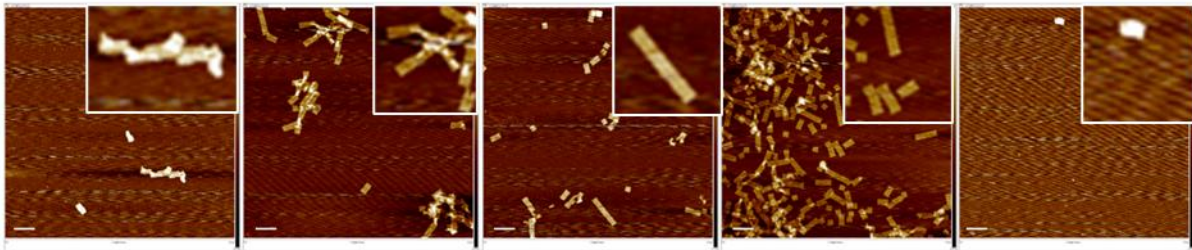


Figure 127 1 dimensional strings of DNA origami breadboards created by conjoining monomers with lattice strands via a secondary thermal cycle step. From left to right – 3:1 2:1 1:1 1:2 and 1:3 – lattice staple DNA:DNA origami. White lines - 100 nanometers

While direct AFM visualisation of secondary step lattice formation using the methods described above was partially successful, seen figure 127, it would suggest that AGE analysis of lattice samples created in the 2-step manner is somewhat ineffective. Examples of lack of correlation include the similarities between the 1:2 and 1:3 samples via AGE (Both samples appeared as aggregate proximal to the loading well) which do not translate into direct AFM visualisation (where sample 1:2 contains significant clean lattice growth and sample 1:3 is essentially absent). This contrast could be due to the limits of the AGE method, the technique only detects relative conformation in an indirect manner, so a highly aggregated set of boards and a long string of lattice boards could both present a similar footprint when passing (Or not in the case of aggregate type samples) through an agarose matrix under electrophoresis and return a similar result.

- Two step lattice formation (With initial board formation followed by a lattice aggregation step) is effective at creating 2 dimensional strings of structures but requires careful tuning of the ratio of lattice components to DNA origami breadboards.
- It is possible AGE is ineffective at contrasting/distinguishing long strings of structures and unstructured aggregates.

## 12.7 Imaging and fixation

A key aspect of checking a fabricated structures similarity to any theoretical design motifs is direct inspection/imaging. During this work direct imaging was conducted successfully via AFM in none contact tapping mode. A common substrate used to image DNA origami samples is mica, as both DNA origami and mica share a relatively high negative charge on their surface divalent positive ion bridges can be used to effectively anchor sample to substrate. Conveniently  $MgCl_2$  is very effective in this role, or similar magnesium derivative divalent ion, which are also very commonly used in DNA origami fabrication buffer samples (Including the protocols used in this projects work) which can then be fixed directly to mica post fabrication with little to no modification.

However, while the methodology behind this technique is simplistic, there are other important factors to consider. If a sample is incubated for too long on mica then clear definition of individual structures is lost as they are stacked around and sometimes on top of one another. This image saturation effect is also highly dependent upon DNA origami concentration within the sample being attached to the surface.

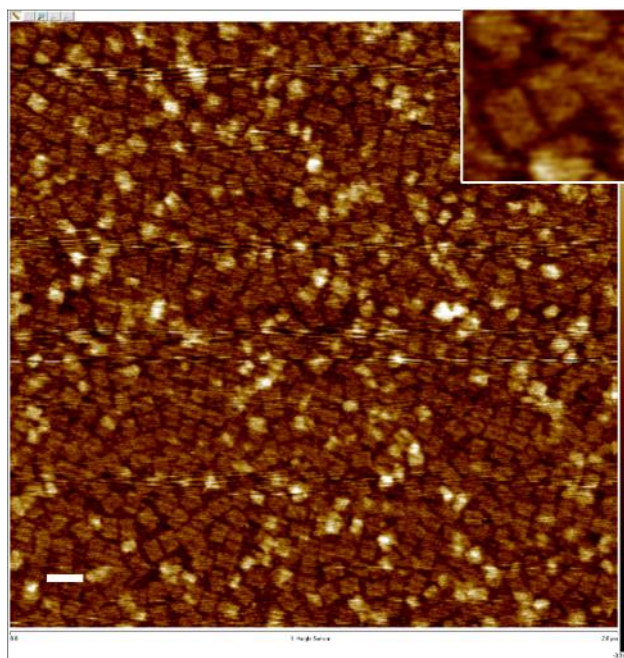


Figure 128 1 microlitre of DNA origami breadboard fabrication solution, with a relative DNA origami concentration of 56 nanomolars, was left for 60 seconds and then washed twice with 100 microlitres of ultrapurified water. Finally the sample was nitrogen dried. White line – 100 nanometers

While the saturation effect in figure 128 is borderline prominent, in that some clear boards are visible but fine structure is lost in almost all cases, it does highlight that while there is clear floor level of correctly attached boards there is detritus attached to both origami and mica surface which juts out significantly from the surface being imaged. This is likely staple/scaffold DNA and DNA origami structures with single strand tendrils anchoring between the gaps in correctly attached origami. It was theorised that the addition of NaCl during attachment, which has demonstrated potential as a semi-permanent fixing agent, could be used to remove single stranded DNA from the mica surface, along with the larger structures attached to it, leaving only correctly folded boards.

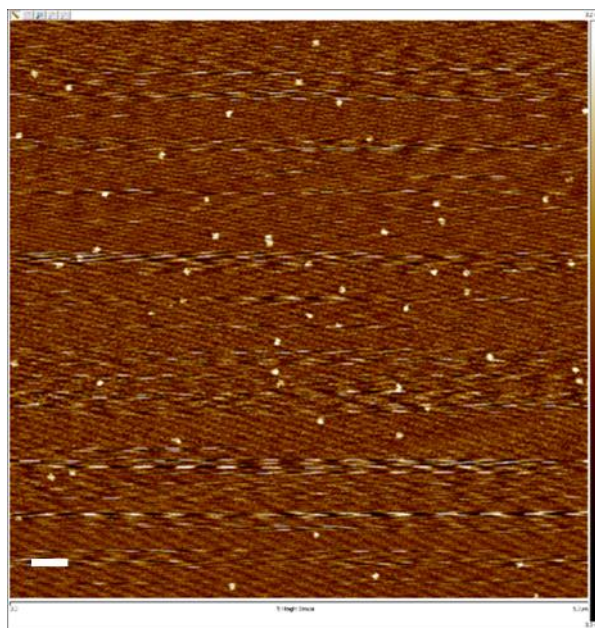


Figure 129 Initially NaCl was added to the solution for attachment at a 100mM concentration and the successful protocol demonstrated in figure 68 was used without further modification. White line – 100 nanometers

Figure 129 shows that when NaCl is introduced to the DNA origami solution being fixed to the mica surface there is significant lowering of structures correctly attached to the mica surface. As NaCl is not present in the fabrication solution employed during this work it was added post fabrication/pre fixation. This addition led to some dilution of the DNA origami solution but at an overall reduction of 33% relative concentration it is unlikely that it is this dilution effect is solely responsible for the significant change in the number of attached DNA breadboards.

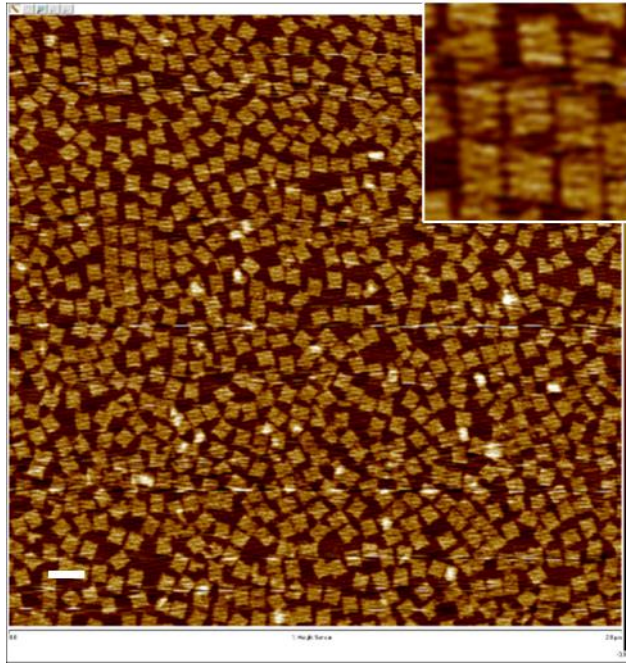


Figure 130 The same solution used in figure 69 is used again but a much longer incubation time is employed. In the ambient conditions in the lab the solution was completely dehydrated on the mica surface and there was visible crystallisation before washing and drying took place. White line – 100 nanometers

Figure 130 demonstrates that with an addition of NaCl to the fixation solution, and a longer incubation period, DNA origami breadboards can be attached to the mica surface in very high number with a significant reduction in excess single stranded DNA and semi fully attach DNA origami structures remaining. This process leads to a significant reduction of noise during imaging providing much higher quality definition of individual structures.

A further observation of the NaCl complete dehydration fixation method was that it allows very robust analysis of a samples overall stability. A sample fabricated successfully over the high folding domain, 46 - 44°C as described above, was contrasted with a sample fabricated in the next 2 degree window (44 - 42°C).

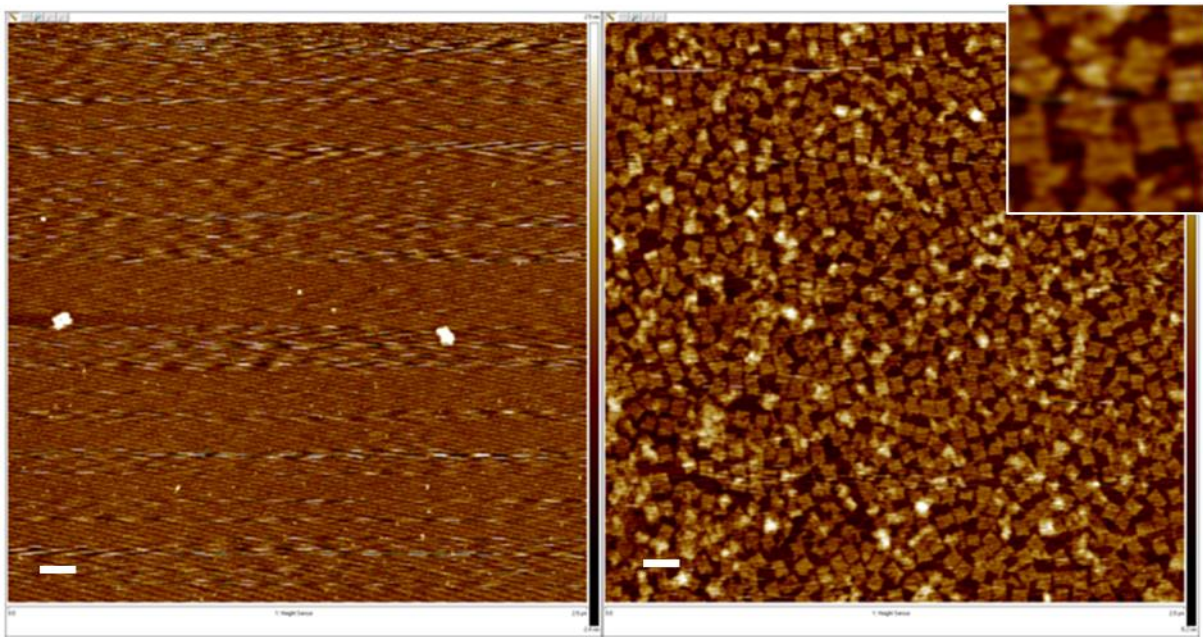


Figure 131 Minimal thermal cycle window samples. Left – 44 to 42 degrees C over 1 hour. Right – 46 to 44 degrees C over 1 hour. Both raw fabrication samples were raised to 100mM NaCl and then left on the substrate until complete dehydration occurred. They were then washed with ultra purified water.

Figure 131 shows that this fixation method can be used to effectively screen samples for any correctly folded contents. There are three significant benefits introduced by this method beyond clean images. Firstly, as shown in figure 71, it is good for quickly identifying similar samples for levels of correctly folded origami. Secondly it is good for high throughput images without the critical time dependencies when creating mica bound samples using the  $MgCl_2$  route. Finally, it allows the effective precipitation of correctly folded structures from a solution, which can also contain ‘junk’, and allow effective imaging and further interaction.

This efficient precipitation of correctly folded structures, and elimination of ‘junk’ from substrate surface, is demonstrated effectively when we contrast a raw DNA origami breadboard sample, created at full staple concentration, and folded across the full temperature sweep with a sample fabricated with a low staple ratio to scaffold using the high efficiency cycling protocol.

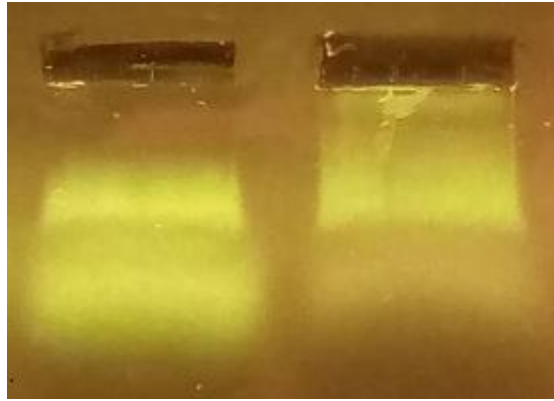


Figure 132 a full concentration, full sweep, sample (left lane) is contrasted with a 2:1 staple to scaffold ratio sample consecutively cycled over the high efficiency temperature range.

The bands in figure 123 would suggest that while the sample on the left, which is universally correctly folded when examined via AFM, is a fairly monomeric species, the sample on the right likely contains some correctly folded tiles and then a variety of unfolded structures and aggregate.

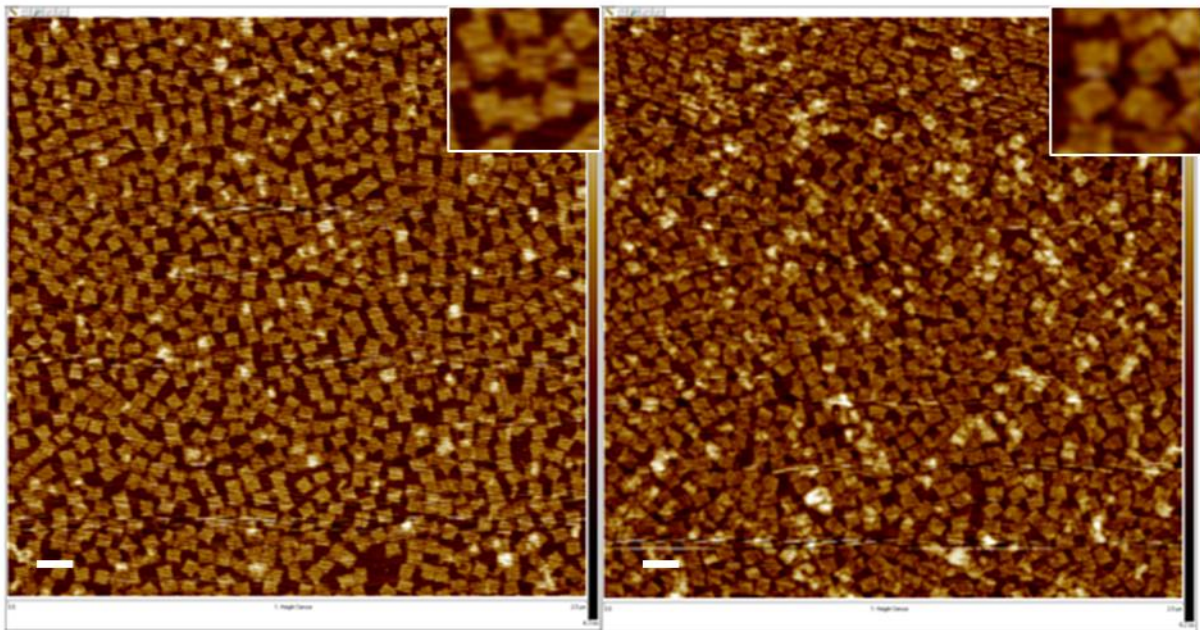


Figure 133 The samples analysed via AGE in figure 72 are imaged directly via AFM post NaCl method fixation. The left image is the full staple concentration, full thermal sweep, sample. The right-hand sample is a 2:1 staple to scaffold concentration sample run over the high efficiency cycling thermal sweep.

Figure 133 shows that the samples are very similar visually and the right-hand sample, which is identical to the poorly define 2X sample discussed above, exhibits a high level of correctly folded boards and low levels of surface aggregate.

A similar effect is exhibited when the 2 step lattice fabrication samples seen section 11.6 (Which provided limited AFM results using standard fixation methods) are examined using a mixed  $MgCl_2/NaCl$  fixation technique.

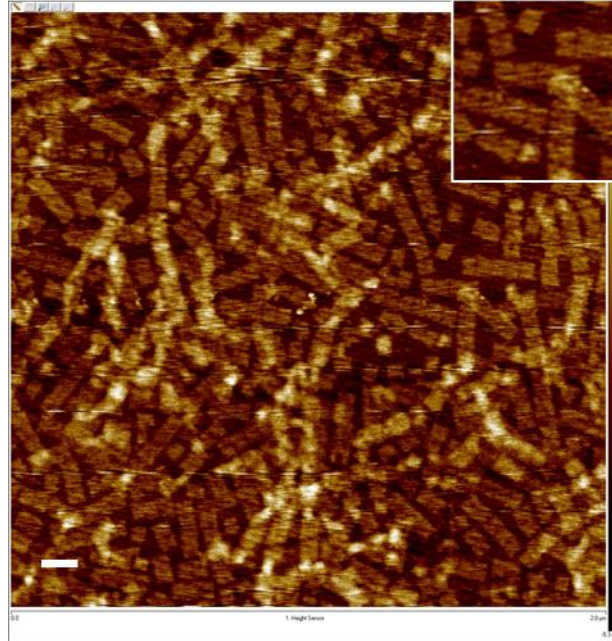


Figure 134 a 1D lattice sample fixed using the modified NaCl method.

Figure 134 highlights that by using a modified NaCl fixation method it is possible to increase the efficiency of surface saturation of correctly folded structures. There are also other potential application for this technique for example ‘bunching’ 2 dimensional strings of DNA breadboards into quasi continuous surface layers.

- NaCl fixation is effective at selectively fixing double stranded samples while excluding single strands.
- This can be used to test the integrity of a DNA origami sample in terms of correctly folded DNA.
- This could be used to increase the fixation efficiency of samples which are challenging to fix using only divalent ions.

## 12.8 DNA purification – Freeze and squeeze

Freeze and squeeze based extraction was used to purify origami from excess staple components.

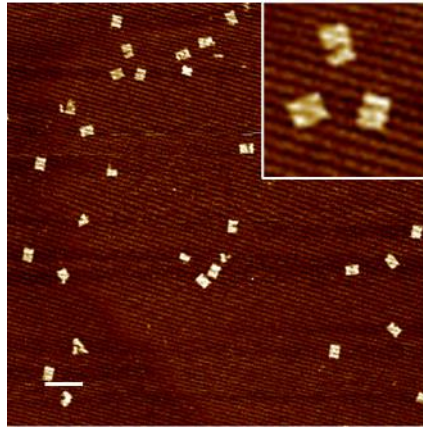


Figure 135 A DNA origami sample purified of excess staple strands via a freeze and squeeze step. White line - 100 nanometers

While the technique was highly successful in removing excess staples from the sample, and also in terms of time and resources, throughput was limited. A significant drop in the number of boards visible via AFM post recovery was observed, imaging a recovered sample via a second AGE step was challenging due to the low intensity of the recovered samples band, and there was a higher level of broken boards visible in freeze and squeeze samples. It should be noted that while this technique is unsuitable for high throughput applications (Such as those this thesis attempts to work towards) it is a very useful tool for initial purification and analysis. The samples created using this technique (In terms of both origami and Au NPs) laid the groundwork upon which all other further experimentation was based.

## 12.9 DNA purification – PEG precipitation

DNA precipitation is a method of both purifying, and concentrating, DNA origami directly from a fabrication solution. This method was employed to try and increase the throughput of purified sample.

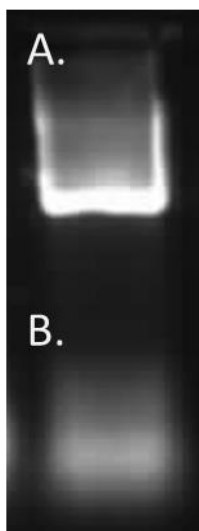


Figure 136 A PEG precipitated DNA origami fabrication solution is examined via AGE. A. the origami band. B. Staple band.

While the PEG method was effective in significantly increasing the concentration of DNA origami within a given (Figure 136 shows that it is possible to increase the origami concentration beyond the running capacity of the gel with the band losing cohesion) there was also evidence that excess staples were present post fabrication (Figure 136 B.). Given that our as fabricated solution could provide surface saturation of a mica substrate for surface/material purposes, without concentration, it seemed that using a high efficiency staple/NaCl fixation protocol was more effective than employing the ~24 hour precipitation step which would create the same surface saturation effect.

It should also be added that the precipitation step relies on pelleting a DNA sample in a similar manner to the Au NP aggregation step conducted pre functionalisation (See chapter 4). However, while Au NPs are highly visible, both in colloid and as a pellet, DNA remains effectively invisible. Given some experience with the technique it was possible to identify where the pellet was located in the container and carefully work around this area but it was not visible enough to image with the lab based camera and several samples were lost due to the pellet being disturbed, decanted with the supernatant, leading to no DNA being present in the final solution.

## 12.10 DNA purification – sucrose lane elution

When we attempted AGE/sucrose based recovery of the DNA origami breadboard yield was very low. Visualisation of DNA origami migration through the system was also problematic. To characterise the system and its mechanism more fully we used a thiol DNA functionalised gold nanoparticle sample as a marker for progression from AGE into the recovery well.

### Boundary between agarose and buffer pool

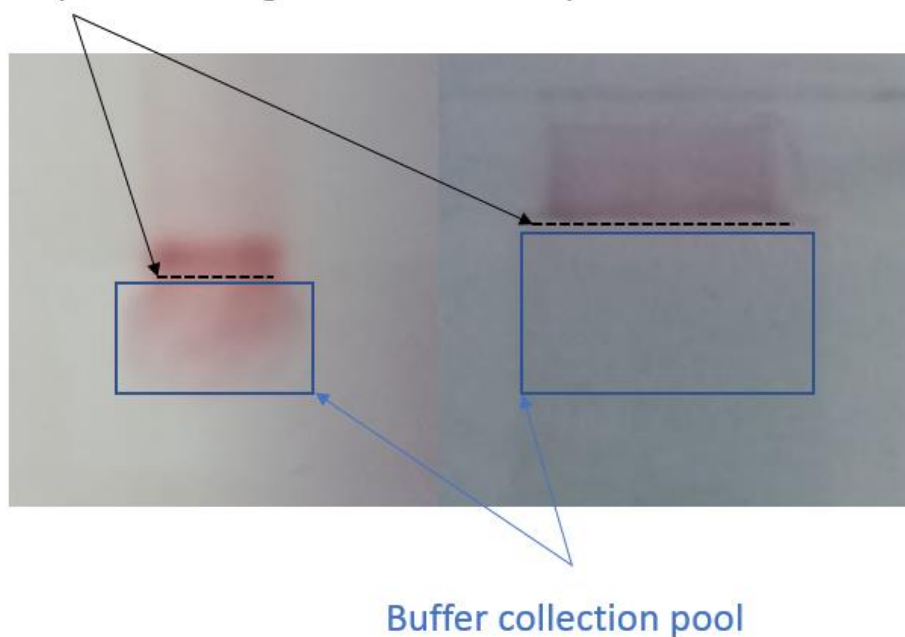


Figure 137 The effect of  $MgCl_2$  on elution of sample from a gel during native AGE. Left – a typical running buffer of 0.5 X TBE allows the sample to escape the agarose and spill into the buffer pool– A like sample does not elute in the same 0.5 X TBE buffer when the  $MgCl_2$  level is raised to 10mM and remains in the agarose with no evidence of sample in the buffer pool

It was observed that when this method of recovery is attempted using functionalised gold nanoparticles, which are highly visible to the naked eye, very little elution occurs in  $MgCl_2$  containing gel. In contrast Au NPs run through the AGE setup which did not contain  $MgCl_2$  would easily elute from the end of a gel and would disperse into the running buffer within the AGE tank.

## 12.11 DNA purification – EMA based purification of DNA origami samples

Initially it was theorised that the sucrose elution method above could be modified, by application of the EMA device, to purify excess staples from DNA origami in a single post fabrication step. There was

very limited initial progress as the charging effect present in  $MgCl_2$  gels described above (Figure 137) mean that a DNA sample within agarose will not elute back into solution. Furthermore, it was also observed when a raw fabrication sample was inserted directly into the recovery reservoir of the EMA device in the hopes that the smaller staple sequences would elute through the dialysis cap leaving only the purified origami, that this charging effect also effected cellulose membranes rendering this method unviable.

The cellulose membrane was replaced with a 30nm pore size polyethersulfone (PES) membrane. Due to this membrane acting as an electrical insulator it was theorised, and observed, that it was unaffected by  $MgCl_2$  based charging effects. Additionally, this membrane size is significantly larger than that of the cellulose dialysis membrane (Pore size  $\sim 1.5nm$ ), much larger than staple DNAs cross section (0.34nm), but still  $\sim 15$  nanometers smaller than the smallest dimension presented by DNA breadboard (45nm). Sample was inserted directly into the recovery well of the EMA device capped with a PES membrane and electrophoresis conducted.

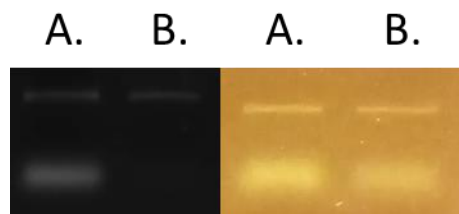


Figure 138 Raw fabrication products and post purified samples using the EMA (PES membrane) for 15 minutes at 50 volts A. Raw sample B. Purified sample

Results of successful EMA based purification seem to indicate the technique is highly effective at removing excess staple strands quickly and with no significant loss of origami sample. Unfortunately, this success was not 100% reproducible and often the sample would be lost completely due to either membrane failing, or adhesive not being completely set, and sample escaping.

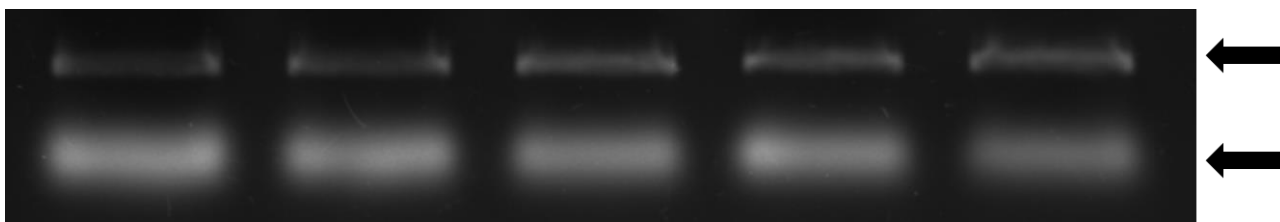


Figure 139 Samples purified for increasing lengths of time in 5 minute steps. (5, 10, 15, 20, 25 minutes left to right) top arrow – DNA origami band, bottom arrow – excess staples

A successful purification run with sample removed every 5 minutes (Figure 139) shows that while there is clear lowering of staple concentration over time there is no visual loss of DNA origami sample in the same time period.

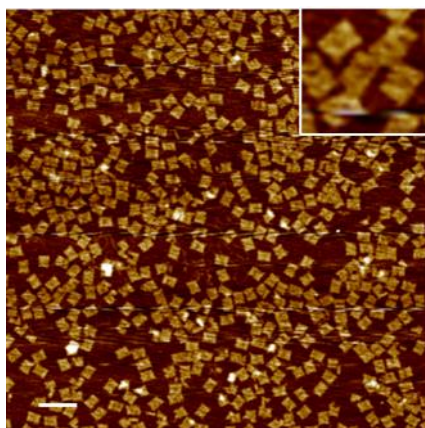


Figure 140 Tiles purified using the EMA method visualised via AFM

Beyond indirect AGE observation AFM observation showed that tiles were present, in high throughput, and there is no evidence of staples strands. There is some evidence of broken tiles, and some long trailing DNA strands (Likely unfolded/defolded scaffold DNA) but this is still at a lower percentage than that obtained using the freeze and squeeze method.

## 12.12 Conclusion

It is important to recognise that DNA origami, while a distinct method of fabrication, can be used to create a plethora of different structures with many different final applications. Rather than relying completely on the semi universal folding cycles which exist predominantly in the literature surrounding DNA origami fabrication it is useful to examine the specific folding patterns of any design.

In terms of fabrication component efficiency, a significant reduction from the 10-fold excess of staples commonly described in fabrication attempts. This reduction significantly reduces the cost of the technique and would be highly appealing when translating small scale fabrications for lab-based experimentation into the batches required for real world applications.

While 2D lattice fabrication (Conducted in single pot fabrication) was only partially successful it did highlight the potential validity of the method, the significant effect specific thermal cycle has on folding dynamics, and that it is possible to effectively recover certain lattice geometries from a lattice solution in a post fabrication purification step. Work on a 2-step fabrication attempt creating 1 dimensional strings of structures highlighted that careful tuning of stoichiometric ratios of DNA breadboards to lattice components is key to increasing fabrication efficiency and reducing non-constructive aggregate folding.

Sample fixation is often overlooked as the typical focus of fabrication throughput/fidelity is on the components used and the process by which they interact. However, by employing a mixed mono and divalent ion fixation protocol we demonstrate substrate attachment/selection can be used as a powerful tool to increase the number of correctly folded structures on a dried surface which is key to real world material fabrication.

Purification of excess staples from a fabrication solution with high throughput remains challenging. While the electrophoresis based system we present does show promise it is still limited due to the fragility of the system. However techniques which can be used quickly and reliably, such as freeze and squeeze based purification, are very effective for confirming initial designs and preparing small scale samples for further use (Such as metallisation or specific fractions of a lattice sample).

## Chapter 13

### 13.0 Gold Nanoparticle synthesis and concentration results

Au NP synthesis was confirmed via UV-vis spectrography and TEM to ensure samples were within the size bands of interest. It is worth noting that while Au NP synthesis techniques can provide samples with very low levels of polydispersity there will always be nanoparticles of differing size within the raw Au NP solution [98].

Au NP samples were measured for absorbance at 450 nanometers wavelength and the specific plasmon resonance of the sample, or SPR, which is defined as the first peak absorbance which occurs after 500 nanometers wavelength.

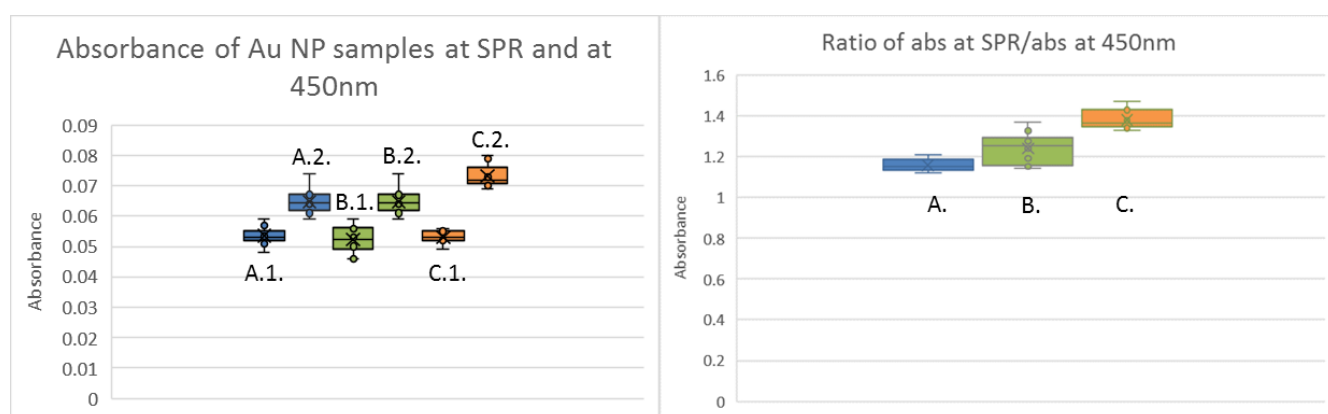


Figure 141 Left - Absorbance of samples at 450 nanometers wavelength (A.1,B.1,C.1) and SPR (A.2,B.2,C.2) and – right - the ratio of absorbance at SPR/absorbance at 450 nanometers. A – 3.5nm sample. B – 5nm sample. C – 9nm sample.

UV-vis results, seen figure 132, demonstrate that the Au NPs provide similar spectral properties to exemplar samples/tabular data relating to Au NPs of their size (Where absorbance at SPR/450nm should be ~1.15 at 3.5nm, 1.25 at 5nm and 1.46 at 9nm). Furthermore the results show relatively low variation suggesting the samples contain Au NPs of mostly similar sizes.

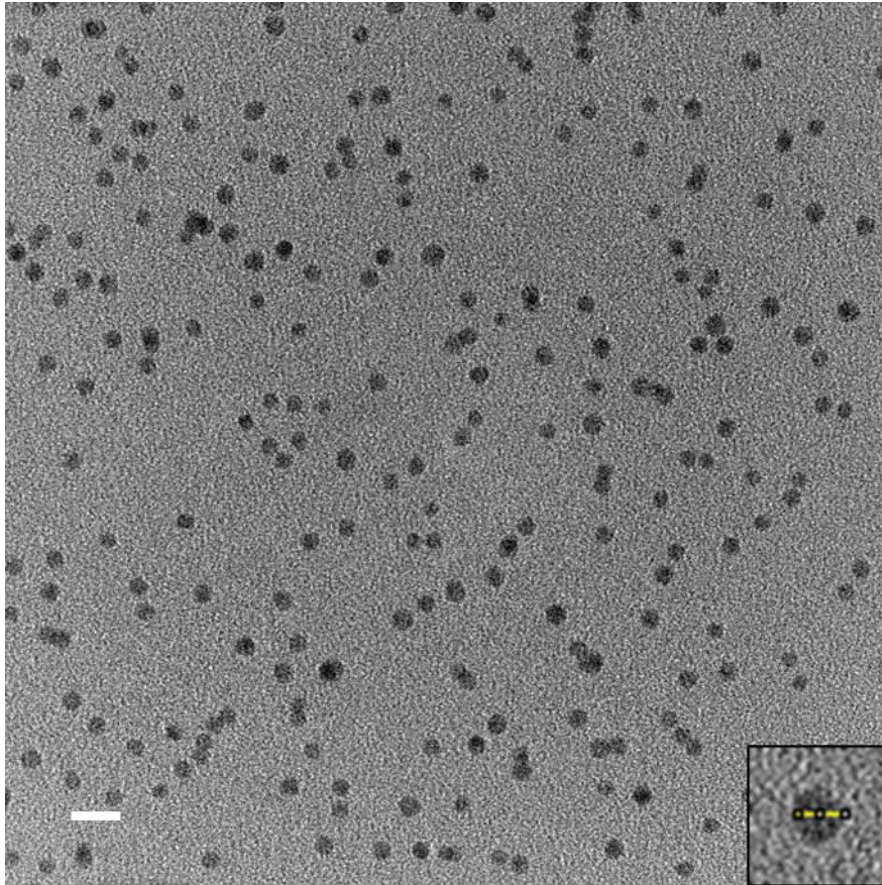


Figure 142 TEM image of a 3.5nm nanoparticle sample. White line – 10 nanometers. Inset right – a nanoparticle overlaid with a 3.5nm yellow line

While it was not possible to attain TEM images of all Au NP samples, due to equipment constraints, successful imaging was conducted on the 3.5nm sample (Figure 142). This successful direct visualisation, combined with the indirect UV-vis results, would indicate that it is likely the Au NP samples are synthesised correctly and within the size range of interest.

### 13.1 Au NP precipitation

Before Au NPs are functionalised, and used for further application, it is likely the relative concentration of the sample must be increased by aggregation of the sample via NaCl (Discussed chapter 5). While this method was successful with 9 nanometer gold nanoparticles some issues were encountered when this method was extended to smaller 5 and 3.5 nanometers diameter gold nanoparticles.

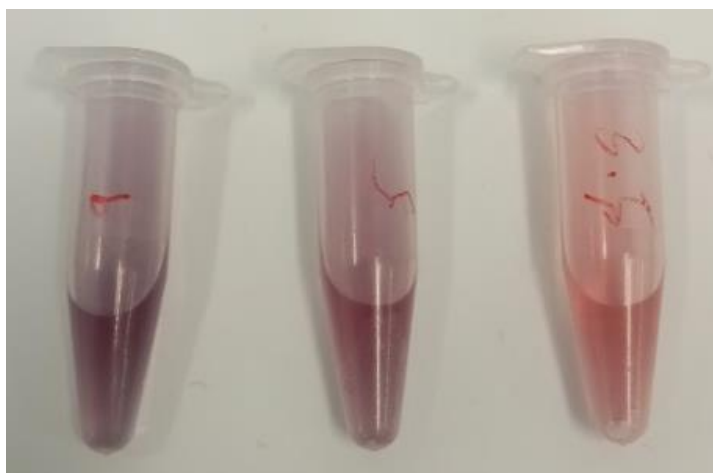


Figure 143 Left to right 9, 5 and 3.5 nanometer gold nanoparticles with 20% W/V solid NaCl added post BSPP stabilisation.

Figure 143 shows that while 9 and 5 nanometer gold nanoparticles can be aggregated relatively easily by the addition of solid NaCl even when 20% W/V NaCl is added to the solution aggregation is not visible in the 3.5 nanometer gold nanoparticles. This presents problems as further addition of NaCl begins to reach the saturation point where NaCl no longer enters solution and remains as noncolloidal solid. If this point is reached then pelleting cannot occur as the Au pellet will be lost in the NaCl crystal also pelleted to the bottom of the test tube. This effect is exacerbated by the methanol step which can precipitate NaCl from solution if the concentrations are high enough, again, effectively destroying the sample. Conversely if less NaCl is added, and complete aggregation does not take place, then a large part of the Au NP colloid will remain in solution post centrifuge and be lost when the supernatant is discarded in the resuspension step.



Figure 144 Pelleted 3.5nm Au NP solution using 10% W/V NaCl and 100 microlitres of methanol

A quick method for the collection of residual nanoparticles, and to ensure complete collection of the sample without very long centrifuge times, is the addition of 100 microlitres of methanol per millilitre of raw nanoparticle solution during the initial NaCl aggregation step. Using this method low concentrations of NaCl (10% W/V as opposed to the >30% W/V to saturation sometimes needed to ensure global aggregation) can be used to reliably aggregate the 3.5 nanometer gold nanoparticles synthesised using the tannic acid/sodium citrate route, without risk of sample destruction, which displayed the most resilience to aggregation during our fabrication attempts (Figure 144).

## 13.2 Freeze and squeeze recovery

Initially purification/recovery of Au NPs was conducted via a ‘freeze and squeeze’ method post AGE separation. This method proved ineffective when recovering sub 10nm Au NP due to relative spread of sample during AGE.

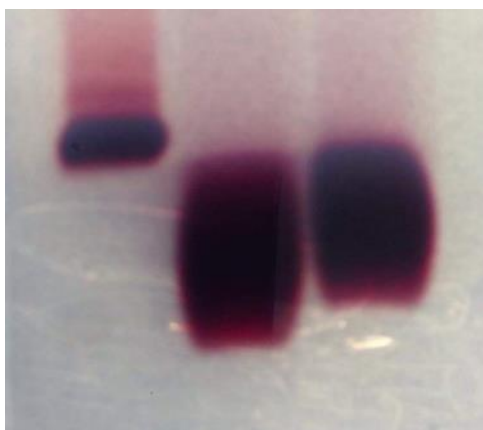


Figure 145 functionalised sub 10 nanometer Au NP samples separated from excess DNA via electrophoresis. Lane 1 – 3.5nm Lane 2 – 9nm Lane 3 – 5nm.

Figure 145 demonstrates that like for like as synthesised volumes of 9, 5 and 3.5nm Au NPs display very different band size dynamics during AGE. Due to the high spread of these samples, it was necessary to excise a relatively large piece of agarose which would then undergo freeze and spin elution. As shown figure 145, as the 3.5nm sample is within an agarose block around 5X larger than that of the 9nm band it will be recovered in a 5X larger volume and at 5X lower relative concentration. While it was possible to lower this relative spread of the Au NP band by increasing the concentration of agarose used to make the gel this also decreases recovery as the Au NP sample now becomes more trapped within the higher concentration agarose matrix.



Figure 146 An EMA purified nanoparticle (Left) and a like sample (Right) separated from excess thiolated DNA via AGE in the same gel and purified via the Freeze and Squeeze approach.

Due to difficulties recovering Au NPs in a suitable quantity using freeze and squeeze recovery it was decided to focus on a novel purification method to increase throughput. Figure 146 displays a clear difference between like for like Au NP samples eluted from the same AGE run. The EMA purified sample remains a dark red colour while the Freeze and squeeze purified sample is lighter in tone, significantly higher in transparency, and due to these visual cues, would imply it is significantly lower in nanoparticle concentration.

### 13.3 Centrifugation

Centrifugation was ineffective for concentration of sub 10 nanometer Au NPs. Typically, and in the case of equipment available for this project, centrifuges capable of operating >100K RCF, which provides suitable force to begin to centrifuge sub 10nm Au NPs (Where the force required to sediment 3.5nm Au NPs is >200K RCF), are relatively large machines which are unsuitable for the microlitre volumes associated with lab based structural DNA nanotechnology. Attempts were made to purify functionalised Au NPs in 50ml batches by sedimentation at 200 RCF followed by supernatant discard/resuspension cycles but inevitably much of the sample was lost during the supernatant discard step, where typically at least 4 cycles are required for purification levels required for fabrication, rendering centrifuge ineffective as little to no sample remained by the end of the process.

## Chapter 14

### 14.0 EMA Results

Initial experimental observation was conducted on areas of the device crucial to effective operation and efficiency. A key component of the column is the dialysis membrane which caps the sample recovery area, and prevents Au NP sample from eluting, while allowing the electrophoresis field to permeate through the device. It was theorised that it may have been necessary to change dialysis membrane depending on diameter of Au NP sample in question, however, when using 12 kilodalton pore size dialysis membrane all Au NP samples (Between 3.5 and 10 nanometers during the entire work conducted) were contained with no loss due to membrane and the elution technique could be conducted in under 1 hour. For this reason, this membrane was used universally when creating purification columns.



Figure 147 agarose, post electrophoresis, stained with Au NP sample

Initially there were small losses of Au NP sample during elution either due to sample re-entering the agarose matrix at the bottom of column or drifting under the agarose completely and travelling back along the device (And becoming irrecoverable) as seen figure 147. This loss of sample was addressed by addition of insulated back plate, which was initially added to prevent re-elution of the sample back into agarose during the run.

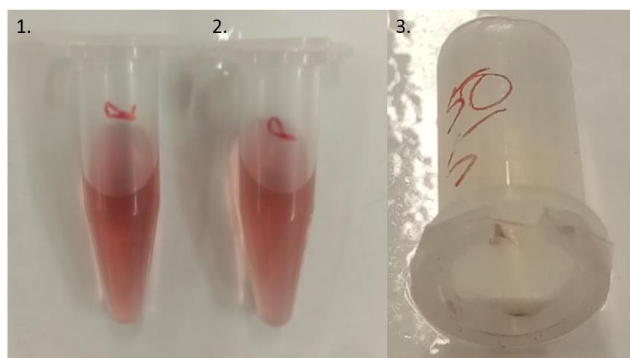


Figure 148 1. Raw mother solution nanoparticles. 2. Gold nanoparticles which have been purified, collected, and resuspended into the original volume they were reduced from. 3. A recovery column post collection of the sample shown in 2.

Figure 140 shows there is no residual Au NP sample remaining the column post elution, and that a recovered solution resuspended into the same volume shows no visual difference to the mother solution it was taken from, this would suggest that the technique now displays very low loss.



Figure 149 Au NP sample collects at the insulated backplate region of the column  
 It was also observed that Au NPs would collect in the electrophoresis free region created by the insulated backplate over time and this effect was used to concentrate sample into a small region of the recovery reservoir.

## 14.1 Au NP recovered sample analysis

Functionalised and purified samples were characterised via UV-vis and compared to existing tabular data in the same process employed when originally characterising synthesised Au NPs, discussed more fully in section 4.4. Initially an experimental goal was to characterise different purification/recovery

techniques and cross compare the results, however, this process was problematic due to specific micro volume spectrometers having a broad ‘preference’ for samples of a certain concentration. Unfortunately, in our case this led to an inability to correctly characterise Freeze and Squeeze purified gold nanoparticle solutions as they could not be recovered in a high enough concentration to provide stable UV-vis results. Other indirect tests confirmed they retained their size, as they did not precipitate under lower gravities than those required for theorised gold colloid within the recovered sample (i.e. a 3.5nm sample could not be pelleted at 10K RCF), and they were correctly functionalised and stable, and could be exposed to 10mM MgCl<sub>2</sub> ionic conditions without irreversible aggregation/destruction of the colloid. Given these observations it was decided that characterisation of the raw and EMA purified samples would continue and the Freeze and Squeeze purified sample would be contrasted only in a broad manner via visual examination that displayed a seemingly lower concentration, or more specifically lower intensity of ruby red hue, when compared to EMA purified samples (As seen figure 137).

Examination was conducted of as synthesised 5nm Au NPs, the same solution with only thiolated DNA present (No functionalisation step), and finally a functionalised solution. The average values of each sample were used to compare the putative diameter of samples against existing tabular data [98].

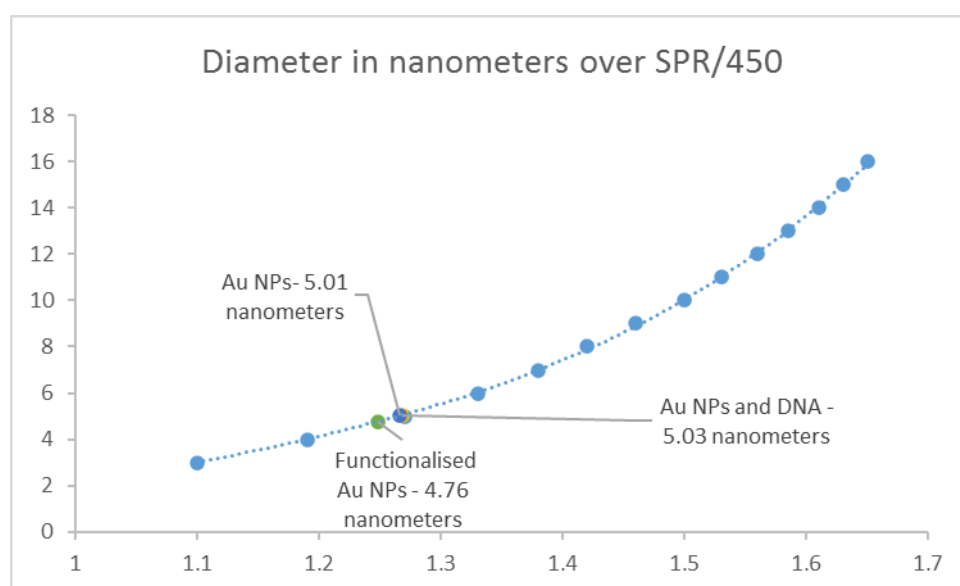


Figure 150 Using the tabular information found in [98] a line of best fit [Blue dotted line] was used to calculate the diameter of nanoparticles [Coloured circles – highlighted via pointer for clarity] from

spectrograph results of as raw Au NPs, the same sample with DNA, and the same sample functionalised

Figure 150 shows that while Au NP samples/DNA containing Au NP samples display very little difference in absorbance ratios/calculated diameter once functionalisation occurs there is a significant drop in putative diameter. Further examination was undertaken comparing like for like functionalised and purified samples using the same process.

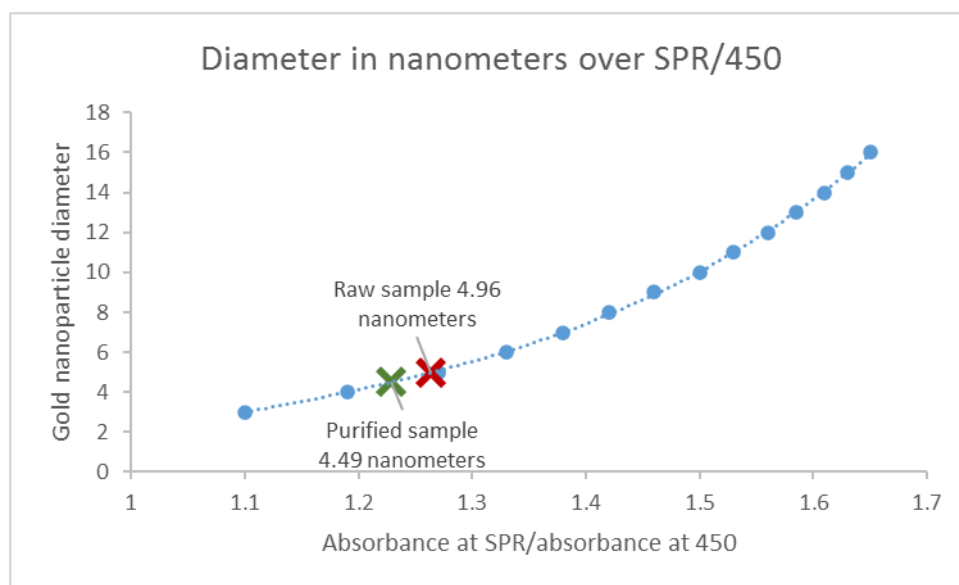


Figure 151 Using the tabular information found in [98], blue dots a line of best fit [Blue dotted line] was used to calculate the diameter of nanoparticles [Green and red cross] from spectrograph results of both raw and purified gold nanoparticle samples.

Figure 151 shows a further drop in absorbance ratios/putative diameter is observed between functionalised and purified samples. These recovered diameter values of the functionalised and purified samples were then used to estimate the extinction coefficient of each sample [98].

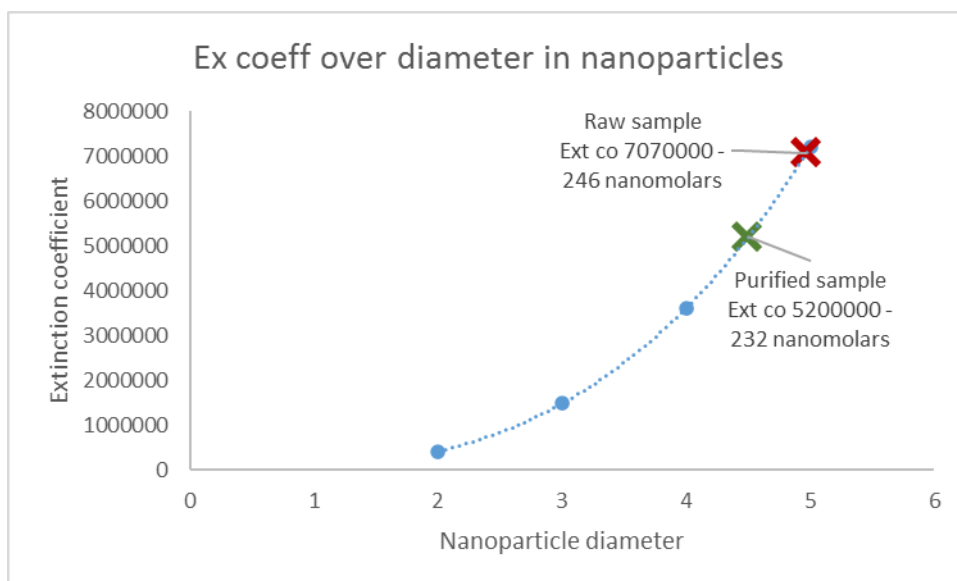


Figure 152 extinction coefficients of known samples taken from the literature [Blue dots] the line of best fit [Dotted blue line] and our sample [Green and red cross]

Once a sample has been assigned a specific extinction coefficient its concentration can be ascertained by Beer-Lamberts law [98].

Raw 450/ext co eff	2.46E-07	246 nanomolars
Pur 450/ext co eff	2.32E-07	232 nanomolars

Table 3 absorbance at 450 nanometers is divided by the samples extinction coefficient to obtain the nanoparticle molar concentration of the sample.

The results in table 3 suggest that EMA purification can be used to recover 94.31% of the nanoparticles present in the original raw sample. However, given that the UV-vis method employed above relies on contrasting an Au NPs specific surface plasmon resonance [98] it is also possible that the binding between the 50+ thiol groups and the Au NP surface during the functionalisation process interferes with this resonance. For this reason, the decision was made to also cross compare samples throughout the functionalisation approach rather than against purely external data of ideal samples.

## 14.2 Functionalisation stepwise examination

Samples were compared in all stages of the functionalisation process: this begins with as synthesised nanoparticles, then an Au NP sample containing excess thiolated DNA pre functionalisation, the correctly functionalised sample with excess thiolated DNA still present, and then the excess thiolated

DNA purified sample. Each sample set was created using the same mother solution and was resuspended to the same volume. When interpreting the change in relative absorbance of each sample it is important to note that any change due to loss of sample is only possible in the final purification step. Each of the preceding steps, representing as synthesised, DNA only, and functionalised Au NP samples, are resuspensions of the synthesised Au NP mother solution and do not include steps where Au NPs could be lost from solution. So, while change in absorbance may be due to loss of sample during the final purification step (Although this loss is likely to be very low given observations described in this chapter) any change in absorbance in the first 3 steps is purely down to the specific difference in component configuration within each system.

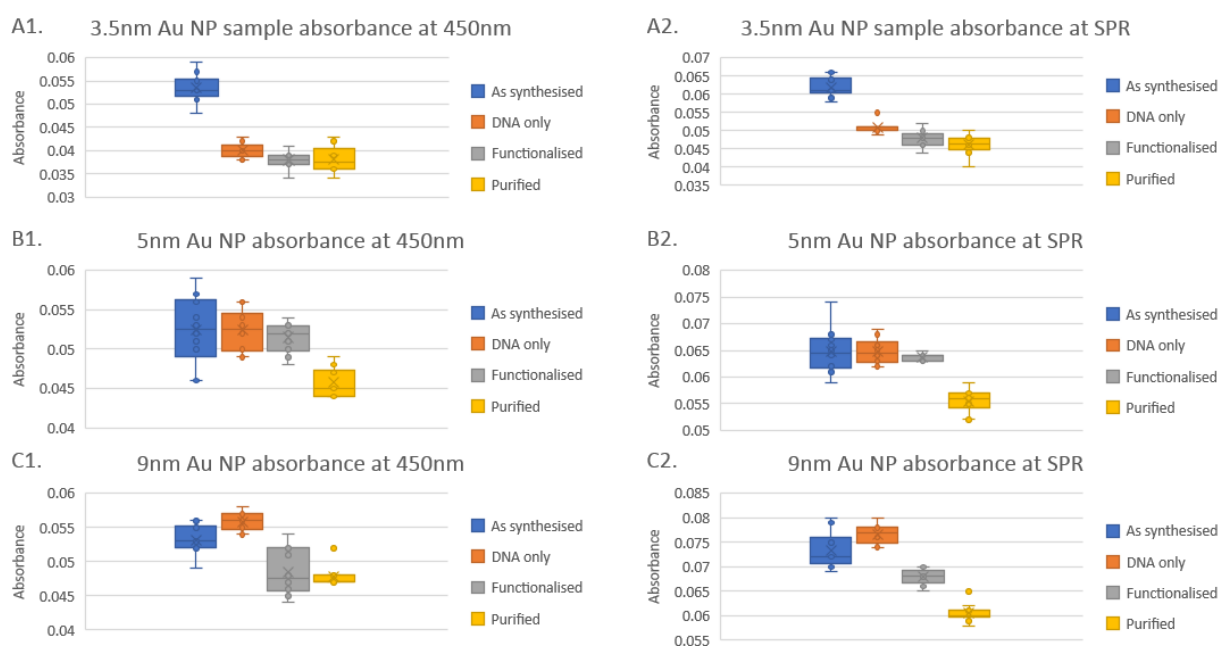


Figure 153 UV vis absorption results of Au NP samples 3.5 (A), 5 (B) and 9 (C) nanometers diameter exposed to 450 nanometers wavelength (A/B/C.1) and at SPR (A/B/C. 2)

UV-vis results, seen figure 145, were examined and cross compared. The smallest nanoparticles examined (3.5nm Au NPs – A1 and A2) display 2 distinct dynamics of absorbance change during the functionalisation/purification process. The first change, a large drop in relative absorbance, is observed when the as synthesised sample is compared to the same sample also containing an excess of thiolated

DNA. There are then smaller drops in absorbance once a sample is functionalised and again when purified.

This pattern of significant absorbance drop between as synthesised Au NPs and a similar DNA containing sample is not replicated in the 5 nanometer samples (B1 and B2), although there is a slight drop in absorbance from as synthesised particles, to the DNA containing group, to the functionalised sample. While these initial stepwise drops in absorbance are relatively small there is a more significant drop between the functionalised and purified groups.

In the largest, 9 nanometer sample (C1 and C2), there is an increase in absorbance observed between the as synthesised and DNA only sample. The same pattern of drop in absorbance observed in DNA only, functionalised, and purified samples in groups A and B is then observed at a higher magnitude.

These results imply that as nanoparticles increase in size the functionalisation/purification steps have more significant effects on the relative absorbance of the nanoparticle sample. This could be due to either the increasing magnitude of SPR observed as nanoparticles increase in size (Where Au NPs below 2 nanometers in size have been shown to display no significant SPR [98]) or the increase in relative concentration of nanoparticles/surface area within the sample as the diameter of the Au NPs within the solution decreases. However, no matter the cause for the shift, there is a clear stepwise change in absorbance, which implies that while absorbance change due to loss of sample is possible another significant factor is the change in spectral properties of the Au NPs within the solution itself.

### 14.3 Collecting specific Au NP sizes within an AGE band

A 9nm sample was separated via AGE, excised, and divided into 3 bands of differing mobility in electrophoresis (The most mobile band, the middle section of the band, and the least mobile section – referred to as front, mid and rear respectively). These samples were then recovered using the method we describe and characterised via UV-vis.

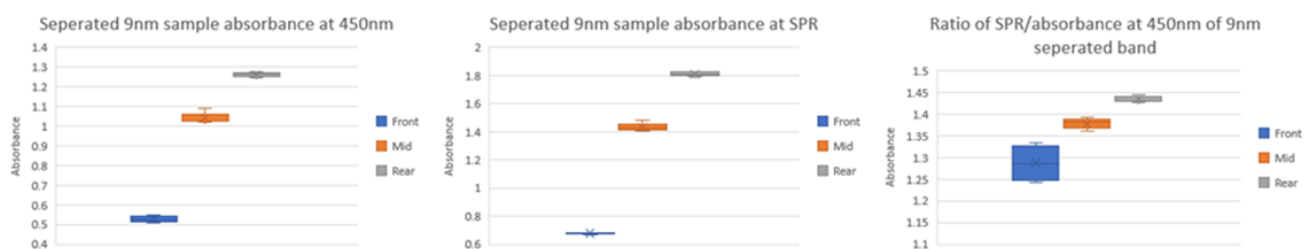


Figure 154 Front, rear and mid samples examined via UV-vis at 450nm wavelength (Left) SPR (Mid) and the ratio of SPR/absorbance at 450nm wavelength

Figure 154 shows that there is a clear increase in absorbance of samples, and the ratio of absorbance at SPR/450 for each sample, from highest to lowest mobility. This would strongly correlate with the general observation highlighted by the UV-vis seminal paper [98] in that as Au NP size increase so does SPR and the ratio of absorbance at SPR/450nm. Furthermore, it is very likely that the purification method presented provides an effective tool for the high throughput recovery not only of functionalised Au NP samples but also of distinct species within a polydisperse solution.

#### 14.4 BSPP resuspension UV-vis observations

While not a key focus of our experimental work, interesting differences, in terms of UV-vis absorbance, were observed between as synthesised samples, samples in which excess BSPP was present, and resuspended samples.

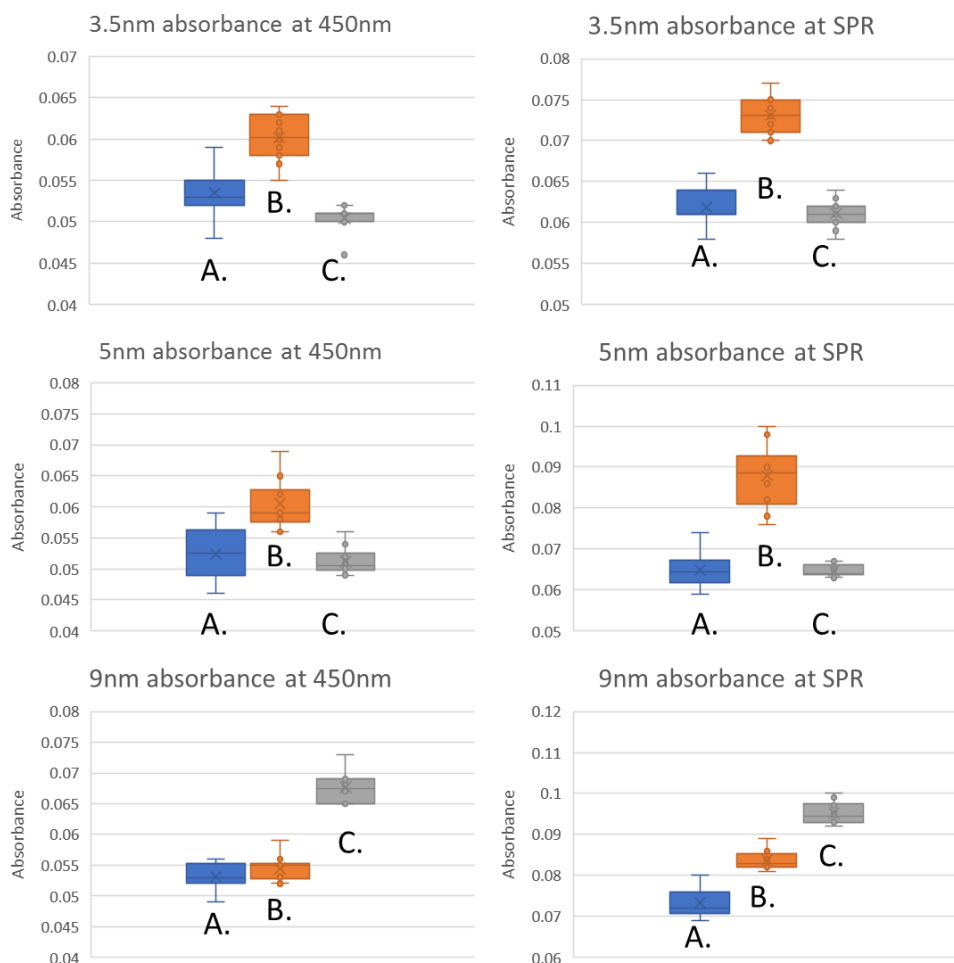


Figure 155 Absorbance of raw as synthesised nanoparticles (A.) these samples post BSPP addition (B.) and samples aggregated via NaCl addition and resuspended into ultra purified water (C.)

Figure 155 would suggest that Au NP samples undergo significant changes in the BSPP addition and resuspension step. It is also of note that in the case of 9nm Au NPs the initial absorbance of as synthesised Au NPs (A.) is distinct from the absorbance of the resuspended solution (C.) meaning that only once the post BSPP resuspension step has been completed can a sample be accurately analysed via UV-vis. For these reasons it is necessary to conduct UV-vis analysis of BSPP resuspended samples to accurately gauge size and concentration results (As opposed to measuring a sample immediately post synthesis).

## 14.5 Conclusion

Tannic acid synthesis was shown to be effective at producing the sub 10nm Au NPs employed during the experimentation we conducted. UV-vis analysis demonstrated a high level of accuracy in describing

samples relative diameter. While TEM was incredibly useful in firmly confirming a samples diameter in a precise manner, it does not give any real indication of relative concentration within the solution being examined and is much more labour intensive in terms of both producing samples and then imaging.

BSPP ligand exchange is cited as a necessary step in Au NP concentration which is required to increase an Au NP samples concentration to fabrication levels. While the addition step was relatively straightforward, and did not effect the samples in any destructive manner, it was demonstrated that it interferes with UV-vis analysis of a sample. Furthermore it was also shown that when resuspending the larger 9nm Au NPs UV-vis results changed between initial, as synthesised observation, and the final resuspended sample. It is likely that good practice would be to conduct BSPP and further precipitation/resuspension before samples are analysed using UV-vis.

The NaCl aggregation step was initially cited in attempts using >10nm Au NP nanoparticles. While still an effective technique at concentrating sub 10nm Au NP samples it requires modification to increase its efficiency to the same near 100% throughput when using the near ultra-small 3.5nm samples. Addition of a small quantity of methanol, as described above, is effective in working with all Au NP sample sizes used in this work.

Conventional purification techniques are limited when applied to sub 10nm Au NPs for large throughputs. However, while centrifuge based purification is not likely to practical for any kind of sub 10nm Au NP manipulation, freeze and squeeze recovery of samples can be conducted quickly for small scale design validation or nonhigh throughput work.

EMA is a very effective system and recovering and concentrating sub 10nm Au NPs. While it is slightly more labour intensive in the initial stages than both centrifuge and freeze and squeeze (Due to having to build and fill a column manually) it is very useful for creating large bulk Au NP samples with little to no loss. An interesting development using the EMA system was the purification of specific species within a more polydisperse sample (Chapter 10) and is likely that this technique could be investigated further and provide very low polydispersity Au NP samples in the future.

## Chapter 15

### 15.0 Metallisation

Initial metallisation attempts were attempted in solution: Au NP and DNA origami samples, completely purified of excess fabrication components, were mixed and analysed via AGE. It seemed logical that the first identification of a viable conjugation method would be to check the effect of ionic conditions of the fabrication solution in the same way this was the first broad examination conducted in naked origami fabrication detailed in chapter 11. This initial step was conducted without a thermal cycle, as it has been suggested that successful metallisation can occur at room temperature incubation [13]. Boards were purified using the Freeze and Squeeze method, a common purification step for metallised origami studies, and were mixed with EMA purified 3.5 nanometre gold nanoparticles.

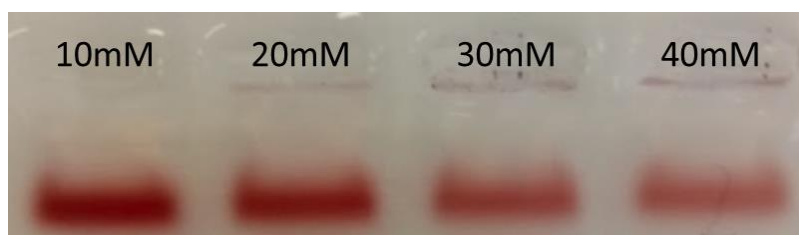


Figure 156 Purified DNA origami breadboards mixed with 5 nanometre functionalised gold nanoparticles at various  $\text{MgCl}_2$  levels.  $\text{MgCl}_2$  levels in the sample are shown above each running lane. Figure 156 shows that the results we obtained contradict other groups successful attempts at fabrication [127], which utilise much higher levels of divalent ion during successful fabrication, where we observed aggregation both when visualising via AGE, seen figure 156, and AFM. This is perhaps due to the significant difference in DNA origami geometry, the AGE identification step employed during our work, or the mica fixation process. Regardless of specific mechanism when  $\text{MgCl}_2$  levels increase to 20mM aggregation of the sample occurs in the loading pocket. This effect increases and is most significant at the 40mM level where the aggregation is significant enough to dull the intensity of the mobile excess nanoparticle band. While very faint, there is a trailing band present in the 10mM solution, suggesting that some DNA origami have conjugated nanoparticles successfully. However as the  $\text{MgCl}_2$

levels increase this band becomes either none present or none visible with the naked eye/laboratory camera.

To increase the throughput of the technique a DNA Origami precipitation step (Section 8.9) was incorporated post DNA origami fabrication. While this step increased throughput there was also evidence of lack of complete metallisation.

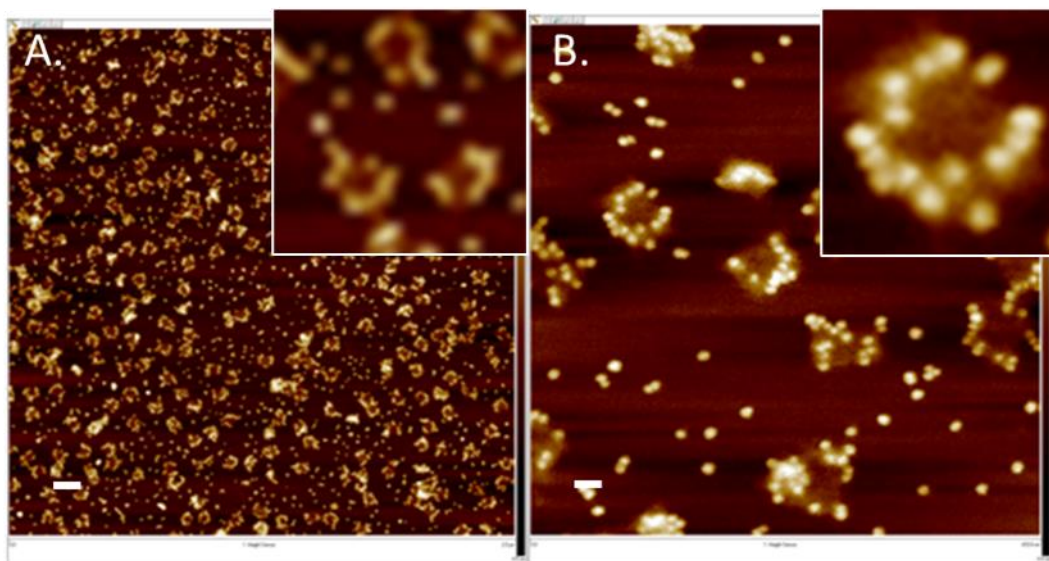


Figure 157 Resonator DNA origami boards with 3.5 nanometre functionalised and purified gold nanoparticles (A.) and 20x zoomed (B.). White line – 100nm (A.) and 20nm (B.)

DNA origami breadboards can be seen in relatively high throughput/surface coverage in figure 149, however, very few designs conform to the envisaged ‘C’ motif, and most have nanoparticles missing in several positions.

The results shown in figure 157 could be interpreted in several ways and each was addressed to ensure higher fidelity manufacture. Missing nanoparticles on the surface of the resonator would likely be due to either deficiency in nanoparticle concentration present in the fabrication solution, interference caused by improper purification/damage to the DNA boards, or insufficient tethers on the DNA origami breadboard to stably bind the required number of nanoparticles in the required ‘C’ motif.

Nanoparticle concentration was easily addressed as the EMA device discussed in chapter 7 meant that gold nanoparticle solution concentration could be significantly increased relatively easily and to

arbitrary levels. Doubling concentration of Au NP used in a functionalisation step did not have a noticeable effect on throughput.

Given that purification is often a source of dilution in relative sample concentration it was decided that examination of unpurified DNA origami breadboard samples conjugated to functionalised gold nanoparticles would take place. Given the partial conjugation demonstrated in figure 157, and the fact that functionalised gold nanoparticles could be purified using the EMA system and added in much higher relative concentration, this now seemed a viable pathway to pursue.

Conjugation of unpurified breadboards created using 10X and 3X staple concentrations would be cross examined. These samples demonstrate a similar throughput to those created when using the DNA precipitation step and a much higher throughput than those purified using the Freeze and squeeze process.

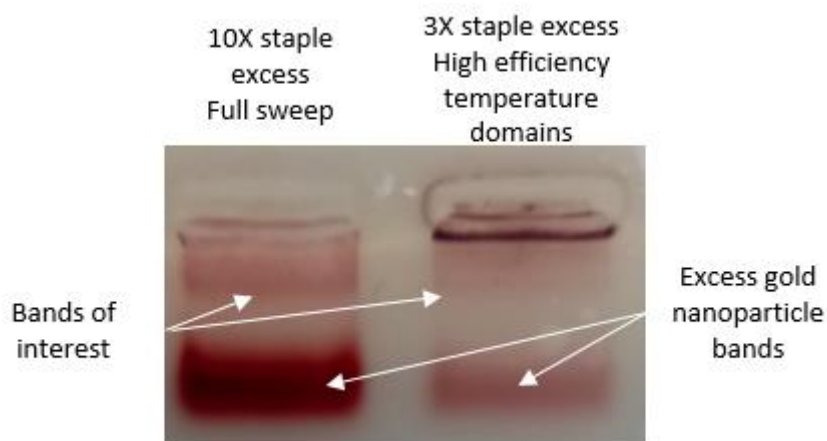


Figure 158 AGE analysis of raw DNA Origami breadboard fabrication samples mixed with a purified 3.5 nanometre gold nanoparticle solution. Left – a 10 fold staple fabrication. Right – a 3 fold staple fabrication.

Initially the results in figure 150 suggest that the high excess staple fabrication product, left, contains a high concentration of metalised structures. This is justified by the high visibility, low mobility, band shown figure 150 - left. In contrast the high efficiency sample, shown figure 150 – right, with low staple count, seems to display a similar species of sample, but at a much lower concentration. Furthermore the

3X sample displays high levels of aggregation at the loading pocket. Given the difference in AGE visualisation between the two samples direct examination was conducted via AFM.

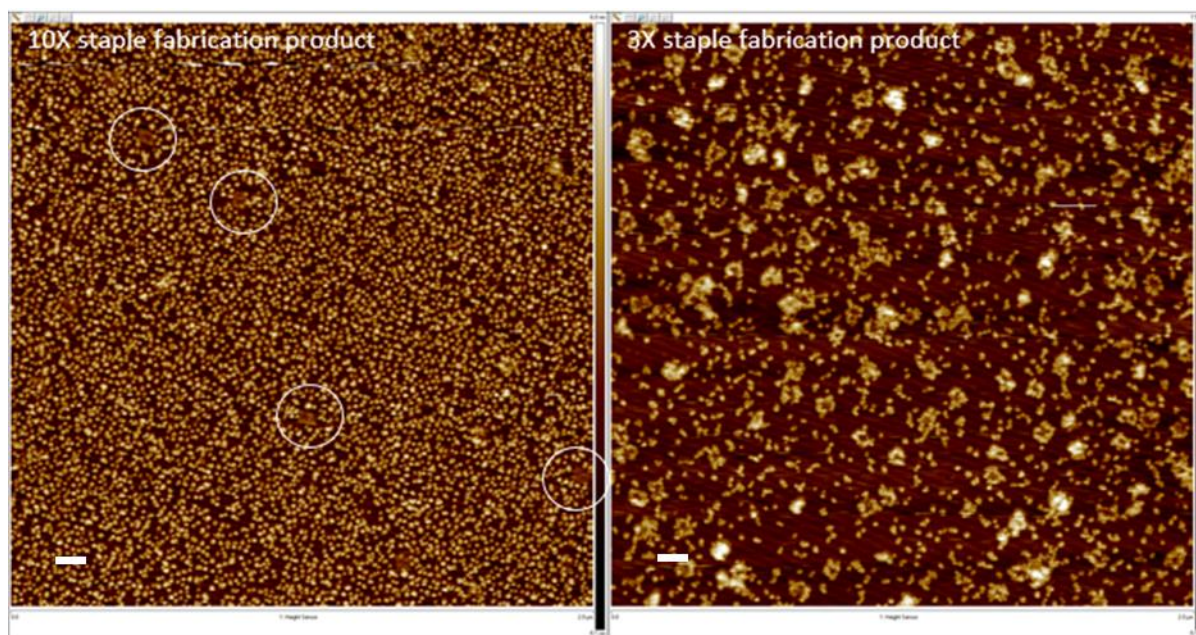


Figure 159 AFM analysis of the samples analysed by AGE in figure 113. Left – 10X staple fabrication. Right – 3X staple fabrication.

Direct AFM analysis (figure 159) of the samples contradicted the initial theorised results provided via AGE. The 10X sample, which displayed a higher intensity band of interest, contained boards which were not functionalised, likely due to conjugation sites being blocked by excess staple strands still in solution. The boards which were present, unfunctionalised, were also present in low number (While it is understood that drying a given sample to mica will not give an exact representation of relative concentration within solution, given both samples were made with like for like concentrations, and applied to the substrate in an identical manner, there does seem to be significant difference in DNA origami breadboard adhesion). In contrast the 3X sample, which showed a lower intensity band of

interest, and significant aggregation at the loading pocket, seems to show a significant number of DNA origami breadboards and each is conforming to the predicted design of binding sites.

It should be noted that while methods for reducing the staple content of a sample to allow for efficient gold nanoparticle conjugation were successful, attempting to conjugate an incorrectly purified thiol DNA gold nanoparticle sample to DNA origami breadboard were not.

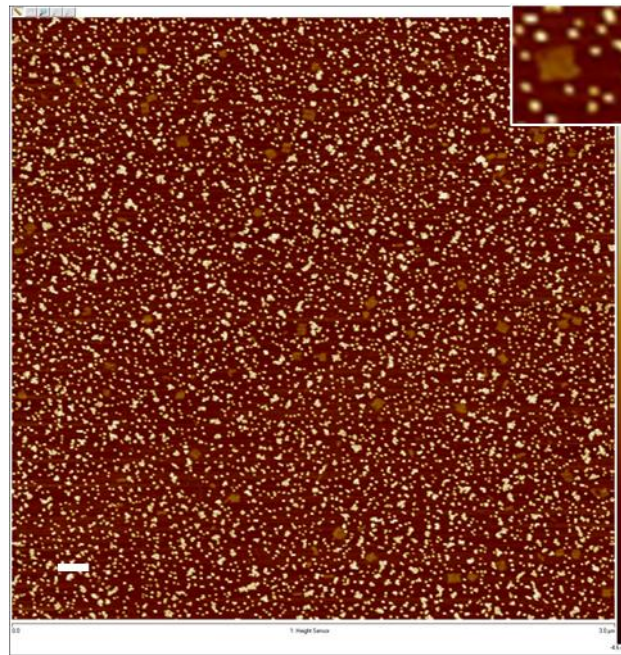


Figure 160 A DNA origami breadboard and incorrectly purified thiol DNA functionalised gold nanoparticle sample analysed by AFM. White line – 200 nanometers

In figure 160 DNA origami breadboards, and gold nanoparticles, can clearly be seen but there is no evidence of even partial conjugation between the two groups. It is notable that no nanoparticles are present on any DNA origami breadboards surface –  $MgCl_2$  is the divalent agent in the buffer that anneals a sample to the mica – and both samples contain negatively charged DNA regions causing them to bind to the mica surface. This would suggest that both DNA origami and gold nanoparticles have high affinity for mica under these conditions but very little between the two groups. In a similar manner there are no DNA origami breadboards present which seem to ‘bulge’ out from the surface of the mica indicating that they have become fixed over a pre-existing nanoparticle already secured to the mica surface.

To address the potentially low number of tethering strands a square resonator board containing significant numbers of tethers in a continuous perimeter sweep of the DNA origami breadboard (Design details are shown in chapter 7) was employed. It is envisaged that use of this high tether density board would allow tuning of the specific number of tethers to create more specific levels of overall metallisation and ensure continuity of a given design motif. Also of significance was that the DNA origami breadboard displayed high levels of attachment even though excess fabrication staples remained in the conjugation solution.

In an effort to increase the overall throughput of substrate affixation the NaCl drying method was used to create a base of structures approaching surface saturation of the mica sheet (Such as those shown in Chapter 11) which would then be conjugated using a functionalised, and purified, gold nanoparticle solution and washed and dried in the conventional manner.

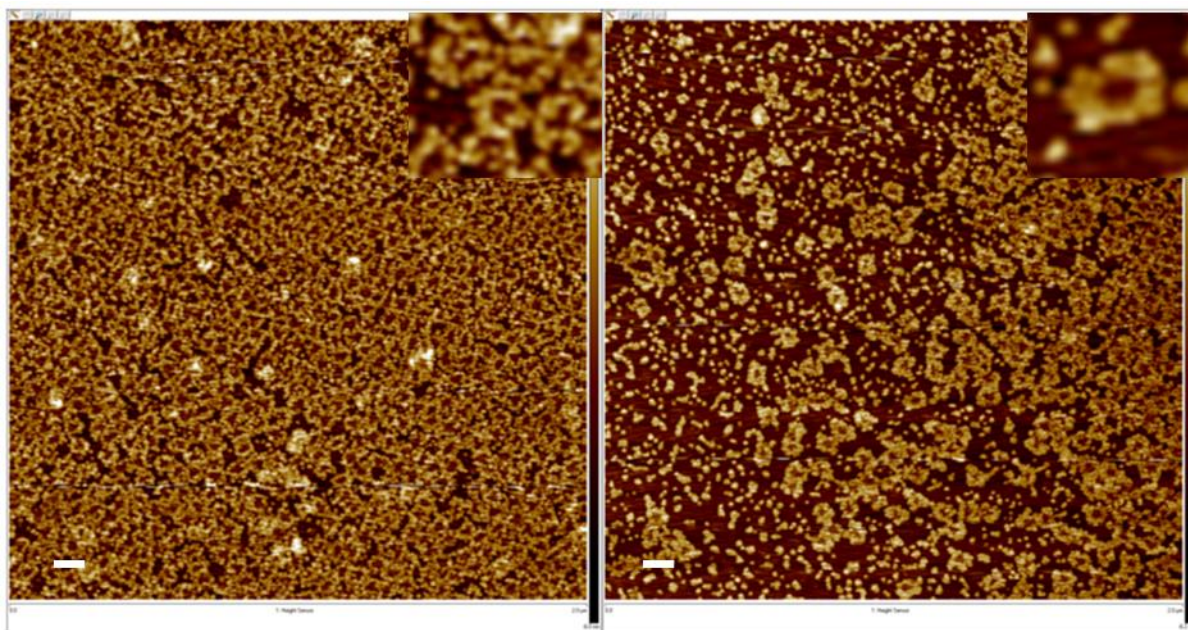


Figure 161 NaCl dried DNA origami breadboard samples functionalised post fixation to substrate. Left – 3.5 nanometre gold nanoparticles surface attached. Right – 5 nanometre gold nanoparticles surface attached.

The images shown in figure 161 would seem to suggest that NaCl drying, followed by functionalisation using a concentrated and purified gold nanoparticle solution, leads to high levels of surface coverage in terms of both individual origami and gold nanoparticles successfully bound to potential attachment sites. While there is strong evidence that the high density tether board design can produce Au NP seeded

designs there is also potentially some overlap between Au NPs on neighbouring boards. This experiment also highlights a dynamic observed in other metallisation attempts with more clarity – all the boards seem to be ‘the right way up’ with tethers extending upwards from the board rather than being trapped beneath it (And being unavailable for complement). This dynamic is highly beneficial to creating fully functionalised surfaces using this method. Initially this post fixation metallisation step was found to be challenging as when gold nanoparticles were applied directly, without ionic modification, it resulted in all DNA origami breadboards being removed from the board and limited gold nanoparticle attachment.

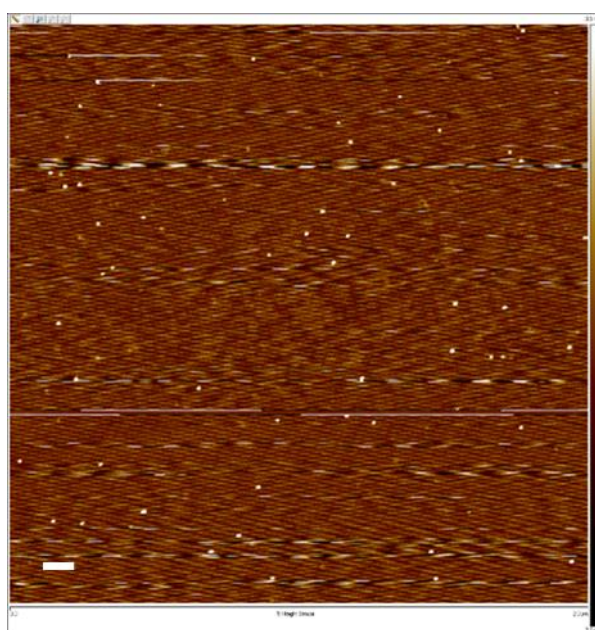


Figure 162 an image recovered from a DNA origami NaCl dried surface where nanoparticles were applied in ultra-purified water. White line – 100 nanometers

Given that ultra-purified water is used commonly to wash mica slides of excess salts and DNA, leaving a thin layer for imaging, it is likely the DNA, or gold nanoparticle, prevalent in the solution applied to the NaCl dried DNA origami structures which causes their complete removal from the mica substrate (As seen in figure 162). This problem is easily rectified by raising the gold nanoparticle solution used to functionalise the boards dried to the surface to 10mM  $MgCl_2$ . When this ionic condition was met boards remained at the high, near complete surface saturation, levels seen in figure 162. Once Au NPs are correctly attached a secondary washing step can be successfully conducted.

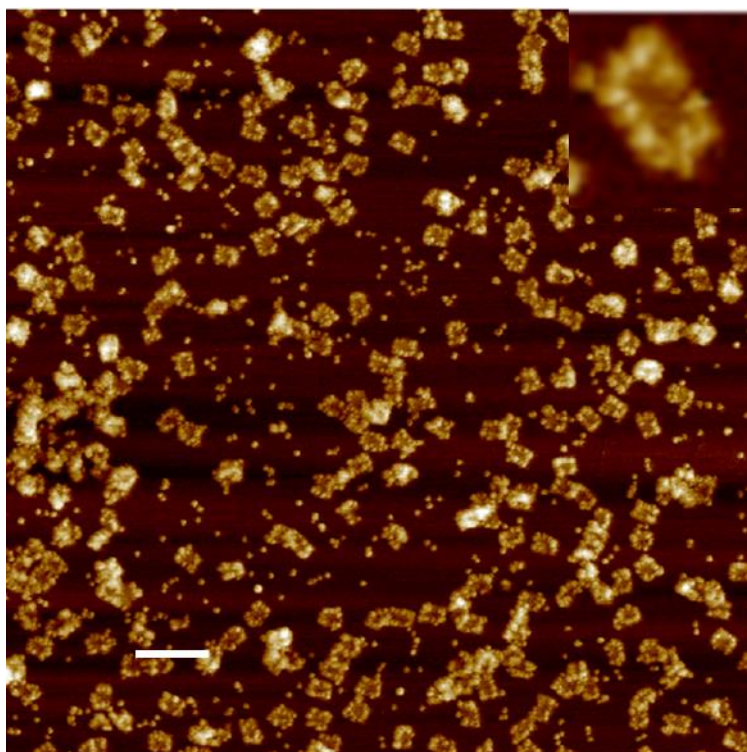


Figure 163 Boards metallised in solution annealed to mica with 50mM NaCl present

When the NaCl fixation method was attempted with a sample metallised in solution it was observed that the sample would degrade and aggregate if left to dehydrate on the mica effectively destroying the sample. However, by employing a lower concentration of NaCl (50mM vs 100mM) and reducing the incubation period (From complete dehydration to a 60 second incubation period) fixation of a stable sample was successful. The number of boards attached using this method is similar to the number attached during the initial metallisation attempt using a PEG precipitation step (Employed to increase to the number of boards present) and higher than that observed using freeze and squeeze purified sample. This method is beneficial over the post NaCl fixing attempts (Figure 163) as there is a lower number of designs sharing nanoparticles while most of the visible structures are still fully metallised. It likely that the NaCl based fixation interferes with the single strand mediated attachment which fix functionalised Au NPs to the mica surface (In the same way it does with other single strands such as staples). Using this method it was possible to create a ~5nm split size with ~5nm feature size, confirmed via nanoscope, which meets the design requirements simulated.

## 15.1 Tether Length

The role of tether length was examined where Au NPs were conjugated to DNA boards fixed to a mica substrate using the NaCl method described above. When conjugation attempts were conducted in solution using tether lengths lower than 20 base pairs no attachment was observed (Which has also been observed by many other groups – and led to 20 base pair tethers being a very common tether length [127]). However, it was theorised that by annealing a breadboard sample to substrate and then applying lower tether length functionalised Au NPs to the surface it could increase conjugation levels. For these experiments a 4 binding site board was employed, with each site located on each corner of the board, in clusters of 3 tethers.

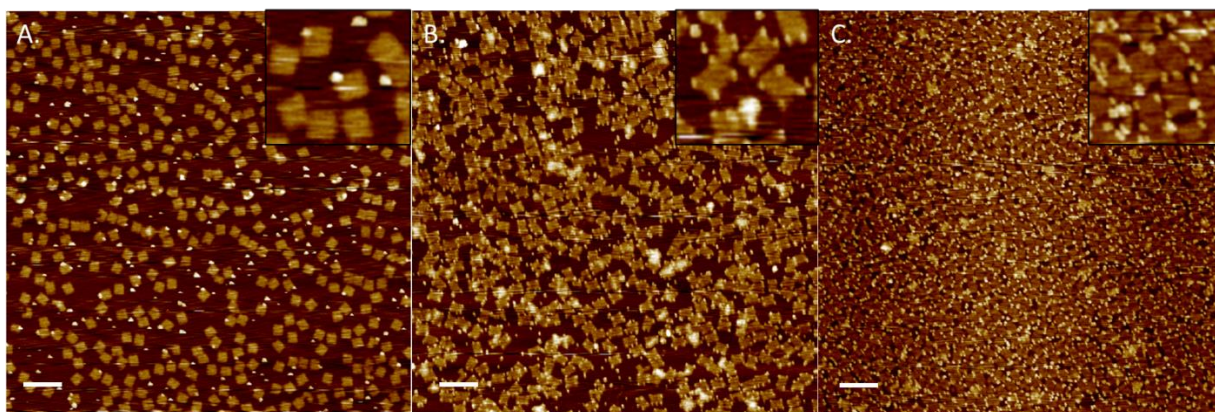


Figure 38 Differing tether length Au NPs undergo conjugation attempts with boards NaCl fixed to the mica surface. A. 5 base pair poly T. B. 10 base pair poly T. C. 15 base pair poly T.

Figure 164 highlights several interesting changes in mechanics when this method is used. Firstly, while the 5 base pair tether length seen figure 156 A. shows some limited conjugation in single corners of the board, in the 10 base pair design a very high number of boards have an Au NP in each corner of the board. If highly examined the same is also true of the 15 base pair design, but, the boards are also sharing tethers and this is having the effect of increasing the surface density of structures. This could either be due to boards becoming mobile during the attachment step (After being pre dried to the mica surface) or due to boards being semi attached via the NaCl fixation method. Given the increasing number of boards A – C it is also possible that Au NP attachment between boards anchors the sample during the conjugation step and lowers the number of boards washed away. The higher the

tether number, the greater the number of linked boards, and the more which are attached to the surface at any given point.

## 15.2 Troubleshooting

It became apparent that 9 and 10nm samples created erroneous bands, seemingly corresponding to a correctly metallised DNA origami band, which were in fact just artifacts and did not relate to correctly fabricated structures.

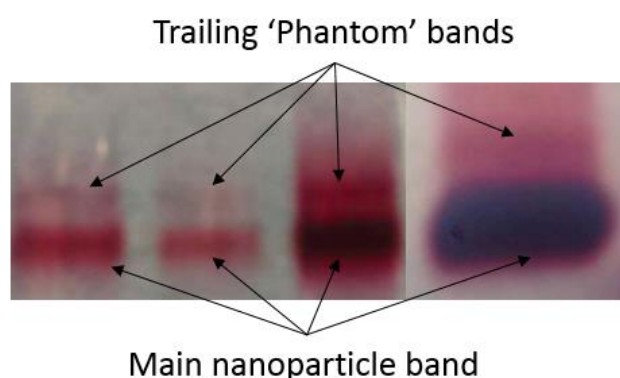


Figure 165 Images of trailing 'phantom' bands. Left image – 10 nanometre functionalised gold nanoparticles displaying a lower mobility trailing band. Right image – a 9 nanometre gold nanoparticle sample displaying a similar lower mobility band.

While the identification method shown in figure 165 can be effective care should be taken to ensure that lower mobility bands are identified correctly. A common phenomenon experienced when examining 9 and 10 nanometre functionalised gold nanoparticles via AGE was a highly defined band displaying a lower mobility than the greater nanoparticle band within the sample, as shown in figure 165. This effect was prominent in both 10 and 9 nanometre diameter samples but was not visualised in any nanoparticle samples of smaller diameter. It should be noted that these samples did not contain any DNA origami or its fabrication components suggesting that the phenomena was entirely due to nanoparticles within the sample.

## 15.3 Enhancement attempts

One of the goals of this project was to work towards creating metallised tracks on the DNA breadboard to provide a system for fabricating high throughput nanocircuitry. It was anticipated that ‘enhancement’, in which an existing Au NP acts as a seed for further metallisation, would be used to bridge the gap between seed particles and create continuous metal tracks. Several attempts at metallisation were attempted but were not successful. When enhancement was conducted within solution aggregation of the sample was observed (The sample shifted from Au NP red to grey or black and the colloid came out of solution).

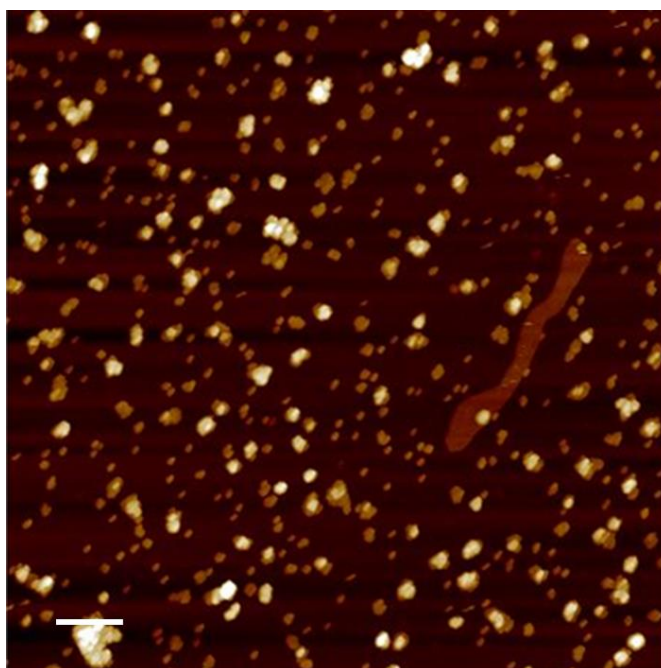


Figure 166 Boards with attached 3.5nm Au NPs on mica post ascorbic acid/AuCl enhancement

Figure 166 shows that enhancement of metallised structures on mica creates large aggregates and destroys, or retards to the point of being none imageable, any fine structure present. Surfactant has been demonstrated as an effective tool to protect Au NPs during the functionalisation step. It was theorised that use of a surfactant could also protect our samples during the enhancement process and experimentation was conducted with surfactant present in the solution.

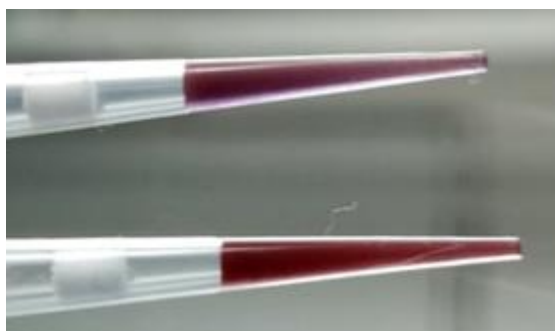


Figure 39 enhanced nanoparticle solution without (Top) and with (Bottom) 10% W/V PEG. Results of enhancement using a surfactant were more promising, as shown figure 167 once a sufficient level of surfactant is present enhancement no longer aggregates the sample (As mentioned previously a color change from red to purple indicates the Au NP solution has aggregated). However while use of surfactant was beneficial we were unable to clearly recover a sample/image from a sample within the solution. When AGE was attempted there was little to no migration observed, suggesting the surfactant prevented electrophoretic force, and images could not be recovered via AFM as the washing process no longer functioned correctly.

One of the methods to be attempted during this work was the use of polyphosphothioate bridges, decorating a breadboard in the same manner as Au NPs in the fabrication attempts described above, to act as seeding site for continuous metalisation. While this wasn't realised some experimentation did highlight the validity of using polyphosphothioate sequences as seeding sites for metalisation/Au NP formation.

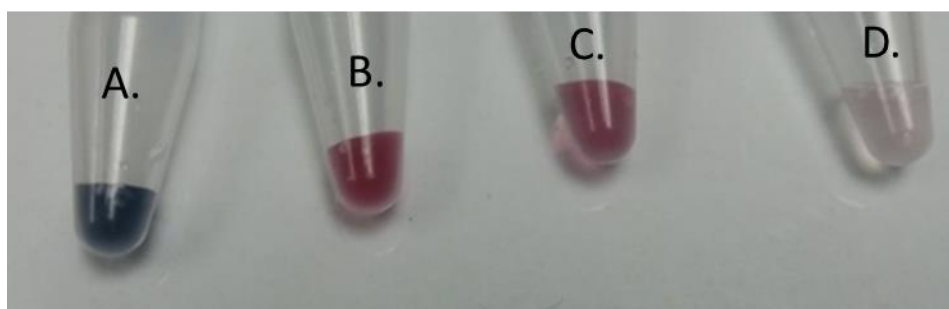


Figure 168 polyphosphothioate DNA sequences, protected with 10% W/V PEG enhanced using 25mM ascorbic acid and A. 1mM AuCl. B. 5mM AuCl. C. 10mM AuCl. D 15mM AuCl.

The sequences enhanced using this manner show distinct and stable colour change which occurs over a period of around an hour. While some of the samples, for instance figure B. and C. display a similar red hue to classical spherical nanoparticles, other samples showed as blue (A.) and pink (D). The only sequences available for experimentation were 20mer poly T phosphothioate backbone strands, and while they provided a multitude of colour changes, it is likely that by altering this length (Rather than just the ionic conditions as we did) it would be possible to create many further permutations. It is also possible that a DNA origami shape could have large sections of its structure complemented to phosphothioate sequences and then metallised to create bespoke metallic circuits and motifs. While this experimentation provides very colourful results, and provides an intriguing pathway for exploration, for our work we were limited by the presence of surfactant in the solution which meant samples could not be accurately measured by either AGE or AFM preventing further inspection.

## 15.4 Conclusion

Initial tests on  $\text{MgCl}_2$  levels effect on conjugation (Between Au NP and origami board) in solution indicated that the sample is not robust above the 10mM level. This led us to abandon ionic control as a method for triggering attachment and look at other methods. These initial samples were created using freeze and squeeze purified boards, were low in throughput, and were difficult to image via AFM and AGE.

A DNA precipitation step was employed to create a high throughput purified origami sample. Origami was mixed with Au NPs in solution and the product examined via AFM. While boards were present in a good number on the mica substrate, the level was not near surface saturation, and there was evidence of unattached Au NPs either through damage, ineffective attachment, or design problems.

To try and understand the dynamics of purifications effect on Au NP/origami conjugation 10X and 3X excess staple fabrications were created and Au NPs added in solution. While attachment was not successful in 10X solution there was evidence of successful attachment in the 3X solution with a throughput in the range of the DNA precipitation attempt.

Surface saturation DNA breadboard samples, created using the NaCl fixation protocol, were used as a base for a metallisation attempt where functionalised Au NPs were applied directly to the substrate. While this technique was successful in attaching nanoparticles in high throughput there was evidence that Au NPs were potentially being shared between tethering sites on separate boards and the design needed to have a lower number of tethers, or a reduced number of tethers on its terminal edges. This method also, crucially, shows that all boards anchor to substrate in the correct orientation with tethers facing upwards and being available for complement.

NaCl fixation of high tether number samples created in solution was more successful. This is likely due to Au NP conjugation occurring in a more controlled manner due to boards being more spaced apart when suspended in solution than when saturated on the mica surface. Using this method presented boards metallised very closely to the design specification. This method presented a measurable sample which displayed the 5nm split size coupled with 5nm feature size we had simulated. While other metallised samples contained structures within this range they also featured significant bleeding between designs. While this could be addressed by reduction of tether length it is likely, in its current format, this method provided the 'best' results in terms of closeness to the simulations we conducted.

Applying a functionalised Au NP solution directly to a NaCl fixed DNA breadboard sample proved effective in reducing the necessary tether length, for ~100% attachment of Au NPs at the correct sites, from 20 to 10 bases. When this length increased to 15 bases there was significant evidence of Au NPs being tethered to multiple boards and this would need to be addressed either by modification of the design to move tethers away from the board's terminal edges or reduction of tether length. While very low in number there was also evidence of Au NPs attaching via 5 base pair tethers and it is possible that this throughput could be increased, either by further ionic modification, or slight increase in tether length, to provide higher resolution metallisation.

Two significant experimental artifacts were observed during our metallisation attempts. The first were the 'phantom' bands appearing in 9 and 10nm Au NP samples which could be mistaken for a correctly metallised DNA origami band. Also when 10X and 3X excess staple attempts were compared there was a lack of correlation between typical AGE analysis, where a higher mobility band is likely a correctly

fabricated one, and aggregation at the loading pocket not signalling destruction of the sample (Typically samples which contain aggregates are effectively destroyed). For this reason when examining metallised samples combined analysis must be undertaken as AGE seems to be less reliable under these circumstances.

When employing an unmodified ascorbic acid/AuCl enhancement step to increase site specific metallisation aggregation and destruction of fine features of the sample was observed. It is likely this could be mitigated by the addition of a PEG surfactant, as under these conditions the Au NP portion of the sample seemed to maintain its spectral qualities, but unfortunately the addition of PEG made AGE and AFM imaging impossible. It is likely that future work to mitigate the deleterious effect of the surfactant would make it a viable pathway for continuous metallisation of these structures.

It was also shown that Au NP formation could occur via an ascorbic acid/AuCl enhancement of a polyphosphothioate modified DNA sequence. This method would possibly benefit over enhancement of an existing Au NP for several reasons. It would allow a lower feature size as it would not require a pre-existing metallic structure. It would also remove the difficulties associated with manipulating sub 10 nanometer Au NPs and attaching them to DNA based structures. However it does suffer from the need of surfactant to protect the reaction which is not readily removed from the sample and prevents further analysis or experimentation.

## Chapter 16

### 16.0 Conclusion

In this conclusion the aims of the project and significant observations and developments achieved during the work will be discussed.

It has been theorised, and demonstrated, that tailorable EM materials can be created using subwavelength periodic geometries with the split ring resonator being an example of a structure which is employed to create artificial magnetic susceptibility. To fulfil the requirement of subwavelength structures, for a material active within the optical regime, a nanofabrication system is required for fabrication. Conventional nanofabrication techniques all display certain characteristics which make optical subwavelength material fabrication and development challenging. DNA origami possesses the throughput combined with design flexibility which could be used to address our fabrication goal.

We designed a modular board, which could be decorated within the feature size range of interest and also be linked into geometric lattice structures (Which fulfils the periodic structure criteria stated above). While simulation of curved structures was challenging, we created a simulation environment which provided realistic feedback when standard structures were compared. We then simulated a series of split ring structures, which demonstrated manipulation of certain EM material parameters and converted these motifs into designs for Au NP decoration of the DNA modular breadboard.

A pathway for fabrication was created, analysed, and a high efficiency protocol developed. This included a significant reduction in thermal cycling time (~20 hours down to ~2) which could be applied to all modular board configurations tested, also inferring that the critical folding mechanic is dominated by the double stranded interaction which makes up the main body of the as fabricated structure, and implies that at least partially universal high efficiency protocols could be used for many variants of our modular design.

Methods for dry lattice fabrication were examined with strings, and sheets, of boards being conjugated. The mechanics of lattice folding were examined, and it was demonstrated that lattice formation and the

formation of individual monomer modular boards occur at significantly differing temperature domains (When the high efficiency protocol was employed). It was also demonstrated that by employing uncomplemented tail regions of the design strings of structures could be effectively created, without a rate limiting purification step, by addition of a specific ratio of lattice components and a secondary thermal cycle. NaCl based fixation (Where  $MgCl_2$  and NaCl were used as dual fixation agents) was shown to allow for highly selective fixation of double stranded DNA to mica which could be used to screen a sample for correctly folded origami structures or to create a layer of quasi purified structures (Where little to no excess fabrication components remain adhered to the board). The NaCl method was also useful for creating a clean surface sheet, where a single layer of boards was clearly visible even after an origami sample had been allowed to dehydrate onto the surface, and this surface saturation modular breadboard layer provides an ideal substrate for creation of a thin sheet of continuous material.

Au NP functionalisation methods were examined and it was shown that by addition of a small quantity of methanol, in the aggregation step, even sub 10 nanometer Au NPs could be condensed and resuspended without displaying significant loss of sample during the process. Conventional techniques for Au NP purification were examined with results being limited when applied to the sub 10 nanometer samples we employ.

We provide detailed information on a system for the quick and effective purification of functionalised sub 10 nanometer Au NPs with little to no observable losses. We also provide the basic principles of operation, how to make the device, and examine a purified sample from synthesis to recovery from the device. This process highlighted that the addition of BSPP, a common procedure in the literature which is used to stabilise an Au NP colloid under mild ionic conditions, significantly affected UV-vis results, and that care should be taken to fully resuspend an Au NP sample before UV-vis measurements (Describing particle size and/or concentration) are obtained.

Metallisation of an NaCl fixed surface saturation level sample was highly successful, in terms of overall metallisation, but evidence of 'bleeding' between designs, where 2 independent boards would share the same Au NP, was observed. When samples were functionalised in solution and fixed on mica this effect was significantly reduced. It was also shown that by employing lower levels of NaCl, and lowering the

incubation period, a metallised sample could be fixed using the NaCl method. We also observed that short 10 base pair tethers could effectively tether functionalised Au NPs (Where classically the tether length is at least 20 base pairs) using the NaCl method and by employing this approach the ‘bleeding’ between designs could be significantly reduced also potentially decreasing site specific feature size.

A key aspect of any material created using the pathway we provide would be the fusing of individual Au NPs bound to the modular breadboards surface into continuous metallisation. When we attempted metallisation of our structures using an ascorbic acid/Au Cl approach sample destruction was observed. It was theorised that addition of PEG surfactant could protect a colloid from aggregation during the enhancement process. While surfactant based protection was successful the presence of PEG made further, AGE or AFM, analysis highly challenging. A novel development was the use of surfactant to protect sulphur containing sequences which could then be enhanced directly (Without Au NP seed site present) using the ascorbic acid/AuCl technique. These samples seemed to display characteristics usually associated with Au NPs/metallic nanoparticles (Such as ruby red colour – or in other cases blue, green, and pink) and if this technique were expanded it may be possible to ‘string’ a polyphosphothioate sequence across an origami board, and then conduct a metallisation step, creating a nanowire between specific points of the breadboard.

In conclusion, certain areas of the project were challenging, such as simulation of curved structures, and enhancement of Au NPs into continuous motifs. However substantial progress was made towards creation of an artificial material and DNA origami was shown to be a promising nanofabrication process for this purpose. By addressing the challenge of bulk purification of sub 10nm Au NPs, creation of surface saturation layers of DNA breadboards, and lowering the necessary tether length for Au NP attachment, we provide tools which can be of significant use when employed in DNA nanotechnology. It is also of note that many of the techniques developed during this work were created by observing and refining existing pathways showing that there is still significant room for development at all stages of DNA based fabrication.

## References

- [1] J. D. WATSON and F. H. C. CRICK, “Molecular Structure of Nucleic Acids: A Structure for Deoxyribose Nucleic Acid,” *Nature*, vol. 171, no. 4356, pp. 737–738, Apr. 1953, doi: 10.1038/171737a0.
- [2] N. C. Seeman and N. R. Kallenbach, “Design of immobile nucleic acid junctions,” *Biophysical Journal*, vol. 44, no. 2, pp. 201–209, Nov. 1983, doi: 10.1016/s0006-3495(83)84292-1.
- [3] P. W. K. Rothmund, “Folding DNA to create nanoscale shapes and patterns,” *Nature*, vol. 440, no. 7082, pp. 297–302, Mar. 2006, doi: 10.1038/nature04586.
- [4] B. Shen, K. Tapio, V. Linko, M. Kostianen, and J. Toppari, “Metallic Nanostructures Based on DNA Nanoshapes,” *Nanomaterials*, vol. 6, no. 8, p. 146, Aug. 2016, doi: 10.3390/nano6080146.
- [5] J. B. Pendry, A. J. Holden, D. J. Robbins, and W. J. Stewart, “Magnetism from conductors and enhanced nonlinear phenomena,” *IEEE Transactions on Microwave Theory and Techniques*, vol. 47, no. 11, pp. 2075–2084, 1999, doi: 10.1109/22.798002.
- [6] Y. Liu and X. Zhang, “Metamaterials: a new frontier of science and technology,” *Chemical Society Reviews*, vol. 40, no. 5, p. 2494, 2011, doi: 10.1039/c0cs00184h.
- [7] Y. Wang and X. Zhang, “Scale-up of the manufacturing of optical metamaterials,” *NPG Asia Materials*, vol. 6, no. 11, pp. e141–e141, Nov. 2014, doi: 10.1038/am.2014.99.
- [8] X. Guo, A. A. Gorodetsky, J. Hone, J. K. Barton, and C. Nuckolls, “Conductivity of a single DNA duplex bridging a carbon nanotube gap,” *Nature Nanotechnology*, vol. 3, no. 3, pp. 163–167, Feb. 2008, doi: 10.1038/nnano.2008.4.
- [9] Z. Chen, C. Liu, F. Cao, J. Ren, and X. Qu, “DNA metallization: principles, methods, structures, and applications,” *Chemical Society Reviews*, vol. 47, no. 11, pp. 4017–4072, 2018, doi: 10.1039/c8cs00011e.
- [10] F. N. Gür, F. W. Schwarz, J. Ye, S. Diez, and T. L. Schmidt, “Toward Self-Assembled Plasmonic Devices: High-Yield Arrangement of Gold Nanoparticles on DNA Origami Templates,” *ACS Nano*, vol. 10, no. 5, pp. 5374–5382, May 2016, doi: 10.1021/acsnano.6b01537.
- [11] C. E. Castro *et al.*, “A primer to scaffolded DNA origami,” *Nature Methods*, vol. 8, no. 3, pp. 221–229, Feb. 2011, doi: 10.1038/nmeth.1570.
- [12] P. Wang, T. A. Meyer, V. Pan, P. K. Dutta, and Y. Ke, “The Beauty and Utility of

- DNA Origami,” *Chem*, vol. 2, no. 3, pp. 359–382, Mar. 2017, doi: 10.1016/j.chempr.2017.02.009.
- [13] A. Kuzyk *et al.*, “DNA-based self-assembly of chiral plasmonic nanostructures with tailored optical response,” *Nature*, vol. 483, no. 7389, pp. 311–314, Mar. 2012, doi: 10.1038/nature10889.
- [14] R. Schreiber *et al.*, “Chiral plasmonic DNA nanostructures with switchable circular dichroism,” *Nature Communications*, vol. 4, no. 1, Dec. 2013, doi: 10.1038/ncomms3948.
- [15] P. D. Halley, R. A. Patton, A. Chowdhury, J. C. Byrd, and C. E. Castro, “Low-cost, simple, and scalable self-assembly of DNA origami nanostructures,” *Nano Research*, vol. 12, no. 5, pp. 1207–1215, Apr. 2019, doi: 10.1007/s12274-019-2384-x.
- [16] V. G. Veselago, “THE ELECTRODYNAMICS OF SUBSTANCES WITH SIMULTANEOUSLY NEGATIVE VALUES OF  $\epsilon$  AND  $\mu$ ,” *Soviet Physics Uspekhi*, vol. 10, no. 4, pp. 509–514, Apr. 1968, doi: 10.1070/pu1968v010n04abeh003699.
- [17] W. E. Kock, “Metallic Delay Lenses,” *Bell System Technical Journal*, vol. 27, no. 1, pp. 58–82, Jan. 1948, doi: 10.1002/j.1538-7305.1948.tb01331.x.
- [18] W. J. Padilla, D. N. Basov, and D. R. Smith, “Negative refractive index metamaterials,” *Materials Today*, vol. 9, no. 7–8, pp. 28–35, Jul. 2006, doi: 10.1016/s1369-7021(06)71573-5.
- [19] J. B. Pendry, “Negative Refraction Makes a Perfect Lens,” *Physical Review Letters*, vol. 85, no. 18, pp. 3966–3969, Oct. 2000, doi: 10.1103/physrevlett.85.3966.
- [20] R. M. Walser, “Electromagnetic metamaterials,” *Complex Mediums II: Beyond Linear Isotropic Dielectrics*, Jul. 2001, doi: 10.1117/12.432921.
- [21] H. Nornikman, B. H. Ahmad, M. Z. A. Abdul Aziz, M. F. bin A. Malek, H. Imran, and A. R. Othman, “STUDY AND SIMULATION OF AN EDGE COUPLE SPLIT RING RESONATOR (EC-SRR) ON TRUNCATED PYRAMIDAL MICROWAVE ABSORBER,” *Progress In Electromagnetics Research*, vol. 127, pp. 319–334, 2012, doi: 10.2528/pier12030601.
- [22] J. Pendry, “Metamaterials in the sunshine,” *Nature Materials*, vol. 5, no. 8, pp. 599–600, Aug. 2006, doi: 10.1038/nmat1697.
- [23] J. A. Liddle and G. M. Gallatin, “Nanomanufacturing: A Perspective,” *ACS Nano*, vol. 10, no. 3, pp. 2995–3014, Feb. 2016, doi: 10.1021/acsnano.5b03299.
- [24] G. E. Moore, “Cramming More Components Onto Integrated Circuits,” *Proceedings of the IEEE*, vol. 86, no. 1, pp. 82–85, Jan. 1998, doi: 10.1109/jproc.1998.658762.

- [25] Hasan, R., 2021. Nanolithography: Status and Challenges. [online] Strathprints.strath.ac.uk. Available at: <[https://strathprints.strath.ac.uk/64171/1/Hasan\\_Luo\\_ICAC\\_2017\\_Nanolithography\\_status\\_and\\_challenges.pdf](https://strathprints.strath.ac.uk/64171/1/Hasan_Luo_ICAC_2017_Nanolithography_status_and_challenges.pdf)>
- [26] Fomenkov, I., Brandt, D., Ershov, A., Schafgans, A., Tao, Y., Vaschenko, G., Rokitski, S., Kats, M., Vargas, M., Purvis, M., Rafac, R., La Fontaine, B., De Dea, S., LaForge, A., Stewart, J., Chang, S., Graham, M., Riggs, D., Taylor, T., Abraham, M. and Brown, D., 2017. Light sources for high-volume manufacturing EUV lithography
- [27] Flynn, C., 2021. The chip-making machine at the center of Chinese dual-use concerns. [online] Brookings. Available at: <<https://www.brookings.edu/techstream/the-chip-making-machine-at-the-center-of-chinese-dual-use-concerns/>>
- [28] Thoss, A., 2021. EUV lithography revisited. [online] Laserfocusworld.com. Available at: <<https://www.laserfocusworld.com/blogs/article/14039015/how-does-the-laser-technology-in-euv-lithography-work>>.
- [29] Microchemicals.com. 2021. SILICON WAFER PRODUCTION AND SPECIFICATIONS. [online] Available at: [www.microchemicals.com/technical\\_information/silicon\\_wafer\\_production\\_specification.pdf](http://www.microchemicals.com/technical_information/silicon_wafer_production_specification.pdf)
- [30] Nayfeh, M., n.d. Fundamentals and Applications of Nano Silicon in Plasmonics and Fullerines.
- [31] Lawson, R. and Robinson, A., 2016. Overview of materials and processes for lithography. Materials and Processes for Next Generation Lithography, pp.1-90.
- [32] N. Parker, A. Brodie and J. McCoy, "High-throughput NGL electron-beam direct-write lithography system", Emerging Lithographic Technologies IV, 2000. Available: 10.1117/12.390042
- [33] Fundamentals and Applications of Nano Silicon in Plasmonics and Fullerines, 2018. Manipulation and Patterning of Surfaces (Nanolithography). pp.89-137.
- [34] Tseng, A., Notargiacomo, A. and Chen, T., 2005. Nanofabrication by scanning probe microscope lithography: A review. Journal of Vacuum Science & Technology B: Microelectronics and Nanometer Structures, 23(3), p.877.

- [35] D. Eigler and E. Schweizer, "Positioning single atoms with a scanning tunnelling microscope", *Nature*, vol. 344, no. 6266, pp. 524-526, 1990. Available: 10.1038/344524a0
- [36] U. Staufer, L. Scandella and R. Wiesendanger, "Direct writing of nanometer scale structures on glassy metals by the scanning tunneling microscope", *Zeitschrift für Physik B Condensed Matter*, vol. 77, no. 2, pp. 281-286, 1989. Available: 10.1007/bf01313672
- [37] Q. Tang, S. Shi and L. Zhou, "Nanofabrication with Atomic Force Microscopy", *Journal of Nanoscience and Nanotechnology*, vol. 4, no. 8, pp. 948-963, 2004. Available: 10.1166/jnn.2004.131
- [38] O. Custance, R. Perez and S. Morita, "Atomic force microscopy as a tool for atom manipulation", *Nature Nanotechnology*, vol. 4, no. 12, pp. 803-810, 2009. Available: 10.1038/nnano.2009.347
- [39] L. Santinacci, Y. Zhang and P. Schmuki, "AFM scratching and metal deposition through insulating layers on silicon", *Surface Science*, vol. 597, no. 1-3, pp. 11-19, 2005. Available: 10.1016/j.susc.2005.05.069
- [40] R. Garcia, A. Knoll and E. Riedo, "Advanced scanning probe lithography", *Nature Nanotechnology*, vol. 9, no. 8, pp. 577-587, 2014. Available: 10.1038/nnano.2014.157
- [41] P. A. Levene and J. A. Mandel, "Über die Konstitution der Thymo-nucleinsäure," *Berichte der deutschen chemischen Gesellschaft*, vol. 41, no. 2, pp. 1905–1909, May 1908, doi: 10.1002/cber.19080410266.
- [42] P. Levene *et al.*, "THE STRUCTURE OF YEAST NUCLEIC ACID. IV. AMMONIA HYDROLYSIS. Downloaded from," *Ber. them. Ges*, vol. 608, no. 2, p. 2020, 1909.
- [43] L. Pray, "Discovery of DNA Double Helix: Watson and Crick | Learn Science at Scitable," *Nature.com*, Dec. 01, 2003. <https://www.nature.com/scitable/topicpage/discovery-of-dna-structure-and-function-watson-397/> (accessed Dec. 01, 2020).
- [44] D. Elson and E. Chargaff, "On the desoxyribonucleic acid content of sea urchin gametes," *Experientia*, vol. 8, no. 4, pp. 143–145, Apr. 1952, doi: 10.1007/bf02170221.
- [45] H. E. Gaub, M. Rief, and H. Clausen-Schaumann, "Sequence-dependent mechanics of single DNA molecules," *Nature Structural Biology*, vol. 6, no. 4, pp. 346–349, Apr. 1999, doi: 10.1038/7582.
- [46] S. Naz and A. Fatima, "Amplification of GC-rich DNA for High-Throughput Family-Based Genetic Studies," *Molecular Biotechnology*, vol. 53, no. 3, pp. 345–350, May 2012,

doi: 10.1007/s12033-012-9559-y.

[47] S. Harteis and S. Schneider, “Making the Bend: DNA Tertiary Structure and Protein-DNA Interactions,” *International Journal of Molecular Sciences*, vol. 15, no. 7, pp. 12335–12363, Jul. 2014, doi: 10.3390/ijms150712335.

[48] S. Y. Taylor and R. Holliday, “Induction of thermotolerance and mitotic recombination by heat-shock in *Ustilago maydis*,” *Current Genetics*, vol. 9, no. 1, pp. 59–63, Dec. 1984, doi: 10.1007/bf00396205.

[49] R. P. D. Bank, “RCSB PDB - 3CRX: CRE RECOMBINASE/DNA COMPLEX INTERMEDIATE I,” *www.rcsb.org*. <https://www.rcsb.org/structure/3CRX> (accessed Dec. 01, 2020).

[50] M. R. Jones, N. C. Seeman, and C. A. Mirkin, “Programmable materials and the nature of the DNA bond,” *Science*, vol. 347, no. 6224, pp. 1260901–1260901, Feb. 2015, doi: 10.1126/science.1260901.

[51] S. M. Douglas, H. Dietz, T. Liedl, B. Högberg, F. Graf, and W. M. Shih, “Erratum: Self-assembly of DNA into nanoscale three-dimensional shapes,” *Nature*, vol. 459, no. 7250, pp. 1154–1154, Jun. 2009, doi: 10.1038/nature08165.

[52] N. C. Seeman, “Nucleic acid junctions and lattices,” *Journal of Theoretical Biology*, vol. 99, no. 2, pp. 237–247, Nov. 1982, doi: 10.1016/0022-5193(82)90002-9.

[53] W. Liu, H. Zhong, R. Wang, and N. C. Seeman, “Crystalline Two-Dimensional DNA-Origami Arrays,” *Angewandte Chemie International Edition*, vol. 50, no. 1, pp. 264–267, Nov. 2010, doi: 10.1002/anie.201005911.

[54] A. Aghebat Rafat, T. Pirzer, M. B. Scheible, A. Kostina, and F. C. Simmel, “Surface-Assisted Large-Scale Ordering of DNA Origami Tiles,” *Angewandte Chemie International Edition*, vol. 53, no. 29, pp. 7665–7668, Jun. 2014, doi: 10.1002/anie.201403965.

[55] H. Dietz, S. M. Douglas, and W. M. Shih, “Folding DNA into Twisted and Curved Nanoscale Shapes,” *Science*, vol. 325, no. 5941, pp. 725–730, Aug. 2009, doi: 10.1126/science.1174251.

[56] D. Han *et al.*, “DNA Gridiron Nanostructures Based on Four-Arm Junctions,” *Science*, vol. 339, no. 6126, pp. 1412–1415, Mar. 2013, doi: 10.1126/science.1232252.

[57] Y. Ke, L. L. Ong, W. M. Shih, and P. Yin, “Three-Dimensional Structures Self-Assembled from DNA Bricks,” *Science (New York, N.Y.)*, vol. 338, no. 6111, Nov. 2012, doi: 10.1126/science.1227268.

[58] L. L. Ong *et al.*, “Programmable self-assembly of three-dimensional nanostructures from 10,000 unique components,” *Nature*, vol. 552, no. 7683, pp. 72–77, Dec. 2017, doi:

10.1038/nature24648.

[59] J.-P. J. Sobczak, T. G. Martin, T. Gerling, and H. Dietz, “Rapid Folding of DNA into Nanoscale Shapes at Constant Temperature,” *Science*, vol. 338, no. 6113, pp. 1458–1461, Dec. 2012, doi: 10.1126/science.1229919.

[60] F. A. S. Engelhardt *et al.*, “Custom-Size, Functional, and Durable DNA Origami with Design-Specific Scaffolds,” *ACS Nano*, vol. 13, no. 5, pp. 5015–5027, Apr. 2019, doi: 10.1021/acsnano.9b01025.

[61] T. Gerling, M. Kube, B. Kick, and H. Dietz, “Sequence-programmable covalent bonding of designed DNA assemblies,” *Science Advances*, vol. 4, no. 8, p. eaau1157, Aug. 2018, doi: 10.1126/sciadv.aau1157.

[62] G. Bellot, M. A. McClintock, J. J. Chou, and W. M. Shih, “DNA nanotubes for NMR structure determination of membrane proteins,” *Nature Protocols*, vol. 8, no. 4, pp. 755–770, Mar. 2013, doi: 10.1038/nprot.2013.037.

[63] B. Kick, F. Praetorius, H. Dietz, and D. Weuster-Botz, “Efficient Production of Single-Stranded Phage DNA as Scaffolds for DNA Origami,” *Nano Letters*, vol. 15, no. 7, pp. 4672–4676, Jun. 2015, doi: 10.1021/acs.nanolett.5b01461.

[64] Eurofins Genomics, “Frequently Asked Questions About Our Products And Services,” [www.eurofinsgenomics.eu](http://www.eurofinsgenomics.eu). <http://www.eurofinsgenomics.eu/en/eurofins-genomics/product-faqs/dna-rna-oligonucleotides/dna-origami/>.

[65] Integrated DNA Technologies, “Oligo synthesis: Coupling efficiency and quality control | IDT,” *Integrated DNA Technologies*. <https://eu.idtdna.com/pages/education/decoded/article/oligo-synthesis-why-idt-leads-the-oligo-industry> (accessed Dec. 07, 2020).

[66] Integrated DNA Technologies, “Do I need to reduce thiol-modified oligos before use?,” *Integrated DNA Technologies*. <https://eu.idtdna.com/pages/support/faqs/do-i-need-to-reduce-thiol-modified-oligos-before-use-> (accessed Dec. 07, 2020).

[67] X. Zhang, T. Gouriye, K. Göeken, M. R. Servos, R. Gill, and J. Liu, “Toward Fast and Quantitative Modification of Large Gold Nanoparticles by Thiolated DNA: Scaling of Nanoscale Forces, Kinetics, and the Need for Thiol Reduction,” *The Journal of Physical Chemistry C*, vol. 117, no. 30, pp. 15677–15684, Jul. 2013, doi: 10.1021/jp403946x.

[68] J. J. Storhoff, R. Elghanian, R. C. Mucic, C. A. Mirkin, and R. L. Letsinger, “One-Pot Colorimetric Differentiation of Polynucleotides with Single Base Imperfections Using Gold Nanoparticle Probes,” *Journal of the American Chemical Society*, vol. 120, no. 9, pp. 1959–1964, Mar. 1998, doi: 10.1021/ja972332i.

- [69] J. Liu and Y. Lu, "Preparation of aptamer-linked gold nanoparticle purple aggregates for colorimetric sensing of analytes," *Nature Protocols*, vol. 1, no. 1, pp. 246–252, Jun. 2006, doi: 10.1038/nprot.2006.38.
- [70] H. Zhang, J. Chao, D. Pan, H. Liu, Q. Huang, and C. Fan, "Folding super-sized DNA origami with scaffold strands from long-range PCR," *Chemical Communications*, vol. 48, no. 51, p. 6405, 2012, doi: 10.1039/c2cc32204h.
- [71] T. L. Schmidt *et al.*, "Scalable amplification of strand subsets from chip-synthesized oligonucleotide libraries," *Nature Communications*, vol. 6, no. 1, Nov. 2015, doi: 10.1038/ncomms9634.
- [72] Z. Zhao, Y. Liu, and H. Yan, "Organizing DNA Origami Tiles into Larger Structures Using Preformed Scaffold Frames," *Nano Letters*, vol. 11, no. 7, pp. 2997–3002, Jul. 2011, doi: 10.1021/nl201603a.
- [73] X. Xu *et al.*, "Cationic Albumin Encapsulated DNA Origami for Enhanced Cellular Transfection and Stability," *Materials*, vol. 12, no. 6, p. 949, Mar. 2019, doi: 10.3390/ma12060949.
- [74] C. Kielar *et al.*, "On the Stability of DNA Origami Nanostructures in Low-Magnesium Buffers," *Angewandte Chemie International Edition*, vol. 57, no. 30, pp. 9470–9474, Jun. 2018, doi: 10.1002/anie.201802890.
- [75] T. G. Martin and H. Dietz, "Magnesium-free self-assembly of multi-layer DNA objects," *Nature Communications*, vol. 3, no. 1, Jan. 2012, doi: 10.1038/ncomms2095.
- [76] K. Matsubara and Y. Takagi, "Electrophoretic separation of single-stranded deoxyribonucleic acid from double-stranded deoxyribonucleic acid," *Biochimica et Biophysica Acta*, vol. 55, no. 3, pp. 389–392, Mar. 1962, doi: 10.1016/0006-3002(62)90797-7.
- [77] P. Y. Lee, J. Costumbrado, C.-Y. Hsu, and Y. H. Kim, "Agarose Gel Electrophoresis for the Separation of DNA Fragments," *Journal of Visualized Experiments*, no. 62, Apr. 2012, doi: 10.3791/3923.
- [78] B. A. Sanderson, N. Araki, J. L. Lilley, G. Guerrero, and L. K. Lewis, "Modification of gel architecture and TBE/TAE buffer composition to minimize heating during agarose gel electrophoresis," *Analytical biochemistry*, vol. 454, pp. 44–52, 2014, doi: 10.1016/j.ab.2014.03.003.
- [79] J. K. Kiviahio *et al.*, "Cationic polymers for DNA origami coating – examining their binding efficiency and tuning the enzymatic reaction rates," *Nanoscale*, vol. 8, no. 22, pp. 11674–11680, 2016, doi: 10.1039/c5nr08355a.

- [80] “Fundamentals of Contact Mode and TappingMode Atomic Force Microscopy,” *AZoNano.com*, May 18, 2012. <https://www.azonano.com/article.aspx?ArticleID=3010> (accessed Dec. 02, 2020).
- [81] N. Jalili and K. Laxminarayana, “A review of atomic force microscopy imaging systems: application to molecular metrology and biological sciences,” *Mechatronics*, vol. 14, no. 8, pp. 907–945, Oct. 2004, doi: 10.1016/j.mechatronics.2004.04.005.
- [82] A. Matković *et al.*, “Enhanced structural stability of DNA origami nanostructures by graphene encapsulation,” *New Journal of Physics*, vol. 18, no. 2, p. 025016, Feb. 2016, doi: 10.1088/1367-2630/18/2/025016.
- [83] Bruker, “PeakForce QNM (Quantitative Nanomechanical Property Mapping),” *Bruker.com*. <https://www.bruker.com/products/surface-and-dimensional-analysis/atomic-force-microscopes/modes/modes/imaging-modes/peakforce-qnm.html> (accessed Dec. 02, 2020).
- [84] J. Turkevich, P. C. Stevenson, and J. Hillier, “A study of the nucleation and growth processes in the synthesis of colloidal gold,” *Discussions of the Faraday Society*, vol. 11, p. 55, 1951, doi: 10.1039/df9511100055.
- [85] J. Piella, N. G. Bastús, and V. Puntes, “Size-Controlled Synthesis of Sub-10-nanometer Citrate-Stabilized Gold Nanoparticles and Related Optical Properties.,” *Chemistry of Materials*, vol. 28, no. 4, pp. 1066–1075, Feb. 2016, doi: 10.1021/acs.chemmater.5b04406.
- [86] A. M. Alkilany and C. J. Murphy, “Toxicity and cellular uptake of gold nanoparticles: what we have learned so far?,” *Journal of Nanoparticle Research*, vol. 12, no. 7, pp. 2313–2333, Apr. 2010, doi: 10.1007/s11051-010-9911-8.
- [87] H. Mühlpfordt, “The preparation of colloidal gold particles using tannic acid as an additional reducing agent,” *Experientia*, vol. 38, no. 9, pp. 1127–1128, Sep. 1982, doi: 10.1007/bf01955405.
- [88] C. A. Mirkin, R. L. Letsinger, R. C. Mucic, and J. J. Storhoff, “A DNA-based method for rationally assembling nanoparticles into macroscopic materials,” *Nature*, vol. 382, no. 6592, pp. 607–609, Aug. 1996, doi: 10.1038/382607a0.
- [89] “Attach oligos to ligands or surfaces,” *Integrated DNA Technologies*. <https://eu.idtdna.com/pages/education/decoded/article/modification-highlight-dithiol-modifier>.
- [90] B. Liu and J. Liu, “Freezing Directed Construction of Bio/Nano Interfaces: Reagentless Conjugation, Denser Spherical Nucleic Acids, and Better Nanoflakes,” *Journal of the American Chemical Society*, vol. 139, no. 28, pp. 9471–9474, Jul. 2017, doi:

10.1021/jacs.7b04885.

[91] M. Zimbone *et al.*, “Dynamic Light Scattering on Bioconjugated Laser Generated Gold Nanoparticles,” *PLoS ONE*, vol. 9, no. 3, p. e89048, Mar. 2014, doi:

10.1371/journal.pone.0089048.

[92] Y. Zhao, Z. Wang, W. Zhang, and X. Jiang, “Adsorbed Tween 80 is unique in its ability to improve the stability of gold nanoparticles in solutions of biomolecules,”

*Nanoscale*, vol. 2, no. 10, p. 2114, 2010, doi: 10.1039/c0nr00309c.

[93] S. J. Hurst, A. K. R. Lytton-Jean, and C. A. Mirkin, “Maximizing DNA Loading on a Range of Gold Nanoparticle Sizes,” *Analytical Chemistry*, vol. 78, no. 24, pp. 8313–8318,

Dec. 2006, doi: 10.1021/ac0613582.

[94] X. Zhang, M. R. Servos, and J. Liu, “Instantaneous and quantitative functionalization of gold nanoparticles with thiolated DNA using a pH-assisted and surfactant-free route,”

*Journal of the American Chemical Society*, vol. 134, no. 17, pp. 7266–9, 2012, doi:

10.1021/ja3014055.

[95] W. Zhou, F. Wang, J. Ding, and J. Liu, “Tandem Phosphorothioate Modifications for DNA Adsorption Strength and Polarity Control on Gold Nanoparticles,” *ACS Applied*

*Materials & Interfaces*, vol. 6, no. 17, pp. 14795–14800, Aug. 2014, doi:

10.1021/am504791b.

[96] J. J. Storhoff, R. Elghanian, C. A. Mirkin, and R. L. Letsinger, “Sequence-Dependent Stability of DNA-Modified Gold Nanoparticles,” *Langmuir*, vol. 18, no. 17, pp. 6666–6670,

Aug. 2002, doi: 10.1021/la0202428.

[97] W. Lu *et al.*, “Quantitative investigation of the poly-adenine DNA dissociation from the surface of gold nanoparticles,” *Scientific Reports*, vol. 5, no. 1, May 2015, doi:

10.1038/srep10158.

[98] N. G. Khlebtsov, “Determination of Size and Concentration of Gold Nanoparticles from Extinction Spectra,” *Analytical Chemistry*, vol. 80, no. 17, pp. 6620–6625, Sep. 2008,

doi: 10.1021/ac800834n.

[99] K. Keren, R. S. Berman, E. Buchstab, U. Sivan, and E. Braun, “DNA-Templated Carbon Nanotube Field-Effect Transistor,” *Science*, vol. 302, no. 5649, pp. 1380–1382, Nov.

2003, doi: 10.1126/science.1091022.

[100] E. Braun, Y. Eichen, U. Sivan, and G. Ben-Yoseph, “DNA-templated assembly and electrode attachment of a conducting silver wire,” *Nature*, vol. 391, no. 6669, pp. 775–778,

Feb. 1998, doi: 10.1038/35826.

[101] J. Liu *et al.*, “Metallization of Branched DNA Origami for Nanoelectronic Circuit

- Fabrication,” *ACS Nano*, vol. 5, no. 3, pp. 2240–2247, Feb. 2011, doi: 10.1021/nn1035075.
- [102] M. Pilo-Pais, S. Goldberg, E. Samano, T. H. LaBean, and G. Finkelstein, “Connecting the Nanodots: Programmable Nanofabrication of Fused Metal Shapes on DNA Templates,” *Nano Letters*, vol. 11, no. 8, pp. 3489–3492, Aug. 2011, doi: 10.1021/nl202066c.
- [103] Y. Geng *et al.*, “Electrically Conductive Gold- and Copper-Metallized DNA Origami Nanostructures,” *Langmuir*, vol. 29, no. 10, pp. 3482–3490, Mar. 2013, doi: 10.1021/la305155u.
- [104] W. Sun *et al.*, “Casting inorganic structures with DNA molds,” *Science*, vol. 346, no. 6210, pp. 1258361–1258361, Oct. 2014, doi: 10.1126/science.1258361.
- [105] S. Helmi, C. Ziegler, D. J. Kauert, and R. Seidel, “Shape-Controlled Synthesis of Gold Nanostructures Using DNA Origami Molds,” *Nano Letters*, vol. 14, no. 11, pp. 6693–6698, Oct. 2014, doi: 10.1021/nl503441v.
- [106] S. Jia *et al.*, “Programming DNA origami patterning with non-canonical DNA-based metallization reactions,” *Nature Communications*, vol. 10, no. 1, Dec. 2019, doi: 10.1038/s41467-019-13507-5.
- [107] “gold nanoparticles properties centrifuge speeds,” *Nanopartz.com*, 2015. <https://www.nanopartz.com/gold-nanoparticles-properties-centrifuge-speeds.asp>.
- [108] E. Stahl, T. G. Martin, F. Praetorius, and H. Dietz, “Facile and Scalable Preparation of Pure and Dense DNA Origami Solutions,” *Angewandte Chemie International Edition*, vol. 53, no. 47, pp. 12735–12740, Oct. 2014, doi: 10.1002/anie.201405991.
- [109] G. O. Humphreys, G. A. Willshaw, and E. S. Anderson, “A simple method for the preparation of large quantities of pure plasmid DNA,” *Biochimica et Biophysica Acta (BBA) - Nucleic Acids and Protein Synthesis*, vol. 383, no. 4, pp. 457–463, Apr. 1975, doi: 10.1016/0005-2787(75)90318-4.
- [110] D. Tautz and M. Renz, “An optimized freeze-squeeze method for the recovery of DNA fragments from agarose gels,” *Analytical biochemistry*, vol. 132, no. 1, pp. 14–9, 1983, doi: 10.1016/0003-2697(83)90419-0.
- [111] G. Bellot, M. A. McClintock, C. Lin, and W. M. Shih, “Recovery of intact DNA nanostructures after agarose gel-based separation,” *Nature Methods*, vol. 8, no. 3, pp. 192–194, Feb. 2011, doi: 10.1038/nmeth0311-192.
- [112] Z. Cendes, “The development of HFSS,” *2016 USNC-URSI Radio Science Meeting*, Jun. 2016, doi: 10.1109/usnc-ursi.2016.7588501.
- [113] Wenshan Cai and V. M. Shalaev, *Optical metamaterials : fundamentals and applications*. New York: Springer, 2010.

- [114] A. M. Nicolson and G. F. Ross, "Measurement of the Intrinsic Properties of Materials by Time-Domain Techniques," *IEEE Transactions on Instrumentation and Measurement*, vol. 19, no. 4, pp. 377–382, Nov. 1970, doi: 10.1109/tim.1970.4313932.
- [115] W. B. Weir, "Automatic measurement of complex dielectric constant and permeability at microwave frequencies," *Proceedings of the IEEE*, vol. 62, no. 1, pp. 33–36, 1974, doi: 10.1109/proc.1974.9382.
- [116] Wenshan Cai and V. M. Shalaev, *Optical metamaterials : fundamentals and applications*. Cham: Springer, 2016.
- [117] F. Costa, M. Borgese, M. Degiorgi and A. Monorchio, "Electromagnetic Characterisation of Materials by Using Transmission/Reflection (T/R) Devices", *Electronics*, vol. 6, no. 4, p. 95, 2017.
- [118] F. Costa, M. Borgese, M. Degiorgi and A. Monorchio, "Electromagnetic Characterisation of Materials by Using Transmission/Reflection (T/R) Devices", *Electronics*, vol. 6, no. 4, p. 95, 2017
- [119] E. Plum, V. Fedotov and N. Zheludev, "Specular optical activity of achiral metasurfaces", *Applied Physics Letters*, vol. 108, no. 14, p. 141905, 2016.
- [120] Q. Le-Van, X. Le Roux, A. Aassime and A. Degiron, "Electrically driven optical metamaterials", *Nature Communications*, vol. 7, no. 1, 2016.
- [121] Handling-solutions.eppendorf.com, 2021. [Online]. Available: <https://handling-solutions.eppendorf.com/sample-handling/photometry/applications/detailview-applications/news/uv-vis-spectrophotometry-easy-and-quick-quantification-of-nucleic-acids/>
- [122] A. Kuzuya and M. Komiyama, "DNA origami: Fold, stick, and beyond," *Nanoscale*, vol. 2, no. 3, pp. 310–322, 2010, doi: 10.1039/b9nr00246d.
- [124] "About", CanDo, 2021. [Online]. Available: <https://cando-dna-origami.org/about/>
- [125] Integrated DNA Technologies. 2020. *Storing Oligos: 7 Things You Should Know*. [online] Available at: <https://eu.idtdna.com/pages/education/decoded/article/storing-oligos-7-things-you-should-know>
- [126] The Scientist Magazine®. 2020. *Thermo Fisher Scientific: Nucleic Acid Sample*

*Storage Solutions*. [online] Available at: <https://www.the-scientist.com/the-marketplace/thermo-fisher-scientific--nucleic-acid-sample-storage-solutions--65289>

[127] E. P. Gates, J. K. Jensen, J. N. Harb, and A. T. Woolley, “Optimizing gold nanoparticle seeding density on DNA origami,” *RSC Advances*, vol. 5, no. 11, pp. 8134–8141, 2015, doi: 10.1039/c4ra15451g.

#### Copyright statement

i. The author of this thesis (including any appendices and/ or schedules to this thesis) owns any copyright in it (the “Copyright”) and s/he has given The University of Huddersfield the right to use such Copyright for any administrative, promotional, educational and/or teaching purposes. ii. Copies of this thesis, either in full or in extracts, may be made only in accordance with the regulations of the University Library. Details of these regulations may be obtained from the Librarian. Details of these regulations may be obtained from the Librarian. This page must form part of any such copies made. iii. The ownership of any patents, designs, trademarks and any and all other intellectual property rights except for the Copyright (the “Intellectual Property Rights”) and any reproductions of copyright works, for example graphs and tables (“Reproductions”), which may be described in this thesis, may not be owned by the author and may be owned by third parties. Such Intellectual Property Rights and Reproductions cannot and must not be made available for use without permission of the owner(s) of the relevant Intellectual Property Rights and/or Reproductions.

## Materials list

Reagents	Supplier
Tris base	Melford
Boric acid	Melford
Agarose technical grade	Melford
Bis(p-sulfonatophenyl)phenylphosphine dihydrate dipotassium salt	Sigma
Methanol	Sigma
Gold trihydrate	Sigma
Sodium citrate	Sigma
Hydrochloric acid	Sigma
Nitric acid	Sigma
Tannic acid	Sigma
Potassium carbonate	Sigma
6X DNA loading buffer	Thermo Fisher
Syber safe DNA stain	Thermo Fisher
Custom DNA sequences	IDT
	Tilibit
P7249/M13MP18 scaffold	Nanosystems

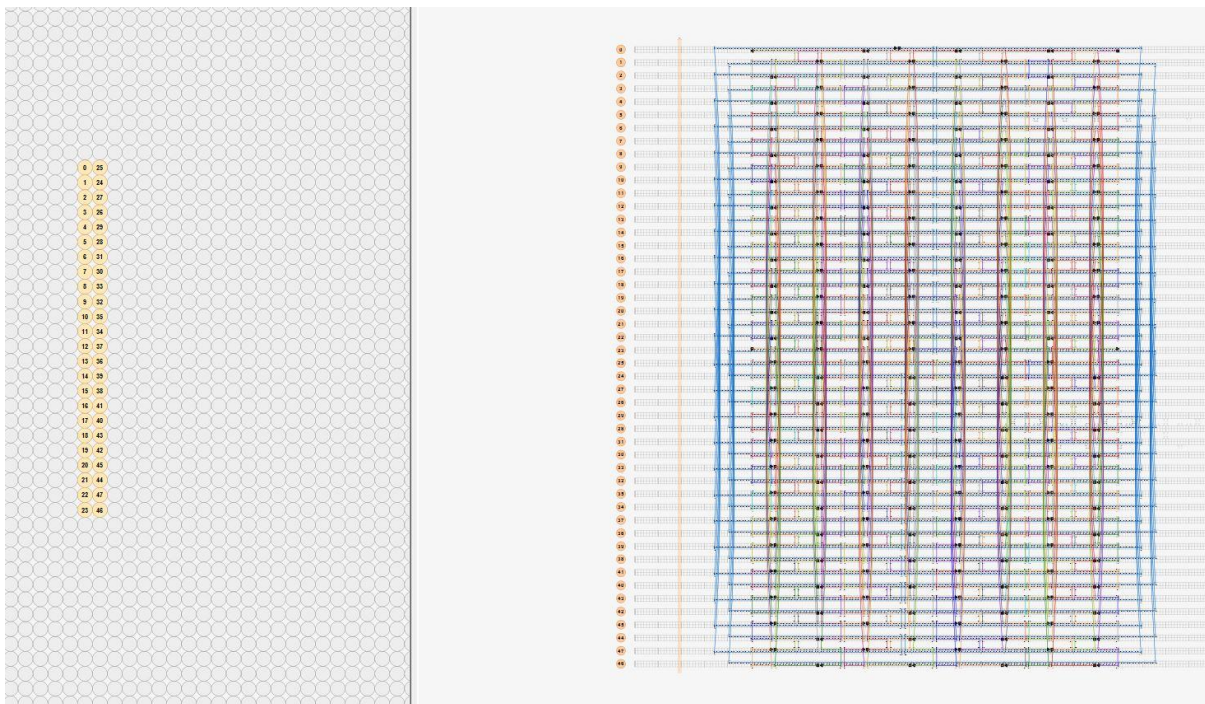
Equipment	
Mini PCR	Cleaver Scientific
Cleaver electrophoresis kit	Cleaver Scientific
Cleaver blue light illuminator	Cleaver Scientific

AFM equipment	
Dimension ICON	Bruker
SNL - 10 tips - C probe	Bruker
Mica slides	Agar Scientific

## Origami designs

Each of the designs was created using the M13MP18 scaffold (as it is notated in caDNAno sequence library) but is sometimes referred to as P7249 (As it is referred to by Tillibit Nanosystems from where our supply was purchased).

Design – Bare board with free edge spacer regions



Start	End	Sequence	Length	Color
19[128]	44[128]	CGGTCATAATTTACCGGGAGGTTGAGTATTAA	32	#f74308
21[64]	46[64]	GGAAGTTTATTTCTTATGAGGCTTTCAACAG	32	#00720
				0
24[95]	3[95]	AAATTTGATCCTGAACTTGCATATGGCCAACG	32	#aaaa0
				0

38[159]	17[159]	GAATTGAGGCAATAATGACTCCTTACAATCAA	32	#cc000 0
3[160]	28[160]	ACATCGCCTTGAGGAATGGCAAATAAAGTTTG	32	#f74308
46[95]	22[80]	TGTATGGGATTTTGCTAAGGCTCCCTTGCTTT	32	#aaaa0 0
35[144]	8[144]	TAAGAATACAAGACAACCTTTTTAGAATCCTT	32	#f7931e
13[64]	38[64]	TTTAAATACGGATTGCCGGAAGCATTAGACTG	32	#33333 3
24[159]	3[159]	AACTCAAATGGCAGATATTCTGGCGCCCTAAA	32	#1700d e
33[144]	6[144]	ATGTGAGTACCTGAGCGATTGCCAGAAATAA	32	#aaaa0 0
20[143]	43[143]	GTCTCTGAGCCCCCTTCGCCACCCTCACCAGT	32	#aaaa0 0
40[159]	19[159]	GACATTCATACCATTAGATAGCAGTTGCCATC	32	#b8056 c
23[64]	47[79]	GAAAATCTCCAAAAAAAACAACCTGCAGGGAG	32	#b8056 c
28[159]	7[159]	AGTAACATAATGGAAGCGTAAAACCTGATTGCT	32	#cc000 0
32[63]	11[63]	GGTAGCTAGGAGACAGCTCATATAAATCGGTT	32	#f74308

44[159]	23[167]	GAACCTATGCCCCGGAACCGCCACCAGTTTCGTCACCAGTA	40	#57bb0 0
41[80]	14[80]	AGAAGTTTGGTAATAGATGACCATATAGTCAG	32	#88888 8
0[111]	24[96]	TTATAATCAAACCGTCCGCCGCTAGCAACAGG	32	#cc000 0
2[47]	25[47]	CAACAGCTGTTGTTCCGAATAGCCGCTGGCAA	32	#88888 8
15[96]	39[111]	AATCAGGTATAAAAACTAGCTATCTTACCAAC	32	#7300d e
30[159]	9[159]	TTTCAATTGAATAACCTTCCCTTAACCTCCGG	32	#7300d e
37[80]	10[80]	AATTCTACAGCATTAAAGACCCTGTGCAAGGAT	32	#1700d e
25[144]	1[159]	GTGCTTTCCTCGTTAGAAAGGGATTGTAGCAA	32	#f7931e
23[40]	47[47]	TGCGAATAATAGAAAGCGCATAAC	24	#f7931e
18[143]	41[143]	TCAGTAGCATAAGTTTAGGGAGGGAGGAAACC	32	#f7931e
31[80]	4[80]	CATTCGCCCCGCAACTGTTCCAGTCTTGCATG	32	#33333 3
22[143]	45[143]	CGCCACCCTTTAACGGAACATGAAAGGCAGGT	32	#57bb0 0

38[63]	17[63]	GATAGCGTAAAATAGCGGAATTACACGGAACA	32	#aaaa0 0
17[96]	41[111]	AGATTTAGAACATATATCATTAAAAAGTAAGC	32	#cc000 0
45[48]	18[48]	GAGATTTGTCAATCATAACAGATGATGCTCATT	32	#88888 8
40[95]	19[95]	ATCGAATTATTGTACCAAGAACCGACCTTCAT	32	#33333 3
42[63]	21[63]	GCAGACGGTATCATCGCTAAAACATTTTCATGA	32	#33333 3
5[160]	30[160]	TATTAAATTATTTGCAGGTTAGAAATTATTCA	32	#cc000 0
7[128]	32[128]	GGGAGAAAAGCGATAGGTACATAAAGAAAAC	32	#57bb0 0
10[111]	34[96]	GTAGGGCTAAGCCTTTAAATTTAAGCCTGTTT	32	#88888 8
2[143]	25[143]	ATAGAACCCACGCAAACCTTGCTGGCGTATAAC	32	#1700d e
13[96]	37[111]	AGTTTCATTTTCATCGTTGCACCCAGTCCTGA	32	#00720 0
9[128]	34[128]	TAGGTCTGCCAGTATATAAATAAGAATAAACA	32	#aaaa0 0

21[160]	46[160]	AACAGTGCGTTTAGTATAGGTGTACAGACAGC	32	#7300d e
26[159]	5[159]	AAAACAGATGGTCAGTGGTTATCTACAACCTCG	32	#aaaa0 0
11[128]	36[128]	AACGCCAAGCACTCATCCCATCCTCTTAAATC	32	#f74308
47[144]	20[144]	TAAGTATATATTCTGAGGTCAGTGAAAGCGCA	32	#f7931e
26[63]	5[63]	ATGAGTGATTATCCGCAGAGGATCATTAAAGTT	32	#f74308
27[144]	0[144]	ATTTACATCTATCGGCTTAACCGTTTTAGACA	32	#cc000 0
30[95]	9[95]	TAA CGCCAAGGAACAAACCCCGGTAAACTAG	32	#00720 0
6[47]	29[47]	TATCGGCCGATGTGCTTATTACGCTTCCTGTG	32	#cc000 0
31[144]	4[144]	TTCTGAATTATCATTTACAATTCGAAAATATC	32	#7300d e
20[111]	44[96]	ACATGGCTCGAAGGCAAACCACCAGATTAGGA	32	#88888 8
41[144]	14[144]	GAGGAACTTAAGCCACACCCTGTTGTTTAA	32	#aaaa0 0
39[80]	12[80]	CAGGTCAGTACCTTTAAAGTACGGTTCCCAAT	32	#b8056 c

15[128]	40[128]	CGGGAGAAGCAAACGTTTACCAGAAAGGTAAA	32	#57bb0 0
32[95]	11[95]	TGAGTTCTCAACCCCTATTTCAACAATACTTT	32	#cc000 0
35[48]	8[48]	GAAAGGCCTTTTTGAGGAGTCTGGTTGTATAA	32	#cc000 0
24[63]	3[63]	CCCTTATAGGTCCACGTCACCAGTGAAACCTG	32	#03b6a 2
3[128]	28[128]	TAGTCTTTCACTAACAAATATCAAAAAGAAAC	32	#88888 8
28[63]	7[63]	GTGCGGGCGGTGCCGGGAGGGGACCTCCGTGG	32	#33333 3
43[80]	16[80]	CTTTAATCACCTTATGAAAGATTCTAATGCAG	32	#7300d e
34[63]	13[63]	CAGGCAAGGGCGCGAGTTTAGTTTCAACATGT	32	#aaa0 0
7[96]	31[111]	GTCACGTTTACAGTAACAAAATTATGGCAATT	32	#33333 3
33[80]	6[80]	TAACCAATTCAAAAATGACCGTAATCGTAACC	32	#cc000 0
35[112]	8[112]	AATACCGATATATTTTGAATTTATAAGACGCT	32	#88888 8

47[112]	20[112]	CAGGCGGAGACTCCTCTACAGGAGAGCGTCAT	32	#1700d e
42[127]	21[127]	GCCACCCTCATTGACATTCCAGTATGTACTGG	32	#33333 3
25[48]	1[63]	GTGTAGCGGTACGCTAACGTGGCACAAGAGT	32	#b8056 c
37[144]	10[144]	AGCATGTAAGTCCAGTTAGGCAGGTTATACA	32	#57bb0 0
16[143]	39[143]	GTATGTTATTAAGTAAATAATAATAATTGTC	32	#03b6a 2
34[95]	13[95]	ATCGTAGTTAATAAACACAGTTGATGTCTGGA	32	#cc000 0
18[47]	41[47]	CAGTGAATTTAATAAAGGACGTTGGACGACGA	32	#b8056 c
45[112]	18[112]	GCCGCCAGCAGAGCCATTTTCATCCCTTAGC	32	#f7931e
47[80]	20[80]	TTAAAGGCGGATCGTCCGGTAAAAAACGAAA	32	#cc000 0
8[111]	32[96]	GAGAAGAGTCATATGTTTTTCATTTTCATCTTC	32	#88888 8
2[79]	25[79]	AGGGTGGTAAAGAACGCCGAAATCCCACCACA	32	#88888 8

44[63]	23[63]	GACAGCATTTCGGTCGCAACAGCTTTTCACGTT	32	#88888 8
22[79]	45[79]	CGAGGTGACCATTAAAACCCCTCAGATTGTGTC	32	#f7931e
24[127]	3[127]	AGAACAATACGCTCAACTGAAAGCATGGCTAT	32	#33333 3
19[160]	44[160]	TTTTCATAATTAAGCATATTCACCTATTTTCG	32	#88888 8
11[64]	36[64]	GTACCAAACGAGTAGACTGAAAAGTTTTGATA	32	#7300d e
26[95]	5[95]	CAAAGCATCCGGAATGGTGCCAAGCACGACGT	32	#f74308
21[128]	46[128]	TAATAAGTTCAGAACCGTCGAGAGAAGTTTTG	32	#33333 3
12[111]	36[96]	GTTTTTATTCCATATAAATAGATAAGCTACAA	32	#88888 8
42[95]	21[95]	CACTGCTCCGACCCAGCCAACCTAATACGTAA	32	#f7931e
20[79]	43[79]	GAGGCAAAGCGCATAGTTAGCCGGAATTTCAA	32	#f74308
40[63]	19[63]	CTCATTATGGGCTTCAAACAAGCACGGTGTA	32	#00720 0
15[160]	40[160]	CAGAGGGTATGATTAACCGGAATAAAAGGGC	32	#f7931e
5[64]	30[64]	GGGTAACGGCCAGTTTAAACCAGGTCTGGCCT	32	#cc000 0

41[48]	14[48]	TAAAAACCCCAATACTCTCAAATGGATTAAGA	32	#33333 3
4[111]	28[96]	CGTCAATAGACGGCCAAAAAATCTCATATTCC	32	#88888 8
7[64]	32[64]	GAACAAACCCCAAAAAAATCAGCCCGGAGAG	32	#b8056 c
9[64]	34[64]	AGAGAATCTTAGAACCTCAAATCAAATCATA	32	#f7931e
29[112]	2[112]	ACCTTGCTCAGTGCCAATTTTTGAGTAAGAAT	32	#aaaa0 0
31[48]	4[48]	CCGCTTCTCTCTTCGCGCAAGGCGCCCGGTA	32	#03b6a 2
43[48]	16[48]	AGTAAATTACCAGTCAACGAACTAGAGGCATA	32	#00720 0
21[96]	45[111]	TGCCACTATTTGATGAAAGAGAAGCCAGAGCC	32	#1700d e
26[127]	5[127]	GCCTGCAAGAACCTCAACTAATAGATTTAGAA	32	#33333 3
7[160]	32[160]	TTGAATACAATTAATTTTGCTTCTGATGCAAA	32	#00720 0
3[96]	27[111]	CGCGGGGACAGACAATCGCTGAGAAAATACCT	32	#33333 3

36[95]	15[95]	TTTGAGAGGATTATATTGACTATTAATCAAA	32	#00720 0
41[112]	14[112]	AGATAGCCAATAGCAAAGGGAAGCTTACAGAG	32	#33333 3
40[127]	19[127]	TATTGACGATTAGAGCCAAGTTTGGGCATTTT	32	#33333 3
43[112]	16[112]	ATTTGGGAGAAATTATAAAGAAACCATACATA	32	#f7931e
47[48]	20[48]	CGATATATCGGAACGAAAAGACTTCTCATCTT	32	#aaaa0 0
10[47]	33[47]	GCAATGCCTTGCCTGAAGATCTACTAAAATTC	32	#1700d e
34[127]	13[127]	ACATGTTCAATAATATCGAGAACAATTACCGC	32	#88888 8
6[143]	29[143]	AGAAATTGCTTTACAATGCGGAACACCCTCAA	32	#f74308
12[47]	35[47]	GATACATTTTCAGAGCATTAGCAAAAAGGGTGA	32	#03b6a 2
9[160]	34[160]	CTTAGGTTGTTTAGTAAATCATAAAAAAGGTA	32	#f7931e
45[144]	18[144]	CAGACGATCTCAGAGCATTAGCGTCACCGTAA	32	#88888 8
13[128]	38[128]	GCCCAATAATGAAAATCCAGAGCCGAGCAAGA	32	#00720 0

6[111]	30[96]	GATGAATAGGTGTAGATCAGATGAATTACATT	32	#88888 8
29[48]	2[48]	TGAAATTGGCTAACTCCCAGTCGGGAGACGGG	32	#b8056 c
14[47]	37[47]	GGAAGCCCATATAATGGATGGCTTCTATATTT	32	#aaaa0 0
30[127]	9[127]	ACAAACATTGGAAACACTTAGATTCAAATCA	32	#cc000 0
22[47]	45[47]	TAGTTGCGTGAGGACTGGGTAGCAGTACAACG	32	#1700d e
19[64]	44[64]	CAGACCAGAGAATACACCTGATAACAGCGAAA	32	#b8056 c
18[111]	42[96]	GTCAGACTATCTTGACGTCACCGAAGAGCCGC	32	#88888 8
42[159]	21[159]	CCGCCTCCTGGCCTTGCAGAATGGCCTTGAGT	32	#f7931e
13[160]	38[160]	TTATCCGGAATAAGAAAGCCATATACCCACAA	32	#00720 0
29[80]	2[80]	CATACGAGAAAGTGTAATGAATCTGGGCGCC	32	#88888 8
1[96]	25[111]	AGGGCGAAAGTGAGGCCAGCCATTCAGGGCGC	32	#aaaa0 0

17[64]	42[64]	ACATTATTATCAACGTGATGGTTTAACGAGGC	32	#7300d e
27[48]	0[40]	CAGCAAGCAATCAAAAAGTTTGGAGAGAAAGGAAGGGAA G	40	#aaaa0 0
17[128]	42[128]	ACCACGGAGACAGAATCAGCAAAATCAGAACC	32	#03b6a 2
34[159]	13[159]	AAGTAATTGAAACCAAAGAACGGGTAGAAGGC	32	#f74308
38[95]	17[95]	GCCGAGGGTGCCACTTCATTCAACATCAGTTG	32	#7300d e
20[47]	43[47]	TGACCCCCGAAAGAGGAAGGGAACGAACGAGT	32	#00720 0
14[111]	38[96]	AGAATAACCTTTACCCCCTGAATCTTACCGAA	32	#88888 8
39[112]	12[112]	GCTAACGATTGCTATTTAGGAATCAGCAAGCC	32	#33333 3
5[128]	30[128]	GTATTAGACGTAGATTATTGTTTGATGATGAA	32	#aaaa0 0
16[47]	39[47]	GTAAGAGCGAATCCCCGCGGAATCTTCGAGCT	32	#aaaa0 0
38[127]	17[127]	AACAATGAGAACAAAGAGAAAATAGCAAAGAC	32	#7300d e

2[111]	26[96]	ACGTGGCAGAGGCGGTGCTCATGGGCCAGCAG	32	#88888 8
36[63]	15[63]	AGAGGTCAAACCAGACATCAAAAACCTTTAAAC	32	#57bb0 0
3[64]	28[64]	TCGTGCCATCGACTCTTCACAATTGGCGATCG	32	#f7931e
16[79]	39[79]	ATACATAAAAACGAGATAAAAATGTAACCTCAA	32	#aaaa0 0
44[95]	23[95]	TTATTGCGCGCTTGCCTTATCAGAAAAGGAG	32	#f7931e
5[96]	29[111]	TGTA AACGATAATACATTATCATAAAGCATC	32	#03b6a 2
22[111]	46[96]	CCACCCTCTGTATCGGGGGTTTTGGAATTTTC	32	#57bb0 0
25[112]	1[127]	GTA CTATGGTTGCTTTATCCTGAGAAAAGAGT	32	#f74308
28[95]	7[95]	TGAGGCTGATTCATTATGGGCGCATGGGATAG	32	#b8056 c
36[127]	15[127]	AAGATTAGGCGTCTTTAGCAGCCTGCATTAGA	32	#f7931e
9[96]	33[111]	CATGTCAATCAATAGTAGTTAATTGAATTACC	32	#03b6a 2
25[80]	1[95]	CCCGCCGCGCTTAATGTATCATTTAACGTCAA	32	#f74308
36[159]	15[159]	CCGACTTGAAATAAACACGATTTTAACAAAGT	32	#33333 3

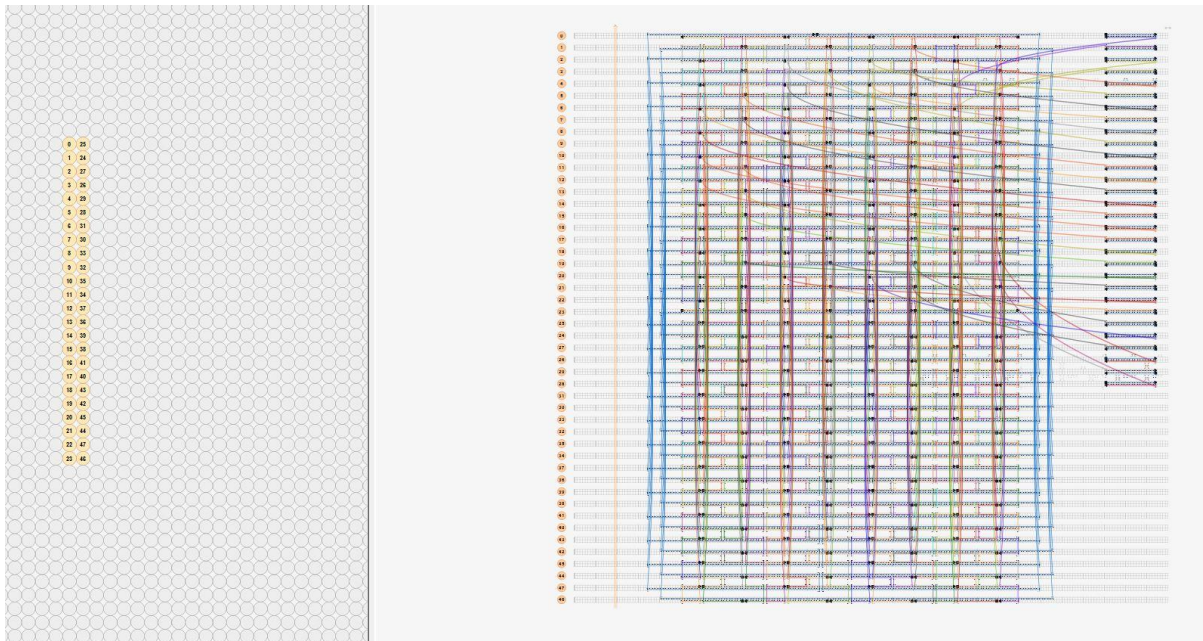
44[127]	23[127]	GAGGCTGATAAGTGCCGCCACCCTAGCCCAAT	32	#7300d e
27[80]	0[80]	GGCGAAAATGGTGGTTTGGACTCCAGAGCTTG	32	#88888 8
0[167]	24[160]	GGCCGATTAATCAGAGAGTAGAAG	24	#b8056 c
1[128]	26[128]	CTGTCCATCTTCTGACTCGTCTGATTAACACC	32	#f7931e
8[143]	31[143]	GAAAACATCAATAACGAAAAGAAGGATTATAC	32	#33333 3
33[112]	6[112]	TTTTTTAACAAGAAAACAGTACCTTAACGTCA	32	#1700d e
14[79]	37[79]	AAGCAAAGTGCAACTAATTGCTCCGTGGCATC	32	#33333 3
46[127]	22[112]	TCGTCTTTCCAGACGTGGATAGCACAGAGCCA	32	#f7931e
31[112]	4[112]	CATCAATAGGAGCGGAATTTGAGGATTAGAGC	32	#f7931e
11[96]	35[111]	TGCGGGAGTAATTGAGCAGAACGCTGGTTTGA	32	#f7931e
17[160]	42[160]	TAGAAAATAAACCATCGCAAGGCCACCGGAA	32	#1700d e
46[159]	22[144]	CCTCATAGTTAGCGTATAAACTGCTCAGAAC	32	#cc000 0
10[143]	33[143]	AATTCTTAAGAGACTAAGAACGCGATCAATAT	32	#7300d e

23[128]	47[143]	AGGAACCCATGTACCGACGATCTAGGTTGATA	32	#00720
				0
6[79]	29[79]	GTGCATCTCCAGGGTTTTGGGAAGCCACACAA	32	#57bb0
				0
39[144]	12[144]	CAGTTACACGGGAGGTATCAGATATATTTAAAC	32	#b8056
				c
12[143]	35[143]	CAAGTACCCATGTAATACGACGACGCGTTAAA	32	#f74308
15[64]	40[64]	AGTTCAGACGCCAAAAGAGAGGCTAGAACTGG	32	#b8056
				c
29[144]	2[144]	TCAATATCGGTGAGGCAACTGATACAACAGAG	32	#aaaa0
				0
8[47]	31[47]	GCAAATATAACAACCCCATCAACATTCCGGCA	32	#b8056
				c
11[160]	36[160]	TCGAGCCATCATTCCATCAATAATCGAACCTC	32	#00720
				0
14[143]	37[143]	CGTCAAAAGCAAGCAATTTGAAGCAATTTACG	32	#b8056
				c
16[111]	40[96]	AAGGTGGCGAATACCATTTAAGAAGGTGAATT	32	#88888
				8
4[143]	27[143]	TTTAGGAGAATGCGCGGGTCAGTAAATGGATT	32	#f7931e
12[79]	35[79]	TCTGCGAAAACATTATCATCCAATCCATCAAT	32	#1700d
				e

19[96]	43[111]	CAAGAGTAGTAGCGCGCCACCCTCCTTGAGCC	32	#1700d e
0[79]	24[64]	ACGGGGAAAGCCGGCGGCGGTAAGGCAAAT	32	#f74308
46[63]	22[48]	TTTCAGCGGAGTGAGAATAATTTTGATACCGA	32	#00720 0
4[47]	27[47]	CCGAGCTCCCCGCTTACATTAATGAGAGTTG	32	#03b6a 2
37[112]	10[112]	ACAAGAAAAGCTAATGAATCGCCAGCTCAACA	32	#7300d e
23[96]	47[111]	CCTTTAATATTTTCAGTAGTAAATCTCAGTAC	32	#1700d e
35[80]	8[80]	ATGATATTAGCTGATAGTAATCGTTGATAATC	32	#f7931e
0[143]	24[128]	GGAACGGTACGCCAGAGACGAGCATAATATCC	32	#cc000 0
30[63]	9[63]	TCCTGTAGTTTTTGTTTCAGGAAGAAGCAAACA	32	#88888 8
43[144]	16[144]	AGCACCATACCGATTGATTTTGTCATTACGCA	32	#cc000 0
1[64]	26[64]	CCACTATTTTTCTTTCTGGTTGGGTGCCTA	32	#aaaa0 0
33[48]	6[48]	GCATTAAACCAGCTTTGTCGGATTGACGACAG	32	#f7931e
39[48]	12[48]	TCAAAGCGTTTTGCGCTGTAGCTGACCATTA	32	#f74308

45[80]	18[80]	GAAATCCGCATGTTACGCTGGCTGGATATTCA	32	#88888 8
1[160]	26[160]	TACTTCTTAAAGGGACTCACCAGTCAGAAGAT	32	#f74308
10[79]	33[79]	AAAAATTTGATGAACGAATTAATGTCATTTTT	32	#00720 0
4[79]	27[79]	CCTGCAGGGCTGCATTAAGCCTGGCCCCAGCA	32	#7300d e
32[127]	11[127]	TTTTCAAACCGTGTGAAAGCCAACACTATTTAAC	32	#1700d e
37[48]	10[48]	TCATTTGGGCAAAGAATAAAGCTATTTTAAAT	32	#f74308
8[79]	31[79]	AGAAAAGCGGCGGATTAATTCGCGCAAAGCGC	32	#7300d e
32[159]	11[159]	TCCAATCGAACACCGGTCATATGCAGGCATTT	32	#03b6a 2
18[79]	41[79]	TTACCCAAACAGGTAGCGATTTTATTTGCAAA	32	#aaaa0 0
28[127]	7[127]	CACCAGAATAATCCTGTTTCAGGTTTTTACATC	32	#aaaa0 0
27[112]	0[112]	ACATTTTGATTACCGCCACCGAGTAAGTGTTT	32	#88888 8

## Design – Board with resonator complementary binding sites



Start	End	Sequence	Length	Color
19[12 8]	44[12 8]	CGGTCATAATTACCGGGAGGTTGAGTATTAA	32	#f7430
21[64 ]	46[64]	GGAAGTTTATTTCTTATGAGGCTTTCAACAG	32	#007200
31[14 4]	1[219]	TTCTGAATTATCATTTACAATTCGAAAATATCAAAAAAAAAAAAAA AAAAAA	52	#7300de
33[14 4]	3[219]	ATGTGAGTACCTGAGCGATTGCCAGAAATAAAAAAAAAAAAAA AAAAAAA	52	#aaaa00

3[160	28[16	ACATCGCCTTGAGGAATGGCAAATAAAGTTTG	32	#f7430
]	0]			8
46[95	22[80]	TGTATGGGATTTTGCTAAGGCTCCCTTGCTTT	32	#aaaa0
]				0
35[14	8[144]	TAAGAATACAAGACAACCTTTTTAGAATCCTT	32	#f7931
4]				e
13[64	38[64]	TTTAAATACGGATTGCCGGAAGCATTAGACTG	32	#3333
]				33
20[14	43[14	GTCTCTGAGCCCCCTTCGCCACCCTCACCAGT	32	#aaaa0
3]	3]			0
32[63	16[20	GGTAGCTAGGAGACAGCTCATATAAATCGGTTAAAAAAAAAAAAA	52	#f7430
]	0]	AAAAAAAAA		8
23[64	47[79]	GAAAATCTCCAAAAAAAAAACAACCTGCAGGGAG	32	#b805
]				6c
28[15	7[159]	AGTAACATAATGGAAGCGTAAAACCTGATTGCT	32	#cc000
9]				0
29[11	5[219]	ACCTTGCTCAGTGCCAATTTTTGAGTAAGAATAAAAAAAAAAAAAA	52	#aaaa0
2]		AAAAAAAAA		0
44[15	23[16	GAACCTATGCCCGGAACCGCCACCAGTTTCGTCACCAGTA	40	#57bb
9]	7]			00
41[80	14[80]	AGAAGTTTGGTAATAGATGACCATATAGTCAG	32	#8888
]				88

0[111	24[96]	TTATAATCAAACCGTCCGCCGCTAGCAACAGG	32	#cc000
]				0
2[47]	25[47]	CAACAGCTGTTGTTCCGAATAGCCGCTGGCAA	32	#8888
				88
15[96	39[11	AATCAGGTATAAAAAGCTATCTTACCAAC	32	#7300
]	1]			de
30[15	9[159]	TTTCAATTGAATAACCTTCCCTTAACCTCCGG	32	#7300
9]				de
37[80	10[80]	AATTCTACAGCATTAAAGACCCTGTGCAAGGAT	32	#1700
]				de
25[14	1[159]	GTGCTTTCCTCGTTAGAAAGGGATTGTAGCAA	32	#f7931
4]				e
23[40	47[47]	TGCGAATAATAGAAAGCGCATAAC	24	#f7931
]				e
18[14	41[14	TCAGTAGCATAAGTTTAGGGAGGGAGGAAACC	32	#f7931
3]	3]			e
24[95	9[219]	AAATTTGATCCTGAACTTGCATATGGCCAACGAAAAAAAAAAAAA	52	#aaaa0
]		AAAAAAA		0
22[14	45[14	CGCCACCCTTTAACGGAACATGAAAGGCAGGT	32	#57bb
3]	3]			00
26[63	11[21	ATGAGTGATTATCCGCAGAGGATCATTAAAGTTAAAAAAAAAAAAA	52	#f7430
]	9]	AAAAAAA		8

38[63	17[63]	GATAGCGTAAAATAGCGGAATTACACGGAACA	32	#aaaa0
]				0
17[96	41[11	AGATTTAGAACATATATCATTAAAAAGTAAGC	32	#cc000
]	1]			0
45[48	18[48]	GAGATTTGTCAATCATACAGATGATGCTCATT	32	#8888
]				88
31[11	7[219]	CATCAATAGGAGCGGAATTTGAGGATTAGAGCAAAAAAAAAAAAA	52	#f7931
2]		AAAAAAA		e
31[80	10[20	CATTCGCCC GCAACTGTTCCAGTCTTG CATGAAAAAAAAAAAA	52	#3333
]	0]	AAAAAAA		33
42[63	21[63]	GCAGACGGTATCATCGCTAAACATTT CATGA	32	#3333
]				33
40[15	28[20	GACATTCATACCATTAGATAGCAGTTGCCATCAAAAAAAAAAAAA	52	#b805
9]	0]	AAAAAAA		6c
33[48	12[20	GCATTA AACAGCTTTGTCGGATTGACGACAGAAAAAAAAAAAA	52	#f7931
]	0]	AAAAAAA		e
5[160	30[16	TATTA AATTATTTGCAGGTTAGAAATTATTCA	32	#cc000
]	0]			0
7[128	32[12	GGGAGAAAAGCGATAGGTACATAAAGAAA ACT	32	#57bb
]	8]			00
10[11	34[96]	GTAGGGCTAAGCCTTTAAATTTAAGCCTGTTT	32	#8888
1]				88

2[143	25[14	ATAGAACCCACGCAAACCTTGCTGGCGTATAAC	32	#1700
]	3]			de
13[96	37[11	AGTTTCATTTTCATCGTTGCACCCAGTCCTGA	32	#0072
]	1]			00
47[11	24[20	CAGGCGGAGACTCCTCTACAGGAGAGCGTCATAAAAAAAAAAAAA	52	#1700
2]	0]	AAAAAAAAA		de
9[128	34[12	TAGGTCTGCCAGTATATAAATAAGAATAAACA	32	#aaaa0
]	8]			0
21[16	46[16	AACAGTGCGTTTAGTATAGGTGTACAGACAGC	32	#7300
0]	0]			de
35[48	14[20	GAAAGGCCTTTTTGAGGAGTCTGGTTGTATAAAAAAAAAAAAAAA	52	#cc000
]	0]	AAAAAAAAA		0
11[12	36[12	AACGCCAAGCACTCATCCCATCCTCTTAAATC	32	#f7430
8]	8]			8
47[14	20[14	TAAGTATATATTCTGAGGTCAGTGAAAGCGCA	32	#f7931
4]	4]			e
27[14	0[144]	ATTTACATCTATCGGCTTAACCGTTTTAGACA	32	#cc000
4]				0
30[95	9[95]	TAACGCCAAGGAACAAACCCCGTAAACTAG	32	#0072
]				00
6[47]	29[47]	TATCGGCCGATGTGCTTATTACGCTTCCTGTG	32	#cc000
				0

20[11	44[96]	ACATGGCTCGAAGGCAAACCACCAGATTAGGA	32	#8888
1]				88
41[14	14[14]	GAGGAACTTAAGCCCACACCCTGTTGTTAA	32	#aaaa0
4]	4]			0
39[80	12[80]	CAGGTCAGTACCTTTAAAGTACGGTTCCAAT	32	#b805
]				6c
15[12	40[12]	CGGGAGAAGCAAACGTTTACCAGAAAGGTAAA	32	#57bb
8]	8]			00
32[95	11[95]	TGAGTTCTCAACCCCTATTTCAACAATACTTT	32	#cc000
]				0
24[63	3[63]	CCCTTATAGGTCCACGTCACCAGTGAAACCTG	32	#03b6
]				a2
3[128	28[12]	TAGTCTTTCACCTAACAAATATCAAAAAGAAAC	32	#8888
]	8]			88
45[14	29[21]	CAGACGATCTCAGAGCATTAGCGTCACCGTAAAAAAAAAAAAAAAA	52	#8888
4]	9]	AAAAAAAAA		88
43[80	16[80]	CTTTAATCACCTTATGAAAGATTCTAATGCAG	32	#7300
]				de
7[96]	31[11]	GTCACGTTTACAGTAACAAAATTATGGCAATT	32	#3333
	1]			33
33[80	6[80]	TAACCAATTCAAAAATGACCGTAATCGTAACC	32	#cc000
]				0

35[11	8[112]	AATACCGATATATTTTGAATTTATAAGACGCT	32	#8888
2]				88
40[95	21[21	ATCGAATTATTGTACCAAGAACCGACCTTCATAAAAAAAAAAAAAA	52	#3333
]	9]	AAAAAAA		33
25[48	1[63]	GTGTAGCGGTCACGCTAACGTGGCACAAGAGT	32	#b805
]				6c
37[14	10[14	AGCATGTAAGTCCAGTTAGGCAGGTTATACA	32	#57bb
4]	4]			00
16[14	39[14	GTATGTTATTAAGTAAATAATAATAATTGC	32	#03b6
3]	3]			a2
34[95	13[95]	ATCGTAGTTAATAAACACAGTTGATGTCTGGA	32	#cc000
]				0
18[47	41[47]	CAGTGAATTAATAAAGGACGTTGGACGACGA	32	#b805
]				6c
45[11	18[11	GCCGCCAGCAGAGCCATTTTCATCCCTTAGC	32	#f7931
2]	2]			e
8[111	32[96]	GAGAAGAGTCATATGTTTTCATTTTCATCTTC	32	#8888
]				88
2[79]	25[79]	AGGGTGGTAAAGAACGCCGAAATCCCACCACA	32	#8888
				88
42[95	23[21	CACTGCTCCGACCCAGCCAACCTAATACGTAAAAAAAAAAAAAAAAA	52	#f7931
]	9]	AAAAAAA		e

44[63	23[63]	GACAGCATTTCGGTCGCAACAGCTTTTCACGTT	32	#8888
]				88
22[79	45[79]	CGAGGTGACCATTAAAACCTCAGATTGTGTC	32	#f7931
]				e
19[16	44[16	TTTTATAATTAAGCATATTCACCTATTTTCG	32	#8888
0]	0]			88
11[64	36[64]	GTACCAAACGAGTAGACTGAAAAGTTTTGATA	32	#7300
]				de
26[95	5[95]	CAAAGCATCCGGAATGGTGCCAAGCACGACGT	32	#f7430
]				8
21[12	46[12	TAATAAGTTCAGAACCGTCGAGAGAAGTTTTG	32	#3333
8]	8]			33
12[11	36[96]	GTTTTATTCCATATAAATAGATAAGCTACAA	32	#8888
1]				88
20[79	43[79]	GAGGCAAAGCGCATAGTTAGCCGGAATTTCAA	32	#f7430
]				8
15[16	40[16	CAGAGGGTATGATTAACCGGAATAAAAGGGC	32	#f7931
0]	0]			e
40[12	25[21	TATTGACGATTAGAGCCAAGTTTGGGCATTTTAAAAAAAAAAAAA	52	#3333
7]	9]	AAAAAAA		33
5[64]	30[64]	GGGTAACGGCCAGTTTAAACCAGGTCTGGCCT	32	#cc000
				0

41[48	14[48]	TAAAAACCCCAATACTCTCAAATGGATTAAGA	32	#3333
]				33
4[111	28[96]	CGTCAATAGACGGCCAAAAAATCTCATATTCC	32	#8888
]				88
25[11	4[200]	GTA	52	#f7430
2]		ACTATGGTTGCTTTATCCTGAGAAAAGAGTAAAAAAAAAAAAA AAAAAAA		8
7[64]	32[64]	GAACAAACCCCAAAAAAATCAGCCCGGAGAG	32	#b805
				6c
9[64]	34[64]	AGAGAATCTTAGAACCTCAAATCAAATCATA	32	#f7931
				e
42[12	27[21]	GCCACCCTCATTGACATTCCAGTATGTACTGGAAAAAAAAAAAAA	52	#3333
7]	9]	AAAAAAA		33
28[63	13[21]	GTGCGGGCGGTGCCGGGAGGGGACCTCCGTGGAAAAAAAAAAAAA	52	#3333
]	9]	AAAAAAA		33
31[48	4[48]	CCGCTTCTCTTTCGCGCAAGGCGCCCGGTA	32	#03b6
]				a2
43[48	16[48]	AGTAAATTACCAGTCAACGAACTAGAGGCATA	32	#0072
]				00
21[96	45[11]	TGCCACTATTTGATGAAAGAGAAGCCAGAGCC	32	#1700
]	1]			de
26[12	5[127]	GCCTGCAAGAACCTCAACTAATAGATTTAGAA	32	#3333
7]				33

7[160 ]	32[16 0]	TTGAATACAATTAATTTTGCTTCTGATGCAAA	32	#0072 00
3[96]	27[11 1]	CGCGGGGACAGACAATCGCTGAGAAAATACCT	32	#3333 33
36[95 ]	15[95]	TTTGAGAGGATTATATTGACTATTAATCAAA	32	#0072 00
41[11 2]	14[11 2]	AGATAGCCAATAGCAAAGGGAAGCTTACAGAG	32	#3333 33
43[11 2]	16[11 2]	ATTTGGGAGAAATTATAAAGAAACCATACATA	32	#f7931 e
47[48 ]	20[48]	CGATATATCGGAACGAAAAGACTTCTCATCTT	32	#aaaa0 0
10[47 ]	33[47]	GCAATGCCTTGCCTGAAGATCTACTAAAATTC	32	#1700 de
34[12 7]	13[12 7]	ACATGTTCAATAATATCGAGAACAATTACCGC	32	#8888 88
6[143 ]	29[14 3]	AGAAATTGCTTTACAATGCGGAACACCCTCAA	32	#f7430 8
12[47 ]	35[47]	GATACATTTTCAGAGCATTAGCAAAAAGGGTGA	32	#03b6 a2
9[160 ]	34[16 0]	CTTAGGTTGTTTAGTAAATCATAAAAAAGGTA	32	#f7931 e

13[12	38[12	GCCCAATAATGAAAATCCAGAGCCGAGCAAGA	32	#0072
8]	8]			00
6[111	30[96]	GATGAATAGGTGTAGATCAGATGAATTACATT	32	#8888
]				88
29[48	2[48]	TGAAATTGGCTAACTCCCAGTCGGGAGACGGG	32	#b805
]				6c
14[47	37[47]	GGAAGCCCATATAATGGATGGCTTCTATATTT	32	#aaaa0
]				0
30[12	9[127]	ACAAACATTGGAAACACTTAGATTCAAATCA	32	#cc000
7]				0
22[47	45[47]	TAGTTGCGTGAGGACTGGGTAGCAGTACAACG	32	#1700
]				de
19[64	44[64]	CAGACCAGAGAATACACCTGATAACAGCGAAA	32	#b805
]				6c
18[11	42[96]	GTCAGACTATCTTGACGTCACCGAAGAGCCGC	32	#8888
1]				88
42[15	21[15]	CCGCCTCCTGGCCTTGCAGAATGGCCTTGAGT	32	#f7931
9]	9]			e
13[16	38[16]	TTATCCGGAATAAGAAAGCCATATACCCACAA	32	#0072
0]	0]			00
1[96]	25[11]	AGGGCGAAAGTGAGGCCAGCCATTCAGGGCGC	32	#aaaa0
	1]			0

17[64	42[64]	ACATTATTATCAACGTGATGGTTTAACGAGGC	32	#7300
]				de
27[48	0[40]	CAGCAAGCAATCAAAAAGTTTGGAGAGAAAGGAAGGGAAG	40	#aaaa0
]				0
17[12	42[12	ACCACGGAGACAGAATCAGCAAATCAGAACC	32	#03b6
8]	8]			a2
34[15	13[15	AAGTAATTGAAACCAAAGAACGGGTAGAAGGC	32	#f7430
9]	9]			8
38[95	17[95]	GCCGAGGGTGCCACTTCATTCAACATCAGTTG	32	#7300
]				de
20[47	43[47]	TGACCCCCGAAAGAGGAAGGGAACGAACGAGT	32	#0072
]				00
14[11	38[96]	AGAATAACCTTTACCCCTGAATCTTACCGAA	32	#8888
1]				88
39[11	12[11	GCTAACGATTGCTATTTAGGAATCAGCAAGCC	32	#3333
2]	2]			33
5[128	30[12	GTATTAGACGTAGATTATTGTTTGATGATGAA	32	#aaaa0
]	8]			0
16[47	39[47]	GTAAGAGCGAATCCCCGCGGAATCTTCGAGCT	32	#aaaa0
]				0
38[12	17[12	AACAATGAGAACAAAGAGAAAATAGCAAAGAC	32	#7300
7]	7]			de

2[111	26[96]	ACGTGGCAGAGGCGGTGCTCATGGGCCAGCAG	32	#8888
]				88
3[64]	28[64]	TCGTGCCATCGACTCTTCACAATTGGCGATCG	32	#f7931
				e
47[80	22[20	TTAAAGGCGGATCGTCCGGTAAAAACGAAAAAAAAAAAAAA	52	#cc000
]	0]	AAAAAAA		0
16[79	39[79]	ATACATAAAAACGAGATAAAATGTAECTCAA	32	#aaaa0
]				0
44[95	23[95]	TTATTGCGCGCTTGCCTTATCAGAAAAGGAG	32	#f7931
]				e
26[15	2[200]	AAAACAGATGGTCAGTGGTTATCTACAACGAAAAAAAAAAAAAA	52	#aaaa0
9]		AAAAAAA		0
5[96]	29[11	TGTAAAACGATAATACATTATCATAAAGCATC	32	#03b6
	1]			a2
22[11	46[96]	CCACCTCTGTATCGGGGGTTTTGGAATTTTC	32	#57bb
1]				00
28[95	7[95]	TGAGGCTGATTCATTATGGGCGCATGGGATAG	32	#b805
]				6c
36[12	15[12	AAGATTAGGCGTCTTTAGCAGCCTGCATTAGA	32	#f7931
7]	7]			e
9[96]	33[11	CATGTCAATCAATAGTAGTTAATTGAATTACC	32	#03b6
	1]			a2

25[80	1[95]	CCCGCCGCGCTTAATGTATCATTTAACGTCAA	32	#f7430
]				8
37[48	15[21	TCATTTGGGCAAAGAATAAAGCTATTTTAAATAAAAAAAAAAAAAA	52	#f7430
]	9]	AAAAAAA		8
36[15	15[15	CCGACTTGAAATAAACACGATTTTAACAAAGT	32	#3333
9]	9]			33
44[12	23[12	GAGGCTGATAAGTGCCGCCACCCTAGCCCAAT	32	#7300
7]	7]			de
27[80	0[80]	GGCGAAAATGGTGGTTTGGACTCCAGAGCTTG	32	#8888
]				88
0[167	24[16	GGCCGATTAATCAGAGAGTAGAAG	24	#b805
]	0]			6c
39[48	17[21	TCAAAGCGTTTTTTCGCTGTAGCTGACCATTAATAAAAAAAAAAAAAA	52	#f7430
]	9]	AAAAAAA		8
1[128	26[12	CTGTCCATCTTCTGACTCGTCTGATTAACACC	32	#f7931
]	8]			e
8[143	31[14	GAAAACATCAATAACGAAAAGAAGGATTATAC	32	#3333
]	3]			33
33[11	6[112]	TTTTTTAACAAGAAAACAGTACCTTAACGTCA	32	#1700
2]				de
14[79	37[79]	AAGCAAAGTGCAACTAATTGCTCCGTGGCATC	32	#3333
]				33

46[12 7]	22[11 2]	TCGTCTTTCCAGACGTGGATAGCACAGAGCCA	32	#f7931 e
24[15 9]	0[200]	AACTCAAATGGCAGATATTCTGGCGCCCTAAAAAAAAAAAAAAAAAA AAAAAAA	52	#1700 de
11[96 ]	35[11 1]	TGCGGGAGTAATTGAGCAGAACGCTGGTTTGA	32	#f7931 e
17[16 0]	42[16 0]	TAGAAAATAAACCATCGCAAGGCCACCGGAA	32	#1700 de
46[15 9]	22[14 4]	CCTCATAGTTAGCGTATAAACTGCTCAGAAC	32	#cc000 0
10[14 3]	33[14 3]	AATTCTTAAGAGACTAAGAACGCGATCAATAT	32	#7300 de
38[15 9]	26[20 0]	GAATTGAGGCAATAATGACTCCTTACAATCAAAAAAAAAAAAAAAAAA AAAAAAA	52	#cc000 0
40[63 ]	20[20 0]	CTCATTATGGGCTTGAAACAAAGCACGGTGTAAAAAAAAAAAAAAAAAA AAAAAAA	52	#0072 00
23[12 8]	47[14 3]	AGGAACCCATGTACCGACGATCTAGGTTGATA	32	#0072 00
6[79]	29[79]	GTGCATCTCCAGGGTTTTGGGAAGCCACACAA	32	#57bb 00
39[14 4]	12[14 4]	CAGTTACACGGGAGGTATCAGATATATTAAC	32	#b805 6c

12[14	35[14	CAAGTACCCATGTAATACGACGACGCGTTAAA	32	#f7430
3]	3]			8
15[64	40[64]	AGTTCAGACGCCAAAAGAGAGGCTAGAACTGG	32	#b805
]				6c
29[14	2[144]	TCAATATCGGTGAGGCAACTGATACAACAGAG	32	#aaaa0
4]				0
8[47]	31[47]	GCAAATATAACAACCCCATCAACATTCCGGCA	32	#b805
				6c
11[16	36[16	TCGAGCCATCATTCCATCAATAATCGAACCTC	32	#0072
0]	0]			00
14[14	37[14	CGTCAAAGCAAGCAATTTGAAGCAATTTACG	32	#b805
3]	3]			6c
34[63	18[20	CAGGCAAGGGCGCGAGTTTAGTTTCAACATGTAAAAAAAAAAAAA	52	#aaaa0
]	0]	AAAAAAAAA		0
16[11	40[96]	AAGGTGGCGAATACCATTTAAGAAGGTGAATT	32	#8888
1]				88
4[143	27[14	TTTAGGAGAATGCGCGGGTCAGTAAATGGATT	32	#f7931
]	3]			e
12[79	35[79]	TCTGCGAAAACATTATCATCCAATCCATCAAT	32	#1700
]				de
19[96	43[11	CAAGAGTAGTAGCGCGCCACCCTCCTTGAGCC	32	#1700
]	1]			de

0[79]	24[64]	ACGGGGAAAGCCGGCGGCGCGTAAGGCAAAT	32	#f7430
				8
46[63]	22[48]	TTTCAGCGGAGTGAGAATAATTTTGATACCGA	32	#0072
]				00
29[80]	8[200]	CATACGAGAAAGTGTAATGAATCTGGGCGCCAAAAAAAAAAAA	52	#8888
]		AAAAAAA		88
4[47]	27[47]	CCGAGCTCCCCGCTTACATTAATGAGAGTTG	32	#03b6
				a2
37[11]	10[11]	ACAAGAAAAGCTAATGAATCGCCAGCTCAACA	32	#7300
2]	2]			de
23[96]	47[11]	CCTTTAATATTTTCAGTAGTAAATCTCAGTAC	32	#1700
]	1]			de
35[80]	8[80]	ATGATATTAGCTGATAGTAATCGTTGATAATC	32	#f7931
]				e
0[143]	24[12]	GGAACGGTACGCCAGAGACGAGCATAATATCC	32	#cc000
]	8]			0
30[63]	9[63]	TCCTGTAGTTTTTGTTGAGGAAGAAGCAAACA	32	#8888
]				88
24[12]	6[200]	AGAACAATACGCTCAACTGAAAGCATGGCTATAAAAAAAAAAAAA	52	#3333
7]		AAAAAAA		33
43[14]	16[14]	AGCACCATACCGATTGATTTTGTCATTACGCA	32	#cc000
4]	4]			0

1[64]	26[64]	CCACTATTTTTCTTTCTGGTTGGGTGCCTA	32	#aaaa0 0
36[63]	19[21]	AGAGGTCAAACCAGACATCAAAAACCTTAAACAAAAAAAAAAAA	52	#57bb
]	9]	AAAAAAAAA		00
45[80]	18[80]	GAAATCCGCATGTTACGCTGGCTGGATATTCA	32	#8888
]				88
1[160]	26[16]	TACTTCTTAAAGGGACTCACCAGTCAGAAGAT	32	#f7430
]	0]			8
10[79]	33[79]	AAAAATTTGATGAACGAATTAATGTCATTTTT	32	#0072
]				00
4[79]	27[79]	CCTGCAGGGCTGCATTAAGCCTGGCCCCAGCA	32	#7300
				de
32[12]	11[12]	TTTTCAAACCGTGTGAAAGCCAACACTATTTAAC	32	#1700
7]	7]			de
8[79]	31[79]	AGAAAAGCGGCGGATTAATTCGCGCAAAGCGC	32	#7300
				de
32[15]	11[15]	TCCAATCGAACACCGGTCATATGCAGGCATTT	32	#03b6
9]	9]			a2
18[79]	41[79]	TTACCCAAACAGGTAGCGATTTTATTTGCAAA	32	#aaaa0
]				0
28[12]	7[127]	CACCAGAATAATCCTGTTTCAGGTTTTTACATC	32	#aaaa0
7]				0

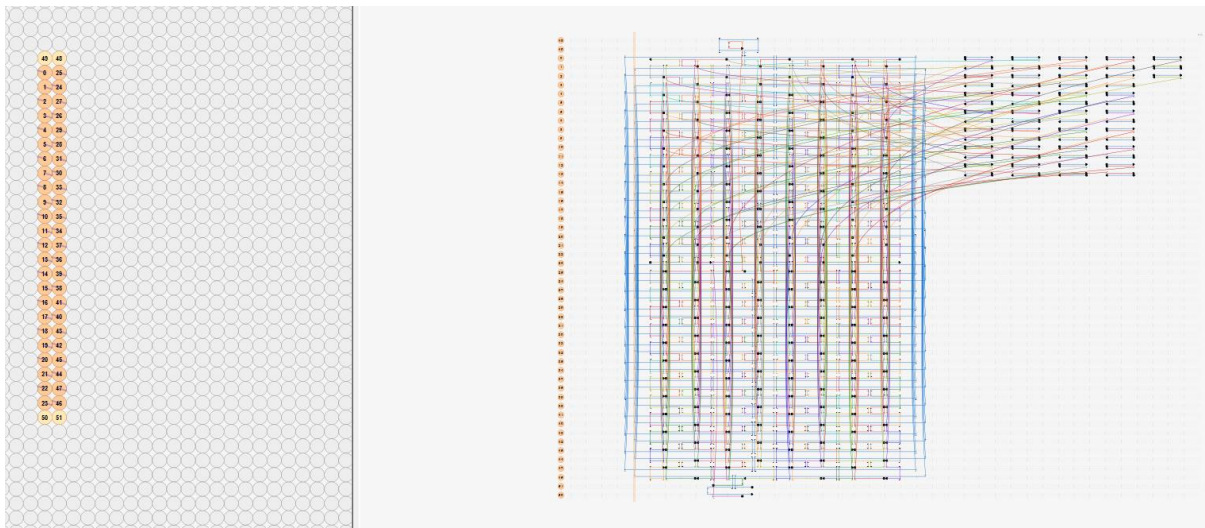
27[11 0[112] ACATTTTGATTACCGCCACCGAGTAAGTGTTT

32 #8888

2]

88

### Design – Square lattice resonator



This board has a much higher tether number than the previous resonator board. The sequences saturate the edge of the design allowing reduction, rather than addition, to be the guiding force in tailoring nanoparticle binding number.

Start	End	Sequence	Length	Color
21[64]	46[64]	GTCTGTCCGCGTAACCTTTCCTCGGCCGTAAA	32	#007200
39[112]	12[112]	AAATGGTCATTCTGCGGATAAGAGAGAGTACC	32	#333333
2[143]	25[143]	ACCGTACTATGGCTTTTTAATGCCCCACCACC	32	#1700de
38[63]	6[248]	ATTATCATATTAATTTGGATTTAGTTGAAAGGAAAAAAAAAAAAAAAAA	47	#aaaa00
5[64]	30[64]	AGAGAATACGGGAGGTACGAGCGTAGTACCGC	32	#cc0000
5[128]	30[128]	TTTATCAGACTACGAAACGAGGGTTGTTACTT	32	#aaaa00

16[143] 39[143]	GTCATTGCGTACCAAACATATATTATATTTTC	32	#03b6a2	
11[128] 36[128]	CCAGAGGGAACAGGTCATCAAAAATAACAGTT	32	#f74308	
43[112] 16[112]	AATTCGCGTGTTAAATTCGTAAAAACAAGAG	32	#f7931e	
43[144] 13[286]	CATCAACATTAATATTCGGTTGATGCTATCAGAAAAAAAAAAAAAAAAA47			#cc0000
18[79] 41[79]	CTGATAGCAAGGTTATCTAAAGCATGAGTAAC	32	#aaaa00	
25[112] 10[200]	CCACCCTCAGAGCCGCTAAAGCCACCAGTAAGAAAAAAAAAAAAAAAAA			47
	#f74308			
9[96] 33[111]	CCAGACGACCCTGACGAAACGAACCCAACCTTT	32	#03b6a2	
33[48] 9[238]	AGCATGTAAGAACAAGTACCGCGCCTTAAATCAAAAAAAAAAAAAAAAAA			47
	#f7931e			
18[143] 41[143]	GACCGTAAATGTACCCTTGTTAAATCAACCG	32	#f7931e	
11[64] 36[64]	AGAAAACCTCTGTAAATCAATAGTTTCATTTTC	32	#7300de	
3[160] 28[160]	CCCAATAGGAACAACCTTTTCAGCGCAACAACC	32	#f74308	
33[112] 6[112]	GAAAGAGGCGAGGCGCTACACTAACCTAAAAC	32	#1700de	
43[80] 16[80]	CTGAGAGCTGAAAAATCTAAAATAGCCGTCAA	32	#7300de	
6[79] 29[79]	CCGACTTGACATAAAAACAGCCATTCTTACCG	32	#57bb00	
17[96] 41[111]	AGCACTAAAACGGTAACAGCTCATCCGGAGAC	32	#cc0000	
11[160] 36[160]	GATAGCGTCTTCAAAGTCAAATATTAAGTAC	32	#007200	
47[112] 4[272]	GCTGCATTGTTGCGCTCGTAATCGATCCCCGAAAAAAAAAAAAAAAAA			47
	#1700de			
1[296] 1[310]	AAAAAAAAAAAAAAAAA	15	#aaaa00	

38[159] 12[272] AAATTTTTGATAAATTCTACAAAGAATCAGAAAAAAAAAAAAAAAAAAAA 47  
#cc0000

40[159] 10[272] TGTAACGTTAAATGTGAACAACTCAGGAAGAAAAAAAAAAAAAAAAAAAA 47  
#b8056c

10[47] 33[47] AGAATAAATTTTCGAGCAACATGTAAATTTACG 32 #1700de

51[72] 13[262] TCAAGTTTTTTCCGTCAAAAAGGGGAAGAAAGGTAGCGGTAAAAAAAAAAAAAAAAAAAA 55  
#007200

37[112] 10[112] AAGCAAAGGACCATAATGCAAAAGAAAACCAA 32 #7300de

15[160] 40[160] AATACTTTTGAGAGATAATGCCGGATTTAAAT 32 #f7931e

17[160] 42[160] AAGCCCCACTCCGTGGGAGCGAGTGGTGCCGG 32 #1700de

46[63] 11[262] GCACTAAATCGGAACCGGAAAGCCCGCCGCGCAAAAAAAAAAAAAAAAAAAAA 47  
#007200

44[159] 23[167] GCCTGGGGTTGCGTATGAGACGGGGGTTCCGAAATCGGCA 40 #57bb00

20[47] 43[47] CTGGTAATACAGAGATGTAATAAATGAGGCGG 32 #007200

0[79] 24[64] TTTTCATCGGCATTTTCCGCCTCTAAAGGTG 32 #f74308

2[79] 25[79] AGAAACGCTAGCAAGTTATTCATCTCAGAGC 32 #888888

36[127] 15[127] GATTCCCAAATAACCTGCAAAGAATAAAGCTA 32 #f7931e

5[160] 30[160] AACAGCTTGTTCATGACTAAAGATAAATTG 32 #cc0000

35[48] 11[238] AGTATCATACAACGCCAGTAATAACAATAGAAAAAAAAAAAAAAAAAAAA 47  
#cc0000

35[144] 1[214] CAACTAATATACCAGTGAGATGGTTTACCCAAAAAAAAAAAAAAAAAAAA 47  
#f7931e

18[111]	42[96]	TGGGCGCAGGCTATTAGAACGCCACGGTGCGG	32	#888888	
27[80]	2[224]	GGAGGGAAGACGGAAACCGGAAACGTAGCGCGAAAAAAAAAAAAAAAA			47
		#888888			
13[96]	37[111]	CAGTACATCTCCTTTTAACGAGTAATAGTCAG	32	#007200	
40[63]	8[248]	CTGAACCTAACACCGCATCGCCATTCTGACCTAAAAAAAAAAAAAAAAA47			#007200
44[95]	2[272]	AGTAACAGAGCTACGGTGGCAAGTCGAAAGGAAAAAAAAAAAAAAAA			47
		#f7931e			
27[112]	13[214]	AAGAGAAGACCTATTATTACCGTTGAATGGAAAAAAAAAAAAAAAA			47
		#888888			
31[144]	5[214]	CTACAGAGCGCATAACCGAGGTGATGCGAATAAAAAAAAAAAAAAAAA			47
		#7300de			
24[159]	6[200]	GTGCCCGTGGCGGATACCGGAATAATAGCAAGAAAAAAAAAAAAAAAA			47
		#1700de			
24[63]	5[238]	AATTATCAAAGGGCGACACGGAATGATTAAGAAAAAAAAAAAAAAAA			47
		#03b6a2			
28[127]	7[127]	TGAGGCTTGCATCGGAGGCACCAAAACTCA	32	#aaaa00	
32[95]	11[95]	CAACTCAACAACGCATATTTAATGAGTTAATT	32	#cc0000	
37[80]	10[80]	CAAAATCAAGACTACCTATATTTGTTTGAAA	32	#1700de	
7[160]	32[160]	AACAAAGTAAGAACCGACCTTCATTAAGAACT	32	#007200	
6[111]	30[96]	GAAAGAGGACGCGAGGCGTCACCCAATCATAA	32	#888888	
34[127]	13[127]	ACGAGAATCGGATTGCAGGATTAGGTCATTTT	32	#888888	

42[95] 1[286] GCCTGAAATCGTCTCTGTAATAACGTTGTAGCAAAAAAAAAAAAAAAAAA 47  
#f7931e

3[96] 27[111] AAAATACACCACCCTCAGCGTAACGACTCCTC 32 #333333

8[47] 31[47] TAAGTCCTGGAATCATCAAGCCGTTTATCCTG 32 #b8056c

50[87] 47[79] ACTACGTGAACCATCAAAGGAAGGGTCGAGGTTTAGAATC 40 #b8056c

20[143] 43[143] CATGCCTGGACGACAGCATTGCCCCAGCTTT 32 #aaaa00

14[111] 38[96] ATTAAGCACAAAATTAATTAGATAAGATTCAA 32 #888888

23[40] 47[47] CTTGACGGCTAAAGGGCTTTGACG 24 #f7931e

4[47] 27[47] GATAACCCCCAAAAGAGGAAACGCCAGCGCC 32 #03b6a2

25[48] 4[224] AGAGCCACCACCGGAACGGTCATAGTAGCACCAAAAAAAAAAAAAAAAAA 47  
#b8056c

28[159] 2[200] ATCGCCCAGCTTTGAGTAAACGGGAAGCGCGAAAAAAAAAAAAAAAAA 47  
#cc0000

11[96] 35[111] TCATCTTCGAGGCTTTATCAAAAAGTAGAAAG 32 #f7931e

26[95] 5[95] GTTGAAAATTTAATTGGAACACCCGCGCATT 32 #f74308

28[63] 10[224] TCCAATCCAACGCTATTTGAAGCCAATAGCAAAAAAAAAAAAAAAAAA 47  
#333333

47[80] 0[272] AGAGCGGGGAGGCCGAAATTAACCATCACTTGAAAAAAAAAAAAAAAAA 47  
#cc0000

3[128] 28[128] GAGCCACCTTCACGTTTGTATGGGTCGGTCGC 32 #888888

21[96] 45[111] AATACTTCGCTCGAATTCAGTCCACGCCAGC 32 #1700de

1[128] 26[128] CGTCATACCAGGAGGTTTAGCGGGATTCCACA 32 #f7931e

27[48] 0[40] AAAGACAACCGTCACCAATCACCAGCCCCCTTATTAGCGT 40 #aaaa00

10[143] 33[143] ACCCTCGTTTGGGCTTCAGGACGTCAGACCAG 32 #7300de

47[144] 7[286] GAGGCGGTTGCCTAATAAATTGTTCAAGCTTGAAAAAAAAAAAAAAAAA 47  
#f7931e

28[95] 7[95] CGGAGTTATTGCCGATCGTTTTAGATCCGGTA 32 #b8056c

25[88] 0[224] TCAGAACCAGCACCGTGTACCAAAAAAAAAAAAAAAAAA 39 #03b6a2

14[79] 37[79] AAATAAAGTTGAATTAGCGAATTAGAATTTAT 32 #333333

19[160] 44[160] ATCGCACTAAACGACGGGTTTTCCAGTGTA 32 #888888

24[127] 11[214] ATTTCCGGAGATTAGGATTAGTACCCACCCTCAAAAAAAAAAAAAAAAAA 47  
#333333

45[48] 7[262] GGAAAAACCACGACCAAGAACCCTTAAAAATAAAAAAAAAAAAAAAAAA 47  
#888888

19[128] 44[128] GAGGGGACCAGGTCGATGCTGCAATAACTCAC 32 #f74308

29[80] 3[238] AAGCCCTTGTAAGCAGATGTTAGCCATATAAAAAAAAAAAAAAAAAA 47  
#888888

46[159] 8[272] AGGGTTGAGTGTTGTTTTGATGGTCAACAGCTAAAAAAAAAAAAAAAAA 47  
#cc0000

15[64] 40[64] TTATACTTACATTTGATAAAAGTTTCACCTTG 32 #b8056c

25[144] 8[200] AGAGCCGCCGCCAGCAGCCTTGATCAGGAGTGAAAAAAAAAAAAAAAAA 47  
#f7931e

21[128] 46[128] AGCTGTTTTTCACCGCGGCCAACGGAACAAGA 32 #333333

17[128] 42[128]	TCAATCATTGGGATAGTCCTGTAGATTCAGGC	32	#03b6a2
8[79] 31[79]	AATGCAGACAGATATATTAACCACTTTCCAG	32	#7300de
20[111] 44[96]	GGTACCGATTTGATTATCGCTATTCGCTTTCC	32	#888888
0[167] 24[160]	GACGATTGTTGACAGGGAGTAACA	24	#b8056c
0[143] 24[128]	ACAAATAAATCCTCATCACCAGAACCCTGCCT	32	#cc0000
37[144] 10[144]	GGAAGCCCCAAATGCTTAAATGTCTATCATA	32	#57bb00
44[63] 12[248]	CAGGAACGTAACGTGCACCACACCGGCGAACGAAAAAAAAAAAAAAAAA	47	#888888
30[95] 9[95]	GGGCCAAGTCATTAACAACAACATAATTCTGT	32	#007200
13[64] 38[64]	AATTCATAAATTGCGCGCCTGATGGAGCGGA	32	#333333
13[128] 38[128]	TGCGGATGCAGGCAAGTTTAGCTTTAAATGC	32	#007200
4[79] 27[79]	GTCAGAGGTACGCAGTATAGCCGACGATTGAG	32	#7300de
19[64] 44[64]	GAAAGCGTGAAGAACTAAATACCTATTTTAGA	32	#b8056c
31[112] 4[112]	GAAAGACAGCAGGGAGCCTTTAATCCAAAAA	32	#f7931e
12[111] 36[96]	TTTAATTGAAATCAATTGACTATTGATTTAGT	32	#888888
12[143] 35[143]	CAAACCTCCGTAATAGTTAAACAGACCACATT	32	#f74308
23[64] 23[71]	TGGCGAGA	8	#b8056c
45[80] 18[80]	ACGCTCAATGGATTATGTGGCACATGCGCGAA	32	#888888
25[80] 49[87]	CGCCACCCATCAAGTTGTCAGACT	24	#f74308
41[80] 14[80]	ATTATCATAAAGAACTGGAAGGGTAAAACAG	32	#888888

41[112]	14[112]	AGTCAAATAGTAATGTTTCAGAGCATTAGCAAA	32	#333333	
4[111]	28[96]	AAGGCTCCAATTAACCTTCGTCTTTTCGCTTTTG	32	#888888	
31[48]	7[238]	AATCTTACCAAATAAGATAGCAGCATCAGAGAAAAAAAAAAAAAAAAA			47
		#03b6a2			
44[127]	6[272]	ATTAATTGAATGAATCCTGGCCCTTGCCCCAGAAAAAAAAAAAAAAAAA			47
		#7300de			
26[159]	4[200]	AGTACAAATTCAACAGAAAGGAATATTTCTTAAAAAAAAAAAAAAAAA			47
		#aaaa00			
38[127]	17[127]	AATGCCTGCACCATCACTGGAGCACTAGCATG	32	#7300de	
34[159]	13[159]	ATCCCCCTGAAAGACTCGAACCAGCTGAATAT	32	#f74308	
46[127]	3[286]	GTCCACTATTAAGAACGCTGGTTGAGAGAGTAAAAAAAAAAAAAAAAA			47
		#f7931e			
32[63]	0[248]	CATATTTAATGCGTTAAATAAGGCAGAACGCGAAAAAAAAAAAAAAAAA			47
		#f74308			
9[128]	34[128]	GTAGTAAATTACCAGATTAGGAATTTTCAGAAA	32	#aaaa00	
43[48]	5[262]	TCAGTATTCAAATATCATCAACAGAAGTATTAAAAAAAAAAAAAAAAAA			47
		#007200			
22[47]	45[47]	TTAATGCGTCAGTGAGGAATCCTGTTGCAACA	32	#1700de	
29[48]	6[224]	GAAACAATGAAACCGAACTGGCATAAGTTTATAAAAAAAAAAAAAAAAAA			47
		#b8056c			
12[79]	35[79]	CCTTGCTTTTTTCAAATTTTAACTTACCAG	32	#1700de	

34[63] 2[248] TAGGTTGGGAGAAGAGCGTCGCTACATTTAACAAAAAAAAAAAAAAAAAAAA 47  
#aaaa00

22[143] 45[143] GATTGCCCCCTGTGTGGAGTGAGCGGCGATTA 32 #57bb00

22[111] 46[88] TGCAGCAATAGGGCGCGAAACCTGCCAACGTCAAAGGGCG 40 #aaaa00

16[79] 39[79] TAGATAATCTGAATAACACCAGAATGCTTTGA 32 #aaaa00

21[160] 46[160] ACAATTCCTCACCAGTTGGGCGCCCCCGAGAT 32 #7300de

27[144] 9[214] CAGTACCAATAAACAGTGATGATAATTCACAAAAAAAAAAAAAAAAAAAA 47  
#cc0000

40[127] 19[127] TAAATTTTTCTGGCCTGTCACGTTGCCAGTTT 32 #333333

41[48] 3[262] CGAACGTTTCATATTCCATCCTGATCAGGTTTA???????????????? 47 #333333

2[47] 25[47] TTTGTCACGCCAGCAAGACTTGAGCCGGAACC 32 #888888

40[95] 19[95] CAAGCAAACAGCATAGGTCTTTAAGACAATAT 32 #333333

1[160] 26[160] TACTGGTAAGTATAGCAGTGCCGTTTCGTCACC 32 #f74308

29[112] 12[200] TAGTAAATTCATAGTTAGAACC GCGCCACCCTAAAAAAAAAAAAAAAAAAAA 47  
#aaaa00

5[96] 29[111] GACGGGAGAAAAGGAGTTAAAGGCCCAGACGT 32 #03b6a2

30[63] 12[224] ACTCATCGGAAACCAAGTTTATCAAGAGAATAAAAAAAAAAAAAAAAAAAAA 47  
#888888

33[80] 6[80] TTTCTTAAACGGGTAGAAAGGCTTCGAACCTC 32 #cc0000

42[159] 9[286] AAACCAGGAACGCCAGGCCAGTGCATCCGCTCAAAAAAAAAAAAAAAAAAAAA 47  
#f7931e

34[95]	13[95]	TTACTGAGTAGGTCCCATATGTGAAATGGAAA	32	#cc0000	
26[127]	5[127]	GACAGCCCGAATTTTCGAAAATCTTGTATCGG	32	#333333	
18[47]	41[47]	CCGAACGAGTTGGCAAAAACCTCCCTTTGCC	32	#b8056c	
15[128]	40[128]	AATCGGTTCTGAGAGTATATGATAATTCGCAT	32	#57bb00	
7[128]	32[128]	TCTTTGACAACAAAGCACGGTGTATGGGAAGA	32	#57bb00	
6[47]	29[47]	AAGATTAGAAATGAAAAACGATTAAGAGCAA	32	#cc0000	
31[80]	4[80]	AGCCTAATCAAAATAAACAGGGAATGAACAAA	32	#333333	
42[63]	10[248]	ACCAGTCAGCTCATGGCAAACCTATGTAAAAGAAAAAAAAAAAAAAAAAAAA			47
		#333333			
14[143]	37[143]	AAATCATAGCTTAGAGATTCCATAGATTAAGA	32	#b8056c	
8[143]	31[143]	ATCAACGTCCCCAGCGCTGCTCCAAGCAACGG	32	#333333	
36[63]	4[248]	AATTACCTAACGGATTTAGATTTTTGTTTGGAAAAAAAAAAAAAAAAAAAA47			#57bb00
39[48]	1[262]	GAAACAATGAGCAAAAATTAATTATTAATTAATAAAAAAAAAAAAAAAAAAAAA			47
		#f74308			
13[160]	38[160]	AATGCTGTATAGTAGTGAAAAGGTAAGGATAA	32	#007200	
0[111]	24[96]	AGCGCAGTTCGATAGCGCCACCCTCATGAAAG	32	#cc0000	
32[159]	11[159]	GGCTCATTGCAGATACGAGCAACATTAGACTG	32	#03b6a2	
24[95]	1[238]	TATATATTGGTAATAAGGTGGCAAAAACGTAGAAAAAAAAAAAAAAAAAAAA			47
		#aaaa00			
35[80]	8[80]	TATAAAGCCAGTAGGGGGTAAAGTGTTTCAGCT	32	#f7931e	
38[95]	17[95]	AAGGGAACCTTTCGGGTAGATTAGATCTTTAGG	32	#7300de	

4[143]	27[143]	ATAATTTTACCCTCATCCTGTAGCGTTTTGCT	32	#f7931e	
10[111]	34[96]	AATAGCGATGACCTAATATTACAGTCAGGTCT	32	#888888	
10[79]	33[79]	TACCGACCCGACAAACTTAATTGCGGCTGTC	32	#007200	
45[112]	18[112]	TGGCGAAATGTTGGGAGTGCATCTGGTGTAGA	32	#f7931e	
3[64]	28[64]	CTCCTTATGTAATTGAAATAGCTAATTATTTA	32	#f7931e	
42[127]	5[286]	TGCGCAACGGGGGATGCTCTAGAGATGGTCATAAAAAAAAAAAAAA			47
		#333333			
35[112]	8[112]	ATTCATCACGTTAATAAGAAACACCAGTGAAT	32	#888888	
39[80]	12[80]	ATACCAAGGCGCAGAGCCTTTTTTGTGAATAA	32	#b8056c	
16[111]	40[96]	AATCGATGCAACTAATGAGAAAGGTTTTTAAC	32	#888888	
6[143]	29[143]	GTAATGCCCTTGCTTTTCGATATATATTTTGCT	32	#f74308	
23[128]	47[143]	CAGGCGAAAATCCTGTCCAGTTTGCGCGGGGA	32	#007200	
45[144]	11[286]	AGTTGGGTCAAAGCGCTATCGGCCGGCGGATTAAAAAAAAAAAAAA			47
		#888888			
30[159]	0[200]	TGTCGAAAGCTGGCTGGATATTCATTAATTTCAAAAAAAAAAAAAA			47
		#7300de			
23[96]	47[111]	GCGGGCGCGCGGTCCACGTGGACTTCGTGCCA	32	#1700de	
16[47]	39[47]	GACTTTACTCAATATATGATTATCCATCGGGA	32	#aaaa00	
9[64]	34[64]	TAAAGTACGTGTGATATACAAATTCTCCGGCT	32	#f7931e	
20[79]	43[79]	CCTGAGTAAAGAATACTTACATTGGTGCCACG	32	#f74308	
8[111]	32[96]	AAGGCTTGCGACAATACGAAGTATAACGGAA	32	#888888	

33[144] 3[214] GGCATAGTCCGCGACATTATACCTAAAATACAAAAAAAAAAAAAAAAAAAA 47  
#aaaa00

37[48] 13[238] AAGACGCTGTTATATACAAGACAAGTTAAATAAAAAAAAAAAAAAAAAAAAA 47  
#f74308

30[127] 9[127] AGCCGAAACAGATGATGCTCATT CAGAACGA 32 #cc0000

7[64] 32[64] AAGCAAATACGCGCCTTCAATAATAGAATCGC 32 #b8056c

12[47] 35[47] TTTCCCTTCCAATCGACTATATGGCCTGTTT 32 #03b6a2

36[95] 15[95] TTGAAATCTTACAACCTTTGCACGTTAGAACC 32 #007200

7[96] 31[111] TTCTAAGACAAAAGAAAGACGGTCTCAGCAGC 32 #333333

1[64] 26[64] ATTACCATAAAGACACCATTCAACACAAAGTT 32 #aaaa00

41[144] 2[296] TTCTAGCTAGAACCCCTAACATTATCATCCAATAAAAAAAAAAAAAAAAAAAAA 47 #aaaa00

19[96] 43[111] TTTTGAATTCGTAACCAGGGCGATTCAAAAAT 32 #1700de

17[64] 42[64] AATTGAGGCCTAAAACCTGCAACAGCAGATTC 32 #7300de

22[79] 45[79] CACGCTGCATCACGCATTAAAGGGACATTTTG 32 #f7931e

2[111] 26[96] CAGAACCGTACATAAAGAGGCTGAGATCTAAA 32 #888888

1[96] 25[111] TGAAACCACTCTGAATTTCTGAAACAGAGCCA 32 #aaaa00

26[63] 8[224] ACCAGAAGGAAATAGCGCGCTAATCTTTACAGAAAAAAAAAAAAAAAAAAAA 47  
#f74308

29[144] 7[214] AAACAACCTCTACAACGTTTCAGGGGGTGTATCAAAAAAAAAAAAAAAAAAAAA 47  
#aaaa00

9[160] 34[160] AACTTTAACATAGTAAATAACGCCTTCATTGA 32 #f7931e

39[144] 12[144] ATTTGGGGGAAGTTTCCTTAATTGACCGGAAG 32 #b8056c

15[96] 39[111] TACCATATATAAAGCCGTAGGTAACATTTTCGC 32 #7300de

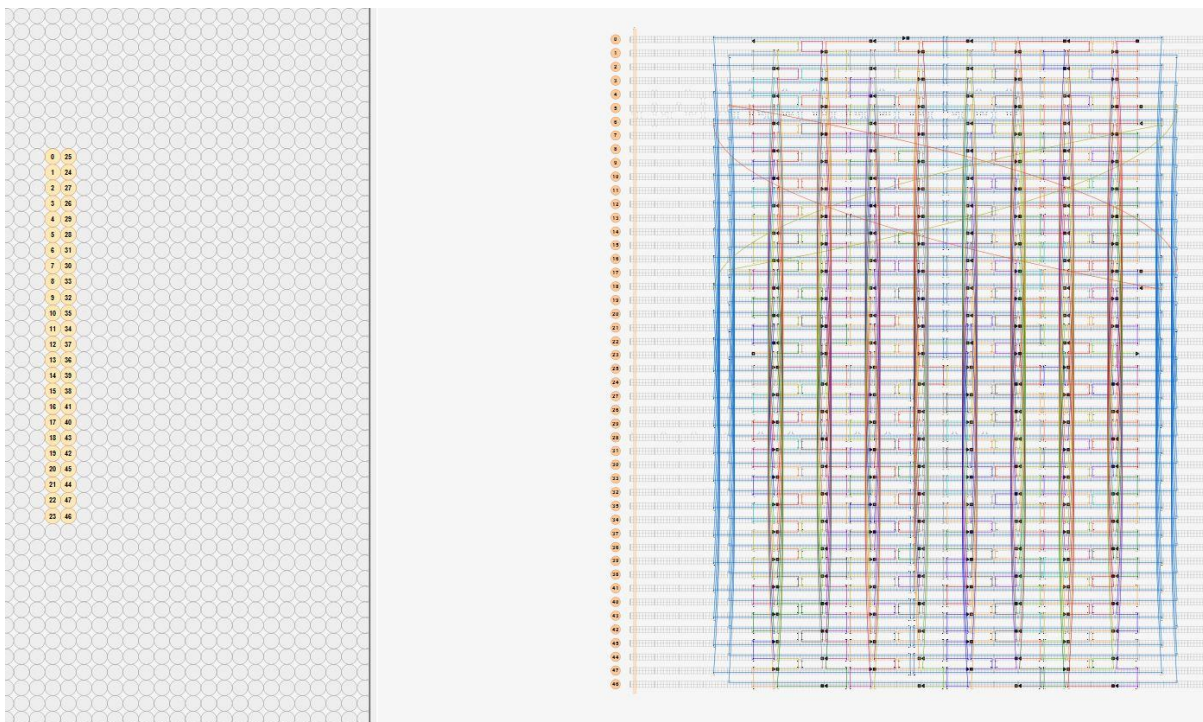
36[159] 0[296] GGTGTCTGCGCGAGCTAGCATTAAAGACCCTGTAAAAAAAAAAAAAAAAA 47  
 #333333

14[47] 37[47] ACGTCAGAAAAACAAAGAAGATGACTTAGATT 32 #aaaa00

32[127] 11[127] AAAATCTAGTTGAGATCGACGATAAAGTTTTG 32 #1700de

47[48] 9[262] AGCACGTAGTACGCCAGCCACCGACGGCCTTGAAAAAAAAAAAAAAAAA 47  
 #aaaa00

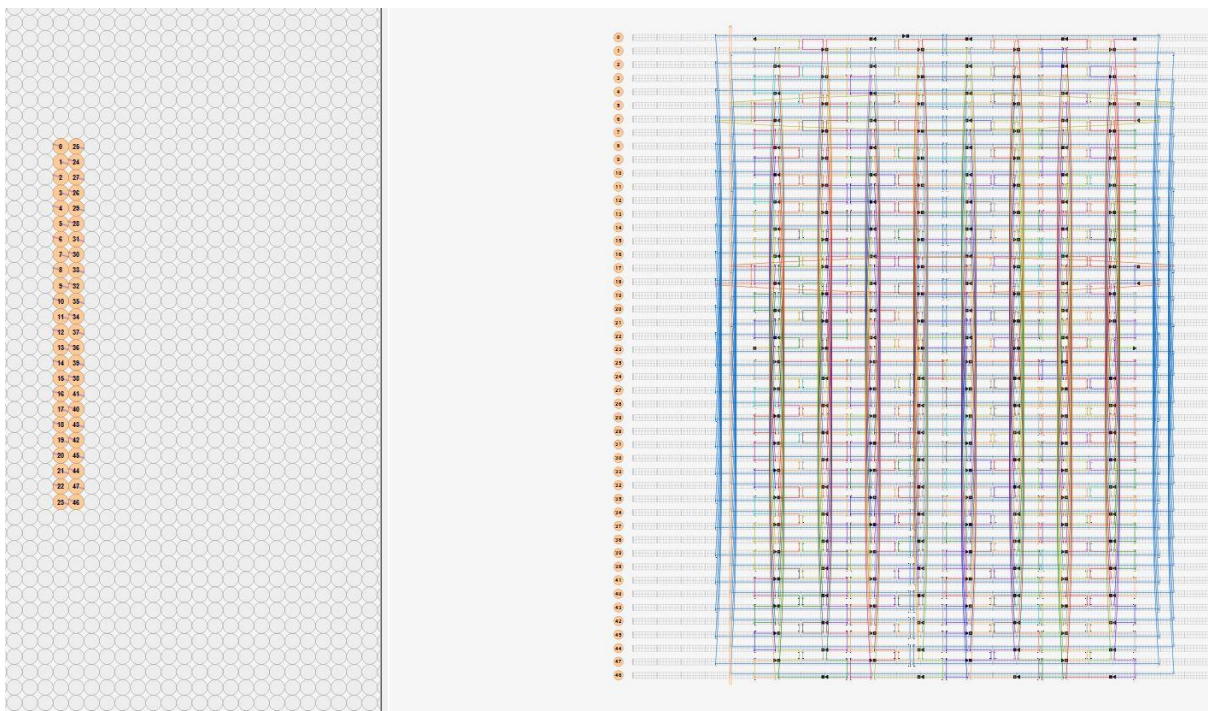
Design – Lattice points expanding in X and Y



As this board is essentially identical to the bare board design show above only the two lattice sequences are noted below. Every other sequence is identical to the design listed at the beginning of this section.

5[168]	6[168]	CCTTTGCCCGAACAAATCTACGAAGGCTTGCCCTGATCAAAT	42	#aaaa0
				0
17[168]	18[168]	TCATATGGTTTACGAAAGGGGTCAGGAAGATCGCCACCAAT	42	#f7430
]	]	G		8

Design – Lattice points expanding only in X



As with the expanding X and Y lattice only the sequences unique to this design are included. All other sequences are shared with the bare board described at the beginning of the design list.

5[168]	6[168]	CCTTTGCCCGAACGAAAGGGGTCAGGAAGATCGCATCAAAA	42	#aaaa0
		T		0
17[168]	18[168]	TCATATGGTTTACAATCTACGAAGGCTTGCCCTGCACCAATG	42	#f7430
]	]			8